Brahim Safi
Abdelhakim Daoui
Hamza Mechakra
Youcef Ghernouti *Editors*

# Proceedings of the 4th International Symposium on Materials and Sustainable Development

## Volume 2: Waste Recycling and Environment

Springer

Proceedings of the 4th International Symposium on Materials and Sustainable Development

Brahim Safi · Abdelhakim Daoui ·
Hamza Mechakra · Youcef Ghernouti
Editors

# Proceedings of the 4th International Symposium on Materials and Sustainable Development

## Volume 2: Waste Recycling and Environment

Springer

*Editors*
Brahim Safi
Faculté de Technologie
Université M'hamed Bougara Boumerdes
Boumerdès, Algeria

Hamza Mechakra
Université M'hamed Bougara Boumerdes
Boumerdès, Algeria

Abdelhakim Daoui
Université M'hamed Bougara Boumerdes
Boumerdès, Algeria

Youcef Ghernouti
Université M'hamed Bougara Boumerdes
Boumerdès, Algeria

ISBN 978-3-030-43210-2 ISBN 978-3-030-43211-9 (eBook)
https://doi.org/10.1007/978-3-030-43211-9



This Springer imprint is published by the registered company Springer Nature Switzerland AG
The registered company address is: Gewerbestrasse 11, 6330 Cham, Switzerland

# Preface

As part of the scientific events which took place within the M'hamed Bougara University of Boumerdes, the Research Unit: Materials, Processes and Environment of the Faculty of Technology, organizes, from 12 to 14 November 2019, the 4th International Symposium on Materials and Sustainable Development (ISMSD2019).

This scientific, technological and environmental gathering will strive to improve by trying:

1. To deepen the subject relating to nanomaterials and their incorporation in other materials.
2. To take an interest in sustainable development by focusing on renewable energies, recycling and recovery of materials, the quality of which will contribute to improving environmental protection.
3. To deepen the university–industry complementarity by multiplying the contacts between them in order to possibly bring solutions to the problems hampering the technological processes.
4. To energize the partnership, collaboration and development of relations between our university and certain foreign universities by working on joint projects to allow, among other things, our doctoral students to benefit from joint supervision and to facilitate exchanges between our students and foreign students.
5. To foster links between national researchers who will take note of the work presented by dissecting it to draw inspiration from it, as far as possible.
6. To choose the best work by rewarding the winners.

To this end, this symposium will focus on:

Theme 1: Nanomaterials, Nanotechnology and Emerging Intelligent Materials
Theme 2: Cementitious Materials and Material Properties
Theme 3: Renewable Energies, Sustainable Development, Recycling and Environment
Theme 4: Materials, Processes and Transformations

We would like to express our gratitude and appreciation for all of the reviewers who helped us maintain the high quality of manuscripts included in the proceedings published by Springer Nature. We would also like to extend our thanks to the members of the organizing team for their hard work. It is hoped that this volume will be of help to many researchers working in diverse topics present in the ISMSD2019.

It is a great privilege for us to present the proceedings of ISMSD2019 to the authors and delegates of the event. We hope that you will find it useful, exciting and inspiring.

Brahim Safi
Abdelhakim Daoui
Hamza Mechakra
Youcef Ghernouti

# Objectives of the 4th International Symposium on Materials and Sustainable Development

This book presents the proceedings of the 4th International Symposium on Materials and Sustainable Development ISMSD2019 (CIMDD2019) that was held during 3-day (12–14 November) and organized by the Research Unit: Materials, Processes and Environment and M'hamed Bougara University of Boumerdes (Algeria) in partnership with University of Reims - Champagne-Ardenne (France). This symposium follows the success of CIMDD 2013-2015-2017 and continues the traditions of the highly successful series of international conferences on the materials, processes and environment. The symposium will provide a unique topical forum to share the latest results of the materials and sustainable development research in Algeria and worldwide.

## Organization

Research Unit: Materials, Processes and Environment and M'hamed Bougara University of Boumerdes in partnership with and University of Reims Champagne-Ardenne

# Scientific and Advisory Committee

| | |
|---|---|
| A. Zerizer | Univ. Boumerdes, Algeria |
| A. Li | Univ. Reims, France |
| M. T. Abadlia | Sci. Res. Tech. Coun., Algeria |
| A. Benmounah | Univ. Boumerdes, Algeria |
| A. Bezazi | Univ. Guelma, Algeria |
| B. Safi | Univ. Boumerdes, Algeria |
| T. A. V. Phan | Ton Duc Thang Univ, Vietnam |
| Y. Ghernouti | Univ. Boumerdes, Algeria |
| M. F. R. Al-Khatib | Int. Islamic Univ. Malaysia |
| K. Boumchedda | Univ. Boumerdes, Algeria |
| M. Kadri | Univ. Boumerdes, Algeria |
| R. Tala Ighil | Univ. Boumerdes, Algeria |
| H. Essawy | Nat. Res. Centre, Egypt |
| D. Aboutaleb | Univ. Boumerdes, Algeria |
| T. Bouziani | Univ. Laghouat, Algeria |
| C. Derail | Univ. Pau, France |
| R. Chaid | Univ. Boumerdes, Algeria |
| A. Oudia | Univ. Toulouse, France |
| M. Hamiane | Univ. Boumerdes, Algeria |
| M. Arif Kamal | Univ. Aligarh Muslim, India |
| M. Hachemi | Univ. Boumerdes, Algeria |
| M. Bououdina | Univ. Bahrain, Bahrain |
| S. Kebbouche-Gana | Univ. Boumerdes, Algeria |
| M. Z. Messaoud-Boureghda | Univ. Boumerdes, Algeria |
| G. Goli | Univ. Florence, Italy |
| T. Hassaine Douadji | Univ. Tiaret, Algeria |
| K. Mohammedi | Univ. Boumerdes, Algeria |
| K. Bouakaz | Univ. Tiaret, Algeria |
| S. Willfor | Univ. Åbo Akademi, Finland |
| A. Daoui | Univ. Boumerdes, Algeria |
| K. Chahour | Univ. Tizi Ouzou, Algeria |

| | |
|---|---|
| H. Mechakra | Univ. Boumerdes, Algeria |
| N. H. Kamel | CRNA, Algeria |
| B. Benothmane | Univ. Boumerdes, Algeria |
| J. Mitterpach | Tech. Univ. Zvolen, Slovakia |
| F. Bensouci | Univ. Boumerdes, Algeria |
| S. Bahamida | Univ. Boumerdes, Algeria |
| F. T. Kheloui | Univ. Tizi Ouzou, Algeria |
| M. Ould Ouali | Univ. Tizi Ouzou, Algeria |
| M. Tazrout | Univ. Boumerdes, Algeria |
| K. Amara | Univ. Ain-Temouchent, Algeria |
| B. Rabehi | Univ. Boumerdes, Algeria |
| A. Chellil | Univ. Boumerdes, Algeria |
| L. Hammadi | Univ. Oran, Algeria |
| M. Almansba | Univ. Tizi Ouzou, Algeria |
| K. Yahiaoui | Univ. Boumerdes, Algeria |
| M. Driss | Univ. Mascara, Algeria |
| M. Saidi | Univ. Boumerdes, Algeria |
| M. Sonebi | Queen's Univ. Belfast, UK |
| H. Aksas | Univ. Boumerdes, Algeria |
| S. Kennouche | Univ. Bouira, Algeria |
| S. Lecheb | Univ. Boumerdes, Algeria |
| B. Amrane | Univ. Bouira, Algeria |
| R. Benzerga | Univ. Rennes 1, France |
| B. Bezzazi | Univ. Boumerdes, Algeria |
| H. Trouzine | Univ. Sidi Bel-Abbes, Algeria |
| A. Limam | CNERIB, Algeria |
| A. Flilissa | Univ. Setif, Algeria |
| C. Aribi | Univ. Bouira, Algeria |

## Organization

Research Unit: Materials, Processes and Environment and M'hamed Bougara University of Boumerdes in partnership with and University of Reims Champagne-Ardenne

# Contents

# Physicochemical and Foaming Properties of Crude Acid Whey Treated by Ultrafiltration

K. Acem[1(✉)], C. Fersi[2], and A. Yahia[2]

[1] Laboratory of Plant Physiology Applied to Soilless Crops, Faculty of Nature Sciences and Life, University of Tiaret, BP 78, 14000 Tiaret, Algeria
kamel_acem@yahoo.fr

[2] Laboratory of Materials, Treatment and Analysis, INRAP, Biotechpole Sidi-Thabet, 2032 Ariana, Tunisia

**Abstract.** The crude acid whey is a cheese rejection derived from the manufacture of soft cheeses and fresh dough, by its fermentable biomolecules; it represents a real factor of biological pollution of freshwater ecosystems (Wadi of Mina, Relizane, Algeria). Our study aims to analyze the effect of membrane treatment (ultrafiltration) on the physicochemical parameters (COD, turbidity, Brix, pH, salinity and electrical conductivity) and foaming properties (foaming capacity and diameter of air bubbles) of crude acid whey by applying physical, chemical and interfacial analysis methods. The results have shown that a variability has been noted for the physicochemical parameters COD(CAW: 1159 mg/l, PCAW: 525 mg/l and CCAW: 1355 mg/l), turbidity(CAW: 237.66NTU, PCAW: 0.86NTU and CCAW: 72.1NTU), Brix(CAW: 7.45%, PCAW: 5.8% and CCAW: 10%), pH(CAW: 4.6, PCAW: 4.6 and CCAW: 4.9), salinity(CAW: 3.58 g/l, PCAW: 3.95 g/l and CCAW: 3.77 g/l) and electrical conductivity(CAW: 5.8 mS/cm, PCAW: 6.39 mS/cm and CCAW: 6.4 mS/cm) and interfacial properties (foaming capacity and diameter of air bubbles) of crude acid whey and its fractions after ultrafiltration (concentrate and permeate). It is concluded from this study that the ultrafiltration of crude acid whey has changed its physicochemical and foaming behavior in function to the operating conditions and to the composition of the studied whey.

**Keywords:** Crude acid whey · Ultrafiltration · Pollution · Foam · Valorization

## 1 Introduction

The crude acid whey is a co-product and an effluent of soft cheeses and fresh dough. According to Mollea et al. (2013) global whey production was estimated at 180–190 tons/year. In Algeria and in other countries of the world, this rejection accounts for about 85% of milk processed into cheese (FAO 1995; Gana and Touzi 2001). Rejected in the environment without prior treatment (case of dairy and cheese industry SIDI SAADA, YELLEL, RELIZANE, Algeria), the latter may be a favorable factor in the biological pollution of freshwater ecosystems following its native biochemical composition (Acem


B. Safi et al. (Eds.): ISMSD 2019, *Proceedings of the 4th International Symposium on Materials and Sustainable Development*, pp. 1–11, 2020.
https://doi.org/10.1007/978-3-030-43211-9_1

et al. 2016, 2017). Its valorization is an economic and ecological stake since one liter of the whey has a Biological Demand in Oxygen (BDO) is between 30 and 45 g/l of oxygen and therefore requires the oxygen of 4500 l of oxygen unpolluted water, making it a pollutant that can no longer be released into the environment (Juillerat and Badoud 2010).

Whey proteins are widely used in the food industry because they possess, inter alia, good functional properties (Bottomley et al. 1990; Acem and Choukri 2017). The whey proteins have in particular the properties to retain water, to act as foaming and/or emulsifying agent and to form aggregates (or gels) (Kinsella and Whitehead 1989; Acem and Choukri 2017).

According to Cheftel et al. (1985), Acem and Choukri (2012a, b) the whey proteins have functional properties which vary according to the preparation treatments they have undergone (ultrafiltration, fixation on ion exchangers, precipitation by chemical or thermal agents).

According to Gaucheron and Tanguy (2009), membranes technologies are now very interesting for the purification of milk proteins or peptides, they allow to separate and purify on a large scale the different molecules or particles present in the milk or liquid according to their size.

Therefore, a pre-concentration of the milk proteins by ultrafiltration at the right concentration factors is interesting for the transformer, because it reduces the time and operating costs of energy-intensive processes such as evaporation (Rehman et al. 2003). Few scientific studies have begun and published on the influence of membrane treatment on the physicochemical and foaming behavior of crude acid whey, and for this purpose, the present study aims to analyze the impact of ultrafiltration on the physicochemical and foaming properties of crude acid whey.

## 2 Material and Methods

### 2.1 Crude Acid Whey

Crude acid whey is prepared at the laboratory level from skimmed milk powder (0% Fat) made from cow's milk by SOLAREC SA, route de St, Hubert, 756,800 RECOGNE BELGIUM. Crude acid whey (CAW) is prepared by adjusting the pH of reconstituted milk to 10% at the isoelectric pH of the insoluble proteins; after a rest period, the crude acid whey is recovered after centrifugation fixed at 3500 rpm/5 min (ROTINA 380 centrifuge, Hettich ZENTRIFUGEN) and is stored at 4 °C.

### 2.2 Membrane Treatment

1000 ml of crude acid whey was treated by ultrafiltration (GE Osmonics assembly) whose characteristics of the organic membrane used are (Trade name: GK Osmonics, active surface: 140 $cm^2$, composition: polyamide/polysulfone, type: plane, cut-off point: 2 kDa) under a transmembrane pressure fixed at 5 bar and an ambient temperature of the laboratory (20 °C).

### 2.3 Physicochemical Properties

The physicochemical parameters controlled for the three compartments (CAW, PCAW and CCAW) are: the chemical oxygen demand (COD) and the turbidity measured by multi-parameter photometer (WTW photoFlex), Brix degree (°Brix) by refractometry (refractometer ABBE), pH by pH meter (pH meter CG 822 GHS), salinity and electrical conductivity by multi-parameter conductivity meter (ProLine).

### 2.4 Foaming Properties

For the formation of the foam, 20 ml of the whey is whipped by a Blinder (Bomann, STABMIXER SM 354 CB-hand blender) at 18,000 rpm during 1 min. The estimation of its foaming power was made by controlling the mean diameter of the air bubbles and the foaming capacity (Martínez et al. 2011) whose average diameter of the air bubbles is observed and determined under a photonic microscope (PHYWE, hund WETZLAR, GERMANY) using an ocular micrometer graduated from 0 to 10 whose graduations are distant from each other others of 0.1 μm.

The experimental data are analyzed statistically by R software.

## 3 Results and Discussion

### 3.1 Physicochemical Properties

The Fig. 1 shows some physicochemical parameters measured for crude acid whey (CAW) and modified by ultrafiltration (permeat: PCAW and concentrate: CCAW).

The modification of the crude acid whey by ultrafiltration into two fractions (permeate and concentrate) modulated their physicochemical parameters, namely °Brix (CAW: 7.45%, PCAW: 5.8% and CCAW: 10%, Fig. 1a), pH (CAW: 4.6, PCAW: 4.6 and CCAW: 4.9, Fig. 1a), salinity (CAW: 3.58 g/l, PCAW: 3.95 g/l and CCAW: 3.77 g/l, Fig. 1a), electrical conductivity (CAW: 5.8 mS/cm, PCAW: 6.39 mS/cm and CCAW: 6.4 mS/cm, Fig. 1a), COD (CAW: 1159 mg/l, PCAW: 525 mg/l and CCAW: 1355 mg/l, Fig. 1b) and turbidity (CAW: 237.66NTU, PCAW: 0.86NTU and CCAW: 72.1NTU, Fig. 1b).

From the results, we have noted that the parameters (pH, EC and salinity) measured for the three compartments (CAW, PCAW and CCAW) are characterized by stable values, while a high concentration of dry matter represented by °Brix ( Brix degree) was noted in the CCAW compared to those found in the CAW and PCAW (Fig. 1a). In parallel, we have recorded a high chemical oxygen demand (COD) in the CCAW compared to those in the CAW and PCAW, however a higher turbidity was marked in the CAW compared to those measured in the CCAW and PCAW (Fig. 1b). These results can be explained by the composition of the crude acid whey and the operating conditions used during the ultrafiltration.

Ultrafiltration (UF) process is the most important membrane technology and has the ability to concentrate any substance with molecular weight between 1 to 1000 kDa especially for concentrating the whey protein (Atra et al. 2005). UF membranes are performed by applying a specific pressure in order to separate the particles according to their sizes and molecular weight (El-Gazzar and Marth 1991). In case of separation

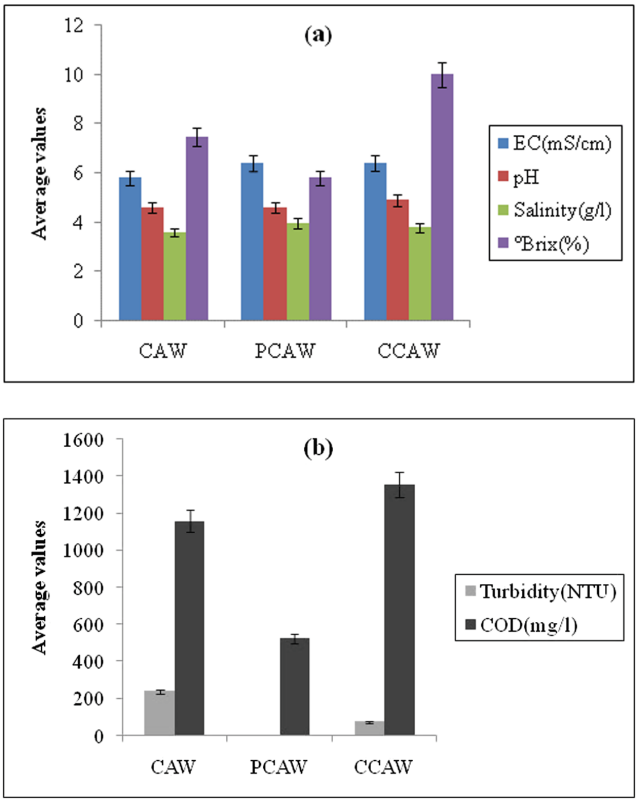


**Fig. 1.** Average values of physicochemical parameters of crude acid whey (CAW) and modified by ultrafiltration (a and b) at 20 °C.

of whey components, by using UF process, the protein and fat can be recovered with accumulating on the surface or the pores of membrane as the retentate while lactose, minerals and water pass through the membrane pores as the permeate by using particular driven pressure (El-Gazzar and Marth 1991).

The performance and selectivity of the membrane filtration system was clearly dependent on the processing conditions, such as pH and temperature, the composition, such as mineral content, and the protein interactions, such as electrostatic and hydrophobic interactions in the feed (Chandrapala et al. 2016).

According to Iltchenco et al. (2018), the viability of the whey protein concentration process by membranes depends, largely, of the conditions as the membrane properties, flow type, membrane-solute affinity, solution temperature, pressure, among others.

The whey represents about 85 to 90% of the total volume of milk used for cheese production, and contains approximately 55% of milk nutrients, including proteins, lactose, soluble vitamins and minerals (Brandelli et al. 2015).

Ultrafiltration of crude acid whey is operated according the size of its composants. According to Krissansen (2007), the β-lactoglobulin (β-LG) and α-lactalbumin (α-LA) are the two biggest protein fractions in cheese whey. These fractions, together, account

for 70 to 80% of total proteins in whey, but concentration of β-LG is twice that of α-LA. Moreover, the molecular weight (MW) of α-LA is 14 kDa and MW of β-LG is 18.4 kDa, the rest of the whey proteins are serum albumin with MW of 66.5 kDa and immuneglobulin (MW 150–1000 kDa), Glycomacropeptide (MW 6.8 kDa), Proteose-peptone (MW 4–22 kDa), Lactoferrin (MW 78 kDa), Lactoperoxidase (MW 89 kDa).

The decrease in turbidity may be related with the presence of carbohydrate compounds that might contribute to protein stabilization and so, fewer or smaller particles formation, as the carbohydrate concentration increases. When a hydrophilic solute is diluted in water it will establish hydrogen bonds with it creating an unfavorable environment to protein denaturation due to lower water availability. It is well known that the turbidity of aggregated proteins depends on the number and size of aggregates along with the scatter factor of their particles; the large size and high scatter factor of particles usually lead to the high turbidity of the solution (Kehoe and Foegeding 2011).

Chemical oxygen demand (COD) is generally used to indirectly determine the amount of organic compounds in aquatic systems. High COD indicates presence of all forms of organic matter, both biodegradable and nonbiodegradable and hence the degree of pollution in waters, this makes COD useful as an indicator of organic pollution in surface waters. The estimation of COD along with BOD is helpful in indicating toxic conditions and the presence of nonbiodegradable substances (Sawyer et al. 2003).

The results obtained are similar to those found by Baldasso et al. (2011), Belhamidi et al. (2015) and Iltchenco et al. (2018).

According to Belhamidi et al. (2015), the physicochemical properties (electrical conductivity, pH, salt content, lactose, proteins, lipids, chemical oxygen demand (COD) and biological oxygen demand ($BOD_5$) of crude acid whey modified by ultrafiltration(concentrate and permeate) vary with transmembrane pressure, temperature, and volume reduction factor (VRF).

### 3.2 Foaming Properties

The Fig. 2 indicates the foaming capacity of crude acid whey and modified by ultrafiltration (permeate and concentrate).

According to Fig. 2, at time t = 0 min, we found that the foaming capacity of the CCAW (120%) is higher than that noted in the CAW (100%) and PCAW (0%).

The concentration of crude acid whey by ultrafiltration increased its foaming capacity for CCAW compared to that marked in CAW and PCAW, the latter did not manifest by the formation of the foam from the time t = 0 min.

These results are strongly linked to the high concentration of dry matter (proteins) noted in the CCAW than those recorded in the CAW and the PCAW.

The main proteins in whey are β-lactoglobulin (β-LG), α-lactalbumin (α-LA) and bovine serum albumin (BSA) and they account for 70% of total whey proteins (Cayot and Lorient 1997). These proteins are responsible for the functional properties of whey proteins, such as solubility in water, viscosity, gelation, emulsification, foaming, colour, and flavor and texture enhancement and offer numerous nutritional advantages to formulated products (Krešic et al. 2008).

Protein foams are dependent on protein surface activity and film forming properties, which are governed by protein structure (Phillips et al. 1990a). According to Firebaugh

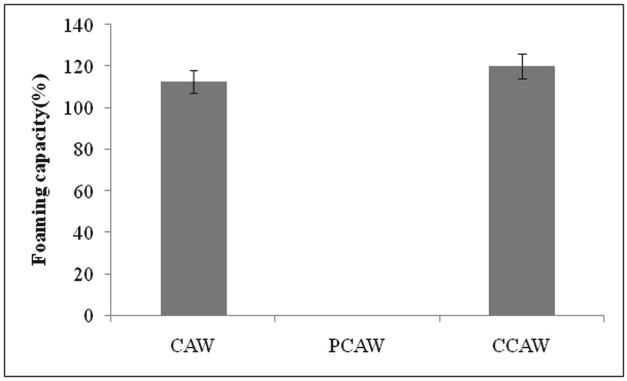


**Fig. 2.** Foaming capacity of CCAW, PCAW and CAW controlled at 20 °C.

and Daubert (2005), surface active functional performance of whey proteins is directly linked to protein structure, which varies based on several environmental factors (pH, ionic strength, and protein concentration).

Moreover, Patino and Pilosof (2011) have concluded that the foaming properties or surface activities of proteins are closely related to the protein conformational properties, such as structure, size, shape, and amino-acid composition.

Proteins due to their amphiphilic character can adsorb at fluid interfaces; the adsorption of proteins at interfaces and other dynamic surface properties such as film viscoelasticity are known to play an important role in the formation and stability of food dispersed systems as foams and emulsions (Dickinson 1992).

According to Zayas (1997), the foaming properties of proteins are influenced by the source of the protein, methods and process parameters, including protein isolation, temperature, pH, protein concentration, mixing time, method of foaming. Among many factors influencing foaming capacity (FC) of proteins, the type of foaming equipment and method of agitation are important.

The basic function of proteins in foams is to decrease interfacial tension, to increase viscous and elastic properties of the liquid phase and to form strong films. Protein foamability is correlated with its capacity to decrease surface tension at the air-liquid interface. Proteins possess the ability to adsorb at the interface and reduce surface tension (Zayas 1997). The foamability increased with the protein concentration (*C*p), until a plateau value was reached; upon increasing (*C*p) above the plateau value, the foam wetness kept increasing du to the decreasing size of the formed bubbles (Marinova et al. 2009).

Functional properties of whey proteins such as emulsification, foaming and gelation are affected by their structure and mainly reflect the functionality of β-lactoglobulin as the most abundant protein, which has the ability to adsorb at the water oil and air–water interfaces (Nakai and Li-Chane 1993).

According to Damodaran (2005), factors impacting foam stability include disjoining pressure, surfactant film viscoelasticity, and interfacial tension, proteins like β-LG behave like surfactants due to their amphiphilic nature which are also enhanced by mixing with other surfactants. Factors that affect foaming properties of proteins include

intrinsic factors, such as molecular flexibility (Engelhardt et al. 2013) and external environment factors such as pH, ionic strength, and heating condition directly affect protein structure and its interfacial properties, thus impact the foaming properties of whey protein (Phillips et al. 1989, 1990b, 2006; Clark et al. 1994; Zhu and Damodaran 1994; Raikos et al. 2007).

The surface dilatational viscoelasticity of surfactant layers reflects the force working against the shrinkage of the bubbles (Dickinson 2006). Globular proteins, e.g., β-lactoglobulin, irreversibly adsorb at the air–water interface and form highly viscoelastic films, thus they are suitable to stabilise foams in long-term (Dickinson 2006).

The foaming properties of globular proteins are determined by their rate of diffusion and rate of adsorption to the interface, the ability to unfold their globular molecular structure and their aggregation at the interface (Borcherding et al. 2008).

However, whey protein fractions differ in their adsorption behaviour; the unfolding of the molecular structure, respectively the tertiary structure, during adsorption of α-lactalbumin is taking place more rapidly than for β-lactoglobulin (Cornec et al. 1999).

The changes in pH affect the conformation and the net charge of the adsorbed protein layers at the interface (Phillips et al. 1994). Moreover, the pH of protein solution may affect the solubility of proteins by changing the repulse among molecules (Peligrine and Gasparetto 2005).

At pH 5.0, the net charge was minimized, and the aggregation of whey proteins was the highest due to a reduction in electrostatic repulsion between proteins and rigid protein films (Lam and Nickerson 2015).

Nastaj and Sołowiej (2020) have deducted that the overrun (OR) values of the foams depend on the preparation type and pH. For all preparations, the highest ORs were observed for the 10% protein concentration. For lower concentrations, it decreased proportionally. Also the highest values of OR were observed at pH 5.0 and 9.0 and the lowest values at pH 3.0, as the pH value increased from 9.0 to 11.0, a significant OR decrease was found.

The behavior of whey proteins differs according to their native (crude) and individual (isolate) environment; Davis and Foegeding (2004) recorded a superior foaming of whey protein isolate (WPI) at pH 4.5, the moderate at pH 7.0 and the lowest at pH 3.0. An improved whey protein isolate (WPI) foaming at pH 5.0 is associated with the α-lactalbumin transformation into an intermediate state at its isoelectric point; the isoelectric point for α-lactalbumin is at pH between 4.1 and 4.8 and for β-lactoglobulin at pH 5.2. Thus, these conditions promote the formation of foams with the maximum overrun (Nastaj and Sołowiej 2020).

Figure 3 shows the microscopic aspect of the best foam prepared from concentrate of crude acid whey (CCAW).

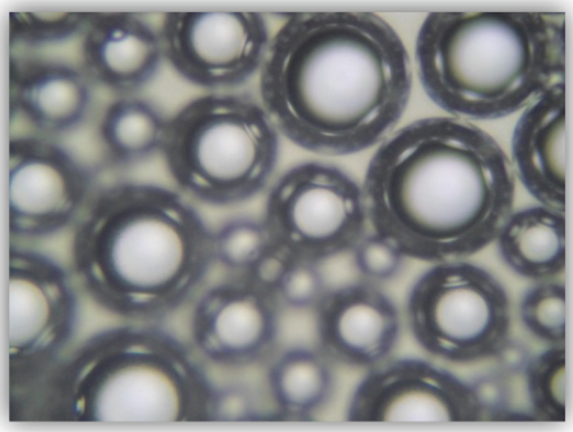

**Fig. 3.** Microscopic aspect (×100) of the foam studied at time 0 min showing the influence of ultrafiltration on the size of air bubbles: case foam of CCAW(average diameter of air bubbles = 1 μm).

## 4 Conclusion

The ultrafiltration application gave satisfactory results on the physicochemical and foaming properties of whey fractions (concentrate and permeate); on the one hand, we noted a remarkable reduction in the chemical oxygen demand (COD) compared to that observed in crude acid whey (45.30% reduction for permeate) or the concentrate was characterized by an increase in COD (117%) due to the variability of the dry matter content in the two compartments (concentrate: 10%, permeate: 5.8%), and on the other hand an improvement in the foaming capacity of the concentrate compared to that recorded in permeate and crude acid whey. In the future, in order to complete our study we will analyze the foaming stability of concentrate crude acid whey over the time.

## List of Abbreviations

| | |
|---|---|
| CAW | Crude acid whey |
| CCAW | Concentrate of crude acid whey |
| PCAW | Permeate of crude acid whey |
| COD | Chemical oxygen demand |
| EC | Electrical conductivity |

## References

Acem, K., Choukri, A., Moulai Mostefa, N., Mettai, K., Kadi, S., Fetouhi, B.: Analyse et valorisation des propriétés émulsifiantes des lactosérums déprotéinés. In: Conférence scientifique internationale sur l'environnement et l'agriculture (CSIEA), Hammamet, Tunisie, 24 au 25 Avril 2017 (2017)

Acem, K., Choukri, A.: Etude du comportement interfacial des lactosérums bruts dans une émulsion alimentaire. Revue d'écologie-environnement. Revue ecologie-environnement. Laboratoire de recherche d'agro-biotechnologie et de nutrition en zones semi-arides et laboratoire de physiologie végétale appliquée aux cultures hors sol, université Ibn Khaldoun, Tiaret, Algerie, no. 13, pp. 17–20 (2017)

Acem, K., Choukri, A.: Study of the effect of power's ultrasound on the protein's emulsifying properties of crudes wheys. Adv. Environ. Biol. **6**(10), 2689–2697 (2012a)

Acem, K., Choukri, A.: Study of the emulsifying properties of whey proteins in crude and modified environments. J. Appl. Sci. Res. **8**(7), 3293–3303 (2012b)

Acem, K., Mettai, K., Kadi, S., Fetouhi, B., Choukri, A., Moulai Mostefa, N.: Caractérisation et valorisation des propriétés polluantes du lactosérum brut. 1er colloque international en toxicologie et santé (ICTH). Faculté des Sciences de la Nature et de la Vie et Sciences de la Terre et l'Univers. Université 8Mai 1945, Guelma, 28–29 November 2016 (2016)

Atra, R., Vatai, G., Bekassy-Molnar, E., Balint, A.: Investigation of ultra-and nanofiltration for utilization of whey protein and lactose. J. Food. Eng. **67**, 325–332 (2005)

Baldasso, C., Barros, T.C., Tessaro, I.C.: Concentration and purification of whey proteins by ultrafiltration. Desalination **278**(1), 381–386 (2011)

Belhamidi, S., Larif, M., Achatei, A., Habziz, S., Zouhri, N., Rafiq, M., Chouni, S., Elhannouni, F., Elmidaoui, A.: Recovery and purification of whey with the concentration, reincorporation and reuse protein and lactose. J. Mater. Environ. Sci. **6**(3), 861–868 (2015)

Borcherding, K., Lorenzen, P.C., Hoffmann, W., Schrader, K.: Effect of foaming temperature and varying time/temperature conditions of pre-heating on the foaming properties of skimmed milk. Int. Dairy J. **18**, 349–358 (2008)

Bottomley, R.C., Evans, M.T.A., Parhiason, C.J.: Whey proteins. In: Harris, P. (ed.) Food Gels. Applied Science, pp. 435–466. Elsevier, London, New York (1990)

Brandelli, A., Daroit, D.J., Corrêa, A.P.F.: Whey as a source of peptides with remarkable biological activities. Food Res. Int. **73**, 149–161 (2015)

Cayot, P., Lorient, D.: Structure-function relationships of whey proteins. In: Dekker, M. (ed.) Food Proteins and their Applications, New York, USA (1997)

Chandrapala, J., Duke, M.C., Gray, S.R., Weeks, M., Palmer, M., Vasiljevic, T.: Nanofiltration and nanodiafiltration of acid whey as a function of pH and temperature. Sep. Purif. Technol. **160**, 18–27 (2016)

Cheftel, J.C., Cuq, J.I., Lorient, D.: Protéines Alimentaires. Tec et Doc, p. 308 (1985)

Clark, D.C., Wilde, P.J., Marion, D.: The protection of beer foam against lipid-induced destabilization. J. Inst. Brew. **100**(1), 23–26 (1994)

Cornec, M., Cho, D., Narsimhan, G.: Adsorption dynamics of α-lactalbumin and β-lactoglobulin at air-water interfaces. J. Colloid Interface Sci. **214**, 129–142 (1999)

Damodaran, S.: Protein stabilization of emulsions and foams. J. Food Sci. **70**, R54–R66 (2005)

Davis, J.P., Foegeding, E.A.: Foaming and interfacial properties of polymerized whey protein isolate. J. Food Sci. **69**, 404–410 (2004)

Dickinson, E.: Structure and composition of adsorbed protein layers and the relationship to emulsion stability. J. Chem. Soc. **88**, 2973–2983 (1992)

Dickinson, E.: Interfacial particles in food emulsions and foams. In: Binks, B.P., Horozov, T.S. (eds.) Collodial Particles at Liquid Interfaces, pp. 298–327. Cambridge University Press, Cambridge (2006).

El-Gazzar, F.E., Marth, E.H.: Ultrafiltration and reverse osmosis in dairy technology: a review. J. Food. Protect. **54**, 801–809 (1991)

Engelhardt, K., Lexis, M., Gochev, G., Konnerth, C., Miller, R., Willenbacher, N., Peukert, W., Braunschweig, B.: pH effects on the molecular structure of beta-lactoglobulin modified air-water interfaces and its impact on foam rheology. Langmuir **29**(37), 11646–11655 (2013)

FAO: Lait et produits laitiers dans la nutrition humaine, p. 262. FAO, Rome (1995)
Firebaugh, J.D., Daubert, C.R.: Emulsifying and foaming properties of a derivatized whey protein ingredient. Int. J. Food Prop. **8**(2), 243–253 (2005)
Gana, S., Touzi, A.: Valorisation du lactosérum par la production de levures lactiques avec les procédés de fermentation discontinue et continue. Rev. Energ. Ren. **1**, 51–58 (2001)
Gaucheron, F., Tanguy, G.: Modifications de la qualité biochimique des laits et des produits laitiers par la technologie. Renc. Rech. Ruminants. **16**, 131–134 (2009)
Iltchenco, S., Preci, D., Bonifacino, C., Fraguas, E.F., Steffens, C., Panizzolo, L.A., Cole, R., Fernandes, I.A., Abirached, C., Valduga, E., Steffens, J.: Whey protein concentration by ultrafiltration and study of functional properties. Ciência Rural. Santa Maria. **48**(5), 1–11 (2018)
Juillerat, M.A., Badoud, R.: Acides aminés et protéines. In: Sciences et technologie des aliments: principes de chimie des constituants et de technologie des procédés. Presses polytechniques et universitaires romandes, CH-1015 Lausanne, pp. 47–104 (2010)
Kehoe, J.J., Foegeding, E.A.: Interaction between beta-casein and whey proteins as a function of pH and salt concentration. J. Agric. Food Chem. **59**(1), 349–355 (2011)
Kinsella, J.E., Whitehead, D.M.: Proteins in whey: chemical, physical, and functional properties. Adv. Food Nutr. Res. **33**, 343–438 (1989)
Krešic, G., Lelas, V., Jambrak, A.R., Herceg, Z., Brncic, S.R.: Influence of novel food processing technologies on the rheological and thermophysical properties of whey proteins. J. Food Eng. **87**, 64–73 (2008)
Krissansen, G.W.: Emerging health properties of whey proteins and their clinical implications. J. Am. Coll. Nutr. **26**, 713–723 (2007)
Lam, R., Nickerson, M.: The effect of pH and temperature pre-treatments on the physicochemical and emulsifying properties of whey protein isolate. LWT-Food Sci. Technol. **6**, 427–434 (2015)
Marinova, K.G., Bashera, E.S., Nenova, B., Temeslska, M., Mirarefi, A.Y., Campbell, B., Ivanov, I.B.: Physicochemical factors controlling the foamability and foam stability of milk proteins: sodium caseinate and whey protein concentrates. Food Hydrocoll. **23**, 1864–1876 (2009)
Martínez, K.D., Ganesan, V., Pilosof, A.M., Harte, F.M.: Effect of dynamic high-pressure treatment on the interfacial and foaming properties of soy protein isolatehydroxypropylmethylcelluloses systems. Food Hydrocoll. **25**(6), 1640–1645 (2011)
Mollea, C., Marmo, L., Bosco, F.: Valorization of cheese whey, a by-product from the dairy industry. In: Agricultural and Biological Sciences: Food Industry, Chap. 24, pp. 549–588 (2013)
Nakai, S., Li-Chane, E.: Recent advances in structure and function of food proteins: QSAR approach. Crit. Rev. Food Sci. **33**, 477–499 (1993)
Nastaj, M., Sołowiej, B.G.: The effect of various pH values on foaming properties of whey protein preparations. Int. J. Dairy Technol. **0**, 1–12 (2020)
Patino, J.M.R., Pilosof, A.M.: Protein-polysaccharide interactions at fluid interfaces. Food Hydrocoll. **25**(8), 1925–1937 (2011)
Peligrine, D., Gasparetto, C.: Whey proteins solubility as function of temperature and pH. Lebensm-Wiss U-Technol. **3**, 77–80 (2005)
Phillips, L., Whitehead, D., Kinsella, J.: Structure-Function Properties of Food Proteins. Academic Press, Inc., London (1994)
Phillips, L., Yang, S., Kinsella, J.: Neutral salt effects on stability of whey protein isolate foams. J. Food Sci. **56**(2), 588–589 (2006)
Phillips, L., Yang, S., Schulman, W., Kinsella, J.: Effects of lysozyme, clupeine, and sucrose on the foaming properties of whey protein isolate and β-lactoglobulin. J. Food Sci. **54**(3), 743–747 (1989)
Phillips, L.G., German, J.B., O'Neil, T.E., Foegeding, E.A., Harwalkar, V.R., Kilara, A., Lewis, B.A., Mangino, M.E., Morr, C.V., Regenstein, J.M., Smith, D.M., Kinsella, J.E.: Standardized procedure for measuring foaming properties of three proteins, a collaborative study. J. Food Sci. **55**(5), 1441–1453 (1990a)

Phillips, L.G., Schulman, W., Kinsella, J.E.: pH and heat treatment effects on foaming of whey protein isolate. J. Food Sci. **5**, 1116–1119 (1990b)

Raikos, V., Campbell, L., Euston, S.: Effects of sucrose and sodium chloride on foaming properties of egg white proteins. Food Res. Int. **40**, 347–354 (2007)

Rehman, S., Farkye, N.Y., Yim, B.: Use of dry milk protein concentrate in pizza cheese manufactured by culture or direct acidification. J. Dairy Sci. **86**, 3841–3848 (2003)

Sawyer, C.N., McCarty, P.L., Parkin, G.F.: Chemistry for Environmental Engineering and Science, 5th edn. McGraw-Hill, New York (2003)

Zayas, J.F.: Foaming properties of proteins. In: Functionality of Proteins in Food. Springer, Heidelberg (1997)

Zhu, H., Damodaran, S.: Effects of calcium and magnesium ions on aggregation of whey protein isolate and its effect on foaming properties. J. Agric. Food Chem. **42**, 856–862 (1994)

# CoSoTIA Project: Decision Support for the Choice of Concentrated Solar Technologies for Electricity Generation

M. Aissani[1(✉)], K. Mohammedi[2], A. Zitouni[1], M. Boukraa[1], T. Chekifi[1], and A. Mehiris[1]

[1] Research Center in Industrial Technologies CRTI, P.O. Box 64, 16014 Cheraga, Algiers, Algeria
m.aissani@crti.dz, aissani_mld@yahoo.fr
[2] URMPE/MESO, M. Bougara University, 35000 Boumerdes, Algeria

**Abstract.** The CoSoTIA (Concentrated Solar Technologies for Industrial Applications) project initiated by the CRTI center in collaboration with the URMPE unit concerns the study and development of CSP solar concentrators for industrial applications. In the present work, we present decision support tools for the choice of a solar concentration technology for sites in Algeria. They will be used for the comparison between different technologies of solar concentration e.g.: cylindro-parabolic, parabolic, solar tower, etc. The models used include project costs and site characteristics; they incorporate also engineering knowledge (economic, social, technical and environmental). The information needed for decision-making produced by these tools is: the total cost of the project, indicators with economic, social, technical and environmental aspects. The case studies presented were conducted under the SAM Advisor environment, which was developed to evaluate the capacities to implement CSP project in order to produce expertise for the different actors through an application on a given site (by the client). Four case sites in Algeria and for two types of solar concentrator plant are studied and presented. A comparative study was conducted and for each site the best CSP was deduced and commented.

**Keywords:** Decision support · Multicriteria analysis · Solar concentration · CSP · SAM advisor

## 1 Introduction

The environmental problems caused by greenhouse gas emissions during the exploitation of fossil fuels and the increasing demand for electricity have spurred the search for alternative energy resources. Concentration solar technologies offer the possibility of satisfying the world's demand for electricity (Goetzberger and Greubel 1977, Seitz et al. 2014, Imenes and Mills 2004) but are still conditioned by the weather conditions of the sites, the high cost of kWh and the need for optimal storage capacity (Sylvain 2007) for continuous operation, etc.


B. Safi et al. (Eds.): ISMSD 2019, *Proceedings of the 4th International Symposium on Materials and Sustainable Development*, pp. 12–22, 2020.
https://doi.org/10.1007/978-3-030-43211-9_2

Making a decision usually requires the simultaneous optimization of several often contradictory objectives. Tools such as multi-criteria analysis are therefore very useful for the decision maker (Mena 2000, Tsoukiàs 2007). The multicriteria approach makes it possible, based on multiple criteria and decision maker preference conditions, to choose the best type of CSP technology taking into account a maximum of criteria. In many new thermal plants installation projects (Stoddard et al. 2006), decision-makers are faced with complex problems of large size and multi-purpose. To achieve these goals, effective decisions must be made to avoid the following problems:

– The incompatibility of installation site with the type of CSP technology.
– Increased installation costs of the project.

The CoSoTIA (Concentrated Solar Technologies for Industrial Applications) project initiated by CRTI center in collaboration with URMPE focuses on the study and development of CSP solar concentrators for industrial applications, assisted with a decision support system.

The decision support tools for the choice of a CSP technology were applied for some sites in Algeria; and they are used in the current study by SAM Advisor for calculations and the comparison. The applied models of SAM integrate several informations: project costs, site characteristics and engineering knowledge.

So, four sites in Algeria and two types of solar concentration plant were chosen and studied.

## 2 Decision Support

### 2.1 Concept and Definition

Decision support is a scientific approach to decision problems in all socio-economic contexts. It is a discipline that targets a broad audience ranging from business executives to the private individual, designers and other decision makers.

Decision support can intervene and provide solutions for decision-makers at each stage of the decision-making process (Amarache 2012). It can be defined as a "model-based" activity, offering some answers to the questions a stakeholder asks in a decision process. It will provide the decision-maker with solutions that can meet the decision-making objectives, in a complete or partial way.

### 2.2 Source of Decision-Making and Decision-Making Modes

- Decision-making is influenced by the individual's personality and its values.
- Can also take its source from the function or status of the individual (for example: we made the decision of an arbitrator).
- Experience, that is, someone who has to make decisions often will be less afraid than the person who never takes them.
- Credible information (Documents/references/testimonials …), all the elements that could enlighten us in our decision-making. Indeed, by the informations gathered we will be able to make the most thoughtful decision.

The main modes of decision-making within a group are cited as: Authoritarian, majority, minority and unanimity. They are summarized by the schema of Fig. 1:

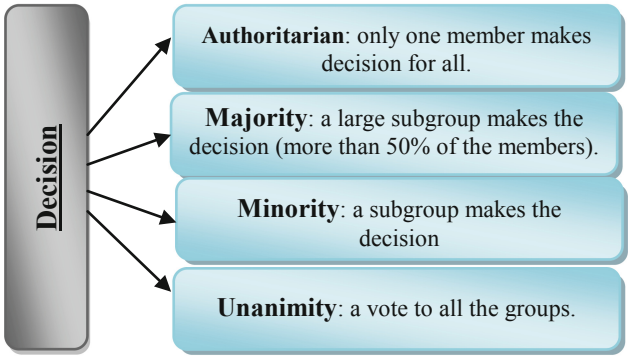


**Fig. 1.** Main decision modes, deduced from Vodoz (2012) and wiki/Prise_de_décision (2019).

### 2.3 Decision Support Process

The concept of decision support is broader than theories of decision-making, the moment that contains both theoretical and practical contributions to the conduction of what we call the "decision support process". This latter is shown schematically by the Fig. 2. Also the evaluation and analysis of past decisions is complementary to decision-making.

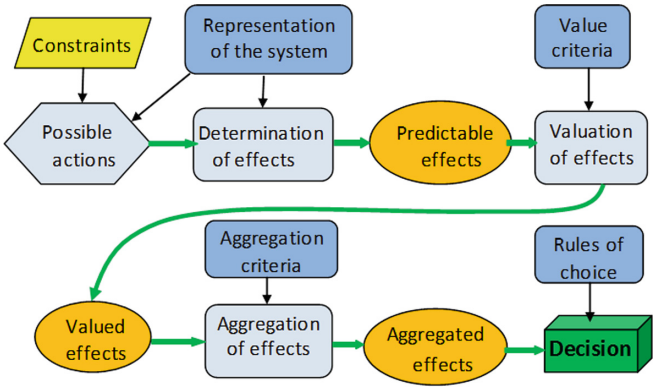


**Fig. 2.** Decision process deduced from the theory of Cyert and March (2017)

## 3 Introducing the SAM Advisor Code Analysis Environment

This software is a multi-model application allowing the analysis of the technical and economic data of a project in the field of renewable energies; it is a decision-making tool

for the choice and the selection among several competing technologies. SAM (System Advisor Model) includes several analysis models such as thermodynamic solar power plants, photovoltaic power plants, wind turbines, geothermal energy as well as solar water heaters. SAM is a technical performance and financial model to facilitate decision-making for those involved in the renewable energy industry, such as:

- Project Managers and Engineers.
- Policy analysts.
- Technology developers.
- Researchers.

SAM makes predictions of performance and cost of energy estimates for projects. These grid connected plant projects are based on the installation and operating costs and system design parameters that you specify as inputs to the model. Projects can be either the customer side of the electricity meter, the purchase and sale of electricity at retail prices, or on the utility side of the device, the sale of electricity to a price negotiated through a power purchase agreement.

For input variables, either use the default value or change its value. Some examples of input variables are:

- Installation costs, including equipment purchases, labor, engineering and other project costs, land costs, operations and maintenance costs.
- The number of modules and inverters, the type of monitoring, the factors of decommissioning of photovoltaic installations for example.
- Collector and receiver type, multiple, storage capacity, solar power block capacity for parabolic trough collector (PTC) sensor systems.
- Analysis period, actual discount rate, inflation rate, tax rates, target internal rate of return, or purchase price for utility financing models.
- Building load and detail of usage time rates for commercial and residential financing models.
- Taxes and cash incentive amounts and rates.

The multicriteria analysis based decision support system methodology follows three main steps:

The first step consists of, after fixing all solar concentrator technologies CSPs (to be studied and subject to choice) and the various sites to explore set by the customer or the state; the most important criteria influencing the choice of decision are investigated and determined.

Then, we determine the main input parameters (technical, socio-economic, …) for the calculation of design and parametric estimation of CSPs according to the region, which to be carried out under the SAM software.

In a second step, we proceed to the various calculations under this software and the mathematical formulas of certain criteria. In the last step, we collect all the results to be analyzed, then will be presented to decision-makers (client, …) with recommendations.

# 4 Case Study in Algeria: Technico-Economic Evaluation of PTC and Central Receiver Types Solar Power Plants

## 4.1 Evaluation of Radiometric Data

Our study is done for the following four sites in Algeria: Algiers, Batna, Bechar and Tamanrasset. The radiometric data are summarised in the Table 1.

**Table 1.** Radiometric data of the studied sites

| DATA | Algiers | Batna | Bechar | Tamanrasset |
|---|---|---|---|---|
| Time zone | GTM+1 | GTM+1 | GTM+1 | GTM+1 |
| Elevation (m) | 25 | 1052 | 772 | 1377 |
| Latitude (°) | 36.72 | 35.55 | 31. 62 | 22.78 |
| Longitude (°) | 3.25 | 6.18 | 2.33 | 5.51 |
| Direct Normal (kWh/m$^2$) | 1446.4 | 1907.3 | 2568.9 | 2759.4 |
| Global Horizontal (kWh/m$^2$) | 1683.0 | 1765.4 | 2114.6 | 2364.4 |
| Dry-bulb T (°) | 17.7 | 14.0 | 21.8 | 22.7 |
| Wind speed (m/s) | 3.0 | 4.5 | 4.4 | 3.6 |

## 4.2 Technical Characteristics of Solar Power Plants

### 4.2.1 The Characteristics of the Parabolic Trough Collector Power Plant

The Parabolic trough collector power plant is a 30 MWe (Megawatts electric) station, with a storage capacity of 6 hours per day (6 h/d) and it uses a heat transfer fluid that has the characteristics indicated by the Table 2. The parameters of the solar field and the heat-carrying fluid in the plant are issued by SAM and shown in Fig. 3, and then the electric power with some data are shown in Fig. 4a and 4b.

**Table 2.** Characteristics of the heat transfer fluid of the Parabolic trough collector power plant.

| Name | Type | Min of the Optimal temperature (°C) | Max of the optimal temperature (°C) | Temperature freezing point (°C) |
|---|---|---|---|---|
| Therminol VP-1 | Mixture of biphenyl - diphenyl oxide | 12 | 400 | 12 |

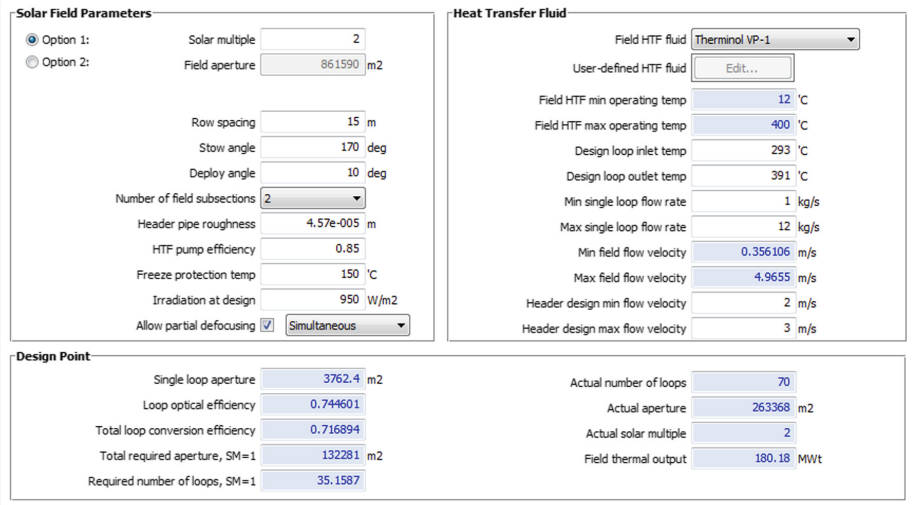


**Fig. 3.** The parameters of the solar field and heat transfer fluid in the Parabolic trough collector power plant.

### 4.2.2 The Characteristics of the Solar Tower

The 30 MWe solar tower power plant is design with 6 hours per day storage system. The melting salt heat transfer fluid (HTF) characteristics are given in Table 3:

With all the data needed to size the tower, according to the software SAM Advisor, the length of the tower must be **163.5** m, and about the powers of the tower see Fig. 5.

## 5 Results and Interpretation

### 5.1 LCOE (Levelized Cost of Energy)

LCOE is the total cost of installing and operating a project expressed in dollars per kiloWatt-hour of electricity produced by the system over its lifetime.

By definition, the equivalent annual cost $C_n$ of a project is the product of LCOE by the amount of electricity $Q_n$ generated by the system this year (see Eq. 1):

$$C_n = Q_n \times LCOE \tag{1}$$

The costs of the project $C_n$ include installation, operation and maintenance, financial charges and taxes, and also account for incentives and salvage value.

The SAM performance model calculates the annual energy $Q_n$ for $n = 1$. For $n > 1$, $Q_n$ decreases year by year, so year-to-year decrease in the value of production on the *setting page performance* is greater than zero.

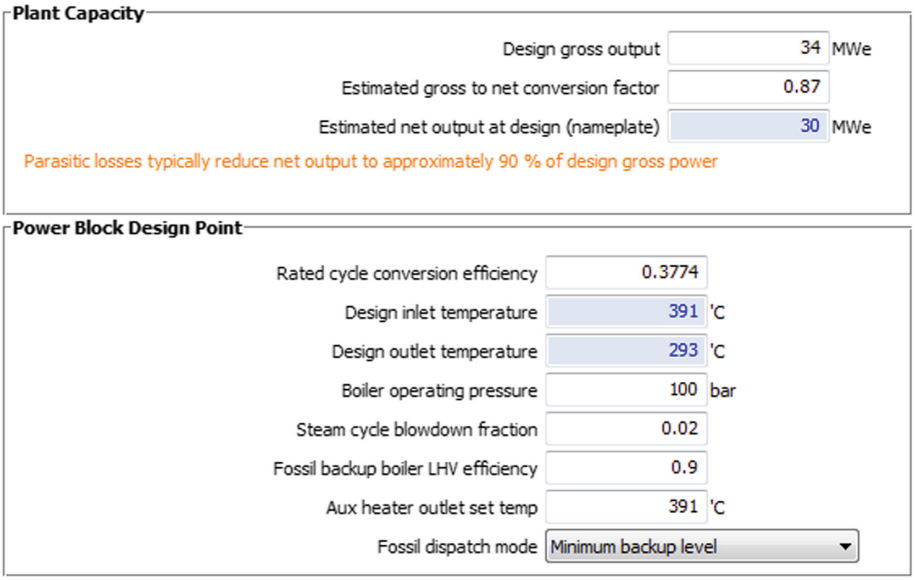


(a)

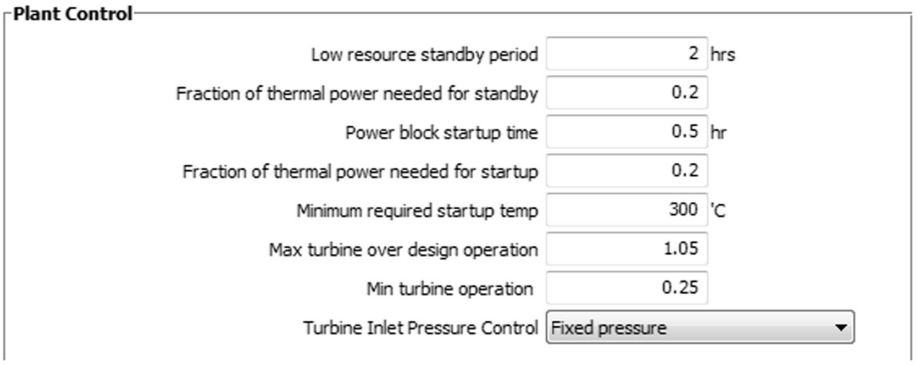


(b)

**Fig. 4.** (a) The electric Power and some data of the Parabolic trough collector power plant. (b) Some control data of the Parabolic trough collector power plant.

**Table 3.** Heat transfer fluid characteristics

| Name | Type | Min of optimal temperature (°C) | Max of optimal temperature (°C) | Temperature freezing point (°C) |
|---|---|---|---|---|
| Hitec solar salt | Nitrate salt | 238 | 593 | 238 |

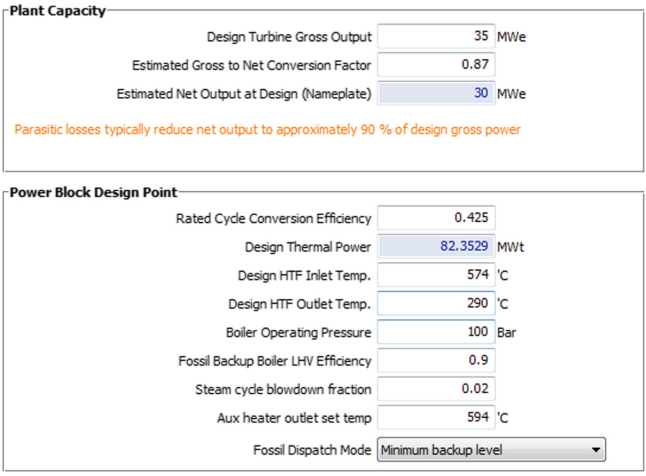


**Fig. 5.** The power of the solar tower plant

This Eq. (1) must be valid for all N years of the project life, and the total LCOE cost is obtained as follow (2):

$$LCOE = \frac{\sum_{n=0}^{N} \frac{C_n}{(1+d)^n}}{\sum_{n=0}^{N} \frac{Q_n}{(1+d)^n}} \tag{2}$$

The results shown by Fig. 6 depict that the calculated LCOE for Algiers site is the highest compared to the other sites. However, the value of this LCOE is doubled compared to those of the southern regions (as Bechar and Tamanresset), this regardless of the type of power plant. While, according to the type of CSP: with the tower plant the cost LCOE is the most expensive than the Parabolic trough collector power plant, regardless of the site.

For a better illustration of these comparative analysis results, the graphical representation of both plants through sites is (shown in Fig. 6).

### 5.2 Total Land Area

The total land area which is necessary for the power plants project with solar tower trough collectors are estimated by SAM Advisor. According to the results obtained by the calculation, we found that the surface of the tower plant is more than three times higher than that of the parabolic trough collector power plant (Table 4 and 5), while the total cost of the installation and the operation LCOE is close between these both projects for the same site or region.

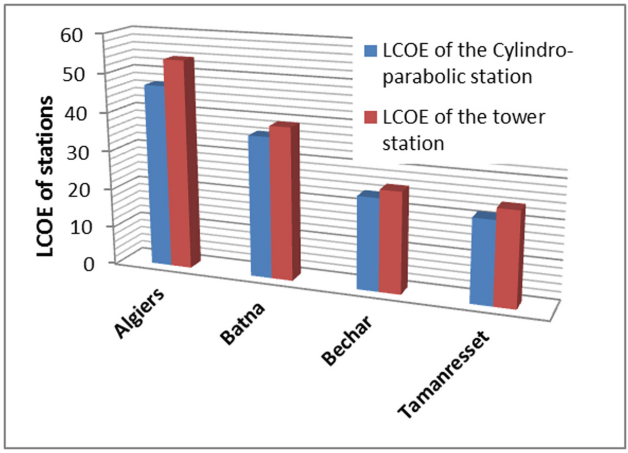


**Fig. 6.** The total cost LCOE results through the sites and the types of plant

**Table 4.** The total project area of the parabolic trough collector plant.

| Total land area *Algiers.epw* | Total land area *Batna.epw* | Total land area *Bechar.epw* | Total land area *Tamanresset.epw* |
|---|---|---|---|
| 273.329 | 273.329 | 273.329 | 273.329 |

**Table 5.** The total project area of the tower plant

| Total land area *Algiers.epw* | Total land area *Batna.epw* | Total land area *Bechar.epw* | Total land area *Tamanresset.epw* |
|---|---|---|---|
| 1029.56 | 1029.56 | 1029.56 | 1029.56 |

### 5.3 Annual Water Consumption

The annual water consumption is calculated by the following Eq. (3), the results with the four case studies are presented in Tables 6 and 7 for the parabolic trough collector and central receiver technologies respectively.

$$\textit{Annual water consumption}\ (m^3) = \textit{Cooling water}\ (m^3) + \textit{Water used for washing mirrors}\ (m^3) \quad (3)$$

According to the results obtained under SAM Advisor simulation environment, the annual consumption of water of the parabolic trough collector power plant project is slightly superior to that of the central tower of about 20 to 18% according to the north or south zones. It is confirmed also by these calculations that for the same plant at the

**Table 6.** The annual water consumption of the parabolic trough collector plant project ($m^3$/year)

| Annual water usage\|Algiers | Annual water usage\|Batna | Annual water usage\|Bechar | Annual water usage\|Tamanrasset |
|---|---|---|---|
| 240463 | 290529 | 413512 | 457929 |

**Table 7.** The annual water consumption of the tower power plant project ($m^3$/year)

| Annual water usage\|Algiers | Annual water usage\|Batna | Annual water usage\|Bechar | Annual water usage\|Tamanresset |
|---|---|---|---|
| 203526 | 254907 | 363680 | 381776 |

southern sites consume more water than those in the north; it is about less than double. Of course, we should be aware of the scarcity and costs of water in the southern areas.

### 5.4 Annual Energy Production (AEP)

The Annual Energy Production AEP in kWh/year is calculated by the following Eq. (4), the results according to the different sites studied are presented in Fig. 7, for the parabolic trough collector (PTC) and solar tower power plants respectively.

$$\begin{aligned} \textit{Annual Energy}\ (kWh/year) = \textit{Sum of hourly energy delivered} \\ \times\ \textit{Percentage of annual production} \end{aligned} \tag{4}$$

The annual production of energy by the cylindro-parabolic power plant project is slightly higher than the production of the tower power plant. The max values are about **7.4%** and **6%,** according in northern and southern region respectively, as seen in Fig. 7.

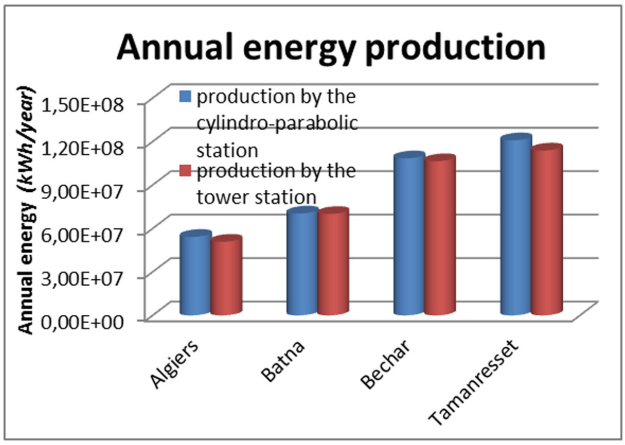


**Fig. 7.** The Annual energy production through the sites and the type of plant

## 6 Conclusions

The multicriteria analysis allows us to shift from a subjective decision to an objective decision making based on several criteria.

According to the results obtained by calculations using the SAM Advisor software and the evaluation of some main criteria, the parabolic trough collector (PTC) power plant project performances are significantly better compared to the tower plant project, regardless of the sites. Therefore it is highly recommended to decide to choose it.

But, when it comes to implement a CSP power plant in north Africa, soiling effects are important, one has to keep in mind water availability in the north, and water scarcity in the southern part even if the solar irradiation potential is important.

## References

Goetzberger, A., Greubel, W.: Solar energy conversion with fluorescent collectors. Appl. Phys. **14**, 123–139 (1977). https://doi.org/10.1007/BF00883080

Imenes, A.G., Mills, D.R.: Spectral beam splitting technology for increased conversion efficiency in solar concentrating systems. Sol. Energy Mater. Sol. Cells **84**(1–4), 19–69 (2004)

Mena, S.B.: Introduction to multi-criteria decision support methods (Introduction aux méthodes multicritères d'aide à la décision). Biotechnol. Agron. Soc. Environ. **4**(2), 83–93 (2000)

Tsoukiàs, A.: On the concept of decision aiding process: an operational perspective. Ann. Oper. Res. **154**(1), 3–27 (2007)

Vodoz, L.: Decision-making by consensus (La prise de décision par consensus). Environnement et Société, pp. 57–66. Lausanne – EPFL (2012)

Stoddard, L., Abiecunas, J., O'Connell, R.: Economic, Energy, and Environmental Benefits of Concentrating Solar Power in California. United States, Technical Report: N, pp. 1–69 (2006).https://doi.org/10.2172/881924

Seitz, M., Cetin, P., Eck, M.: Thermal storage concept for solar thermal power plants with direct steam generation. Energy Procedia **49**, 993–1002 (2014)

Sylvain, Q.: Concentrating solar power plants (Les Centrales Solaires à Concentration). Report, University of Liège, Faculté des sciences appliquées, pp. 1–34 (2007)

Amarache, S.: Decision support system for the supply of a multi-source system integrating renewable energies (Système d'aide a la prise de décision pour l'approvisionnement d'un système multi sources intégrant des énergies renouvelables). Report (2012)

Cyert, R., March, J.G.: Behaviorist theory of the firm (Théorie behavioriste de la firme) (2017). wikiberal.org. https://www.wikiberal.org/wiki/Th%C3%A9orie_behavioriste_de_la_firme

Wikipedia. Decision making (Prise de décision) (2019). https://fr.wikipedia.org/wiki/Prise_de_d%C3%A9cision

# Mechanical Strength Analysis and Damage Appraisal in Carbon/Perlon/Epoxy Composite for Orthopedic Prostheses

L. Alimi[1,2(✉)], Y. Menail[2], K. Chaoui[2], K. Kechout[2], S. Mabrouk[2], N. Zeghib[2], A. Belhamzaoui[2], N. Metrane[1], and K. Bedoud[1]

[1] Research Center in Industrial Technologies (CRTI), P.O. Box 64, 16014 Cheraga, Algeria
latifaalimi@yahoo.fr

[2] LR3MI, Mechanical Engineering Department, Badji Mokhtar University, P.O. Box 12, 23052 Annaba, Algeria

**Abstract.** Nowadays, the choice of composite materials to manufacture medical orthopedic prostheses is largely accepted for its intrinsic resistance, ease of molding and machining, compatibility with human skin and also for economic aspects. Because of population aging and the need to repair broken or damaged human members, composite materials offer a very large variety of solutions to strongly satisfy such demands in the form of prostheses. These materials consist mainly of a consolidated resin reinforced with glass, carbon or natural fibers. Advantageous properties made them the most requested materials in the manufacturing of prosthetic devices for orthopedic use by people with movement disabilities. The present work considers a composite material made with carbon fibers, perlon (insulating layer) and an epoxy-based orthocyclic laminating resin. Both mechanical and morphological properties are analyzed. It is found that the composite made of carbon fibers/perlon/epoxy resin lower has lower mechanical resistance compared to carbon fiber/epoxy resin composite, but its adherence and its contact with human skin are ameliorated. For the fibrous reinforcements, carbon, glass or perlon, the mechanical properties on the proposed composite material (PVA- (C-4P-C) -PVA) are comparable to literature values. Based on uniaxial tensile tests, the elastic modulus is 626 MPa and the yield stress which is 57 MPa. Finally, SEM observations revealed that both composites exhibit similar damage mechanisms with higher intensity when perlon is present. This is due to the nature of the perlon in the composite material which exhibits more anisotropy. The main encountered damage mechanism is laminate decohesion which takes places between carbon plies and perlon. Such condition contributes to more interlaminar delamination and more brittleness of the material when subjected to high loads.

**Keywords:** Composites · Carbon fiber · Perlon · Prosthesis · Mechanical properties · Delamination · Anisotropy


B. Safi et al. (Eds.): ISMSD 2019, *Proceedings of the 4th International Symposium on Materials and Sustainable Development*, pp. 23–33, 2020.
https://doi.org/10.1007/978-3-030-43211-9_3

## 1 Introduction

Generally composites materials consist of proportionate mixtures of fibers and polymeric resins and can be ideal solutions to a variety of problems expressed by orthopedic surgeons and physicians (Ambrosio 2017). In recent decades, rapid developments of biomaterials have greatly improved both integrity and comfort of life of people suffering from mechanical functional problems. Biomaterials are non-living materials used in medical devices which are intended to interact with any biological system. They can be metallic, ceramic, polymeric, natural or composite (Berthelot (2012); Rajak et al. (2019); Plummer et al. (2001)). As in many technological applications, composites have found a wide basis for human health maintenance principally because of 3 advantages when compared to metals: *(i)* lighter weight, *(ii)* higher strength and *(iii)* lesser chemical reactivity with human body (Iftekhar 2004). The interest shown in composites in this field lies in the desire to reduce the weight of the structure and to ensure good mechanical strength while facing simple and inexpensive formability. Bone implants prostheses of all kinds, screws and stems to repair a fractured bone and also to use in instruments. Composites, which are often blends of fibers and polymer resins, offer even more solutions to surgeons and medical doctors. They can replace metals and plastics, or even offer new properties; however, these advances remain discreet as composite quantities used in for medical and health applications remain smaller compared to those consumed by aeronautic and automobile industries. Composites in health care sector represent a minute percentage of the global composites market which averages 90 $10^9$ US$ (Composites Market, Global Forecast to 2020–2024).

Unfortunately, there is no single definition of a composite material. Alternatively, two criteria are emphasized: *(i)* a composite is a heterogeneous material, formed of at least two constituents with different phases or; *(ii)* these constituents are arranged according to a geometric organization, which gives the composite properties that are superior to those of the constituents taken separately (hybrid materials). The term "superior properties" encompasses two distinct concepts. In the first case, the composites are generally designed so as to judiciously combine the best properties of their constituents; in the second one, the geometric organization of composites (or the structure) can sometimes bring out, at the global level, properties that their constituents do not have. This is the case of some ductile ceramic-based composites, whereas the ceramics themselves are brittle. This is due to the resulting spatial structure, which hinders the propagation of cracks (Lionel Gendre 2019). Composite material consist mainly of *(i)* a matrix, thermoplastic resin (TP) or thermosetting resin (TD); and *(ii)* a reinforcing structure consisting of fibers, usually glass, carbon, aramid or natural fibers (flax, hemp, sisal) (Berthelot (2012); Rajak et al. (2019))

In the orthopedic prosthetic device manufacturing industry for people with disabilities, fiberglass-reinforced acrylic resin composite materials remain the materials of choice (Ambrosio 2017). They allow meeting all the requirements of shape and cadence by successive layers to have laminates that must not have any defect, or undergo treatment likely to hide the defects. Carbon fiber (CF) offers many unique physical, chemical and biological characteristics that can be exploited for many diverse applications. CF possesses high heat tolerance, high strength-to-weight ratio, resistance to corrosion and to adequate conductivity. As in other industrial sectors, CF physical properties have led

to many advances in medical implants, health devices and/or instruments. CF medical solicitations range from dental orthodontics to medical limb prosthetic fabrication; literally from head to toe illustrative applications are found on the market (Ambrosio 2017; Iftekhar 2004; Hillock and Howard 2014; Research carbon fiber 2013). Despite this increased use of composite materials, adopted as technological solutions in various fields, it appears that problems related to manufacturing are rather the cause of a large number of parts failures and structures based on reinforced polymers. Premature failures may be due to certain defects introduced at the time of processing, factors not correctly considered in the design or the misuse of manufactured parts Rajak et al. (2019).

The objective of this work is to establish a mechanical characterization of a laminated composite material for orthopedic use made of an epoxy matrix reinforced with layers of perlon fabrics and carbon fibers.

## 2 Experimental Methods

### 2.1 Raw Materials

The raw materials of the composite used in this study are provided by the ONAAPH (Algerian National Office of Accessories and Apparatuses for Disabled Persons), located in Annaba, Algeria. The manufacturing of orthopedic prostheses is based on the combination of a generic resin, carbon fiber reinforcement and perlon which is an absorbent material. An epoxy-based clear and orthocyclic laminating resin is used to obtain thin-walled stable laminates. Such resin is characterized by satisfactory impregnation and perfect binding to reinforcing fibers which allows manufacturing components with an optimal quality and a higher structural rigidity.

The reinforcement is represented by the extremely fine carbon fiber diameter of the order of 5 to 15 μm mainly derived from carbon atoms. Several carbon fibers wrap together to form a wire of 80 to 100 carbon fibers layers. This is a form of graphite in which the sheets, formed by carbon atoms bonded into hexagonal ring, are long and thin.

Perlon is a variety of synthetic polyamide fiber which is largely used in the textile industry under trade names of Nylon or Rilsan. Such fibers have a limited usage in composite materials because of high sensitivity to humidity which may reduces its mechanical resistance by ~20% as water absorption can reach 4 to 5% by weight in normal conditions. The elongation at break is very significant as it could vary from 15 to 30%.

The association of perlon fibers (PF) with glass fibers is mainly due to *(i)* economic reasons as it increases the reinforcement rate at a minimal cost and *(ii)* combination of both perlon and glass fibers improves the composite strength and the adherence to organic resins. This condition gives better resistance to delamination, reduces the weight and protects the glass fabric. It is important to note the under traction mode perlon tissues are capable of showing a significant elongation before break. In orthopedic applications, it is a good choice because of its softness and zero allergies for humans.

### 2.2 Elaboration of Composite Material

The production method adopted in this study is the same as that used by the ONAAPH to manufacturing prostheses in the shop. The wooden male part of the mold is fixed on a vise

and then is covered by an insulating PVA film in order to prevent the viscous resin from sticking to the wood. The reinforcements are then stacked in a given order for a selected time portion. The chosen stack configurations of this study are symmetrical: *(i)* (PVA-(C-C-C)-PVA) and *(ii)* (PVA-(C-4P-C)-PVA). The products are test specimens made of CF reinforced laminates, a perlon layer and an epoxy resin. Intentionally, perlon is stacked on the surface for both aesthetic reasons and resistance to atmospheric moisture. Reinforcements must be pulled and tightened in the direction of stacking. The set is then covered by a plastic bag (ONAAPH 2018).

### 2.3 Preparation of Testing Specimens

The specimens are cut from molded plates using a hardened steel disc saw. On purpose, a hole is drilled on the fat face of the specimen in order to evaluate the created damage around such heterogeneity. With and without drilled holes, the specimens are prismatic in shape, 225 mm long, 30 mm wide and 3 mm thick as shown in Fig. 1. The preparation is in accordance with both ISO 527 parts 4 and 5 and ASTM D 5083 relative to tensile tests specific to composite materials with fibrous reinforcements (ISO 527–4 (1997); ASTM D5083 (2017)). The surface sides have been milled and then polished using a special grinding machine to eliminate any cracking defects from causing detrimental delamination between layers.


**Fig. 1.** Specimen preparation (a) wooden mold, (b) final composite product, (c) specimen without hole, (d) specimen with hole

### 2.4 Test Devices

#### 2.4.1 Uniaxial Traction

The tests are carried out under monotonic traction mode using a Zwick/Roell/Z050 traction machine. Its maximum capacity is 50 kN and it is equipped with an automatic

load–displacement data acquisition system managed by the TestXpert software. The moving crosshead speed is set at 1 mm/min. All tests are conducted to complete break at laboratory temperature.

### 2.4.2 SEM Observations

SEM is used to analyze surface quality and to observe the events that occurred during loading and final specimen failure. The aim is to understand the underlying failure mechanisms that governed the ruin process the composite. A possible correlation with measured mechanical properties is highly sought.

## 3 Results and Discussion

### 3.1 Stress–strain Curves

The stress–strain (σ-ε) behaviors of the 3 cases studied here are presented in Figs. 2, 3 and 4. Reproducibility is acceptable although the materials are heterogeneous because of the nature and the manufacturing process. However, the overall trend in all cases is quite similar. Figure 2 illustrates the case of composite reinforced with CF. Figures 3 (a) and (b) show the evolution of stress–strain curves for the CF/perlon/epoxy resin composite. The architecture (PVA-(C-4P-C)-PVA) is the configuration chosen for this study. From tensile tests, it is seen that stress–strain curves show a typical behavior. Mainly, an initial linear elastic zone is followed by a nonlinear portion representing a zone enduring plastic deformation and subsequently final abrupt failure. The inclination of the slopes of the linear part of these curves denotes a slight variation of tensile modules; this could be caused by geometrical and dimensional variations encountered during manufacturing and cutting processes.

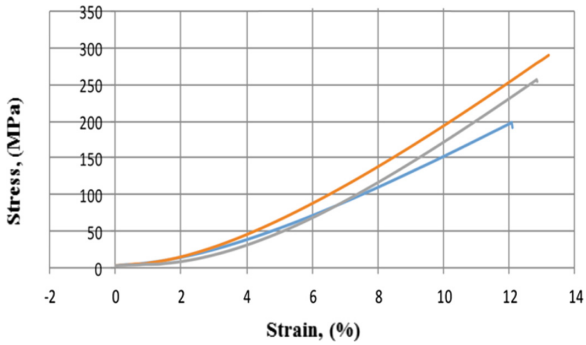


**Fig. 2.** Stress–strain curves for carbon/epoxy specimens

In addition, the occurrence of matrix cracks well before the final rupture is at the origin of the fluctuations which appear on the σ-ε curves. The diffuse and progressive damage that takes place within the structure before total failure is mainly caused by a multi-cracking of the matrix, a mechanism of loosening and detachment of the fibers,

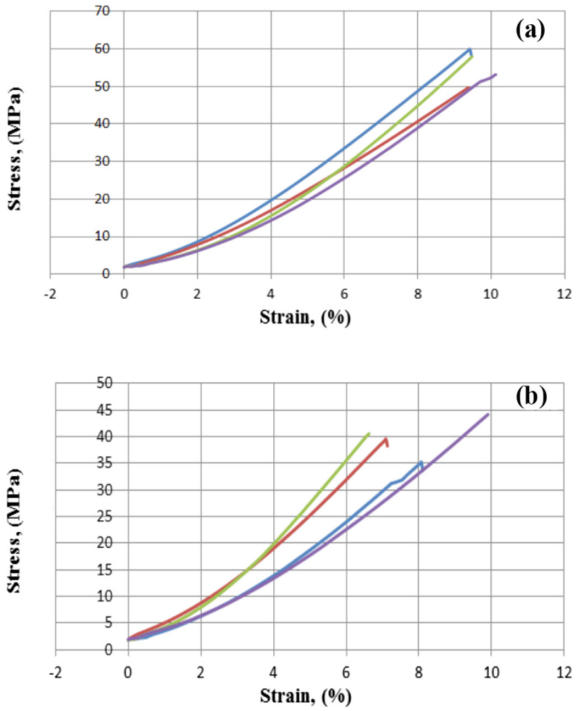


**Fig. 3.** Stress–strain curves for carbon/perlon/epoxy specimens: (a) Plain (no hole), (b) With central hole.

fiber-matrix decohesions (fiber pull out) which limit or prevent the stress continuity between the broken fibers and the unbroken fibers as well as individual breaks in the fibers that are estimated as minor in this case. The breakage is reached at the maximum value of the load. Just after and quite abruptly the load drops indicating the saturation of the phenomenon of multi-cracking and the rupture of the specimen (Berthelot and Lecorre 2001; Fantozzi 1990).

The damaged part is relative to the rupture of both the matrix and the reinforcements. Crack propagation is in the form of a composite tearing. Substantially, during the test, the mechanism operates with frequent change in the direction of the tear. The orientation of this tear probably follows the path of the fabric nodes as well as the matrix fiber interface. The dominant mechanism of damage remains transverse cracking (Berthelot 2012; Rajak et al. 2019; Berthelot and Lecorre 2001; Fantozzi 1990).

Table 1 recapitulates several mechanical properties deduced from Figs. 2, 3 and 4. Four important mechanical parameters are presented, namely, the elastic modulus, the stress at flow, the stress at break and finally the strain at break on test pieces of different sections. It is observed that the material composed solely of carbon reinforcement has clearly superior mechanical properties. For instance, the elastic modulus is of the order of 1365 MPa and the flow stress is around 248 MPa in the composite consisting solely of carbon, while these two properties have decreased to 626 MPa and 57 MPa in the composite made of a mixture of carbon and perlon respectively. These properties show

that the carbon-reinforced composites are more resistant. It is seen that the introduction of perlon lowered the mechanical properties. The mechanical properties of test specimens without holes are significantly better than those with a hole (1). We found an elastic modulus $E$ close to 680 MPa, the stress at the plastic flow threshold $\sigma_y$ close to 55 MPa, the tensile stress $\sigma_f$ is close to 50 MPa and finally the deformation at break $\varepsilon_f$ is 8%. The introduction of the hole is supposed to simulate the case of setting screw to assemble different pieces or give an idea about damage growth close or around such discontinuity.

**Table 1.** Mechanical properties of Carbon/Perlon/Epoxy composite.

| Cases | Test Nb | $E$ (MPa) | $\sigma_y$ (MPa) | $\varepsilon_f$ (%) | $\sigma_f$ (MPa) |
|---|---|---|---|---|---|
| 1: CF | 1 | 1233.32 | 198 | 11.1 | 198 |
| | 2 | 1464.15 | 291 | 12.1 | 291 |
| | 3 | 1397.68 | 257 | 11.0 | 257 |
| Average | | **1365.05** | **248.67** | **11.4** | **248.67** |
| Std. Dev | | **97.02** | **38.42** | **0.50** | **38.42** |
| 2: CF/PF | 1 | 680 | 59.91 | 8.31 | 59.81 |
| | 2 | 570 | - | 8.26 | 49.74 |
| | 3 | 700 | 57.95 | 7.57 | 57.95 |
| | 4 | 610 | 53.17 | 8.28 | 53.17 |
| Average | | **626.67** | **57.01** | **8.11** | **55.17** |
| Std. Dev | | **52.44** | **2.83** | **0.31** | **3.96** |
| 3: CF/PF (Central hole) | 1 | 561 | 35.22 | 6.39 | 35.22 |
| | 2 | 640 | 39.52 | 6.06 | 39.52 |
| | 3 | 770 | – | 5.17 | 40.56 |
| | 4 | 510 | – | 8.38 | 44.16 |
| Average | | **620.25** | **39.52** | **6.50** | **39.87** |
| Std. Dev | | **98.08** | **2.15** | **1.05** | **2.85** |

The obtained results are compared with literature experimental data from literature with different matrix reinforcements intended for prosthetic sockets (Table 2), (Kahtan et al. 2014; Walke and Pandure 2017; Abbas 2018; Achouri and Redjel 2014).

In Prosthetic Socket (basis: PMMA matrix/reinforcement).

**Table 2.** Properties comparison of some composite material used in prosthetic socket (basis: PMMA matrix/reinforcement).

| Reinforcement | *E* (GPa) | $\varepsilon_f$ (%) | $\sigma_y$ (MPa) | Ref |
|---|---|---|---|---|
| 8 PF | 1.5 | 1.833 | 12.39 | Kahtan et al. (2014) |
| (3 PF + 2 CF + 3PF) | 2.586 | 2.1 | 38.8 | |
| (3 PF + 2GF + 3PF) | 2.5 | 2.375 | 20.82 | |
| (3 PF + 2 (CF + GF) + 3PF) | 2.8125 | 2.763 | 62.7 | |
| (3PF + 2(CF + GF) + 3PF) + 3%(nano + micro) $SiO_2$ powder | 1.6 | 5.04 | 42.94 | |
| CF | – | – | 13.2 | Walke and Pandure (2017) |
| Kevlar | – | – | 15.00 | |
| GF | – | – | 10.00 | |
| (3 PF + 1CF + 3PF) | 2.5 | – | 89.1 | Abbas (2018) |
| (3 PF + 1GF + 3PF) | 2 | – | 42.5 | |
| (3PF + 1 n-GF + 3PF) | 11.4 | – | 1.25 | |
| (3 PF + 2CF + 3PF) | 117 | – | 1.9 | |
| (3 PF + 1GF + 3PF) | 42 | – | 1.32 | |
| (3PF + 2 n-GF + 3PF) | 43 | – | 1.13 | |
| 4 PF | 10.12 | – | 1.16 | |
| 6 PF | 33.6 | – | 0.8 | |
| 8 PF | 34.45 | – | 1.01 | |
| (2 PF + 2 GF + 2PF) | 1.274 ± 16% | – | 25.5 ± 12% | Achouri and Redjel (2014) |
| (1GF + 4PF + 1GF) | 1.009 ± 10.5% | – | 22.5 ± 10.5% | |
| (1PF + 1GF + 2PF + 1GF + 1PF) | 1.307 ± 6.5% | – | 25.5 ± 8.5% | |

### 3.1.1 Fracture Surface Analysis

Electron microscopy allowed visualizing closely the various damage phenomena after final specimen failure. Figures 4a, 4b, 4c, and 4d highlight the effects of traction on the carbon/perlon/epoxy composite material. These events are manifested by documented damage mechanisms, namely: *(i)* matrix cracking, *(ii)* interlaminar delamination, *(iii)* decohesion and finally *(iv)* fiber breakage.

For matrix cracking, damage takes place first and propagates until the end of matrix extension giving localized cracks, which over time form a front in a preferred direction and the contribute to interlaminar delamination (Fig. 4a). On the other hand, interlaminar

delamination consists of material cracking at interfaces (Fig. 4b). It usually contributes to the degradation of the composite by creating voids (pockets) between the different strata capable of storing moisture that can leach the resin reducing the life of the material.

Also, during molding, the resin usually binds to the fibers more or less depending on the nature of the sizing resin used on the fibers in manufacturing process. In tension, the resin and the fibers do not stretch in the same way, which creates internal stresses between the resin and the fibers. Such stresses contribute to the decohesion mechanism, which weakens both the resin and the fibers and ultimately hands up by fiber failure (Fig. 4c). Even though they are strong, fibers undergo breakage for high loads. This is the critical part of damage as it appears just before composite material degradation (Fig. 4d). Weakened by the cracking of the matrix, delamination and decohesion, the fibers undergo the direct effects of traction and start to break in collapse, presaging the end of the material's life.

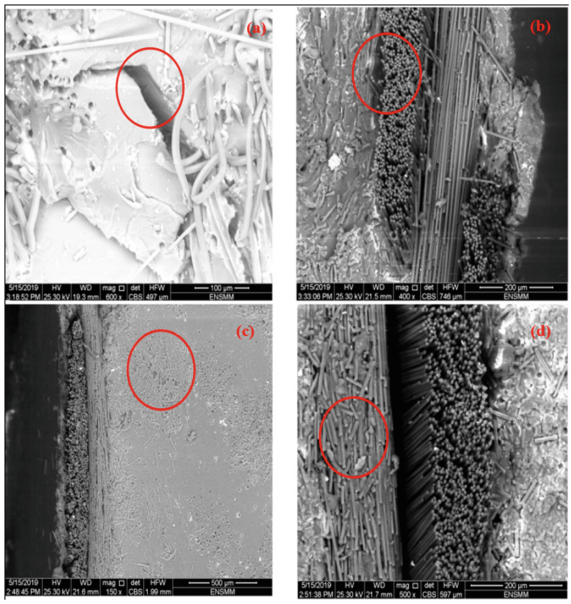


**Fig. 4.** SEM observations of the carbon/perlon/epoxy composite: (a) matrix failure (b) delamination (c) decohesion (d) fiber failure

## 4 Conclusion

This experimental work on tensile fracture of carbon/perlon/epoxy reinforced orthopedic laminates allowed to measure some important mechanical properties and to identify accompanying damage mechanisms at ultimate failure. As predicted, the fracture phenomenon is influenced by the heterogeneous nature of the composite structure which induces random damage phenomena and some dispersion of the mechanical properties. Some specific conclusions can be drawn:

1. The measured mechanical characteristics are characterized by some dispersion. This is mostly true for stress components (E, $\sigma_y$ and $\varepsilon_f$). This is mainly due to the heterogeneity of the material as well as the presence of defects within the volume of the specimen because of manufacturing processes (production and cutting).
2. The addition of perlon layer lowered the mechanical properties; for instance, E is decreased by 54%. The properties remain largely acceptable for an orthopedic prosthesis.
3. The introduction of a physical discontinuity (i.e. a circular hole) within the composite led to a slightly lower rigidity but the decreases in other properties is much important. It indicates that the designer ought to define the less critical location for any assembling perforation or creating a discontinuity in the whole prosthesis structure to reduce stress concentration points and induced damage zones.
4. Electron microscopy allowed indentifying the various damage mechanisms which may be encountered in such material. Indeed, at least 4 mechanisms have been observed to occur during the loading until failure of a carbon/perlon/epoxy composite material (matrix cracking, interlaminar delamination, decohesion and fiber breakage).

**Acknowledgements.** The authors wish to express their gratitude towards the ONAAPH technicians of Annaba (Algeria) for raw material supply, facility operations, and fruitful discussions. Parts of this work are conducted within 2 PRFU projects authorized by the DGRSDT of the Algerian Ministry of Higher Education and Scientific Research. https://www.univ-annaba.dz

Project code: A11N01UN230120190010, "Contribution à l'étude du comportement d'un matériau composite à base de fibres de carbone pour la réalisation de prothèses orthopédiques".

Project code: A11N01UN230120190008 "Etude du comportement mécanique et de la durée de vie restante des tubes en PE soumis aux conditions de l'exploitation et de l'environnement".

## Nomenclature

| | |
|---|---|
| CF: | *Carbon fiber* |
| GF: | *Glass fiber* |
| PF: | *Perlon fiber* |
| TP: | *Themoplastic resin* |
| TS: | *Thermosetting resin* |
| ONAAPH: | *National Office of Accessories and Apparatuses for Disabled Persons* |
| PVA: | *polyvinyl alcohol (film)* |
| E: | *Elastic modulus (MPa)* |
| $\sigma_y$: | *Yield stress (MPa)* |
| $\sigma_f$: | *Failure stress (MPa)* |
| $\varepsilon_f$: | *Failure strain (%)* |

## References

Ambrosio, L.: Biomedical Composites, 2nd edn., p. 616. Elsevier Woodhead Publishing, Cambridge (2017)

Berthelot, J.M.: Matériaux Composites: Comportement Mécanique et Analyse des structures, 5ème Lavoisier, Paris (2012)

Rajak, D.K., Pagar, D.D., Menezes, P.L., Linul, E.: Fiber-reinforced polymer composites: manufacturing, properties, and applications. Polymers **11**(10), 1667 (2019). https://doi.org/10.3390/polym11101667

Plummer, C.J.G., Bourban, P.-E., Månson, J.-A.E.: Polymer matrix composites: matrices and processing. In: Encyclopedia of Materials: Science and Technology, pp. 7388–7396 (2001). https://doi.org/10.1016/B978-0-12-803581-8.02386-9

Iftekhar, A.: Biomedical composites. In: Standard Handbook of Biomedical Engineering and design, Downloaded from Digital Engineering Library. McGraw-Hill (2004). www.digitalengineeringlibrary.com

Composites Market by Fiber Type (Glass Fiber Composites, Carbon Fiber Composites, Natural Fiber Composites), Resin Type (Thermoset Composites, Thermoplastic Composites), Manufacturing Process, End-use Industry and Region, Global Forecast to 2020–2024. https://www.marketsandmarkets.com/Market-Reports/composite-market-200051282.html

Lionel Gendre, L.: Matériaux composites et structures composites. https://eduscol.education.fr/sti/si-ens-cachan/. Reviewed October 2019

Hillock, R., Howard, S.: Utility of carbon fiber implants in orthopedic surgery: literature review, JISRF Reconstructive Rev. **4**(1), 23–32

https://www.utsi.edu/research/carbonfiber/CF.htm. Reviewed 12 Aug 2013

ONAAPH Manufacturing protocol. Reviewed 2018

ISO 527–4: Plastiques — Détermination des propriétés en traction — Partie 4: Conditions d'essai pour les composites plastiques renforcés de fibres isotropes et orthotropes (1997)

ASTM D5083: Standard Test Method for Tensile Properties of Reinforced Thermosetting Plastics Using Straight-Sided Specimens (2017)

Berthelot, J.M., Lecorre, J.F.: Fissuration transverse et délaminage dans les stratifiés croisés essais monotones et essais de fatigue, XVe Congrès français de mécanique, Nancy (2001)

Fantozzi, G.: Rupture des matériaux : 1ère et 2ème parties, recueil, Département Génie physique des Matériaux et Génie Mécanique Développement, 5ème année, p. 447. INSA Lyon, France (1990)

Kahtan Al-Khazraji, K., Kadhim, J., Sahbah Ahmed, P.: Effect of reinforcement material on fatigue characteristics of trans-tibial prosthetic socket with PMMA matrix. In: The 4th International Scientific Conference of Salahaddin University-Su Erbil, Kurdistan, 18–20 October 2011

Walke, K.M., Pandure, P.S.: Mechanical properties of materials used for prosthetic foot: a review. IOSR J. Mech. Civil Eng. (IOSR-JMCE) (2017). e-ISSN: 2278–1684, p-ISSN: 2320–334X 61–65

Abbas, S.M.: Effects of composite material layers on the mechanical properties for partial foot prosthetic socket. Al-Nahrain J. Eng. Sci. (NJES) **21**(2), 253–258 (2018)

Achouri, S., Redjel, B.: Experimental study and probabilistic analysis of the tensile fracture behavior of glass-perlon-acrylic reinforced composites for orthopedic use. Rev. Sci. Technol. Synthèse **29**(59), 76 (2014)

# Study of the Mechanical Properties of the Sand Concrete Lightened by Lignocellulosic Materials

B. Belhadj[1(✉)], A. Goullieux[2], M. Bederina[1], N. Montrelay[2], and M. Quéneudec[2]

[1] SREML Laboratory, University of Amar Telidji, Laghouat, Algeria
b.belhadj@lagh-univ.dz
[2] Research Unit EPROAD, University of Picardie Jules Verne, Amiens, France

**Abstract.** The article aims to study the mechanical properties of the studied concretes, namely sand concrete without lignocellulosic materials (SC), sand concrete lightened by barley straw which content is 15 kg/m$^3$ (BSC), sand concrete lightened by barley straw and wood shavings which content is 35 kg/m$^3$ (BWSC) and sand concrete lightened by wood shavings which content is 60 kg/m$^3$ (WSC). The objective is to target the best composition of the three lightweight sand concretes, which constitutes the best compromise between the studied properties. The first part was devoted to study the mechanical properties, namely the flexural strength, compressive strength, elasticity modulus in flexion and elasticity modulus in compression. However, the second part was reserved to study the cracking analysis of studied concretes by video microscope in order to appreciate the lignocellulosic materials effect on toughness and ductility.

The results show that as the content of lignocellulosic materials increases, the mechanical properties decrease as was predictable. Another relation was found between the porosity accessible to water and the compressive strength of the studied concretes. This relation was defined according to a polynomial equation whose correlation coefficient approaches 1. The cracking analysis shows the advantageous barley straw effect, separate and in combination for cracking propagation compared to wood shavings alone. Nevertheless, the advantage is in favour of concrete (BSC), from the point of view of improving the deformation capacity of concrete, that is to say ductility and toughness, this is mainly due to the particularity of barley straw in terms of tensile strength, straw flexibility, geometric shape and surface appearance. This barley straw particularity is an advantage compared to the wood shavings, it may contribute favourably to improve the ductility and consequently to increase the propagation resistance of the crack.

**Keywords:** Lightweight sand concrete · Lignocellulosic materials · Mechanical properties · Cracking · Ductility

## 1 Introduction

In recent years, there has been renewed interest in the use of plant fibers as constituents in composite materials based on polymer or mineral matrix, such as cement, plaster or


B. Safi et al. (Eds.): ISMSD 2019, *Proceedings of the 4th International Symposium on Materials and Sustainable Development*, pp. 34–47, 2020.
https://doi.org/10.1007/978-3-030-43211-9_4

lime Hamzaoui et al. (2014). However, Khazma et al. (2012) the lightweight concretes formulation by local lignocellulosic materials is one way of contributing to sustainable development in the construction sector. Therefore, according Pacheco-Torgal et al. (2011) to promote the use of cement-based building materials reinforced with plant fibers could be a way to achieve a more sustainable construction, because according to Claramunt et al. (2011), the plant fibers was obtained from renewable, biodegradable sources and therefore respectful of the environment.

Merta et al. (2013), the concrete is resistant to compression, however, as a very fragile material, has a low tensile strain capacity and therefore low toughness. Moreover, Babafemi et al. (2015) the incorporation of the fibers into a cementitious matrix makes it possible to improve the bending strength of the concrete or the mortar and to reduce its fragility, that is say, the increase of the absorption capacity energy of the concrete that is well known. The hypothese according to which the fibers make it possible to control the mechanism of cracking by delaying the departure of the crack and by controlling it once it appears Khenfer et al. (2000).

In this context, there is a number of studies (Reis 2012) and Merta et al. (2013), that study the fracture energy of concretes reinforced with plant fibers, but there is a lack in the analysis of cracking. Nevertheless, Hamzaoui et al. (2014) and Savastano et al. (2005), for the microstructure analysis, there are several researches cementitious matrix concretes reinforced by plant fibers.

In this study, the studied concretes compositions was inspired of previous work Belhadj et al. (2014) and Belhadj et al. (2016), which are the sand concrete without lignocellulosic materials (SC), the sand concrete lightened by 15 kg/m$^3$ of barley straw (BSC), the sand concrete lightened by 35 kg/m$^3$ of lignocellulosic materials, i.e. 30 kg/m$^3$ of wood shavings and 5 kg/m$^3$ of barley straw (BWSC), and finally the sand concrete lightened by 60 kg/m$^3$ of wood shavings (WSC). The three lightweight sand concretes have a workability are getting closer, the slump test with Abrams cone is from 5 cm to 6 cm. The objective is to have a lightweight sand concrete with plastic consistency of the fresh concrete.

Indeed, this study focuses on the lignocellulosic materials effect on the physico-mechanical properties of studied concretes, as well as the cracking analysis on specimens ($4 \times 4 \times 16$ cm$^3$) subjected to the elasticity modulus tests in flexion. The objective is to target the best composition, that constitutes the best compromise between the studied properties.

## 2 Materials Used and Methods

### 2.1 Materials Used

The contribution of using two different sands (Dune sand (DS) and alluvial sand (AS)) falls under the option of the valorisation of local materials in construction, especially the materials little or not exploited, such as dune sand. The sand used is a mixture of two sands, a dune sand (DS) with a maximum grain diameter about 0.63 mm and an alluvial sand (AS) with a maximum diameter 5 mm. The proportions of this mixture was prepared according to a specific mass ratio by correcting the granulometric curve of the alluvial sand, in its fine part, by adding dune sand. Bederina et al. (2005) studied

the mixture of the same sands (alluvial sand and dune sand) and found that the optimum compacity can be obtained with the report AS/DS = 1.7. Table 1 lists all the physical characteristics of the sand used.

**Table 1.** Physical characteristics of the sand used

| | |
|---|---|
| Apparent density (kg/m$^3$) | 1590 |
| Specific density (kg/m$^3$) | 2485 |
| Fineness modulus | 2.81 |
| Compactness (%) | 0.66 |
| Porosity (%) | 0.34 |
| Visual sand equivalent (%) | 93.2 |
| Piston sand equivalent (%) | 80.3 |

The cement used is CPJ limestone Portland cement CEM/II AL 42.5 R. This type of binder is a new class of cement, which provides a similar performance to that of conventional Portland cement, but emits a decrease $CO_2$ up to at 10%. The limestone fillers used were obtained by sieving at 80 μm the waste from the aggregates produced in the quarries locate in the Laghouat region. It is also part of the valorisation of waste. In addition, for economic and technical reasons, mineral powders have been added by substitution of cement. Belhadj (2016) studied the substitution of the same minerals powders (limestone, natural pozzolana and hydraulic lime) and found that the optimum combination can be obtained with 10% of mineral powders (1/3 limestone, 1/3 natural pozzolana and 1/3 hydraulic lime), which are obtained by sieving at 80 μm.

In addition to these used materials, barley straw was introduced into sand concrete, separated and in combination with wood shavings, to obtain lightweight sand concrete. The barley straw lengths are 2 cm for molds (4 × 4 × 16 cm$^3$). The straw diameter is about between 1 and 4 mm. Belhadj et al. (2014) was determined an average percentage of the barley straw used, which is 70% in the form tubular straws and 30% broken straws in the form of fibers and straw blankets. This mixture is representative of the natural mixture composition of the straw, as shown in Fig. 1 (a, b). Figure 1 (c) shows that the outside shape of the barley straw is in corrugated form, as well as it is regular narrowing, which facilitates the adhesion of the straw to the cement matrix. The inside form of barley straw is in the form of longitudinal fibers crossed almost transversely by microfibers (Fig. 1 (d)), which facilitates adhesion between the straw and the cement matrix.

The wood shavings used are part of the reuse of carpentry waste. At the video microscope magnification scale, the fibrous structure of wood shavings appears as an irregular and rough structure (Fig. 2), which facilitates adhesion between wood shavings and the cement matrix.

The superplasticizer used is the “SP MEDAPLAST 40” type, in accordance with EN 934-2. It is a superplasticizer high-water reducer that allows to obtain high quality concrete and mortar.

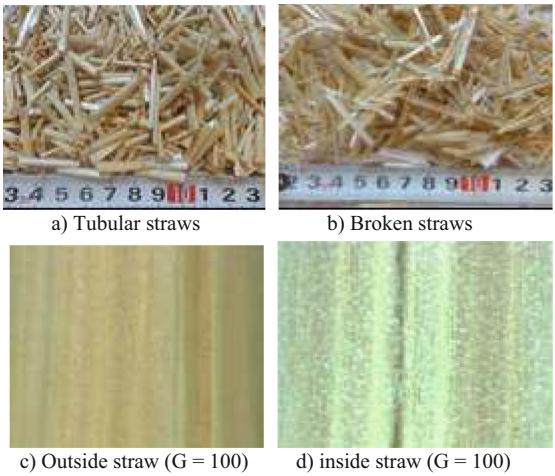


**Fig. 1.** General appearance of barley straw.


**Fig. 2.** General appearance of wood shavings.

## 2.2 Methods

Table 2 groups together the differents studied concretes compositions, which was inspired of previous work Belhadj et al. (2014) and Belhadj et al. (2016).

In order to best homogenize the mixture, to ensure a good quality of the concrete and thus to control the various properties of the finished product, the mixing was carried out by a mixer of the "Controls" type, according to the following procedure: a dry mix of the cement and mineral powders for one minute at low speed, then the sand and limestone fillers was added to a dry mix for another three minutes at low speed.

When the dry mixture is perfectly homogeneous, the lignocellulosic materials, separated and in combination was introduced in the saturated state, while continuing to mix for three minutes at a low speed. Finally, the mixing water was added gradually to the mixture without interruption, to ensure homogenization of the mixture for three minutes at a low speed Bederina et al. (2016). After mixing, the material was introduced into molds ($4 \times 4 \times 16\ cm^3$).

**Table 2.** Compositions used for the studied concretes

| Studied concrete | SC | BSC | BWSC | WSC |
|---|---|---|---|---|
| Sand (kg/m$^3$) | 1316 | 1245 | 1150 | 1030 |
| Cement (kg/m$^3$) | 315 | 315 | 315 | 315 |
| Mineral powders (kg/m$^3$) | 35 | 35 | 35 | 35 |
| Limestone (kg/m$^3$) | 135 | 135 | 135 | 135 |
| Water (l/m$^3$) | 210 | 229 | 252 | 281 |
| SP* (%) | 2 | 2 | 2 | 2 |
| Barley straw (kg/m$^3$) | 0 | 15 | 5 | 0 |
| Wood shavings (kg/m$^3$) | 0 | 0 | 30 | 60 |

* Mass percentage relative to the amount of cement.

The specimens was remolded after 24 h of their manufacture and the specimens are kept until the day of the test, in the same room where the climatic conditions inside the laboratory room is closer to the conditions actual weather conditions of local construction sites, i.e. the temperature is 20 °C ± 5 °C, while the relative humidity is 50% ± 10%.

The elasticity modulus in flexion was determined by a Shimadzu type press (Fig. 3 (a, b)) at a ramp rate equal 50 N/s, according to the EN-196-1 standard and the NBN EN 1015-11 standard. The elasticity modulus in compression was determined by a Shimadzu type press (Fig. 3 (a, c)) at a ramp rate equal 500 N/s, in accordance with the standard NBN EN 1015-11. The equipment used is linked to a computer (Fig. 3 (a)) which consists

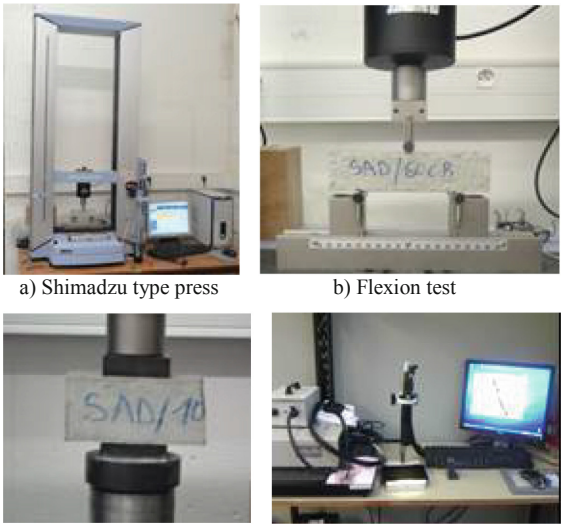


a) Shimadzu type press b) Flexion test

c) Compression test d) video microscope

**Fig. 3.** Shimadzu type press and video microscope.

in observing all the results obtained for each test and the figures (Displacement according to the flexion stress and compression stress), as well as the synthesis of the results by type of concrete.

For example, when the maximum stress in flexion is reached the test stops and the values of the elastic modulus as well as figure, are observed on the computer.

Crack analysis as well as general views of the matrix with lignocellulosic materials was done by optical imaging. The equipment is linked to a computer, which consists of observing with a video microscope type Controlab (Fig. 3 (d)), magnifications up to 300 with 25x–175x and 150x–300x, it is associated with a color screen containing 507–688 pixels, a low circular illumination and VIDEOMET software (Controlab). This software makes it possible to measure the geometrical characteristics by a simple observation.

## 3 Results and Analysis

### 3.1 Flexural Strength and Compressive Strength

The results of the flexural strength and compressive strength of the studied concretes are mentioned in Table 3. When the lignocellulosic material content increases, the flexural strength and the compressive strength decrease as it is predictable, following polynomial equations whose tendencies are negatives and having the correlation coefficients closer to 1 as shown in Fig. 4 and Fig. 5. Another relation was found between the porosity accessible to water and the compressive strength of the studied concretes, following polynomial equation whose tendencie is negative and having correlation coefficient is closer to 1 as shown in Fig. 6. The trend of this relationship is almost similar to the work of some researchers Lian et al. (2011) and Chen el al. (2013).

**Table 3.** Flexural strength and compressive strength at 28 days

| Studied concretes | Flexural strength (MPa) | Compressive strength (MPa) |
|---|---|---|
| SC | 4.12 ± 0,39 | 19.44 ± 0.43 |
| BSC | 3.08 ± 0,30 | 10.50 ± 0.35 |
| BWSC | 2.53 ± 0,21 | 8.13 ± 0.22 |
| WSC | 1.93 ± 0,08 | 7.05 ± 0.24 |

### 3.2 Elasticity Modulus in Flexion and Compression

The results of the elasticity modulus in flexion ($4 \times 4 \times 16\ cm^3$) and compression (4x4 cm) on the two prisms was obtained by flexion of the studied concretes are mentione in Table 4.

Figure 7 shows the existence of a very strong correlation between the maximum stress in flexion and the elasticity modulus in flexion of the studied concretes, whose correlation coefficient $R^2 = 0.99582$.

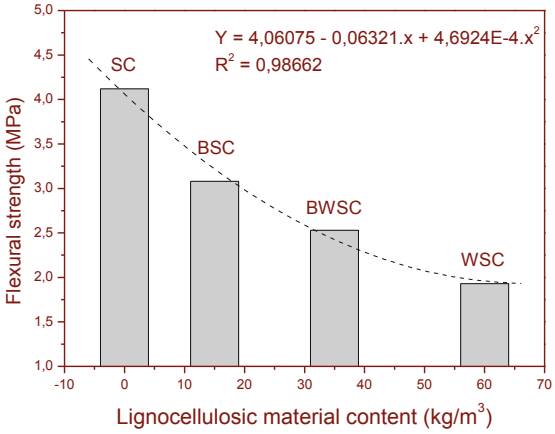


**Fig. 4.** Relationship between lignocellulosic material content and flexural strength.

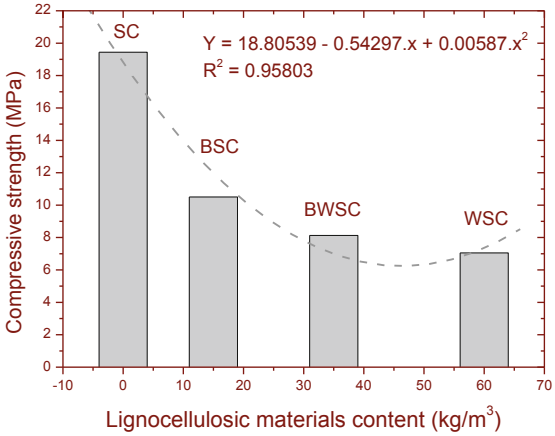


**Fig. 5.** Relationship between lignocellulosic material content and compressive strength.

The flexural strength values given in Table 4 represent the average of three tests carried out on the test ($4 \times 4 \times 16$ cm$^3$) specimen. On the other hand, the value of the bending stress presented in Fig. 8 represents the result of a single test for composition (BSC) which is given just as an example.

Figure 8 shows the results of the test of elasticity modulus in flexion, which shows the maximum stress in flexion in the elastic part for the concrete (BSC). However, Fig. 9 shows the results of the test of elasticity modulus in compressive, which shows the maximum stress in compression in the elastic part for the concrete (BSC).

Finally, from the values of the elasticity modulus in compression of the studied concretes, it was found that the values are getting closer.

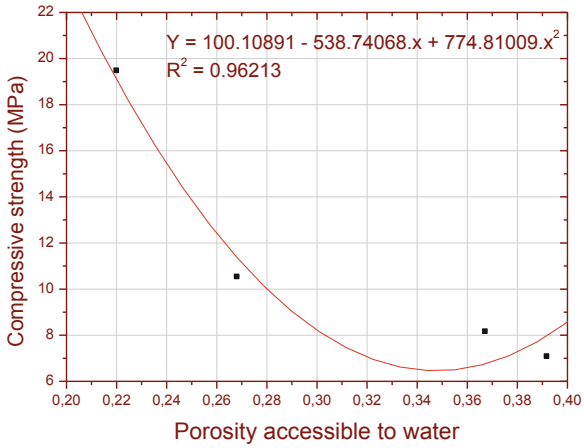


**Fig. 6.** Relationship between porosity accessible to water and compressive strength.

**Table 4.** Elasticity modulus in flexion and compression of studied concretes

| Studied concretes | Elasticity modulus in flexion (MPa) | Elasticity modulus in compression (MPa) | Maximum stress in flexion (MPa) |
|---|---|---|---|
| SC | 1228.04 ± 34,44 | 419.73 ± 4,93 | 7.90 ± 0.49 |
| BSC | 846.27 ± 42,73 | 407.86 ± 6,18 | 4.29 ± 0.15 |
| BWSC | 870.51 ± 86,32 | 405.12 ± 4,71 | 3.60 ± 0.11 |
| WSC | 823.92 ± 15,74 | 402.26 ± 6,45 | 3.26 ± 0.18 |

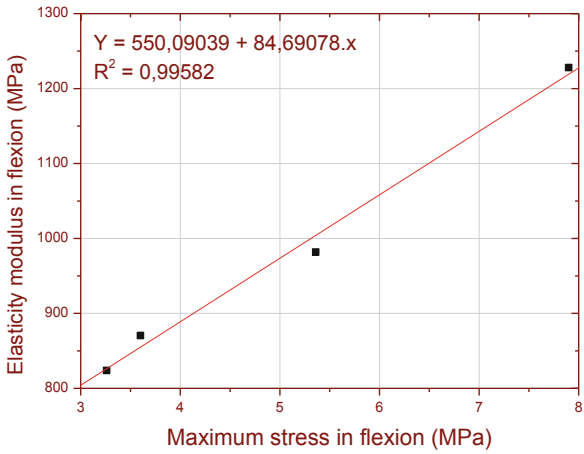


**Fig. 7.** Relationship between the maximum stress in flexion and elasticity modulus in flexion.

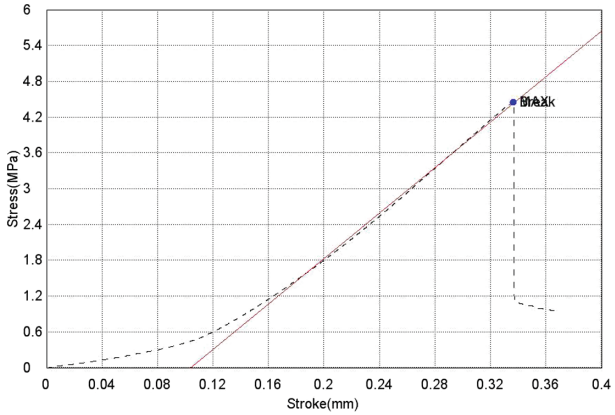


**Fig. 8.** Displacement according to the flexion stress of the (BSC).

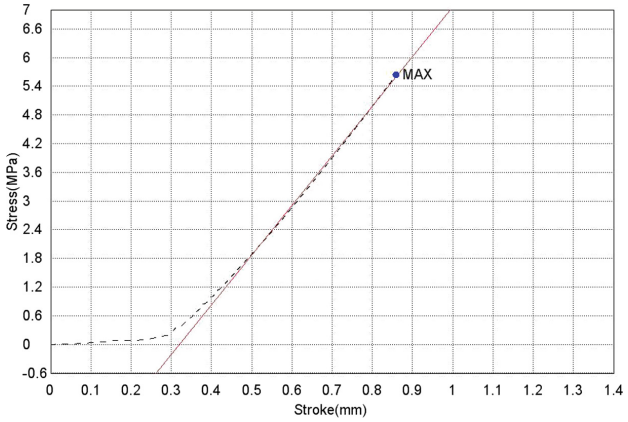


**Fig. 9.** Displacement according to the compressive stress of the (BSC).

The cross interpretation of the results was showed the existence of a strong linear regression whose correlation coefficient approaches 1, between the elasticity modulus in flexion and the elasticity modulus in compression as shown in Fig. 10.

### 3.3 Analysis of Cracking

After the tests of the elasticity modulus in flexion on ($4 \times 4 \times 16$ cm$^3$) specimen, it was found that cracks are illegible for concretes (BSC) and (BWSC) compared to the concrete (WSC) that is legible (Fig. 11 (a, b, c)).

Hence the need for a study of cracking proves necessary by a video microscope to appreciate the beneficial barley straw effect. It was also found that barley straw contribute favourably to improve the ductility of the sand concrete lightened by barley straw and the sand concrete lightened by wood shavings and barley straw, for example see Fig. 12 (a, b) for concrete (BWSC).

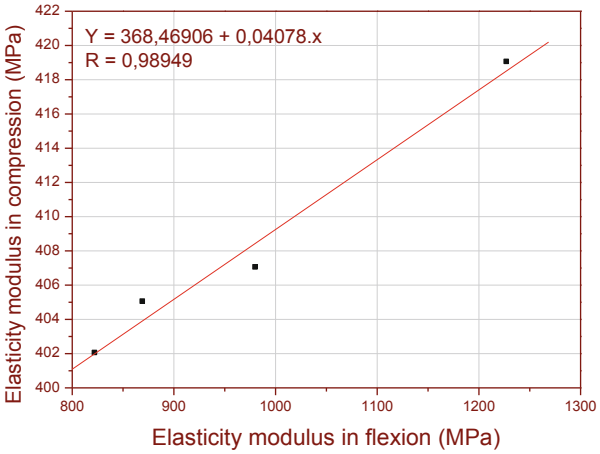


**Fig. 10.** Relationship between elasticity modulus in flexural and elasticity modulus in compressive.

a) Illegible crack after tests (BSC).

b) Illegible crack after tests (BWSC).

c) Legible crack after tests (WSC).

**Fig. 11.** Crack After the tests of the elasticity modulus in flexion.

In general way, we can say that the results show that the ductility of the sand concrete lightened by barley straw (BSC) is slightly best than the ductility of the sand concrete lightened by wood shavings and barley straw(BWSC). This can be explained by the following syntheses:

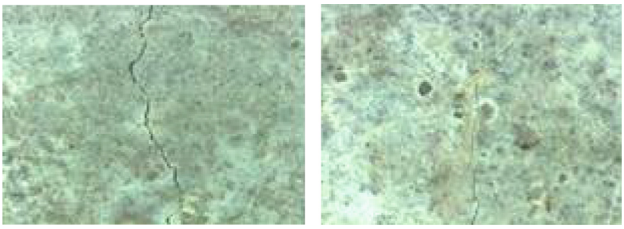

a) Lower part (G = 25) b) Upper part (G = 100)

**Fig. 12.** Concrete lightened by wood shavings and barley straw (BWSC).

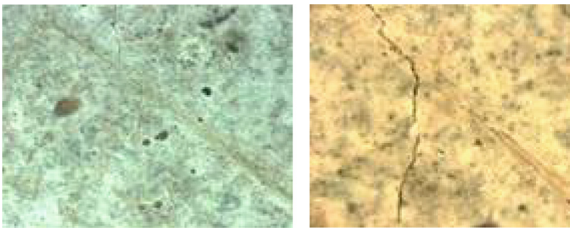

a) G = 50 b) G = 150

**Fig. 13.** Effect of wood shavings fibers and barley straw on ductility.

- After several measurements of the opening of the crack which has been determined a gap between the minimum and the maximum. In the lower part of the specimen (BWSC), the crack is narrower and varies from 14 μm to 90 μm.
- Fig. 13 shows the adhesion and orientation of the barley straw relative to the matrix in the lower part. On the other hand, Fig. 14 shows the effect of the grain of sand and the fiber on the deflection of the crack.
- Barley straw has reinforced the role of wood shavings as fibers, knowing that the effect of straw orientation is almost always horizontal (vibration effect) implies almost perpendicular to the force.

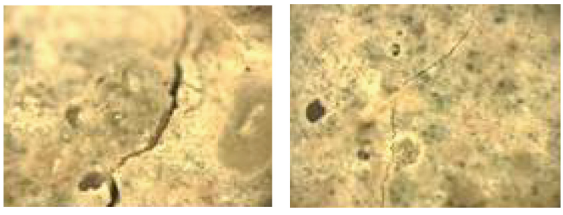

a) G = 150 b) G = 150

**Fig. 14.** Effect of sand grain and fiber on deflection of crack.

It should also be noted that the concrete containing 15 kg/m$^3$ of barley straw (BSC) has showed a different behavior from that of (BWSC). Indeed, it has been found by video microscope the existence of three parts:

1) Low part: It represents almost 1/4 of the height of the test specimen. The opening of the crack varies from 60 to 120 μm (Fig. 15 (a, b)).
2) Middle part: It represents almost half of the height of the specimen. The opening of the crack varies from 30 to 70 μm. The crack was propagated through two directions, one on the left and the other on the right. This is probably due to the effect of the barley straw content as well as their orientation (Fig. 15 (c, d, e)).
3) Upper part: It represents almost 1/4 of the height of the test specimen. The disappearance of the crack is complete (Fig. 15 (f)).

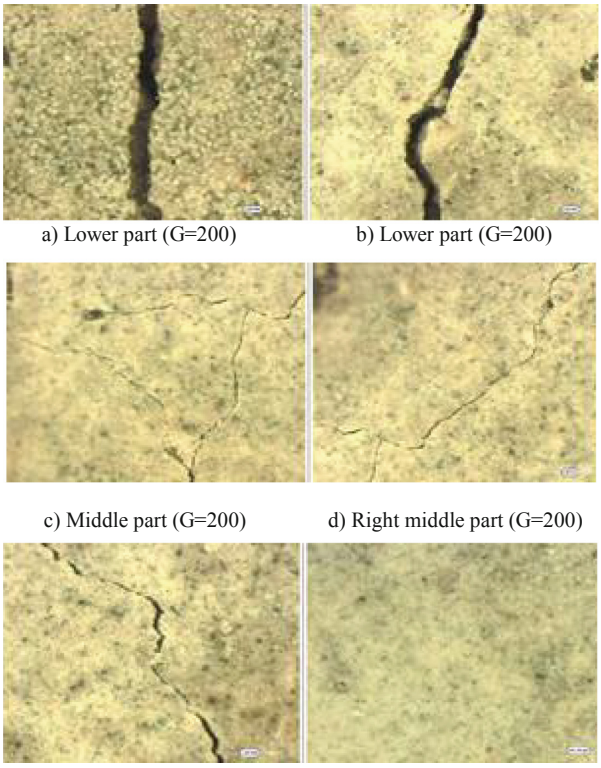

a) Lower part (G=200) b) Lower part (G=200)

c) Middle part (G=200) d) Right middle part (G=200)

e) Left middle part (G=200) f) Upper part (G=200)

**Fig. 15.** Cracking of the concrete (BSC).

In general, the results show that the ductility of the concrete (BSC) is slightly best than the ductility of the concrete (BWSC).

Finally, it can be concluded that the behavior of the test specimen ($4 \times 4 \times 16\ cm^3$) made with straw fibers having a length 2 cm is similar to the test specimen ($7 \times 7 \times 28\ cm^3$) made with straw fibers having a length 3.5 cm Belhadj et al. (2016), this explains that the effect of barley straw length has a similar influence on the role of ductility, hence the beneficial effect of barley straw on improving the capacity of barley straw deformation of lightweight sand concrete from the point of view of ductility and toughness.

After separation of the two prisms, Fig. 16 shows views of the matrix with barley straw and wood shavings which have been found to have good adhesion matrix versus lignocellulosic materials and the presence of an interesting porosity at the level of the cement matrix.

On the video microscope magnification scale, good adhesion between the barley straw and the cement matrix has been found, and the holes in the straw are empty. This adhesion can be explained by the outside shape of barley straw which is in corrugated or corrugated form, as well as regular narrowing (see Fig. 1.c). As well as the inside shape of the barley straw is in the form of longitudinal fibers crossed almost transversely by microfibers, which are well bonded, which facilitates the adhesion between the straw and the cement matrix (see Fig. 1). It has been found good adhesion between the wood shavings and the cement matrix, as well as the high porosity in the cementitious matrix, as shown in the images (Fig. 16).

The fibrous structure of the wood shavings appears as an irregular and rough structure at the scale of the enlargement, which facilitates the adhesion between the wood shavings and the cement matrix.

a) Concrete (BSC) b) Concrete (WBSC)

**Fig. 16.** Porosity at the level of the cement matrix.

## 4 Conclusions

This study shows, when the lignocellulosic material content increases, the mechanical properties decreases as it is predictable of the sand concrete lightened by lignocellulosic materials for the flexural strength, the compressive strength, the elasticity modulus in flexion and the elasticity modulus in compression. The results advantage shows that the studied concretes remains in the range of lightweight structural concretes, which are intended for the outside walls construction in arid regions.

The crack analysis shows the beneficial barley straw effect, separated and in combination for the propagation of cracking compared to wood shavings alone.

Nevertheless, the advantage is in favor of sand concrete lightened by barley straw from the point of view of improving the deformation capacity of the concrete, that is to

say the ductility and the tenacity, this is mainly due to the natural characteristics of the barley straw.

Finally, in the study of the microstructure mounted a double porosity at the scale of the matrix and at the scale of the lignocellulosic materials, which contributes favourably to improve the thermophysical properties of the studied concretes. In addition, it has been found good adhesion between the cement matrix and the lignocellulosic materials.

## References

Hamzaoui, R., Guessasma, S., Mecheri, B., Eshtiaghi, A.M., Bennabi, A.: Microstructure and mechanical performance of modified mortar using hemp fibres and carbon nanotubes. Mater. Des. **56**, 60–68 (2014)

Khazma, M., Goullieux, A., Dheilly, R.M., Quéneudec, M.: Coating of a lignocellulosic aggregate with pectin/polyethylenimin mixtures: effect on flax shive and cement-shive composite properties. Cement Concr. Compos. **34**, 223–230 (2012)

Pacheco-Torgal, F., Jalali, S.: Cementitious building materials reinforced with vegetable fibres: a review. Constr. Build. Mater. **25**, 575–581 (2011)

Claramunt, J., Ardanuy, M., Garcia-Hortal, J.A., Toledo Filho, R.D.: The hornification of vegetable fibers to improve the durability of cement mortar composites. Cement Concr. Compos. **33**, 586–595 (2011)

Merta, I., Tschegg, E.K.: Fracture energy of natural fibre reinforced concrete. Constr. Build. Mater. **40**, 991–997 (2013)

Babafemi, A.J., Boshoff, W.P.: Tensile creep of macro-synthetic fibre reinforced concrete (MSFRC) under uni-axial tensile loading. Cement Concr. Compos. **55**, 62–69 (2015)

Khenfer, M.M., Morlier, P.: Characterization and microstructure of cements reinforced with cellulose fibers. Bull. Pavement Bridges Lab. 224 REF **4236**, 49–58 (2000). (in French)

Reis, J.M.L.: Sisal fiber polymer mortar composites: Introductory fracture mechanics approach. Constr. Build. Mater. **37**, 177–180 (2012)

Savastano, H., Warden, P.G., Coutts, R.S.P.: Microstructure and mechanical properties of waste fibre-cement composites. Cement Concr. Compos. **27**, 583–592 (2005)

Belhadj, B., Bederina, M., Montrelay, N., Houessou, J., Quéneudec, M.: Effect of substitution of wood shavings by barley straws on the physico-mechanical properties of lightweight sand concrete. Constr. Build. Mater. **66**, 247–258 (2014)

Belhadj, B., Bederina, M., Makhloufi, Z., Dheilly, R.M., Montrelay, N., Quéneudec, M.: Contribution to the development of a sand concrete lightened by the addition of barley straws. Constr. Build. Mater. **113**, 513–522 (2016)

Bederina, M., Khenfer, M.M., Dheilly, R.M., Quéneudec, M.: Reuse of local sand: effect of limestone filler proportion on the rheological and mechanical properties of different sand concrete. Cem. Concr. Res. **35**, 1172–1179 (2005)

Belhadj, B.: Contribution to the valorisation of local materials and waste to the formulation of insulating-carrier lightweight sand concretes intended for the construction in arid environments (Case of Laghouat city). Doctoral thesis, University of Laghouat, Algeria (2016). (in French)

Bederina, M., Belhadj, B., Ammari, M.S., Gouilleux, A., Makhloufi, Z., Montrelay, N., Quéneudec, M.: Improvement of the properties of a sand concrete containing barley straws – treatment of the barley straws. Constr. Build. Mater. **115**, 464–477 (2016)

Lian, C., Zhuge, Y., Beecham, S.: The relationship between porosity and strength for porous concrete. Constr. Build. Mater. **25**, 4294–4298 (2011)

Chen, X., Wu, S., Zhou, J.: Influence of porosity on compressive and tensile strength of cement mortar. Constr. Build. Mater. **40**, 869–874 (2013)

# Physical and Mechanical Properties of Concrete Containing PVC Waste as Aggregate

M. Belmokaddem[1,2(✉)], A. Mahi[1], Y. Senhadji[3,4], and B. Y. Pekmezci[2]

[1] Laboratoire LM2SC, Université des Sciences et de la Technologie d'Oran Mohamed Boudiaf, USTO-MB, Oran, Algeria
mohammed.belmokaddem@univ-usto.dz
[2] Istanbul Technical University, Civil Engineering Faculty, Maslak, Istanbul, Turkey
[3] Civil Engineering Department, University of Mascara, Mascara, Algeria
[4] Laboratory Lab-Mat, ENPO Maurice Audin, Oran, Algeria

**Abstract.** The global annual production of plastics rose sharply from 1.5 up to 359 million tons during the period between the years 1950 and 2018. A large proportion of plastic products and goods, such as bottles of water and soda, food packaging, etc., are thrown away right after their first use, causing the generation of considerable amounts of post-consumer plastic waste. Reusing solid plastic wastes to produce other innovative materials, such as recycled plastic aggregate concrete, is considered as one of the most economical and cost-effective alternatives. This work is part of an ambitious sustainable development program. For this purpose, PVC waste is used in the form of aggregates (sand 0/3 and coarse aggregate 3/8) in the preparation of a number of concrete specimens. These plastic aggregates were used as partial replacement of natural aggregates at the following substitution rates: 25%, 50% and 75%. The experimental results obtained indicate that there is a difference between the physical and mechanical properties of plastic wastes-based concretes and those containing natural aggregates. The use of plastic aggregates in concrete improves the thermal insulation of concrete which can be considered as part of a construction solution, to improve a building's thermal efficiency.

**Keywords:** PVC wastes aggregate · Lightweight concrete · Waste valorization · Thermal insulation

## 1 Introduction

Plastics have been increasingly used, since their development in the 1930s and particularly between the years 1950 and 2018. The global annual production of plastics rose sharply from 1.5 up to 359 million tons during that period (www.statista.com). Nowadays, a large proportion of plastic products and goods, such as bottles of water and soda, food packaging, etc., are thrown away right after their first use, causing the generation of considerable amounts of post-consumer plastic waste. The production of this type of waste is still going to increase in the future. In fact, it has been estimated that the annual production of plastic wastes doubles every 10 years (Iadav 2008). Although many


B. Safi et al. (Eds.): ISMSD 2019, *Proceedings of the 4th International Symposium on Materials and Sustainable Development*, pp. 48–56, 2020.
https://doi.org/10.1007/978-3-030-43211-9_5

recycling opportunities are available today, reusing solid plastic wastes to produce other innovative materials, such as recycled plastic aggregate concrete, is considered as one of the most economical and cost-effective alternatives (Saikia and de Brito 2014). Several researchers have addressed the technical viability of incorporating selected plastic wastes into concrete; they also studied the effects of such incorporation on the mechanical and durability properties of the new materials obtained. It can be seen from the literature that plastic waste has also found application in the production of building composites as a substitute for traditional aggregates and as reinforcing fibers in concretes and mortars (Benosman et al. 2017). Aattache et al. (2013) reported that this waste can also be used as a substitute for blended Portland cement. In general, adding plastic waste aggregates decreases the unit weight of the composite. Moreover, the modulus of elasticity of the composite decreases, and the formulated specimens show a more ductile behavior as the amount of incorporated plastic aggregate increases. However, the inclusion of plastic waste aggregates causes a reduction in the compressive strength, flexural tensile strength, and splitting tensile strength of cement-based composites. In addition, water absorption increases as the amount of plastic waste aggregates rises (Senhadji et al. 2015). The present study has to do with sustainable development. This work aims to conduct an experimental investigation on the behavior of concrete specimens containing PVC waste aggregates, at different substitution percentages, i.e. 25, 50, 75%, by volume.

## 2 Material and Methods

### 2.1 Cement

The cement used in the preparation of concretes is of type.

CPJ CEM II 42.5 N, from the LAFARGE cement factory in Oggaz (north-western Algeria).

### 2.2 Natural Aggregates

Two grades of crushed and calcareous coarse aggregates were used, i.e. the first one is medium, 3–8 mm aggregate and the second is coarse, 8–15 mm aggregate. The fine aggregate used is local natural sand. The physical properties of natural aggregates are shown in Table 2.

### 2.3 Plastic Aggregates

Plastic wastes were used to replace a fraction (by volume) of natural sand and medium aggregate in the mixtures, in order to achieve low-density concrete. The plastic wastes used were PVC plastic aggregates, as shown in Fig. 1. The plastic wastes were ground into small granules; they were then classified as fine or medium aggregates with size ranges 0–3 and 3–8 mm, respectively. The physical properties of the plastic wastes are shown in Table 2.

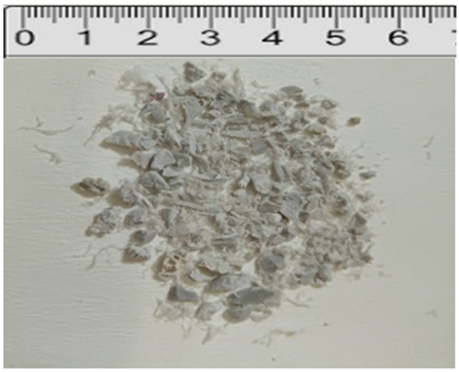


**Fig. 1.** PVC aggregate

### 2.4 Superplasticizer

UNICUM PC6 is a polymer-based super-plasticizer of the latest generation. It is characterized by a very high reduction performance of the W/C ratio; it also helps concretes to develop very high initial and final strengths (Table 1).

**Table 1.** Physical and chemical characteristics of the superplasticizer

| Designation | Physical state | Color | Dosage |
|---|---|---|---|
| UNICUM PC 6 | Liquid | Yellow | 0,4–1,1% |

**Table 2.** Physical properties of the aggregates

| Properties | Natural sand | Medium aggregate | Coarse aggregate | PVC sand | PVC aggregate |
|---|---|---|---|---|---|
| Density ($g/cm^3$) | 2.68 | 2.59 | 2.66 | 1.40 | 1.43 |
| Grain size (mm) | 0–3 | 3–8 | 8–15 | 0–3 | 3–8 |
| Shape | Angular | Angular | Angular | Angular | Angular |

## 3 Experimental procedures

Four formulations were prepared by partial volume replacement of natural aggregates by PVC plastic wastes, with percentages 0%, 25%, 50% and 75%, respectively, as shown in

Table 3. The superplasticizer was used to adjust the workability. For each formulation, specimens of dimension 10 × 10 × 10 cm3 were prepared. After demolding, they were cured in lime saturated water until the day of testing. The unit weights of fresh concrete and dry concrete were measured at 28 days. The compressive strength of the concrete specimens was tested and evaluated according to Standard EN 12 390–3 (2003), at 7 and 28 days.

**Table 3.** Concrete composition for a meter cube

| Composites | Weight Kg/m$^3$ | | | |
|---|---|---|---|---|
| | RC | PCPVC | | |
| | | 25% | 50% | 75% |
| Portland cement CEM II | 350 | 350 | 350 | 350 |
| Natural sand (0/3) | 602 | 451.52 | 301 | 150.49 |
| PVC sand (0/3) | 0 | 79 | 157 | 236 |
| Medium aggregate (3/8) | 900 | 675 | 450 | 225 |
| PVC aggregate (3/8) | 0 | 124 | 248 | 373 |
| Coarse aggregate (8/15) | 270 | 270 | 270 | 270 |
| Water (Kg) | 168 | 168 | 168 | 168 |
| Water/Cement ratio (%) | 0.48 | 0.48 | 0.48 | 0.48 |
| Superplasticizer( %) | 0.6 | 1 | 0.80 | 0.60 |

Three specimens were prepared from each mixture in order to measure the compressive strength at each age; the average of the three measurements was considered in this study. The unit weight of concrete was also measured at 28 days. After the compression test, a microstructural analysis was carried out on different samples using scanning electron microscopy (SEM) by means of a Hirox SH-4000 M Scanning Electron Microscope. The thermal conductivity was measured using the ISOMET 30 Quickline equipment.

## 4 Results and discussion

### 4.1 Fresh and Dry Densities of Concrete

The fresh and dry densities of the different mixtures are summarized in Table 4 and Fig. 2. One can clearly note that the fresh and dry densities of concrete diminish as the PA content goes up. The increase in the PVC content by 25, 50 and 75% results in a decrease in the fresh density by 9.39, 17.31 and 27.75%, respectively; with respect to that of the reference concrete (RC). However, when the PVC content rises by the same percentages (25, 50 and 75%), the dry density decreases by 10, 19.35 and 29.56%, respectively, as compared to that of the reference concrete. This decline in the density of concrete can certainly be attributed to the lower density of plastic aggregates and also to the increase

in porosity. These findings proved to be in good agreement with the conclusions of some authors (Badache et al. 2018; Hannawi et al. 2010). According to ACI CT-13 (2013) which identifies an upper limit for lightweight concretes (1920 kg/m$^3$), PCPVC25 and PCPVC50 can be considered as lightweight concretes.

**Table 4.** Fresh and hardened densities of concretes

| Mixture name | Fresh density (kg/m$^3$) | Dry density −28 days (kg/m$^3$) |
|---|---|---|
| RC | 2385 | 2439 |
| PCPVC25 | 2161 | 2195 |
| PCPCV50 | 1972 | 1967 |
| PCPVC75 | 1723 | 1718 |

RC: Reference Concrete
PC25: Concrete contain 25% of plastic
PA: Plastic aggregate

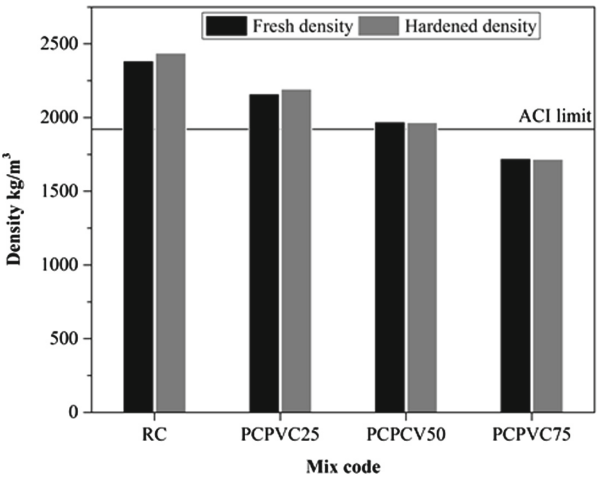


**Fig. 2.** Fresh and hardened densities of concretes

## 4.2 Compressive Strength

The compressive strength values of the composites obtained were calculated in the laboratory; they are summarized in Table 5. The results presented in Table 5 and Fig. 3 show a systematic reduction in the compressive strength with the increase in plastic aggregate content. Incorporating 25, 50 and 75% of recycled PVC aggregates into concrete engendered a compressive strength decrease of 26, 42 and 63% for concretes mixtures PCPVC25, PCPVC50 and PCPVC75, respectively, at 28 days. Reducing in the compressive strength of concrete incorporating plastic aggregates (PA) can be attributed to

the increase in matrix porosity which would cause the decrease in density and thus in compressive strength (Benosman et al. 2017) or low compressive strength of lightweight aggregates. These findings are consistent with those of Senhadji et al. (2015), Badache et al. (2018), Hannawi et al. (2010), Latroch et al. (2018), (Herki and khatib, 2017), and Akçaözoğlu et al. (2013), who demonstrated that poor contact between a plastic LWA and the matrix leads to a drop in the compressive strength. Concretes PCPVC25, PCPVC50 can be classified as structural lightweight concrete because their compressive strengths presented in Fig. 3 were equivalent to or higher than 17 MPa; in accordance with the specification of ASTM C330/C330M -17a (2017) definition which state that, the compressive strength of a structural lightweight concrete at 28 d should be higher than 17.24 MPa.

**Table 5.** Development of compressive strength of concretes

| Mixture name | Compressive strength (MPa) | | | |
|---|---|---|---|---|
| | 7 days | % of loss | 28 days | % of loss |
| RC | 30.64 | – | 35.05 | – |
| PCPVC25 | 23.60 | 23 | 25.96 | 26 |
| PCPCV50 | 16.93 | 45 | 20.50 | 42 |
| PCPVC75 | 11.18 | 64 | 12.79 | 63 |

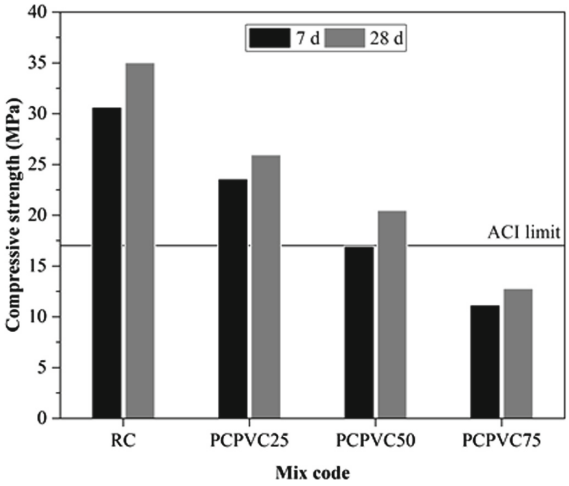


**Fig. 3.** Evolution of the compressive strength of concretes

### 4.3 SEM Images

Some scanning electron microscope (SEM) images of samples of PCPVC75 composite concrete and reference concrete (RC) were taken and are displayed in Figs. 4 and 5,

respectively. The interfacial transition zone (ITZ) between the PVC aggregates and cement paste turned out to be weaker than that between the cement matrix and natural aggregates. The ITZ width is even wider PVC aggregate concrete. The quality of the ITZ was not determined but it might have lower strength than that of natural aggregate concrete depending on the hydrophobic structure of PVC. This last finding may also help to explain the decreased compressive strength of composite concrete.

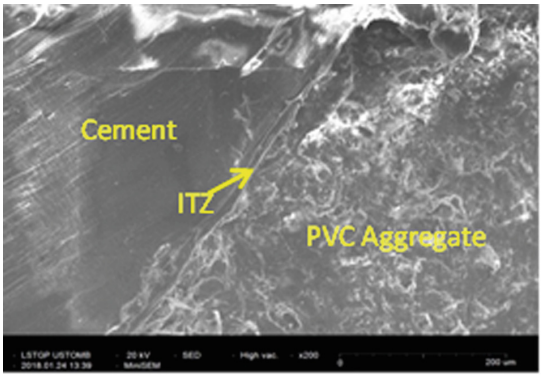


**Fig. 4.** SEM images of PCPP75 composite

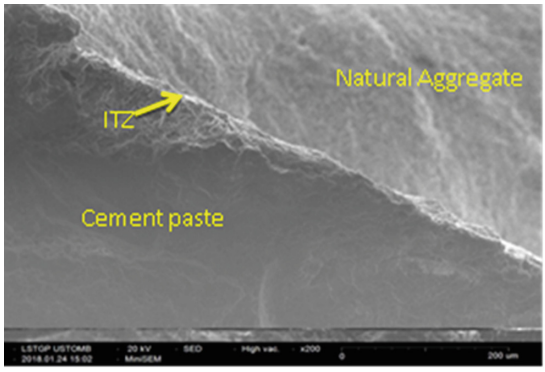


**Fig. 5.** SEM images of RC reference concrete

### 4.4 Thermal Conductivity

Table 6 shows the thermal conductivity variation of concretes. We can clearly say that all concretes containing PVC aggregates have experienced a decrease in thermal conductivity as compared to the reference concrete. It also indicates that the thermal conductivity decreases as the percentage of PA increases. Incorporating 25, 50 and 75% of recycled PVC aggregates into concrete caused the thermal conductivity to decrease by 32.2, 52.1 and 67.2% for concrete mixtures PCPVC25, PCPVC50 and, PCPVC75, respectively.

The decrease in thermal conductivity can be explained by the low thermal conductivity of PVC (≈0.081 W/m. K) (Latroch et al. 2018).

**Table 6.** Variation in the thermal conductivity of concrete

| Mixture name | Thermal conductivity (W/m.k) | % of loss |
|---|---|---|
| RC | 1.86 | – |
| PCPVC25 | 1.26 | 32.2 |
| PCPCV50 | 0.89 | 52.1 |
| PCPVC75 | 0.61 | 67.2 |

## 5 Conclusions

The present experimental study allowed showing that there is a difference between the evolution of the physical and mechanical performances of concretes containing PVC wastes, and the evolution of the physical and mechanical performances of natural aggregate concrete.

The following conclusions may be drawn:

- The density of composite concrete decreases significantly as the plastic aggregates content rises,
- The compressive strength of composite concrete decreases significantly as the plastic aggregates content goes up,
- The composite concrete has a wider ITZ as compared to that of reference concrete,
- The use of PVC aggregates leads to a decrease of a thermal conductivity to 67% for the PCPVC75 compared to RC. It's clear that the use of plastic aggregates in concrete improves the thermal insulation of concrete which can be considered as part of a construction solution, to improve a building's thermal efficiency.

## References

https://www.statista.com/statistics/282732/global-production-of-plastics-since-1950/

Iadav, I.: Laboratory investigations of the properties of concrete containing recycled plastic aggregates. Patiala, India: Civil Engineering Department, Thapar University (2008)

Saikia, N., de Brito, J.: Mechanical properties and abrasion behaviour of concrete containing shredded PET bottle waste as a partial substitution of natural Aggregates. Constr Build Mater **52**, 236–244 (2014)

Benosman, A.S., Taïbi, H., Senhadji, Y., Mouli, M., Belbachir, M., Bahlouli, M.L.: Plastic Waste Particles in Mortar Composites: Sulfate Resistance and Thermal Coefficients. Progr. Rubber Plast. Recycl. Technol. J. **33**, 127–158 (2017)

Aattache, A., Mahi, A., Soltani, R., Mouli, M., Benosman, A.S.: Experimental study on thermo-mechanical properties of polymer modified mortar. Mater. Des. **52**, 459–469 (2013)

Senhadji, Y., Escadeillas, G., Benosman, A.S., Mouli, M., Khelafi, H., OuldKaci, S.: Effect of incorporating PVC waste as aggregate on the physical, mechanical and chloride ion penetration behavior of concrete. J. Adhes. Sci. Technol. (2015). https://doi.org/10.1080/01694243.2014.1000773

EN 12 390–3.: European committee for standardization. Test for hardened concrete – Part 3: Compressive strength of test specimens. EN 12 390–3 (2003)

ACI Concrete Terminology ACI CT-13.: Farmington Hills, Michigan: American Concrete Institute (2013)

Badache, A., Benosman, A.S., Senhadji, Y., Mouli, M.: Thermo-physical and mechanical characteristics of sand-based lightweight composite mortars with recycled high-density polyethylene HDPE. Constr. Build. Mater. **163**, 40–52 (2018)

Hannawi, K., Kamali-Bernard, S., Prince, W.: Physical and mechanical properties of mortars containing PET and PC waste aggregates. Waste Manag. **30**, 2312–2320 (2010)

Latroch, N., Benosman, A.S., Bouhamou, N.E., Senhadji, Y., Mouli, M.: Physico-mechanical and thermal properties of composite mortars containing lightweight aggregates of expanded polyvinyl chloride. Constr. Build. Mater. **175**, 77–87 (2018)

Herki, B.A., Khatib, J.M.: Valorisation of waste expanded polystyrene in concrete using a novel recycling technique. Eur. J. Environ. Civ. En. **21**(11), 1384–1402 (2017)

Akçaözoğlu, S., Akçaözoğlu, K., Atis, C.D.: Thermal conductivity, compressive strength and ultrasonic wave velocity of cementitious composite containing waste PET lightweight aggregate (WPLA). Compos. B **45**, 721–726 (2013)

ASTM C330/C330M−17a.: Standard specification for lightweight aggregates for structural concrete (2017)

# A Statistical Analysis of Size, Shape and Tensile Properties of Fibres Extracted from Date Palm (*Phoenix Dactylifera L.*) Rachis

H. Boumediri[1(✉)], A. Bezazi[1], G. Garcia del Pino[2], B. Bezzazi[3], A. Toufik Moussai[1], F. Scarpa[4], and A. Dufresne[5]

[1] Laboratoire de Mécanique Appliquée des Nouveaux Matériaux (LMANM), Université 8 Mai 1945, Guelma, Algérie
haithem.boumediri@yahoo.com
[2] Escola Superior de Tecnologia (EST), Universidade do Estado do Amazonas, UEA, Av. Darcy Vargas 1200, Parque Dez, Manaus, AM, Brasil
[3] Research Unit Materials, Processes and Environment, University M'Hamed Bougara, 35000 Boumerdes, Algeria
[4] Department of Aerospace Engineering, University of Bristol, Queens Building, University Walk, Bristol BS8 1TR, UK
[5] Univ. of Grenoble Alpes, CNRS, Grenoble INP, LGP2, 38000 Grenoble, France

**Abstract.** Algeria is the largest country in Africa by in terms of land area, which makes it contain large quantities of agricultural residues. The aim of this study is the valorisation of the huge amount of agricultural residue of date palm rachis available in Algeria to be used as reinforcement in bio-composite materials for various industrial applications. The analysis of the morphology of the of the date palm rachis cross-section allowed us to identify two main types of fibres according to their microstructure: vascular bundles and fibre strands. The chemical and molecular structure analysis of the date palm rachis fibres was examined by Fourier transform infrared spectroscopy (FTIR). The tensile properties of the fibre extracted were investigated under tensile loading test. The experimental results obtained for the tensile strength, Young's modulus and strain at break of the fibres have been analysed, because of their dispersion, using three-parameter and two-parameter Weibull statistical laws. The tensile strength and Young's modulus of the fibre strand were found to be about than four times higher than for the vascular bundle and their predicted model was determined. The tensile properties obtained for the investigated fibre were compared with other lignocelluloses fibres, existing in the literature, and it shows its great potential for use as reinforcement in bio-composite materials.

**Keywords:** Statistical analysis · Tensile properties · Fibre strand · Vascular bundle · Date palm rachis


B. Safi et al. (Eds.): ISMSD 2019, *Proceedings of the 4th International Symposium on Materials and Sustainable Development*, pp. 57–70, 2020.
https://doi.org/10.1007/978-3-030-43211-9_6

## 1 Introduction

In recent years, natural fibres have increasingly grown in popularity for use in industry sectors as substitute for synthetic ones in many various applications such as automobiles, furniture, packaging, kayaks, prosthetics, aerospace, etc. (Amroune et al. 2015; Al-Oqla et al. 2015; Mhatre et al. 2019; Saba et al. 2015). This is due to their many advantages, such as their abundant availability in the form of fibres, biodegradability, renewability, low cost, and low-density when compared to synthetic fibres (Amroune et al. 2015; Bezazi et al. 2020; García del Pino et al. 2020; Maache et al. 2017).

Algeria is one of the countries with the highest potential for natural resources in the world, because of its vast area; it is the largest country in Africa. Many plants grow there such as date palms, Alfa, Juncus effuses L., Agave, Lygeum spartum L., Diss, Doum, etc. (Amroune et al. 2015; Belaadi et al. 2013; Belouadah et al. 2015; Bezazi et al. 2014; Bezazi et al. 2015; Bezazi et al. 2020; Bourahli et al. 2018; Maache et al. 2017). These various resources were investigated with the objective to be used in different applications such as packing, furniture, automobiles, and construction. The results obtained were very promising, which can give the local industry other sources of raw materials. This enables Algeria to valorise these abandoned resources and create jobs and maintain foreign exchange reserves by reducing importations, which contributes to raising the national economy.

The date palm (*Phoenix dactylifera L.)* is considered as one of the most important fruit crops in Algeria with more than 950 types of date palms classified according to the external quality of the date fruit in three categories: the palm produces soft dates, semi-soft dates and the dry ones (Biglari et al. 2008; Bouguedoura et al., 2015). Based on the FAO statistics (FAOSTAT) it is the world's fourth-largest producer of dates in 2018 with a total of more than 20 million date palms trees, which can produce about 720,000 tons of date palm petioles and leaves, and 210,000 tons of fruit bunches (Boumediri et al. 2017, 2019).

The date palm petioles and leaves are an abundant resource of lignocellulosic materials but are considered as a big waste. They mostly dumped into landfill and only small quantities used as feed for animals and in a traditional craftsman (Agoudjil et al. 2011; Boumediri et al. 2019). While this waste can be developed and valorised to be used as reinforcement in composite materials, this has attracted the attention of researchers for developing industry sectors throughout the last few years (Jawaid et al. 2011).

In this context, the main objective of this investigation is to promote local natural Algerian resources in order to integrate them into the industrial sector. Therefore, the purpose of the present work is an experimental characterization of the fibres extracted from date palm leaves of a palm tree called Gears harvested from a Farm in El-Oued located in southern Algeria. The morphology of the fibre was examined using optical microscope and scanning electron microscopy (SEM). The chemical and molecular structure analysis of the date palm rachis fibres was identified out by Fourier transform infrared spectroscopy (FTIR), and its mechanical properties investigated using a tensile machine with linear regression model to predict them. The obtained results have been compared with those found in the literature for other natural fibres.

## 2 Materials and Methods

### 2.1 Material

Algeria has many date palm varieties. The variety used in this research was date palm tree called Gears taken from a local farm of El-Oued located in the south of Algeria, collected from date palm leaves in October 2018. This rachis (Fig. 1) was obtained by removing all the leaflets and cut into a length of about 10 inches using a cutter. The fibres extraction from the rachis involves the degumming of fibrous straw in an autoclave in boiling water at 120 °C for 1 h and 30 min.

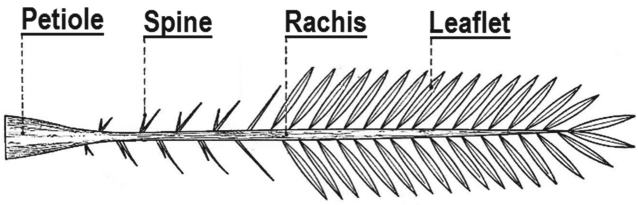


**Fig. 1.** Date palm leaf details

The fibres were extracted and separated from each other by hand peeling after cooling the rachis. Once the fibres were extracted, they were thoroughly washed and cleaned with water and then dried at room temperature for seven days. Broad dispersion was observed in their diameter, which leads to classify them into two types, as shown in Fig. 2 for further investigations.

**Fig. 2.** The extracted fibres from date palm rachis

### 2.2 Optical Microscopy

A Motic BA310 optical microscope was used to identify the shape and morphology of the fibres and their dispersion in the base and tip of the rachis. The pictures were taken under × 5 magnification using Motic image plus 2.0 software with a microscopic camera (Moticam 5.0 MP).

### 2.3 Scanning Electron Microscopy

A Quanta 200-FEI environmental scanning electron microscope (ESEM) was used to study the morphology of the date palm rachis fibres. A thin conductive gold layer coated all the samples before recording the micrographs. The acceleration voltage was set at 10 kV and the working distance at about 10.5 mm.

### 2.4 Fourier Transform Infrared Spectrometry (FTIR)

FTIR spectra were recorded on an ATR-FTIR using a Thermo Scientific Nicolet iS10 FT-IR spectrometer equipped with a single reflection ATR accessory (Specac Golden Gate). The FTIR spectral analysis was recorded in the range of 4000–500 $cm^{-1}$ region with an accumulation of 32 scans at a resolution of 1 $cm^{-1}$.

### 2.5 Technical Fibre Tensile Tests

Tensile tests were carried out on a universal testing machine Zwick/Roell model Z2.5 according to ASTM D 3822–07 using a gauge length of 30 mm. The crosshead speed was of 1 mm/min using a 200 N load cell attached to an automatic data acquisition system. Testing was done using twenty samples that were analysed for each group at room temperature of 23 °C and relative humidity of 45%.

The technical fibres are assumed to be cylindrical, and their diameter was determined using a MOTIC optical microscope equipped with a Motic-BA310 Met digital camera running with Motic image plus 2.0 software. Three measurements have been taken along the effective fibre length in different points, and an average value has been calculated. The obtained tensile results were analysed statistically by two parameters and three parameters Weibull distribution model using the Minitab software.

## 3 Results and discussion

### 3.1 Morphological Analysis

The observation of the cross-section of date palm rachis presented in Fig. 3a and 3b show a lot of fibres which occur randomly throughout the parenchymatous tissue with intercellular spaces in the beginning and before 20 cm of the tip of rachis. The observed fibres can be classified according to their microstructure into two types, one that contains at least one large void called vascular bundle (VBs) and the other fibre strand (FSs) does not contain any a large void.

As depicted in Fig. 4b and c, VBs are the thickest fibres and have at least one main void in the middle responsible for the conduction of food, other organic material, and water in the tree. Their microstructure showed that it was an almost circular elliptical shape, the main void diameter being between 90 and 160 μm with a large number of spherical microfibrils of smaller diameter in the range 5 and 25 μm, aligned and bound together by lignin and other non-cellulosic materials. While, the FSs are the smallest and do not contain any main voids, which contain many individual microfibrils with a diameter between 4 to 12 μm, compactly arranged to form a technical fibre whose

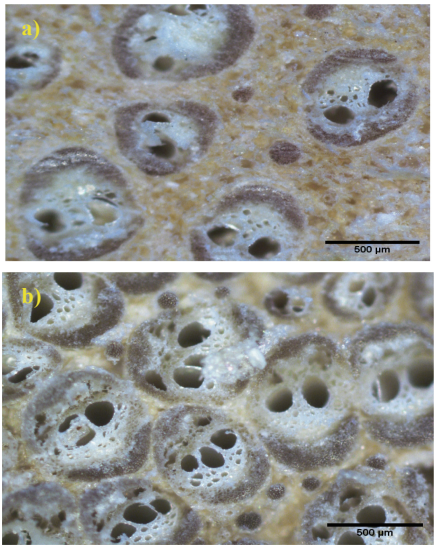


**Fig. 3.** Optical microscope images of the cross-section of the date palm rachis: a) At the beginning of the rachis, b) before 20 cm of the tip of rachis

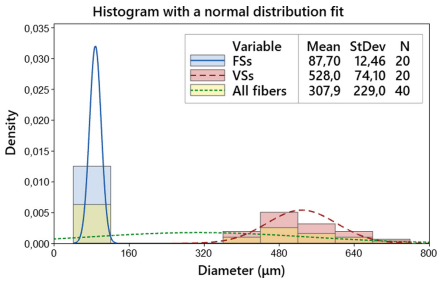


**Fig. 4.** Distribution of the diameter normal plot for (VBs) and (FSs)

shape is approximately cylindrical and whose diameter is found in the range of 85 to 120 microns.

A diameter analysis of extracted fibres performed using normal method distribution shows a low standard deviation for the mean diameter about 14% (Fig. 5). However, the average diameter for all the fibres (20 VBs + 20 FSs) shows a significant standard deviation around 75%. These results show the importance of classification for each type of fibre for proper use.

### 3.2 FTIR Analysis

The FTIR analysis performed for VBs and FSs fibres shows different chemical functional groups and molecular structure (Fig. 6 and Table 1). It exhibits a small band at 900 $cm^{-1}$

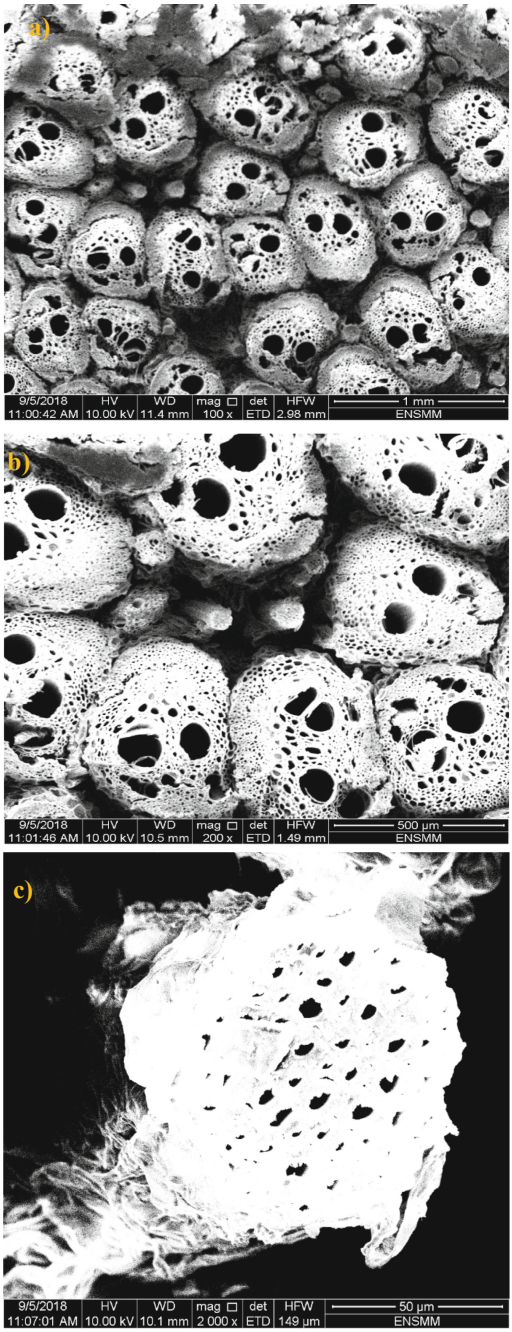


**Fig. 5.** SEM micrographs of the cross-section before 30 cm of the tip of the rachis: a) Zoom X100, b) Zoom X200, and c) FSs (zoom X2000)

indicating the presence of C–O–C stretching of the β-glycosidic linkage between the monosaccharides.

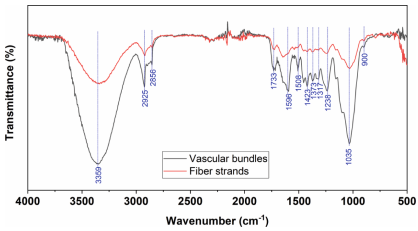


**Fig. 6.** FTIR spectra for (VBs) and (FSs)

**Table 1.** The chemical composition

| Wavenumber range ($cm^{-1}$) | Vibration assignment | Source |
|---|---|---|
| 900 | C–O–C stretching | β -glycosidic linkage in Cellulose |
| 1035 | C–O stretching ring | Cellulose, |
| 1238 | C=O Stretching | Hemicellulose |
| 1317 | CH2 rocking vibration | Cellulose |
| 1373 | C–H deformation vibration | Cellulose |
| 1423 | CH2 bending | Cellulose |
| 1508 | C=C of aromatic skeletal vibration | Lignin |
| 1596 | C=O stretching of carboxylic acid and ester | Lignin |
| 1733 | C=O stretching vibration of the acetyl | Hemicellulose |
| 2856 | CH2 symmetric stretching | Cellulose, Hemicellulose |
| 2925 | CH2 asymmetrical stretching | Cellulose, Hemicellulose |
| 3359 | O–H stretching | Hydroxyl groups |

The peak that appears at 1035 $cm^{-1}$ corresponds to the presence of C–O stretching ring, which belongs to polysaccharide in cellulose (Maache et al. 2017). The wave number at 1238 $cm^{-1}$ corresponds to the C = O stretching groups of hemicellulose. The peaks at 1317 $cm^{-1}$, 1373 $cm^{-1}$, and 1423 $cm^{-1}$ are attributed to the CH2 rocking vibration, C–H deformation vibration and CH2 bending, respectively, groups of cellulose (Amroune et al. 2015). Following two peaks are characteristic of lignin at 1508 $cm^{-1}$ and 1596 $cm^{-1}$ indicate the presence of C = C of aromatic skeletal vibration and C = O stretching of carboxylic acid and ester, respectively (Saaidia et al. 2017).

The peak localized at 1733 $cm^{-1}$ is attributed to the C = O stretching vibration of the ester group in hemicellulose. The two peaks observed at 2856 $cm^{-1}$ and 2925 $cm^{-1}$ are

indicative of the presence of $CH_2$ symmetric stretching and $CH_2$ asymmetrical stretching groups of cellulose and hemicellulose, respectively (Saaidia et al., 2015). The largest absorbance peak at 3359 $cm^{-1}$ corresponds to O–H stretching vibration and hydrogen bond of the hydroxyl groups (Bezazi et al., 2014).

### 3.3 Technical Fibre Tensile Tests

Figure 7a shows the typical stress–strain curves for both VBs and FSs under tensile tests. They exhibit quasi-linear and non-linear behaviour, respectively, until they reach their ultimate stress where a sudden rupture is obtained.

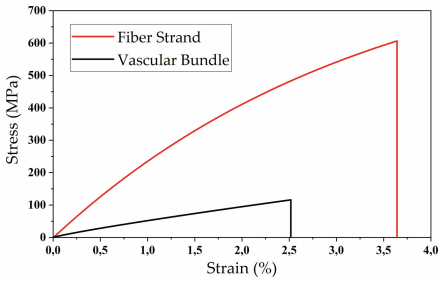


**Fig. 7.** Typical stress–strain curve for VBs and FSs

From the experimental data, the strength, Young's modulus and the strain at failure were determined for VBs and FSs. It was found 129.1 ± 47.3 MPa and 530.5 ± 115.2 MPa for the strength, 5.88 ± 1.84 GPa and 21.90 ± 3.96 GPa for the Young's modulus and 2.67 ± 0.57% and of 3.60 ± 0.95 for the strain at failure, respectively. These results were higher than those obtained from Juncus effusus L. fibres with a strength of 113 ± 36 MPa, strain at break of 2.75 ± 0.68%, and Young's modulus of 4.38 ± 1.37 GPa (Maache et al. 2017). Also, the present results were bigger than were obtained from date palm fruit branches technical fibres which reported 117 ± 35 MPa and 3.13 ± 0.70% (Amroune et al. 2015). The average diameter for VBs and FSs was 520 μm with a standard deviation of 72 μm and 88 μm with a standard deviation of 12 μm, respectively. Consequently, the VBs have a larger fibre diameter than FSs, but the later has higher properties.

The analysis of the curves representing the variation of the tensile properties versus diameter for VBs and FSs, are presented in Fig. 8, which show that the strength, Young's modulus and strain at failure decrease with increasing fibre diameter for both types of fibres. The experimental results reveal that date palm rachis fibres have dispersions in their tensile properties, so a statistical study taken them into account is necessary.

Figure 9 illustrates the 2 and 3 parameters Weibull distributions of the tensile properties obtained from the test data for all the 20 trials carried out for VBs and FSs. The plot helps to estimate statistical parameters such as shape and scale factors of the distribution and also confirms the integrity of the data acquired with the Weibull distribution (Fiore 2014; Maache et al. 2017).

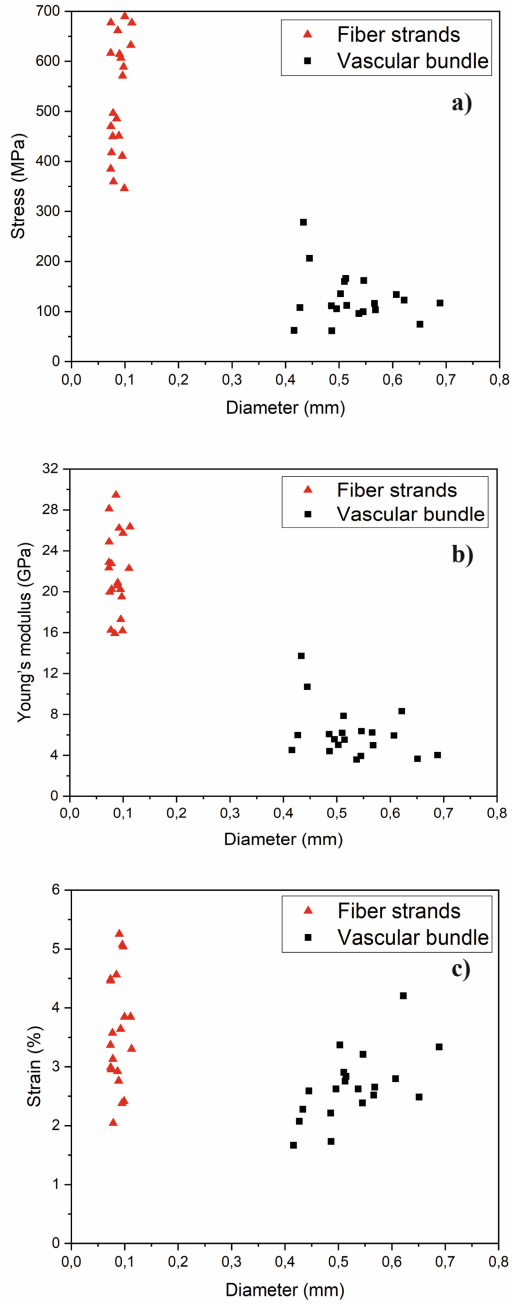


**Fig. 8.** Effect of the fibre diameter on the tensile properties for VBs and FSs: a) tensile strength, b) Young's modulus, and c) strain at break

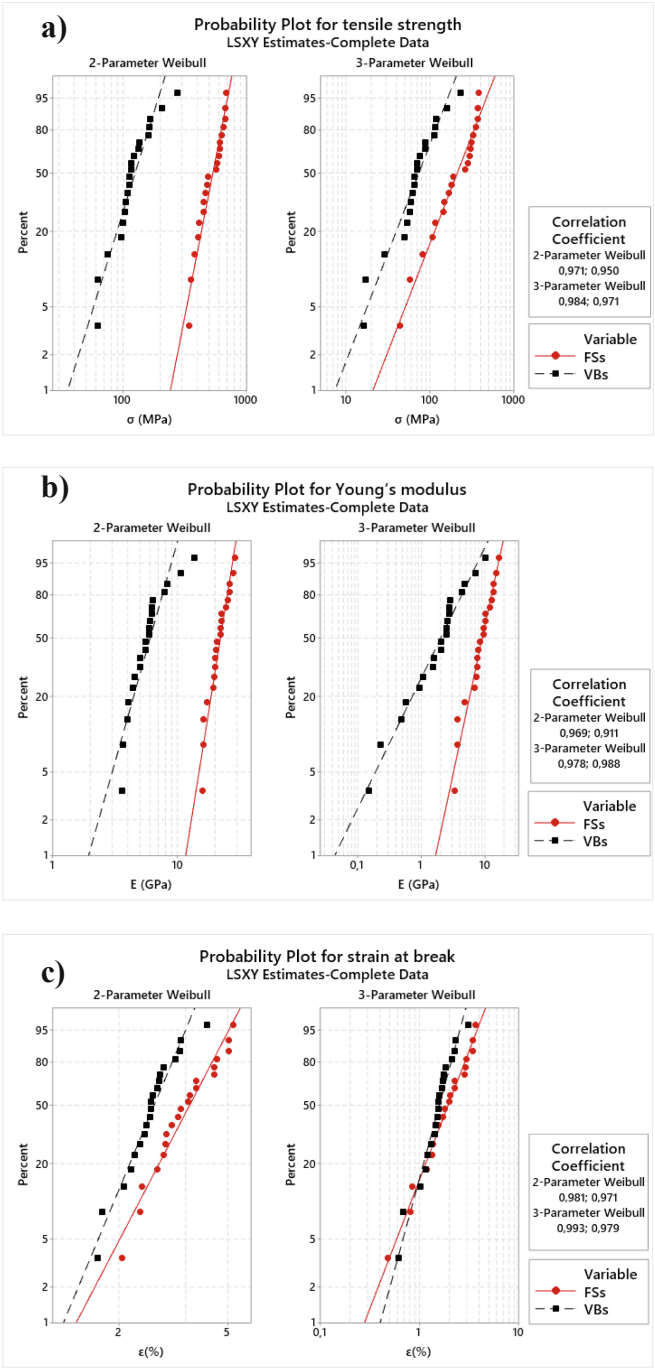


**Fig. 9.** Two-parameter and three-parameter Weibull distribution for VBs and FSs for: a) tensile strength, b) Young's modulus, and c) strain at break

**Table 2.** Tensile properties

| Fibre type | Experimental results | | | 2-P Weibull | | | 3-P Weibull | | |
|---|---|---|---|---|---|---|---|---|---|
| | Σ (MPa) | E (GPa) | Ɛ (%) | σ (MPa) | E (GPa) | Ɛ (%) | σ (MPa) | E (GPa) | Ɛ (%) |
| **VBs** | 129.1 ± 47.3 | 5.88 ± 1.84 | 2.67 ± 0.57 | 125.08 | 6.01 | 2.65 | 126.10 | 6.18 | 2.65 |
| **FSs** | 530.5 ± 115.2 | 21.90 ± 3.96 | 3.60 ± 0.95 | 528.74 | 21.83 | 3.59 | 533.37 | 21.89 | 3.61 |

Also, this analysis allows studying the effect of the variation of fibre diameter on the tensile properties. It can be observed that the experimental values are close to the Weibull lines, the correlation factor varying from 0.911 to 0.981 in 2-parameters Weibull distributions and from 0.971 to 0.993 in 3-parameters one which is closer to 1. This indicates a good agreement between the linear regression of the fibre tensile properties and the experimental results.

The 2-parameter Weibull distribution for VBs and FSs gives a tensile strength of 125.08 MPa and 528.74 MPa, Young's modulus of 6.01 GPa and 21.83 GPa and strain at failure of 2.65% and 3.59%, respectively. While, the 3-parameter one gives for VBs and FSs a strength of 126.10 MPa and 533.37 MPa, Young's modulus of 6.18 GPa and 21.89 GPa and strain at failure of 2.65% and 3.61%, respectively.

The regression coefficients for the 2-parameter Weibull model are slightly lower than those for the 3-parameter one as shown in Table 2. This indicates that the latter one is more suitable for analysing the tensile properties of VBs and FSs. The dispersion of the experimental result obtained is due to the anisotropy of the diameter of the fibres, the lack of their homogeneity, the existence of flaws and their distributions in the fibre or on their surface, and also on the distribution to the number of main voids and their size.

A linear regression model was used to predict ultimate tensile strength and Young's modulus (Table 3) as a function of the diameter of the fibre with $R^2$ predicted about 80% (Fig. 10).

$$\textit{Regression Equation of } \sigma \textit{ (Mpa)} = 597.3 - 873.1 \textit{ (Diameter of the fibre)}$$
$$\textit{Regression Equation of } \mathrm{E} \textit{ (Gpa)} = 24.669 - 34.61 \textit{ (Diameter of the fibre)}$$

**Table 3.** Model summary

| | R-squared | R-sq(adjusted) | R-sq(predicted) |
|---|---|---|---|
| σ (MPa) | 80.74% | 80.24% | 78.73% |
| E (GPa) | 84,37% | 83,95% | 82,72% |

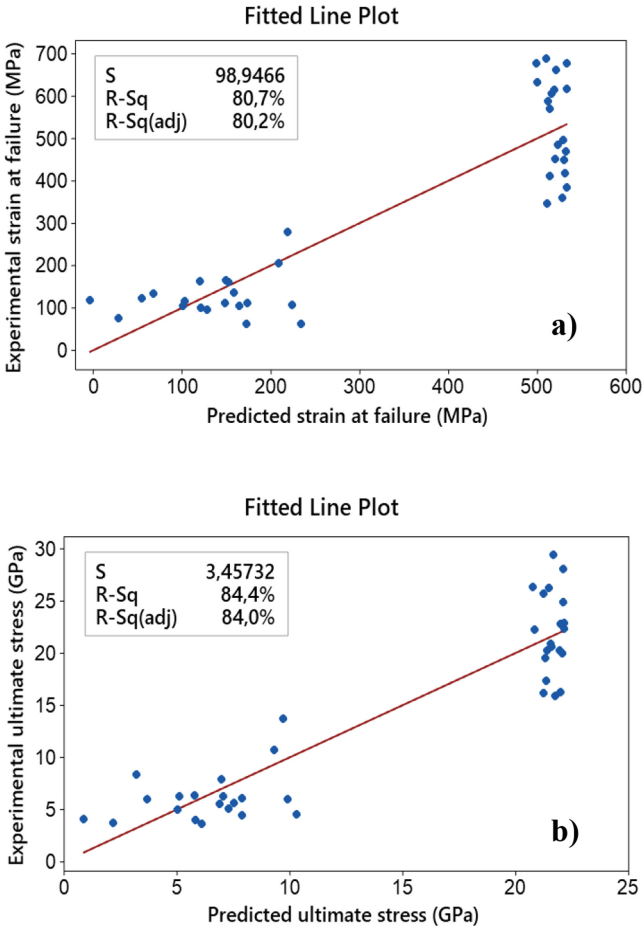


**Fig. 10.** Experimental data vs. predicted data of: a) ultimate tensile strength, b) Young's modulus,

## 4 Conclusions

The extraction and study of the date palm rachis fibres and the examination of their: morphology, chemical and also tensile behaviour lead to the main following conclusions:

- The rachis fibres were extracted without damaging them and two main types of fibres were identified, viz. VBs and FSs.
- The main chemical groups were highlighted by FTIR-ATR spectrum analysis and compared with other lignocellulosic fibres reported in the literature.
- Optical microscopy and SEM observations show that the morphology of VBs consists of microfibrils containing at least one main void between them, while FSs contain only microfibrils aligned and bound together by lignin and other non-cellulosic materials. Besides, the cross-section of the fibres shows their cellular structures.

- The tensile strength and Young's modulus for FSs were found to be at about four times higher than for VBs, while this later has an average diameter almost six times larger than the FSs one.
- The 3-parameter Weibull distribution analysis leads to better results compared to the 2-parameter ones in terms of estimation of the experimental data obtained.
- The linear regression model was used to predict the tensile strength and Young's modulus as a function of the diameter of the fibre with R2 predicted about 80%.
- The date palm rachis fibres have similar characteristics than those of several fibres reported in the literature. The fibre studied shows excellent potential for use as reinforcement for the elaboration of biocomposites in diverse engineering applications such as automobiles, construction and packing.

**Acknowledgements.** The authors gratefully acknowledge the funding by Algerian Ministry of Higher Education and Scientific Research. This study was implemented in the scope of the research project "PRFU: A11N01UN240120190002". The authors would like to thank Mr. Hichem Brahmia & Mr. Mustapha Metiri from ENSMM Annaba for their technical assistance in taking SEM photos.

## References

Agoudjil, B., Benchabane, A., Boudenne, A., Ibos, L., Fois, M.: Renewable materials to reduce building heat loss: characterization of date palm wood. Energy Build. **43**(2–3), 491–497 (2011)

Al-Oqla, F.M., Sapuan, S.M., Ishak, M.R., Nuraini, A.A.: A decision-making model for selecting the most appropriate natural fibre – polypropylene-based composites for automotive applications. J. Compos. Mater. **50**, 543–556 (2015)

Amroune, S., Bezazi, A., Belaadi, A., Zhu, C., Scarpa, F., Rahatekar, S., Imad, A.: Tensile mechanical properties and surface chemical sensitivity of technical fibres from date palm fruit branches (Phoenix dactylifera L.). Compos. Part A Appl. Sci. Manuf. **71**(November), 98–106 (2015)

Belaadi, A., Bezazi, A., Bourchak, M., Scarpa, F.: Tensile static and fatigue behaviour of sisal fibres. Mater. Des. **46**, 76–83 (2013)

Belouadah, Z., Ati, A., Rokbi, M.: Characterization of new natural cellulosic fibre from Lygeum spartum L. Carbohyd. Polym. **134**, 429–437 (2015)

Bezazi, A., Amroune, S., Scarpa, F.: Analyse statistique et effet des traitements chimique sur le comportement physico-mécanique des fibres des bras de grappe des palmiers dattier. Synthèse Revue des Sci. et de la Technologie **31**, 108–120 (2015)

Bezazi, A., Amroune, S., Scarpa, F., Dufresne, A., Imad, A.: Investigation of the date palm fibre for green composites reinforcement: Quasi-static and fatigue characterization of the fibre. Ind. Crops Prod. **146**, 112135 (2020)

Bezazi, A., Belaadi, A., Bourchak, M., Scarpa, F., Boba, K.: Novel extraction techniques, chemical and mechanical characterisation of Agave americana L. natural fibres. Compos. B Eng. **66**, 194–203 (2014)

Biglari, F., AlKarkhi, A.F.M., Easa, A.M.: Antioxidant activity and phenolic content of various date palm (Phoenix dactylifera) fruits from Iran. Food Chem. **107**(4), 1636–1641 (2008)

Bouguedoura, N., Bennaceur, M., Babahani, S., Benziouche, S.E.: Date palm status and perspective in Algeria. In: Date Palm genetic resources and utilization, vol. 11–546 (2015)

Boumediri, H., Bezazi, A., Del Pino, G.G., Haddada, A., Scarpa, F., Dufresne, A.: Extraction and characterization of vascular bundle and fibre strand from date palm rachis as potential bio-reinforcement in composite. Carbohyd. Polym. **222**, 114997 (2019)

Boumediri, H., Bezazi, A., Haddad, A., Saaidia, A., Scarpa, F., Dufrsene, A.: Physico-chemical characterization of date palm leaves (Phoenix Dactylifera-L) of Algeria. In: Ferreira, A.J.M., Viola, E., Tornabene, F., Fantuzzi. N. (eds.) Mechcomp3: 3rd International Conference of Mechanics of Composite, Esculapio, p. 24 (2017)

Bourahli, M.E.H.: Uni-and bimodal Weibull distribution for analyzing the tensile strength of Diss fibres. J. Nat. Fibres **15**(6), 843–852 (2018)

Fiore, V., Scalici, T., Valenza, A.: Characterization of a new natural fibre from Arundo donax L. as potential reinforcement of polymer composites. Carbohydr. Polym. **106**(1), 77–83 (2014)

García del Pino, G., Kieling, A.C., Bezazi, A., Boumediri, H., Rolim de Souza, J., Valenzuela Díaz, F., Luis Valin Rivera, J., Dehaini, J., Hallak Panzera, T.: Hybrid polyester composites reinforced with Curauá fibres and nanoclays. Fibres Polym. **21**, 399–406 (2020)

Jawaid, M., Abdul Khalil, H.P.S.: Cellulosic/synthetic fibre reinforced polymer hybrid composites: a review. Carbohydr. Polym. **86**(1), 1–18 (2011)

Maache, M., Bezazi, A., Amroune, S., Scarpa, F., Dufresne, A.: Characterization of a novel natural cellulosic fibre from Juncus effusus L. Carbohydr. Polym. **171**, 163–172 (2017)

Mhatre, A., Raja, A.S.M., Sujata, S., Patil, P.G.: Environmentally benign and sustainable green composites: current developments and challenges. In: Green Composites, pp. 53–90. Springer, Singapore (2019)

Saaidia, A., Bezazi, A., Belbah, A., Amroune, S., Scarpa, F.: Evaluation of mechanical properties of jute yarns by two-and three-parameters weibull method. Struct. Integrity Life-Integritet I Vek Konstrukcija. **15**, 157–162 (2015)

Saaidia, A., Bezazi, A., Belbah, A., Bouchelaghem, H., Scarpa, F., Amirouche, S.: Mechano-physical properties and statistical design of jute yarns. Measurement **111**, 284–294 (2017)

Saba, N., Jawaid, M., Alothman, O.Y., Paridah, M.T., Hassan, A.: Recent advances in epoxy resin, natural fibre-reinforced epoxy composites and their applications. J. Reinf. Plast. Compos. **35**, 1–24 (2015)

# Study of the Mechanical Behavior of a Reactive Powder Concrete Containing Fibers

M. Chadli[1(✉)], N. Tebbal[2], and M. Mellas[1]

[1] Laboratory of Civil Engineering, Department of Civil Engineering and Hydrology, University of Biskra, BP 145 RP, Biskra 07000, Algeria
mounira.chadli@univ-biskra.dz

[2] Institute of Technical Urban Management, Geomaterials Development Laboratory, University of M'sila, M'sila, Algeria

**Abstract.** The reactive powder concretes (RPC) are new concretes with a particle diameter of not more than 600 μm and very high compressive, tensile strengths and an excellent durability. In this experimental investigation we study this new generation of micro-concretes, in obtaining high initial and final mechanical performances using local materials. The Portland cement, materials rich in silica (slag, silica fume and quartz) and new steel fibers' aspect ratios has been reinforced the concrete RPC. Specimens' preparation, curing regimes and testing procedures to evaluate the effect of heat treatment, steel fiber percentage compressive strength, flexural strength, deformability and modulus of elasticity of RPCFs were discussed. A compressive strength of 134 MPa, indirect tensile strength of 2.7 MPa, heting temperature of 90 °C, 2.5% steel fiber have been achieved for reinforced RPC contains 945 kg/m$^3$ cement content and silica fume content 30% of cement weight. Also, the relationship between the relative value and the modulus of elasticity developed for a fiber-reinforced reactive concrete is greater than that of the unbound fiber. By eliminating the granular phase in the RPC and the abundance of dune sand (southern Algeria) and granulated slag, the use of RPC in Algeria with local materials meets economic and ecological requirements.

**Keywords:** Reactive powder concrete · Mechanical strength · Fibers · Deformability · Elasticity modulus

## 1 Introduction

The high-performance fibered concretes HPFC are very compact and high-strength materials. Due to its excellent properties, UHPC has been widely used as an overlay to repair existing concrete structures, improving its mechanical and durability properties for lesser maintenance work (Azmee and Shafiq 2018). UHPC are cementitious matrix materials with compressive strengths greater than 150 MPa. These materials are supplemented with metal fibers (UHPCF) in order to obtain a ductile behavior in tension. They are also characterized by their strong binding and special selection, the aggregates of which


B. Safi et al. (Eds.): ISMSD 2019, *Proceedings of the 4th International Symposium on Materials and Sustainable Development*, pp. 71–82, 2020.
https://doi.org/10.1007/978-3-030-43211-9_7

are the subject from the point of view of their formulation Shin et al. (2017). Reactive powder concrete (RPC) is a type of

UHPC is distinguished by its compressive strengths ranging between 200 MPA and 800 MPA after pressure and heat treatment, depending on the mixture proportions and the temperature Ye et al. (2018). Also, Ultra-High Performance Fiber Reinforced Concretes (UHPFRC) are cementitious composites with outstanding material properties they have very high strengths (compressive strength > 150 MPa, tensile strength > 8 MPa) Somasekharaiah et al. (2015). The fibers are added to the concretes to increase the tensile strength and to give a ductile character to the fragile concretes by nature. In general, metal, synthetic, glass or vegetable fibers can be incorporated into the concrete. As far as the UHPC is concerned, they may be metallic or organic in nature. Some organic fibers can also increase the fire resistance of UHPCs (Snigdha and Visweswara 2016). Inactive states, have been used in disposal of heavy

Nowadays, studies into concrete durability are no longer limited to a single environment but can be performed taking multiple factors into consideration. Curing plays an important role on strength development and durability of concrete. (Yan and Cui 2015) investigated the influence of a hot spring curing environment on the performance of concrete. This study revealed found that curing temperatures of above 50 °C significantly stimulate the reactivity of cement, through the grinding of fine slag powder and cement, fly ash, silicon ash composite, and gelled material. The Tang et al. (2016) research's demonstrates that the temperature of the environment affects the bond strength and pore structure of concrete support assemblies during construction and early stages. When a given performance is required, the influence of heat curing on the concrete properties must be considered during the concrete design process, because heat can influence the microstructural and durability properties of the concrete García et al. (2016).

Although the limited use of fiber reinforced concrete, there is still debate within the industry as to the benefits they offer. Steel fibers are presently used to good effect in many engineering applications however temperature changes the physical characteristics of the fibers and the composite matrix of fibers and concrete. This paper examines the relationship between fiber performance and curing temperature.

## 2 Research Significance

The purpose of this work is to study some mechanical resistances of reactive powder concrete (RPCC) including compressive, tensile strength of plain reactive powder concrete and reactive powder concrete reinforced with 2.5% steel fiber (RPCF1), by using local available material and curing in 20 °C and 90 °C. This research provides data for the researchers concerning with the main properties of RPC manufacturing using economical available materials.

## 3 Experimental Methods Procedure

### 3.1 Materials

In this study, Portland cement, Quartz powder, Silica fume, granulated Slag, fine sand finely Metal fibers superplasticiser and water available around Biskra area (Algeria) were used for the development of RRPC mix and for the entire tests.

Cement (C): The cement used in this study was Portland cement CEM I 42.5N from the cement plant Enfidha (Tunisia), in conformity with the standard NF EN 197-1. The used cement type has an absolute density, consistency and fineness values of 3.02 g/cm$^3$, 23% and 3714 cm$^2$/g respectively.

Quartz powder (QB): In this sand type quartzes almost the sole component of sand. Similar sandstones are called quartz arenites or orthoquartzites. It is maximum reactive during heat treatment. Its particle size ranges from 10 to 15 μm is made up basically of silicon dioxide ($SiO_2$). It density and surface area were 2.63 g/cm$^3$ and 5714 cm$^2$/g respectively.

Silica fume (SF): A highly reactive silica pozzolan is an essential component of reactive powder concrete. Silica fume is a gray powder from Sika Algeria. The particle size was 0.1 μm lower, the $SiO_2$ content 94% and the bulk density 1560 kg/ m$^3$.

Slag (GS): The granulated slag of the blast furnace come from metallurgical complex (El-hajar) of Annaba (Algeria). Its density and surface area were 2.60 g/cm$^3$ and 7277 cm$^2$/g respectively. The chemical compositions of cement, silica fume, slag and quartz powder are given in Table 1.

**Table 1.** Chemical Compositions of Cement, Silica Fume, Slag and Qquartz Powder (%)

| (%) | $SiO_2$ | $Al_2O_3$ | $Fe_2O_3$ | CaO | MgO | $K_2O$ | $SO_3$ | $Cl^-$ | $Na_2O$ | Loss on ignition |
|---|---|---|---|---|---|---|---|---|---|---|
| C | 20.62 | 4.31 | 4.94 | 63.24 | 2.01 | 1.1 | 1.85 | 0.003 | 0.27 | 1.86 |
| SF | 94 | 1 | 1 | 0.4 | 1 | – | 1.5 | 0.06 | 0.6 | – |
| GS | 35.88 | 8.38 | 0.56 | 30.96 | 4.54 | 0.62 | 1.55 | 0.01 | 0.41 | 2.79 |
| QB | 94.33 | 1.171 | 1.044 | 1.62 | 0.184 | 0.386 | 0.04 | 0.012 | 0.001 | |

Sand (S): Sand should be of good hardness, readily available and low cost. The fine aggregate used in the experimental program was the dune sand (River Djamaa region, El Oued Province (Algeria). Its particle size ranges from 0.15 mm to 0.6 mm according to the European standard (NF EN 933-1). Its apparent bulk, bulk density, finesses modulus and sand equivalent were 1.57 g/cm$^3$, 2.626 g/cm$^3$, 1.98 and 74.90% respectively.

Metal fibers (MF): The steel fibers used in this investigation are crimped metal fibers of 50 mm length with a diameter of 1.05 mm. Throughout the experimental program, number of fiber is 2800 fiber/kg and tensile strength is 1000 MPa/line of fiber were used.

Super plasticizer (SP): In this study a high performance super plasticizing admixture based on acrylic copolymer (SIKA VISCOCRETE TEMPO 12) has been used. It can be used with all types of Portland cement to achieve highest concrete durability and performance according to the standars NF EN 934-2. The main properties are shown in Table 2.

Water: Ordinary drinking (tap) water was used for concrete mixes.

**Table 2.** Characteristics of superplasticizer

| Aspect | Density | Ph | $Na_2O$ content | Extract dry |
|---|---|---|---|---|
| Light brown liquid | 1,06 ± 0,01 | 6 ± 1 | ≤ 1% | 30,2 ± 1,3% |

### 3.2 Test Preparation and Heat Treatment

The investigated mixes were prepared depended on the original mix of reactive powder concreter coined by the inventors (Richard and Cheyrezy 1994), the mix proportions by ($kg/m^3$) are shown in Table 3.

**Table 3.** Mix proportions ($kg/m^3$)

| Mix | C | SF | QB | GS | S | SP/C | W/C | MF (% volume of concrete) |
|---|---|---|---|---|---|---|---|---|
| RPCC | 955 | 219.65 | 219.65 | 143.25 | 1050.5 | 47.75 | 0.20 | – |
| RPCF1 | 945 | 217.35 | 217.35 | 141.75 | 1039.5 | 17.01 | 0.21 | 2.5 |

**RPCC:** Reactive powder concrete without *fibers;*
**RPCF1:** Reactive powder concrete containing *fibers.*

The procedure of mixing can be summarized as follows:

1. Mixing of all dry materials;
2. Addition of about 75% of total water + 50% of superplasticizer;
3. About 5 min, mixing the components;
4. Addition of the remaining liquid quantity (25% of total water + 50% of super plasticizer);
5. Addition of steel fibers;
6. Further mixing for about 5 min.

### 3.3 Mechanical Testing Method

*Compression and Flexural Tensile Strengths:* Prismatic test pieces with dimensions 40 mm × 40 mm × 160 mm were used for the 3 point bending tensile test and the half-test pieces obtained after failure were tested in compression according to standard NF EN 196-1. To determine the average compressive strength, three cubes of each concrete mix are tested after 7, 14 and 28 days, testing under compression testing machine of 180 tones capacity.

– *Curing:* All samples were curing in two conditions:

1. Room temperature at 20 °C,
2. Steam curing: at 20 °C for 1 day,

3. Then at 90 °C in oven 2 day finally at 20 °C up to 28 day.

- *Deformability and modulus of elasticity:* The deformability test was performed on prismatic samples 100 mm × 100 mm × 400 mm at 28 days of age. Increasing forces were applied on the concrete specimen, and the corresponding deformations were measured up to the value of the breaking load Pc, previously measured. The longitudinal and transversal deformations of the crushed sample were measured using the nonstandard equipment following the method exposed by Mezghiche (1996).
- *The shrink swell test:* The measurement of shrinkage was carried out on prismatic specimens of dimensions 40 mm × 40 mm × 160 mm, according to the standard NF P-15-433. These specimens are provided with metal pads on each end and placed vertically in the deformeter which allows monitoring the change in the sample length. Shrinkage of concrete is measured, on a daily basis, after unmolding.

## 4 Results and Discussion

### 4.1 Effect of Steel Fiber Percentage

The used steel fiber percentage is 0 and 2.5%. The effect of this parameter could be observed by studying the hardened properties of mixes RPCC, and RPCF1. Figure 1 shows that the effect of steel fiber on the compressive strength at 7 days, 14 days and 28day age at the presence content. It can be observed that from both treatments environment (with heat treatment 90 °C or at 20 °C) the increasing of steel fiber content from 2.5% increased the compressive strength about 20% at early age 7 days. The average flexural strength of RPCF1with 2.5% steel fibers increase about 6.25, 9 and 18% respectively, compared to mix RPCC without steel fiber (see Fig. 2). The presence of steel fiber percentage from 2.5% caused to significant increase of mechanical strength by 20%. On the other hand, the mechanical strength results of mix containing 2.5% steel fiber comparing to mix without steel fiber were very slightly enhanced about 20%. Figures 1 and 2 demonstrates the effect of increasing the steel fiber content by total volume of RPC on the consistency; it is clear that increasing steel fiber percentage's increases the mechanical strength. This is due to the increased density and cohesion of the mixture. The density of RPC increased when the steel fiber content increases to 2.5%with heat treatment at 90°Cand the pozzolanic reaction, well packing in between cement particles and the densifying of the microstructure that provided by silica fume and slag, could interpret this behavior.

These results correspond to results of Gamal et al. (2019), Benamara et al. (2019), Belouadah et al. (2017).

### 4.2 Effect of Curing Condition

An adequate supply of moisture is necessary to ensure that hydration is sufficient to reduce the porosity to a level such that the desired strength can be attained. The effect of

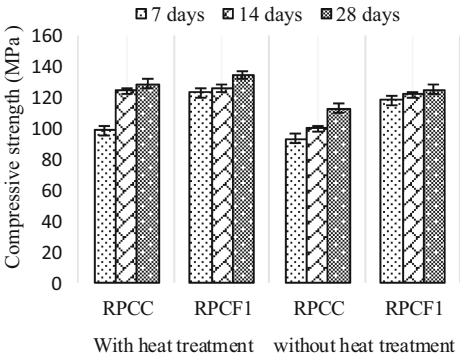


**Fig. 1.** Evolution of the compressive strength of concretes as a function of heat treatment.

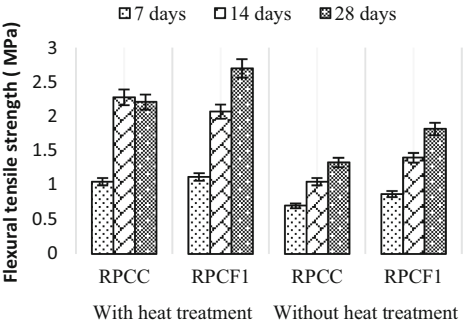


**Fig. 2.** Evolution of the flexural tensile strength of concretes as a function of heat treatment

curing regime on compressive strength under various curing ages is shown in Figs. 1 and 2. The effect of curing condition could be observed by studying the mechanical properties of mixes RPCC and RPCF1, which correspond to two different curing conditions; were normal water curing at 20 °C and hot curing at 90 °C for 2days, also both these mixes containing on constant content of silica fume which were 23% SF.

It can be observed that from Fig. 1, the temperature of curing has significant effect on compressive strength of tested specimens at different ages. The highest effect at age 7 days, where the compressive strength 7 days increased by 20%, and 21% when the temperature of curing water was increased from ambient temperature to 20 °C, 90 °C respectively.

At age 14 days, the corresponding percentages increasing where 4%, 19.89% when the temperature of curing water was increased from ambient temperature to 20 °C and 90 °C respectively. Also, at age 28 days, the corresponding percentages increasing where 7.18% and 12.57%, when the temperature of curing water was increased from ambient temperature to 20 °C and 90 °C, respectively.

The flexural strength results are shown in Fig. 2. It shows that the flexural strength of concrete mix also increases with strength for mixes which curing in hot water 90 °C

for one day which were increases by 32.7%, and 39.3%respectively in comparison with mix curing in normal water 25 °C.

For comparison between the two curing systems, results indicated that RPCF1 system, which included hot treatment curing at 90 °C, had more effect on strength development at 7 days age than later ages. This might be as a result of temperature increase which speeded up the reactions, and consequently the hydration products formation, and led to increasing the early strength. Similar behavior was also found in the literature (Hasan and Arel 2016). These results can be explained by:

- The presence of silica fume combined with granulated slag and water content share the greatest effects on reaching compressive strength targets Tebbal et al. (2016). A more effect of steel fibers can be noticed, as the steel fibers content increased from 2.5% and 23% silica fume with 15% of granulated slag content can be increased from 20% to 21% to keep the strength in the designed target range. The mix RPCC with no steel fiber has high silica fume content of 23% and a less W/C ratio is used to get a compressive strength of 128.32 MPa. The effect of silica fume combined with slag and steel fibers on reactive powder properties were examined, and the gain of cement additions can be noticed not only by its pozzolanic effects but by increasing mix density and enhancing the bond strength between the fine materials and the steel fibers Tebbal et al. (2016), Tang et al. (2016).
- Two curing methods were exercised, one with normal water curing at 20 °C, and other at 90 °C system curing for 48 h. The compressive strength increased by 20% when cured in oven as compared to normal curing. This indicates that curing temperature has a significant effect on the early strength development of RPC. The increased strength is due to the rapid hydration of cement at higher curing temperatures of 90 °C compared to that of 20 °C. Moreover, the pozzolonic reactions are also accelerated by the higher curing temperatures.

XRD patterns of the concretes RPCC are shown in Figs. 3 and 4. The results reveal that the peak of $C_4AH_{13}$ was detected in all the samples and the intensity of its peak sharply increases with the increasing of silica fume content. On the other side, the CSH peaks are intensified with available increase indicating more dense structure and large amounts of additional CSH in the presence of 25 wt% silica fume and 10% of slag. $CaCO_3$ peaks were detected in all the samples. In addition, quartz peaks were also detected as a main constituent of silica fume.

### 4.3 Deformation Modulus *and Elasticity Modulus*

Figure 5 indicates that the deformation modulus decreases as the relative stress increases. The concrete deformation modulus, with the addition of 25 per cent SF, has a higher deformation modulus compared with that of control concrete, and this is in accord with Guettala and Mezghiche (2011); Adnan and Rodger (2013).

Figure 6 shows that the concrete RPCF1 has a modulus of elasticity higher than that of RPCC concrete.

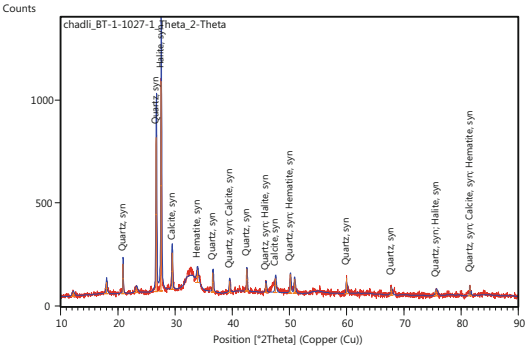


**Fig. 3.** X-ray diffraction diagram of concrete RPCC of 20 °C heat treatment

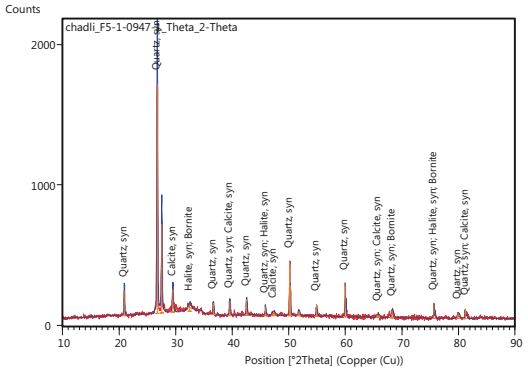


**Fig. 4.** X-ray diffraction diagram of concrete RPCC of 90 °C heat treatment

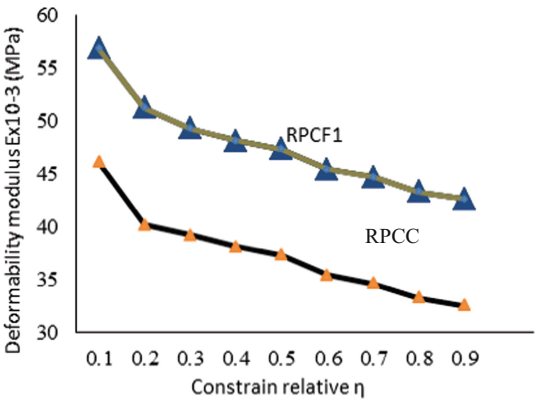


**Fig. 5.** Strain modulus E of concrete as a function of relative stresses η for the series of prisms RPCC and RPCF1

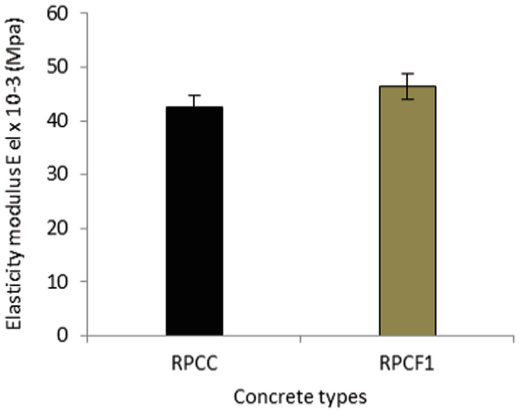


**Fig. 6.** Elasticity modulus of concretes RPCC and RPCF1

### 4.4 The Shrink Swell Result

The Fig. 7 present influence of the nature of additions on concrete shrinkage as a function of time. The results show that:

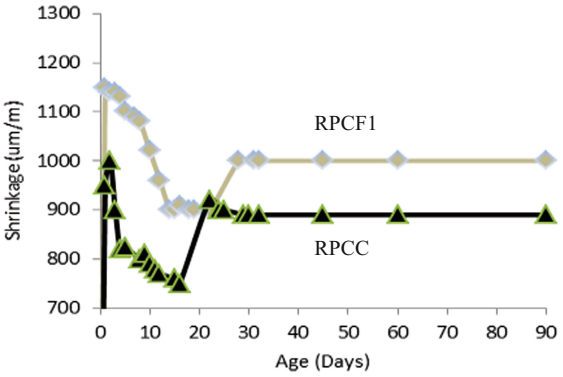


**Fig. 7.** Shrinkage of concretes RPCC and RPCF1

In the first phase, a rapid shrinkage of 1,000 mm/m is observed, during the first three days, for an RPC without metal fibers (RPCC). This shrinkage was 1,150 mm/m for RPCF1 with **W/C = 0.21**. Note that shrinking decreases when the ratio W/C drops from 0.21 to 0.20. Therefore, concrete without fibers has lower shrinking compared with the one containing fibers, at different ages. A rapid decrease in the volume is observed, for all three samples.

– The second phase, between 3 and 20 days, is the swelling phase;
– The third phase, from 20 to 45 days, is the second phase of shrinking in the hardened state;

– Finally, the last phase, beyond 45 days, is represented by the stable part of the curve, where the volume change of the sample continues in the hardened state. The deformation magnitude in concretes with quartz is more important, and this is in accord with Shamsad et al. (2014).

The analysis of the swelling curve (Fig. 8) shows that the swelling kinetics exhibits a trend similar to that of shrinkage.

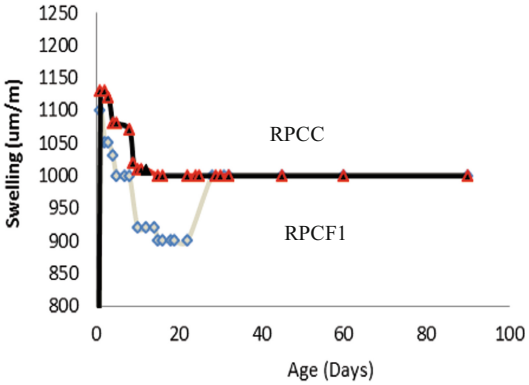


**Fig. 8.** Swelling of concretes RPCC and RPCF1

## 5 Conclusions

The following conclusions based on the results and discussions presented in this study are given below.

1/ The heat treatment and the presence of metal fibers are the major parameters making it possible to obtain high mechanical performances, both in flexion and in compression.

2/ Cement of class CPA42.5 with dune sand, silica-rich fine additions, very low W/C ratio, metal fibers, and heat-treated at temperatures higher than 90 °C, can give exceptional performance to concrete.

3/ Resistance in flexion but it contribute significantly to obtaining high compressive strengths.

4/ The conservation conditions have great impact on the properties of concrete. When it is not protected, it loses its water through evaporation and strength is significantly reduced. Therefore, the internal moisture of concrete varies with the environmental conditions. However, total water retention would be required to have a relatively impermeable concrete, i.e. 100% moisture content.

5/ It is possible to manufacture RPCFs with compressive strength exceeding 140 MPa (at 28 days), with an adequate plasticity, despite the simplicity of means and materials,

6/ Incorporation of the metal fibers into the RPCF cause a good increase in bending tensile strength.

7/The elasticity modulus of cured concrete depends on its mechanical strength. Moreover, the factors affecting the modulus of elasticity are similar to those impacting the strength of concrete. The concretes without fibers have smaller shrinkage deformations compared with those containing fibers. The kinetics of shrinkage and swelling is inversely proportional to the amount of fibers added.

## References


Azmee, N.M., Shafiq, N.: Ultra-high performance concrete: From fundamental to applications, Case Studies in Construction Materials, vol. 9, December 2018

Shin, H.O., Min, K.H., Mitchell, D.: Confinement of ultra-high-performance fiber reinforced concrete columns. Compos. Struct. **176**, 124–142 (2017)

Li, Y., Tan, K.H., Yang, E.-H.: Influence of aggregate size and inclusion of polypropylene and steel fibers on the hot permeability of ultra-high performance concrete (UHPC) at elevated temperature, Constr. Build. Mater. **169,** 629–637 (2018)

Somasekharaiah, H.M., Sajjan, M., Mandela, N.: A study on fiber reinforced high performance concrete using multiple mineral admixtures. Int. J. Res. Eng. Technol. **04**(10), 415–418 (2015)

Malya, S., Visweswara Rao, V.K.: A study on the mechanical properties of reactive powder concrete using granite. Int. J. Innov. Res. Sci. Eng. Technol. **5**(11), 19934– 19944 (2016)

Yan, P.Y., Cui, Q.: Effects of curing regimes on strength development of high-strength concrete. J. Chin. Ceram. Soc. **43**(2), 133–138 (2015)

Tang, Y., Xu, G., Lian, J., Su, H., Qu, C.: Effect of temperature and humidity on the adhesion strength and damage mechanism of shotcrete-surrounded rock. Constr. Build. Mater. **124**, 1109–1119 (2016)

García Calvo, J.L., Alonso, M.C., Fernández, Luco L., Robles Velasco, M.: Durability performance of sustainable self-compacting concretes in precast products due to heat curing. Constr. Build. Mater. **111**, 379–385 (2016)

NF EN 197-1: Cement—Part 1: Composition, Specifications and Conformity Criteria for Common Cements, April 2012

NF EN 933-1, 2006. Essais pour déterminer les caractéristiques géométriques des granulats - Partie 1: Détermination de la granularité - Analyse granulométrique par tamisage (2006)

NF EN 934-2,2012. Adjuvants pour béton, mortier et coulis –Partie 2: Adjuvants pour bétons –Définitions, exigences, conformité, marquage et étiquetage (2012)

Richard, P., Cheyrezy, M.: Composition of reactive powder concrete. Cem. Concr. Res. **25**(7), 1501–1511 (1995)

NF EN 196-1: Méthodes d´essais des ciments, Partie 1 : Détermination des résistances mécaniques

Mezghiche, B.: Résistance et déformabilité des bétons basiques, Actes du Premier Séminaire National En Génie Civil, pp. 86–93 (1996)

NF P15-433 Février 1994, Méthodes d'essais des ciments - Détermination du retrait et du gonflement

Gamal, I.K., Elsayed, K.M., Makhlouf, M.H., Alaa, M.: Properties of reactive powder concrete using local materials and various curing conditions. EJERS, Europ. J. Eng. Res. Sci. **4**(6), June (2019)

Benamara, D., Tebbal, N., Rahmouni, Z.E.A.: Durability of high performance sandcretes (HPS) in aggressive environment. Adv. Concr. Constr. **8**(3), 199–206 (2019)

Belouadah, M., Rahmouni, Z., Tebbal, N.: Effects of glass powder on the characteristics of concrete subjected to high temperatures. Adv. Concr. Constr. **6**(5), 311–322 (2017)

Arel, H.S.: Effects of curing type, silica fume fineness, and fiber length on the mechanical properties and impact resistance of UHPFRC. Results Phys. **6**, 664–674 (2016)

Tebbal, N., Rahmouni, Z., Belagraa, L.: Combined effect of granulated slag and silica fume on the characteristics of high performance concrete. Int. Rev. Civil Eng. (I. RE. CE) **7**(2), 41 (2016)
Yang, T., Su, H., Huang, S., Qu, C., Yang, J.: Effect of curing temperature on the durability of concrete under highly geothermal environment. Advances in Materials Science and Engineering, volume Article ID 7587853, 9 pages (2017)
Guettala, S., Mezghiche, B.: Influence de L'addition Du sable de dune en poudre au ciment sur les propriétés des bétons. Europ. J. Environ. Civil Eng. Taylor Francis **15**(10), 1483–1507 (2011)
Adnan, A.S., Rodger, E.: Behaviour of masonry wallettes made from a new concrete formulation under combination of axial compression load and heat exposure: experimental approach. Eng. Struct. **48**, 193–204 (2013)
Shamsad, A., Ahmed, Z., Mohammed, M.: Effect of the key mixture parameters on shrinkage of reactive powder concrete. Sci. World J. **2014** (2014)

# Effect of Initial Suction on the Hydraulic Properties of an Algerian Waste Landfill Lining

A. Demdoum[1,4(✉)], H. Souli[2], R. Anlauf[3], E. G. Daheur[4], and I. Goual[5]

[1] Department of Hydraulics and Civil Engineering, University of Ghardaïa, BP 455, 47000 Ghardaïa, Algeria
btp.dem@gmail.com

[2] Laboratory of Tribology and Dynamic of Systems, National Engineering School of Saint Etienne, 58 Rue Jean Parot, 42023 Saint Etienne Cedex, France

[3] Faculty of Agricultural Sciences and Landscape Architecture, University of Applied Sciences, Osnabrueck, Germany

[4] Laboratory of Mathematical and Applied Science, University of Ghardaïa, BP 455, 47000 Ghardaïa, Algeria

[5] Department of Civil Engineering, Amar Telidji University, Laghoua, Algeria

**Abstract.** This article investigates the relationship between the initial matric suction and hydraulic conductivity (saturated and unsaturated) and the water retention curve were controlled during a laboratory test. Three materials were used during this study: bentonite and two types of geomaterials (tuff and crushed sand) for use as landfill liners. First, the mixture of 10% bentonite - 20% crushed sand - 70% tuff was selected on the basis of the minimum saturated hydraulic conductivity ($k_{sat}$) by oedometric and triaxial tests. The results showed that the effect of the initial variation in suction from 0.4 MPa to 1.5 MPa does not make a difference in the $k_{sat}$ values; the values are between $10^{-8}$ m/s and $10^{-11}$ m/s. Then, the effect of the initial suction on the water retention curve was studied using suction control methods. The water retention curves showed that the air entry value (AEV) increases with decreasing initial water content and that an AEV for micropores is about 40 MPa for all curves. The unsaturated hydraulic conductivity ($K_w$) study with different initial suction was measured with an original vapor equilibrium technique (VET). The results showed that the $K_w$ varied between $3 \times 10^{-17}$ m/s and $4 \times 10^{-15}$ m/s in all cases of the initial suction over a 90-day period. In addition, the Van Genuchten hydraulic conductivity model is compared to the experimental results. Results measured showed a high affinity with the Van Genuchten model. This allows a $k_w(s)$ function to be established over a large range of suction. Finally, the effect of the initial suction on the saturated and unsaturated hydraulic conductivity of this mixture is not apparent for the much lower ($Sr > 80\%$, $k = k_{sat}$) and very high suction values, respectively.

**Keywords:** Water Retention Curve (WRC) · Tuff (T) · Bentonite (B) · Crushed Sand (CS) · Hydraulic conductivity


B. Safi et al. (Eds.): ISMSD 2019, *Proceedings of the 4th International Symposium on Materials and Sustainable Development*, pp. 83–92, 2020.
https://doi.org/10.1007/978-3-030-43211-9_8

## 1 Introduction

Compacted bentonite-soil mixtures have been preferred as suitable hydraulic barrier materials for landfill liners. At first, the unsaturated state at the time of application of this lining undergoes a very strong suction, especially in geographical zones with arid and semi-arid climatic conditions. Therefore, the suction of this mixture is a fundamental factor in influencing hydraulic properties. Thus, in order to fully understand the behavior and ensure the reliability of the disposal system required for geoenvironmental protection, the saturated and unsaturated hydraulic conductivity ($k_w$) must be thoroughly studied (Iravaniana 2015). As a general rule, the hydraulic conductivity of landfill liners must be less than or equal to $10^{-9}$ m/s (Demdoum et al. 2018).

Laghouat geology area, located in southern Algeria, is composed of very thick of the marl- calcareous rock complex at the base and tuff calcareous crust grouping at the upside (from about 20 cm to around 2 m). Demdoum et al. (2017a, b) show that the saturated hydraulic conductivity ($k_{sat}$) of this tuff by the falling-head parameter is 3.04 $\times 10^{-8}$ m/s. This value is similar to one found by Abeele et al. (1981) for the tuff of Los Alamo's zone (New Mexico-États-Unis). The results of Abeele et al. (1981) indicated that the unsaturated hydraulic conductivity ($k_w$) of crushed Bandelier tuff under matric potential of 195 kPa and a degree of saturation of 22.3%, gives a hydraulic conductivity value of about 5.13 $\times 10^{-11}$ m/s. All the above advantages make these local materials a good choice for use in soil liner engineering.

This paper presents experimental results of saturated hydraulic conductivity by oedometer tests and Water Retention Curves (WRCs) of an optimal mixture of bentonite (B)-crushed sand (CS)-tuff (T), by osmotic measurements under suction between (50–800 kPa) and measurements in vapor equilibrium under strong suction (2.7–348 MPa) with different initial water content (IWC). As the vapor equilibrium method has been proven to be a reliable estimate of the unsaturated hydraulic conductivity ($k_w$) (Gueddouda et al. 2016), the unsaturated hydraulic conductivity ($k_w$) was measured by this method. The results of the unsaturated hydraulic conductivity ($k_w$) tests were compared with the Van Genuchten model to make them more meaningful. The objective of this study is to valorization local Algerian materials for their use as soil linings in landfills.

## 2 Materials and Methods

Three primary materials were used in this study. The first material is Maghnia bentonite (Telmcen, Western Algeria), which is extracted by the Algerian bentonite company - Known as BANTAL. Table 1 summarizes the fundamental physico-chemical characteristics of Maghnia bentonite. The second material is tuff, available in the Laghouat region of southern Algeria (semi-arid area). The tuff was extracted from a Cretaceous age deposit. It is often used in the construction of road platforms. According to USCS classification, the tuff can be classified as silty sands (SM) (see Table 1). The third material is crushed sand, a residue from limestone rock crushing stations located in the north of the Laghouat region (see Table 1). According to USCS classification, the crushed sand can be classified as well graduated clean sands (SW) (see Table 1).

Five mixtures were selected for experiments. For each mixture, the percentage of bentonite is fixed at 10%. The mixtures are named $B_{10}CS_XT_Y$, where X and Y are the

**Table 1.** The physico-chemical characteristics of the bentonite, crushed sand and tuff.

| Parameter | Maghnia bentonite | Crushed sand (CS) | Tuff (T) | Standard used |
|---|---|---|---|---|
| $\Phi \leq 80\mu m$ (%) | 86.00 | 11.50 | 18.00 | NF P94-056 and NF P 94-057 |
| $\Phi \leq 2$ mm (%) | 100.00 | 67.80 | 85.46 | |
| *Cu* | / | 18.80 | 6.57 | |
| *Cc* | / | 2.30 | 0.40 | |
| $\gamma_{dmax}(g/cm^3)$ | 1.20 | 1.95 | 1.72 | NF P 94-093 |
| OWC (%) | 32.50 | 8.75 | 13.85 | NF P 94-093 |
| SE (%) | / | 70 | 30 | EN 933-8 + A1 |
| $S(m^2/g)$ | 462 | 7 | 17 | NF P 94-068 |
| LL(%) | 141 | 17 | 33 | NF P 94-051 |
| PL (%) | 48 | – | 25 | |
| PI (%) | 93 | / | 8 | |
| pH | 10.30 | 9.32 | 7.65 | ASTM D4972 |
| $CaCO_3$ (%) | 5 | 55 | 66 | NF P 94-048 |
| $CaSO_4$, $2H_2O$ (%) | 0 | 0.52 | 0.46 | NF EN 1744-1 |

Symbols of Table 1, *Cu*: uniformity coefficient, *Cc*: coefficient of curvature, $\gamma_{dmax}$: dry density, *OWC*: optimum water content, *PL: plastic limit, LL*: liquid limit, *PI*: plasticity index, *S:* surface area, *SE*: sand equivalent, $CaSO_4$, $2H_2O$: gypsum.

percentages of crushed sand and tuff used complementary to 90%. The mixtures that have been used during experiments are as follows: Mixture (1) ($B_{10}CS_{10}T_{80}$); Mixture (2): ($B_{10}CS_{20}T_{70}$); Mixture (3): ($B_{10}CS_{30}T_{60}$); Mixture (4): ($B_{10}CS_{45}T_{45}$): Mixture (5) ($B_{10}CS_{60}T_{30}$).

The hydraulic conductivity ($k_{sat}$) was obtained from both the coefficient of consolidation $C_V$ ($m^2/s$) evaluated by Taylor's approach and the coefficient of volume change $m_v$ ($m^2/kN$) (Eq. (1)).

$$k_{sat} = C_v \times m_v \times \gamma_w \tag{1}$$

To investigate the effect of initial water content on saturated hydraulic conductivity, different initial states of the optimal mixture (which was chosen on minimal saturated hydraulic conductivity basis) was prepared from OWC, OWC−2% and OWC + 2%.

The results are checked with the triaxial device. The tests were conducted in conformity with the law of Darcy. The test sample size was 38 mm in diameter and 78 mm in height. The sample was constrained by end caps on the top and bottom and by a rubber membrane on the side. Filters stones were placed between the sample and end caps (With permeability of combined thickness of the two filters stone is $5.2 \times 10^{-7}$ m/s). Two pressure control connected for controlled of pressure/volume changes. A test sample compacted at the optimum water content (OWC) was placed on the bottom cap of the cell and then constrained by the porous stones, the top cap, and the rubber membrane.

A vacuum pressure of 60 kPa was applied through the drainage line connected to the top end cap to saturate the sample. Under a confining pressure ($\sigma_3^{'}$) of 100 kPa, back pressure ($U_e$) from the inflow pressure of 40 kPa and outflow pressure of 0 kPa was applied to the GDS, which leads to the bottom and top of the sample, respectively. It is estimated that the sample is saturated when one gets a constant slope and the entering and outgoing flow are equal. After confirming a good saturation (After more than 24 h), permeability testing was started. The hydraulic gradient *i* of the test was 128.2 ($\Delta U =$ 100 kPa). The samples were consolidated according to an experimental program in order to study the effect of effective stresses, which vary from 100 kPa to 800 kPa. Saturated hydraulic conductivity of the mixtures is based on Darcy's law.

The filter stones and the tubing may provide some further resistance to the percolation of the soil, and corrections are, therefore, required to the measured values of hydraulic conductivity. Considering the triaxial sample as a sandwich with a filter stone at each end, which is a three-layer system with flow perpendicular to the stratified layers, the following expression may be derived from the hydraulic conductivity of the soil (Lade 2016) (Eq. (2)).

$$k_{corr} = \frac{H.k_m}{H + 2t(1 - \frac{k_m}{k_f})} \tag{2}$$

In which H is the height of the soil sample, 2t is the combined thickness of the two filters stones, $k_m$ is the measured permeability, and $k_f$ is the permeability of the filter stones. This may be determined separately by simply measuring across the two filter stones in the setup with no sample between them.

The *WRC* is determined at zero effective stress, and the volume changes of soil sample during the determination of *WRC* are ignored (Demdoum et al. 2020). Therefore, the use of methods to impose matric suction is of great interest. In this regard, the osmotic approach and vapor equilibrium method (*VET*), which cover a relatively high suction range, allow in a correct evaluation and control of the matric suction in the bentonite-soil mixture. The initial suction of the samples is measured by the filter paper method (according to the ASTM D 52980-094 standard).

To confirm the results obtained, the Van Genuchten (*VG*) model is used to compare the measured and estimated results. According to Van Genuchten (1980), the function of the *WRC* can be defined as (Eq. (3)):

$$\theta_v = \theta_r + \frac{\theta_s - \theta_r}{(1 + |a.\psi|^n)^m} \tag{3}$$

where, $\theta_\Psi$, volumetric water content at capillary potential $\psi$ ($m^3\ m^{-3}$), $\theta r$, residual volumetric water content which is usually fitted to measured data ($m^3\ m^{-3}$), $\theta_s$, volumetric water content at saturation which is usually not fitted but taken as the measured total porosity (i.e. the volumetric water content at a matric potential of 0) ($m^3\ m^{-3}$), *a, n*, and m are parameters without physical meaning describing the shape of the function; m is usually fixed as $m = 1-(1/n)$.

Van Genuchten's (1980) parametric formulation for *WRC* can be used in combination with a Mualem (Mualem 1976) equation to define the unsaturated hydraulic conductivity

function (Eq. (4)), as follows:

$$k_w = k_s S_e^{\lambda}[1 - (1 - S_e^{\frac{1}{m}})^m]^2 \tag{4}$$

Unsaturated hydraulic conductivity ($k_w$) by vapor equilibrium method is represented by the following relationship (Eq. (5)):

$$k_w(\theta) = \frac{D(\theta)}{\frac{\partial \psi_w}{\partial \theta}} = \frac{D(\theta)}{\triangle\ \psi_w} \times \frac{V_{wT}}{V_T} \tag{5}$$

where, $V_{wt}$, the change in water volume at time t ($mm^3$), $V_{wT}$, the total change in water volume ($mm^3$), $M$ is the slope of the straight line in t, $Ln\ (V_{wT}–V_{w(t)})$ space, and $\psi_w$ is the capillary potential given by the relation $\psi_w = s/\gamma_w$(m).

## 3 Results

### 3.1 Saturated Hydraulic Conductivity ($K_{sat}$)

For all mixtures, saturated hydraulic conductivity ($K_{sat}$) decreases with the increase of the applied vertical stress (Fig. 1).

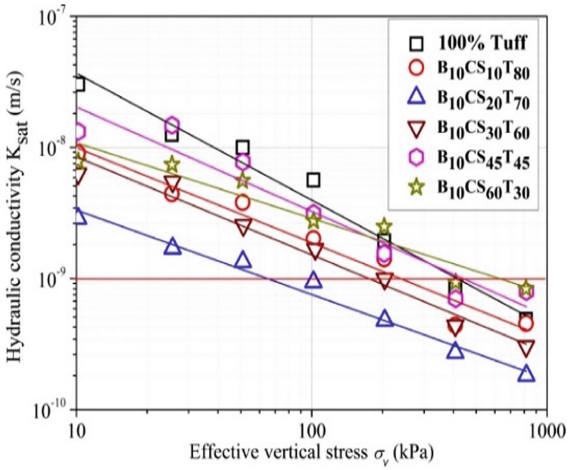


**Fig. 1.** Saturated hydraulic conductivity ($k_{sat}$) versus effective vertical stress for the $B_{10}CS_{\%}T_{\%}$ mixtures.

The hydraulic conductivity values obtained for different mixtures are between 2.0 $10^{-10}$ m/s and 2.0 $10^{-8}$ m/s. For a minimum vertical stress of 10 kPa, $B_{10}CS_{20}T_{70}$ mixture presents the minimum saturated hydraulic conductivity value. It is between 2.0 $10^{-9}$ to 1.83 $10^{-10}$ m/s, for the vertical stresses from 10 to 800 kPa. Generally, the effect of vertical stresses on hydraulic conductivity is less significant, once the vertical stress

exceeds 200 kPa (the effect of stress on the saturation state of the soil becomes weak) (Alston et al. 1997).

After selecting the $B_{10}CS_{20}T_{70}$ mixture as an optimal mixture, we place it in a triaxial cell, and under a permanent hydraulic load. Figure 7 shows the similarity of the hydraulic conductivity results obtained by this test with the oedometer test results. This makes it less demanding to use the triaxial device for hydraulic conductivity estimate for this material type (for ease of use) (Demdoum et al. 2016; Abdellah et al. 2020). Moreover, the effective confining pressure increase does not affect the hydraulic conductivity of this mixture. A similar trend was made by Gueddouda et al. (2016) for a 15% bentonite-85% dune sand mixture. This is the opposite of the great influence of vertical pressure in the odometer test. The hydraulic conductivity values range from $1.7 \times 10^{-10}$ m/s to $4.2 \times 10^{-10}$ m/s. These results are consistent with those found in sand-bentonite and clay-sand mixtures (Gueddouda et al. 2016; Demdoum et al. a, b). This mixture satisfies the principal condition of saturated hydraulic conductivity ($k_{sat} < 10^{-9}$ m/s).

1) **Relationship between saturated hydraulic conductivity ($k_{sat}$) and initial water content (IWC)**

To illustrate the variation of saturated hydraulic conductivity with vertical stresses for samples with various compaction water contents, $B_{10}CS_{20}T_{70}$ mixture samples were used.

Figure 2 shows the evolution of hydraulic conductivity versus vertical stresses in the tests performed for dry density samples of 16.86 kN/m$^3$ with various initial water contents. The hydraulic conductivity decreased from $7.0 \times 10^{-11}$ m/s for the initial water content of 12.35% to $4.4 \times 10^{-11}$ m/s with an initial content of 16.35% under a stress of 1.2 MPa. 50 kPa, hydraulic conductivity decreased from $1.0 \times 10^{-9}$ m/s for a compaction water content of 12.35% to $8.1 \times 10^{-10}$ m/s for a compaction water content of 16.35%. However, these results seem to be validated by the results of previous studies, which found that the range of compaction water contents that gave low hydraulic conductivity is between optimum and over 2% of OWC for soil liners. The results indicate that compacted mixture with OWC, OWC + 2% and OWC-2% have very close saturated hydraulic conductivity values. A similar trend was made by Haug and Wang (1992) for an 8% bentonite - 92% sand mixture; they showed that water content did not affect the saturated hydraulic conductivity. The compacted mixture at OWC-2% is characterized by slightly higher hydraulic conductivity values than the other mixtures in the lower applied stresses of 100 kPa. Above 100 kPa, its hydraulic conductivity decreases with values close to the other mixtures' hydraulic conductivity. The difference in $k_{sat}$ values observed in the OWC, OWC −2% and OWC +2% for low stresses decrease for high stresses to reach a factor of 100 for vertical stress of about 1.2 MPa. Finally, the effect of water content on the saturated hydraulic conductivity of $B_{10}CS_{20}T_{70}$ mixture is small compared to vertical stress impact in the oedometer test.

### 3.2 Water Retention Curve (WRC)

Figure 3 present the *WRCs* in terms of degree of saturation from the average value of the experimental data for the samples prepared at OWC, OWC + 2% and OWC-2%.

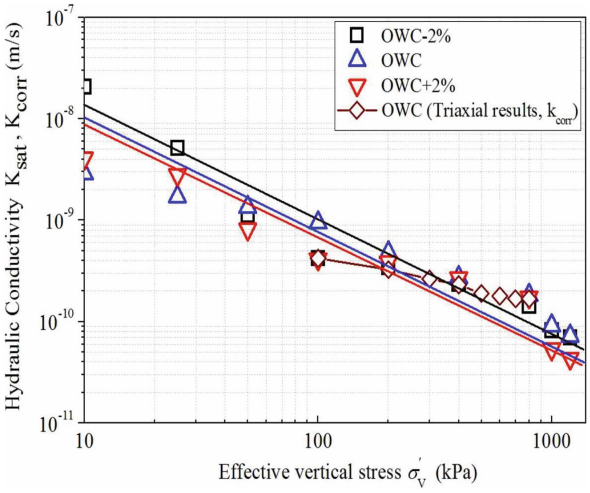


**Fig. 2.** Saturated hydraulic conductivity of $B_{10}CS_{20}T_{70}$ mixture versus effective vertical stress with different initial water content.

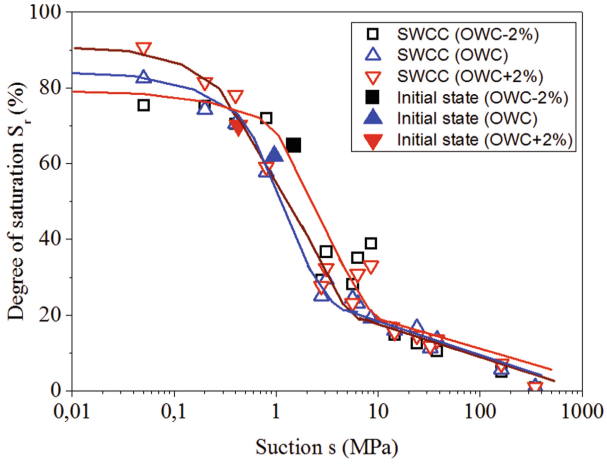


**Fig. 3.** *WRC* of free drying test for the compacted $B_{10}CS_{20}T_{70}$ mixture.

From the initial suction values measured by the filter paper method, the samples follow a drying path for suction values higher than the initial suction values, and a wetting path for values lower than the initial suction values. For suctions lower than 3 MPa (at low suctions), the sample compacted with OWC + 2% gives a saturation degree more than those of the other mixtures: at more than suction of 3 MPa (at high suctions), the difference between the *WRCs* measured is negligible. Generally, *WRC* for optimum dry samples (OWC-2%), characterized by a drying path less than *WRC* at optimum or optimum wet. The same contention has been used by Vanapalli et al. (1999).

The *WRCs* obtained by this prediction model are illustrated in Fig. 4. They show that the shape of the curves obtained $\theta(s)$ is in agreement with the suction points corresponding to the measured results of the *WRCs*. In the desaturation zone ($s \geq 3$ MPa), all the curves of the *VG* model and the measured curves give more similar results.

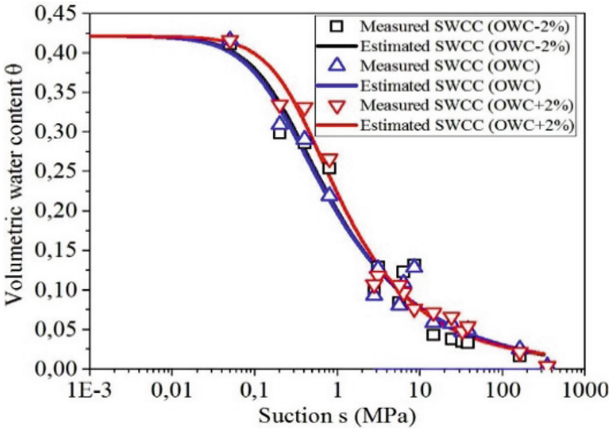


**Fig. 4.** Comparison between the WRCs measured with those of Van Genuchten's model.

### 3.3 Unsaturated Hydraulic Conductivity ($K_w$)

The evolution of the unsaturated hydraulic conductivity ($k_w$) calculated with different imposed suctions is presented in Fig. 5. It can be seen that the compact mixtures have $k_w$ values, which are similar. Figure 4 shows that the minimum hydraulic conductivity $k_W$ values for the degree of saturation levels below 15% in the compact mixture at OWC-2% and in the degrees of saturation above 15% for the compact mixture at OWC. This can be explained by the high initial suction from the dry side to the optimum (continuous air phase and discontinuous water phase) compared to the wet side of the optimum. When suction increased from 2.7 MPa to 348 MPa, the unsaturated hydraulic conductivity ($k_w$) decreased from 4.0 $10^{-15}$ m/s to the order of 3.0 $10^{-17}$ m/s. The unsaturated hydraulic conductivity decreased significantly with the increasing suction. This observation also is clearly indicated in the literature (Ye et al. 2014; Gueddouda et al. 2016; Demdoum et al. 2019a, b).

For very low vertical stresses ($\sigma'_v$ *or* $s \sim 0.01$ MPa), the hydraulic conductivity ($k_{sat}$) of the mixtures at the oedometer $k_{sat}(\sigma'_v)$ and the Van Genuchten model $k_w(s)$ vary by a factor of about 0.5 ($k_{sat(Oed)}/k_{w(VG)}$) ($k_{sat} \sim 2.08\ 10^{-9}$ - $2.88\ 10^{-9}$ m/s in the oedometer and $k_w \sim 1.07\ 10^{-8}$- $2.83\ 10^{-9}$ m/s in the Van Genuchten model) (Fig. 6). For high stresses (or suctions) (0.1 MPa $\leq \sigma'_v$ *or* $s \leq 1.2$ MPa), the sample compacted at the OWC has a high deviation ranging from 3 to 200. The other samples (OWC + 2% and OWC-2%) have low deviations (maximum 10) (Fig. 6), which reflects a good convergence between the mathematical model and the experimental result.

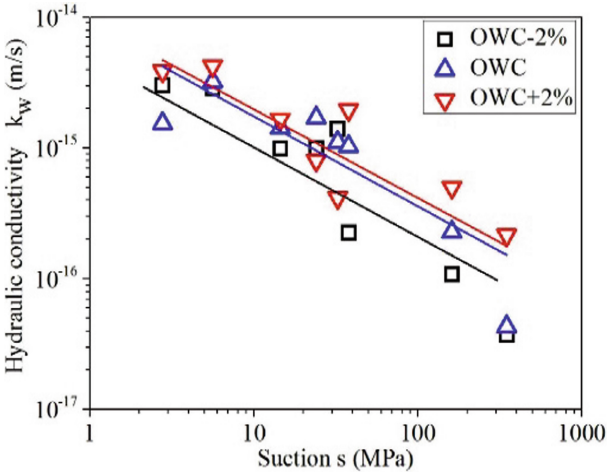


**Fig. 5.** Unsaturated hydraulic conductivity $k_W$ versus suction.

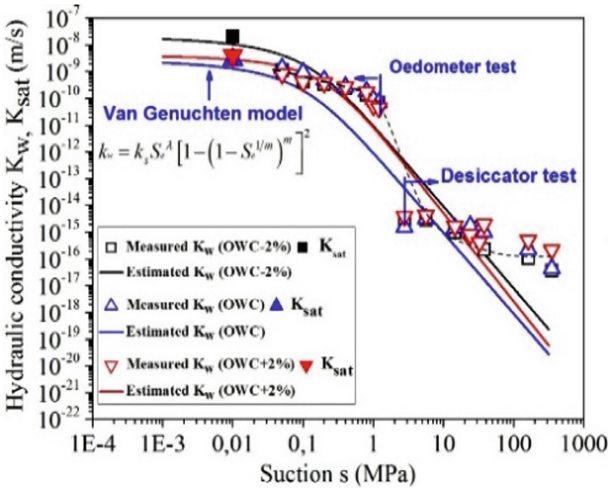


**Fig. 6.** Hydraulic conductivity curves calculated by the Van Genuchten method.

## 4 Conclusions

In the saturated state, the $B_{10}CS_{20}T_{70}$ mixture is the optimal recommended mixture, which satisfies the saturated hydraulic conductivity condition ($k_{sat} = 1.83\ 10^{-10}$ m/s $< 10^{-9}$ m/s). In addition, the increase of more than 30% in the proportion of limestone sand in the mixture has a negative effect on hydraulic conductivity.

In the unsaturated state, *WRC* depends on the initial water content if the suction is less than 3 MPa, beyond this suction (>3 MPa), the WRC is almost identical. Water retention capacity of the $B_{10}CS_{20}T_{70}$ mixture is improved to an initial compact water content of OWC + 2%. The comparison between the hydraulic conductivity $k(\sigma'_v)$ measured with

an oedometer and the hydraulic conductivity $k_w(s)$ deduced from the *WRCs* (using Van Genuchten's model), showed that identical increases in mechanical or suction stresses produce almost the same variation in hydraulic conductivity as long as the soil remains saturated, especially in samples compacted with OWC + 2%.

## References

Abdellah, D., Gueddouda, M.K., Goual, I., Souli, H., Ghembaza, M.S.: Effect of landfill leachate on the hydromechanical behavior of bentonite-geomaterials mixture. Constr. Build. Mater. **234**, 117356 (2020)

Abeele, W.V., Wheeler, M.L., Burton, B.W.: Geohydrology of Bandelier tuff. Los Alamos National Laboratory, USA, Report LA-8962-MS, p. 55 (1981). https://doi.org/10.2172/5575989

Alston, C., Daniel, D.E., Devroy, D.: Design and construction of sand Bentonite liner for effluent treatment lagoon, Marathon, Ontario. Can. Geotech. J. **34**(6), 841–852 (1997)

Demdoum, A., Gueddouda, M.K., Goual, I.: Effect of water and leachate on hydraulic behavior of compacted bentonite, crushed sand and tuff mixtures for use as landfill liners. Geotech. Geol. Eng. **35**(6), 2677–2696 (2017). https://doi.org/10.1007/s10706-017-0270-4

Demdoum, A., Gueddouda, M.K., Goual, I., Souli, H., Anlauf, R., Ghembaza, M.S.: Effect of water content on hydraulic properties of bentonite–geomaterials mixture. Europ. J. Environ. Civil Eng. **23**, 1–26 (2019)

Demdoum, A., Gueddouda, M.K., Goual, I, Berkak, H.: Effect of liquid type on the hydraulic characteristic of compacted local geomaterials for use as hydraulic barriers. In: International Symposium on Materials and Sustainable Development, pp. 451–464. Springer, Cham (2018)

Demdoum, A.: Comportement hydrique et mécanique d'un mélange de Bentonite-Sable Calcaire-Tuf: Application à la conception des Installations de Stockage des Déchets (ISD) (Doctoral dissertation). ⟨tel-02099687⟩ (2019)

Demdoum, A., Gueddouda, M.K., Goual, I., Benabed, B.: Geotechnical characterization of geomaterial blends with bentonite of Maghnia for use as landfill liners. J. Materials Process. Environ. **4**, 48–54 (2016)

Demdoum, A., Gueddouda, M.K., Goual, I.: Experimental study on hydro-mechanical characteristics of compacted bentonite-moderately calcareous soil mixtures for landfill liners purposes. In: International Symposium on Construction Management And Civil Engineering (ISCMCE-2017), Skikda-Algeria (2017b)

Demdoum, A., Gueddouda, M.K., Goual, I., Souli, H.: Unsaturated hydraulic characteristics of compacted local geo-materials for use as landfill liners. Algerian J. Res. Technol. **4**(1), 34–41 (2020)

Gueddouda, M.K., Goual, I., Benabed, B., et al.: Hydraulic properties of dune sand-bentonite mixtures of watertight barriers for hazardous waste facilities. J. Rock Mech. Geotech. Eng. **8**(4), 541–550 (2016)

Haug, M.D., Wong, L.C.: Impact of molding water contention hydraulic conductivity of compacted sand–bentonite. Can. Geotech. J. **29**(2), 253–262 (1992). https://doi.org/10.1139/t92-029

Iravanianam A.: Hydro-Mechanical Properties of Compacted Sand-bentonite Mixtures Enhanced with Cement. Ph.D. thesis, Eastern Mediterranean University (EMU), Cyprus, Turkish (2015)

Mualem, Y.: A new model for predicting the hydraulic conductivity of unsaturated porous media. Water Resour. Res. **12**(3), 513–522 (1976)

Van Genuchten, M.T.: A closed-form equation for predicting the hydraulic conductivity of unsaturated soils. Soil Sci. Soc. Am. J. **44**, 892–898 (1980)

Vanapalli, S.K., Fredlund, D.G., Pufahl, D.E.: The influence of soil structure and stress history on the soil-water characteristics of a compacted till. Géotechnique **49**(2), 143–159 (1999)

Ye, W.M., Borrell, N.C., Zhu, J.Y., Chen, B., Chen, Y.G.: Advances on the investigation of the hydraulic behavior of compacted GMZ bentonite. Eng. Geol. **169**(4), 41–49 (2014)

# Hydromechanical Properties of a Leachate Contaminated Tuff/Sandy Soil/Bentonite Mixture

A. Demdoum[1(✉)], H. Souli[2], R. Anlauf[3], H. Loualbia[4], and M. K. Gueddouda[5]

[1] Laboratory of Mathematical and Applied Science, University of Ghardaïa, BP 455, 47000 Ghardaïa, Algeria
btp.dem@gmail.com

[2] Laboratory of Tribology and Dynamic of Systems, National Engineering School of Saint Etienne, 58 Rue Jean Parot, 42023 Saint Etienne Cedex, France

[3] Faculty of Agricultural Sciences and Landscape Architecture, University of Applied Sciences, Osnabrueck, Germany

[4] Laboratory of Mechanical and Materials Development, University Zaine Achour, 3117 Djelfa, Algeria

[5] Department of Civil Engineering, Amar Telidji University, Laghoua, Algeria

**Abstract.** An empirical study on the chemical characteristics, swelling characteristics, mineralogical characteristics, hydraulic conductivity, shear strength and unconfined compressive strength of compacted tuff /sandy soil/bentonite mixtures used as landfill lining is presented in this paper. Landfill leachate was used to determine the effect of pollution on the parameters of these mixtures for each experiment. To carry out this study, three materials, including bentonite and two types of soils, namely tuff and sandy wastes (crushed sand), were collected in the Laghouat - South Algerian region. A study of the geotechnical properties of all selected materials and mixtures was initially performed. X-ray diffraction (XRD) results showed that the dissolution of minerals and montmorillonite content modified by landfill leachate decreased swelling characteristics and slightly increased saturated hydraulic conductivity. The pH and electrical conductivity measurements of leachate contaminated mixtures revealed a decrease in pH values and an increase in electrical conductivity values. In terms of shear strength, it increased with increased crushed sand content. The shear strength of the previously contaminated optimal mixture showed an increase in cohesion ($C_{uu}$) and a decrease in the friction angle ($\varphi_{uu}$). The results of unconfined compressive strength at the age of 90 days reached 1400 kPa for mixtures containing 70% and 80% tuff. This strength develops with increased deposition of cementitious materials ($CaCO_3$). In addition, the unconfined compressive strength of the contaminated mixture was increased. According to the results, the mixture of 10% bentonite/20% crushed sand/70% tuff responds to the structural criteria for compacted soil liners.

**Keywords:** Landfill liners · Sandy wastes · Conductivity hydraulic · Shear strength · Chemical characteristics · Compressive strength


B. Safi et al. (Eds.): ISMSD 2019, *Proceedings of the 4th International Symposium on Materials and Sustainable Development*, pp. 93–114, 2020.
https://doi.org/10.1007/978-3-030-43211-9_9

## 1 Introduction

The world produces 2.01 billion tons of municipal solid waste annually, of which an extremely conservative estimate is that at least 33% is not managed in an environmentally safe manner (Kaza et al. 2018). Worldwide, waste generated per person per day averages 0.74 kg/day, but varies widely from 0.11 to 4.54 kg/day. For example, Algeria generates 13 million tons of household and similar waste annually and the solid waste production rate per person ranges from 0.8 kg/day to 1.2 kg/day (National Waste Agency 2019). Waste generation in low-income countries is expected to triple by 2050.

Most of the world's waste is currently disposed of in landfill sites. Approximately 37% of waste is disposed of in some form in a landfill, including 8% in sanitary landfills with landfill gas collection systems (Kaza et al. 2018). Open dumps represent about 33% of waste, 19% is recovered by recycling and composting and 11% is incinerated for final disposal. Landfills and open dumps in Algeria are the first solutions for waste disposal. In the future, even if sorting, recycling and composting processes are optimised as much as possible, landfills will remain essential. A better knowledge of the behavior of the sealing materials constituting the waterproof barriers (passive and active) is necessary to ensure good protection of groundwater against leachate migration.

The geological quality and natural protection of groundwater resources is certainly the main and best-known environmental criterion for the design of a new landfill. A key criterion is the long-term availability of a large surface area and volume. Another point is good local availability of cover materials for the construction work at the different stages of the landfill. Controlled landfills require a large volume of these materials to cover the waste. This can be achieved partly by using inert building materials (e.g. crushed sand), but neighbouring quarries are also necessary to provide the necessary materials, because, otherwise, transportation costs will be too expensive to be efficient. . These local quarries can also be the basis for subsequent use as landfill.

The Laghouat geology region in southern Algeria (semi-arid region) is represented by a very thick marl and crushed rock complex at the base and a tuff crust grouping at the surface (from about 20 cm to about 2 m) (Demdoum et al. 2019). However, the tuff crust has an estimated hydraulic conductivity of $3.04 \times 10^{-8}$ m/s (Abeel 1986). Several researchers have studied the mechanical behaviour to assess the cohesion of tuff and crushed sand (crushed stone waste) under dry and wet conditions (Demdoum 2019) with the result, that the addition of sand to the tuff increases the cohesion of the compacted backfill after full saturation (Ben Dhia 1983; Morsli et al. 2007). These characteristics make tuff a good local material in addition to bentonite for use as a landfill liner.

Therefore, sufficiently thick soil-bentonite mixture layers can act as barriers against the migration of many hazardous pollutants. Typical requirements for the design of landfill technical linings are saturated hydraulic conductivity ($k_{sat} \leq 10^{-9}$ m/s), shear strength (internal friction angle: $\varphi' \geq 25°$), compressive strength ($\sigma_c > 200$ kPa), chemical resistance (structural stability of mineralogy), low compressibility and low shrinkage-swelling effects (Abeel 1986; Daniel and Benson 1990; Koch 2002; Guney et al. 2005; Ozcoban et al. 2013; Guney et al. Guney et al. 2014; Li et al. 2015; Demdoum et al. 2017a, b; Demdoum 2019; Abdellah et al. 2020).

Municipal solid waste (MSW) landfill leachate may have an effect on the hydromechanical properties of the soil-bentonite mixture. However, this is not an effect of chemical solutions. Glatsteina and Francisca (2014) showed that the hydraulic behaviour of a compacted 90% silt/10% bentonite mixture can be modified by stimulating microorganisms in the pores of the mixture by injecting the nutrient. They observed a decrease in hydraulic conductivity from $3 \times 10^{-9}$ to $5 \times 10^{-11}$ m/s due to the accumulation of microbial biomass in the pores of the mixture. The authors concluded that biological soil monitoring is useful when the impact of microorganisms is understood in terms of increasing or decreasing the hydraulic conductivity of the silt-bentonite mixture.

MSW landfill leachate may change the compaction, density and strength properties of the soil. However, soil strength varies depending on leachate characteristics and soil texture (Demdoum 2019). Sunil et al. (2009) observed a slight increase in effective cohesion C' (from 18.46 to 20.22 kPa) and a reduction of φ' (from 30.4° to 25.8°) in contaminated lateritic soil (by adding 20% MSW landfill leachate). Harun et al. (2013) conducted unconsolidated undrained triaxial tests (UU) on leachate-contaminated sandy-clay soils. They found that undrained cohesion ($C_u$) was reduced from 156 to 55 kPa with a 0 to 20% addition of MSW landfill leachate. Xue and Zhang (2014) evaluated the impact of the concentration of MSW landfill leachate on the degradation behavior of solidified clay liners. They found that the unconfined compressive strength of the solidified clay decreased significantly with increasing amount of leachate.

The aim of this study is to examine the behavior of local materials (tuff cover crusts and crushed sand) being used as landfill liners in interaction with landfill leachate. For the determination of physico-chemical and hydromechanical parameters (pH, EC, XRD, saturated hydraulic conductivity, shear strength and unconfined compressive strength), two types of liquids were used: tap water and leachate collected from a landfill site in Laghouat city. The results should lead to the proposal of a formulation meeting the regulatory design criteria.

## 2 Materials and Methods

### 2.1 Soil Materials

The first material is Maghnia bentonite (Telmcen, Western Algeria), which is provided by BANTAL company (Maghnia, Western Algeria). Miocene Maghnia bentonite is common in layers a few meters thick (between 0.5 and 9 meters). Its most important mineral components are silica (55–65%) and alumina (12–19%) (Demdoum et al. 2018). The liquid limit (LL) is 141%, the plastic limit (PL) is 48%, the particle density 2.75 g/cm$^3$ and 60% of the particles are less than 2 μm, as shown in Table 1 The total value of the specific surface area obtained by the blue methylene technique is 462 m$^2$/g. Evaluating the pH of the bentonite revealed the fundamental nature of this material. The typical pH of a Ca-bentonite suspension varies from 7 to 8, unlike that of a Na-bentonite suspension whose pH varies from 9 to 10 (Kaufhold et al. 2008). Based on pH results (ASTM D4972-01, 2007, Table 1), Maghnia bentonite can be classified as Na-bentonite.

The second material is tuff, available in the Laghouat region of southern Algeria. It is often used in the construction of roads. The third material is crushed sand, which is a residue from rock crushing stations located in the north of the Laghouat region

**Table 1.** The basic physicochemical characteristics of Maghnia bentonite.

| pH | $CaCO_3$ (%) | $\gamma_{dmax}$ (g/cm$^3$) | Specific surfacearea (S) (m$^2$/g) | OWC (%) | LL (%) | PL (%) | PI (%) | Particle size distribution (%) | |
|---|---|---|---|---|---|---|---|---|---|
| | | | | | | | | 80 μm | 2 μm |
| 10.3 | 5 | 1.2 | 462 | 32.5 | 141 | 48 | 93 | 86 | 60 |

(southern Algeria) (Demdoum et al. 2020). Tuff particles have a maximum diameter ($D_{max}$) of 3 mm with a sand fraction (<2 mm) of about 85%, and more than 5% of the particles have a diameter less than 0/2 μm (identified by laser diffraction - Malvern Mastersizer 2000). According to the USCS classification, the tuff can be classified as silty sand (SM) (see Table 2). The crushed sand has a fine particle content (<2 μm) of about 3%. According to the USCS classification, the crushed sand is classified as well graduated clean sand (SW) (see Table 2).

**Table 2.** Physicochemical characteristics of crushed sand and tuff.

| Parameter | Crushed sand (CS) | Tuff |
|---|---|---|
| Φ ≤80μm | 11.5% | 18% |
| Φ ≤ 2 mm | 67.8% | 85.46% |
| $C_u$ | 18.8 | 6.57 |
| $C_c$ | 2.3 | 0.4 |
| $\gamma_{dmax}$(g/cm$^3$) | 1.95 | 1.72 |
| OWC (%) | 8.75 | 13.85 |
| SE | 70% | 30% |
| S($m^2/g$) | 7 | 17 |
| LL(%) | 17 | 33 |
| PL (%) | – | 25 |
| PI (%) | / | 8 |
| pH | 9.32 | 7.65 |
| Insoluble (%) | 17.20 | 27.70 |
| $CaCO_3$ | 55 | 66 |
| $CaSO_4$, $2H_2O$ | 0.52 | 0.46 |

## 2.2 MSW Landfill Leachate

The leachate used in this study was collected from a Municipal Solid Waste (MSW) landfill site in Laghouat City. Table 3 presents its physical and chemical properties. All

experimental analyses were performed in accordance with the AFNOR standard. The COD value (2160 mg $O_2$/L) indicates a relatively high organic load reflecting a high organic pollutant capacity (Table 3).

**Table 3.** Physicochemical characteristics of landfill leachate.

| Parametre | Resultats | The limit values of reject direct |
|---|---|---|
| T (°C) | 21.3 | 30 |
| pH | 8.04 | 5.5-8.5 |
| Cond (*u*s/cm) | 5600 | 2000 |
| $\eta$(mPa.s) | $\approx 1$ | / |
| COD (mg/l) | 2160 | 120 |
| MES (mg/l) | 91.5 | 30 |
| $BDO_5$ (mg/l) | 143 | 40 |
| $PO_4^{-3}$(mg/l) | 3.18 | 2 |
| Pt (mg/l) | 167 | 2 |
| $NH_4^+$ (mg/l) | 128 | 40 |
| Nt (mg/l) | 142 | 40 |
| N-$NO_2^-$ (mg/l) | 0.25 | 40 |
| N- $NO_3^-$(mg/l) | 16.9 | 40 |
| $Ca^{+2}$ (mg/l) | 86.5 | / |
| $Mg^{2+}$ (mg/l) | 228.4 | / |
| $Na^+$ (mg/l) | 21201 | / |
| Cu (mg/l) | 2.2 | 0.5 |
| Pb(mg/l) | 2.364 | 0.5 |
| Cd(mg/l) | 8.044 | 0.2 |
| Ni(mg/l) | 7.948 | 0.5 |
| $BOD_5$/COD | 0.066 | / |

## 2.3 Experimental Procedures

Practical experience shows that the addition of more than 10% bentonite leads to a less pronounced effect on the $k_{sat}$ value of the mixture and its water retention capacity. This is the critical ratio of the sandy soils/bentonite mixture (Boulanger 2015; Demdoum 2019).

From these materials, five different types of mixtures were prepared. For all mixtures, the proportion of bentonite is set at 10%. The materials and mixtures used are symbolized as follows: bentonite (B), tuff (T), crushed sand (CS), where X and Y are the proportion of tuff and crashed sand. The mixtures use are:

***Mixture (1):*** 10%B-10%CS-80%T, ($B_{10}CS_{10}T_{80}$); ***Mixture (2):*** 10%B-20%CS-70%T, ($B_{10}CS_{20}T_{70}$); ***Mixture (3):*** 10%B-30%CS-60%T, ($B_{10}CS_{30}T_{60}$); ***Mixture (4):*** 10%B-45%CS-45% T, ($B_{10}CS_{45}T_{45}$): ***Mixture (5):*** 10%B-60%CS-30%T, ($B_{10}CS_{60}T_{30}$).

According to USCS classification, all mixtures can be classified as silty sands, as illustrated in Table 4. According to the carbonate content ($CaCO_{3\ \%}$), tuff was classified as marl material (30% to 70%) (NF P 94-048 1996). Table 4 shows that the addition of crushed sand improves the mix by increasing its maximum dry density ($\gamma_{dmax}$) from 16.625 kN/m$^3$ to 17.825 kN/m$^3$; and reducing its Optimal Water Content (OWC) from 14.4% to 9%. The physical, mechanical and chemical properties of the mixtures are given in Table 4.

**Table 4.** Chemical, physical and mechanical properties of all mixtures.

| Parametre | Mixtures | | | | |
|---|---|---|---|---|---|
| | $B_{10}CS_{10}T_{80}$ | $B_{10}CS_{20}T_{70}$ | $B_{10}CS_{30}T_{60}$ | $B_{10}CS_{45}T_{45}$ | $B_{10}CS_{60}T_{30}$ |
| $\Phi \leq 2$ um | 9.68 | 8.27 | 6.23 | 5.50 | 4.45 |
| $\Phi \leq 80$ µm | 26.28 | 22.46 | 20.28 | 17.60 | 15.26 |
| $C_c$ | 0.24 | 0.32 | 0.34 | 0.46 | 0.63 |
| $C_u$ | 7.83 | 8.80 | 12.36 | 13.80 | 15.44 |
| $G_S$ | 2.705 | 2.705 | 2.705 | 2.705 | 2.70 |
| PL (%) | 25.00 | 24.07 | 24.03 | 23.07 | 21.74 |
| LL (%) | 36.77 | 35.54 | 35.20 | 34.39 | 31.79 |
| PI (%) | 11.77 | 11.47 | 11.17 | 11.32 | 10.05 |
| $CaCO_3$ (%) | 58 | 60 | 61 | 62 | 64 |
| OWC (%) | 14.20 | 14.35 | 13.75 | 12.00 | 9.25 |
| $\gamma_{dmax}$ (kN/m$^3$) | 16.625 | 16.86 | 17.10 | 17.38 | 17.82 |

1) **Swelling test**

The free swelling and swelling pressure tests were performed using the conventional oedometer according to XP P94-091 (1995) standard.

The expected maximum swelling pressure (Pg) was determined from the constant volume test (at 0 kPa matrix suction).

2) **XRD Test**

After completion of the free swelling and swelling pressure tests on the base materials (crushed sand, tuff and bentonite), the samples were dried in a furnace at a temperature of 105 °C for 24 h until the mass was constant, then ground to perform X-ray diffraction tests

(XRD) to better understand the results of the resulting swelling. The X-ray diffractometer used is the "XPERT PRO-Powder" with a cobalt source. The scanning of 2ϴ is between 5° and 80° with a step of 0.0167°.

3) **Hydraulic Conductivity (Falling-Head Test)**

The cell used for hydraulic conductivity (Falling-Head test) is a rigid wall permeameter. Liquid from a standpipe flows through the soil. The test is carried out according to NF X 30-441 (2008) standard. Sample preparation of the $B_{10}CS_XT_Y$ mixtures is performed under the following conditions of Optimum Normal Proctor (ONP).

The device consists of a stainless-steel ring with an internal diameter of 101.6 mm and a height of 116 mm. This ring allows the mixture to be placed by direct static compaction in the ring using a computer-controlled press with a constant speed of 1.27 mm/min. It is located between a base and a cover with two porous stones of 101.5 mm diameter. After compacting, the mold is immersed in two different cells; the first is filled with water and the second with leachate. The immersion time is 72 h to allow the sample to saturate. The test is carried out at variable hydraulic load at an initial pressure of 10 kPa. The value of the vertical hydraulic conductivity $k_v$ is determined by Eq. (1):

$$k_v = \frac{a.l}{A.T} x \ln\left(\frac{h_1}{h_2}\right) \tag{1}$$

where, a: pipe cross Sect. (0.28 $cm^2$); A: cross section of the sample (81.03 $cm^2$); T: the time interval between $h_1$ and $h_2$; l: height of the sample.

pH is an important factor for pore structure and hydraulic conductivity (Demdoum 2019), because soil charges affect its hydraulic conductivity and soils have pH-dependent charges. For the pH measurements of contaminated and uncontaminated samples, a HANNA Model (HI 2211 pH/ORP Meter) was used. The pH and electrical conductivity (EC) measurements were performed according to the ASTM standard (ASTM D4972-01 2007; ASTM D1125 2009). The pH measurement in the saturated paste aims to reproduce the conditions of the natural environment as closely as possible (in the form of a suspension).

4) **Strength Property**

The design regulations for a landfill require the backfill material to be sufficiently firm to withstand a static load exerted by the waste cover body. In this respect, the bearing capacity of the landfill bottom liners must be determined.

To simulate the lining of a landfill site, a leachate-contaminated mixture was prepared for each of the mechanical properties tests.: the lowest hydraulic conductivity mixture obtained previously was mixed with 1.5 LL (1.5 x liquid limit) of landfill leachate and left it for about 3 days stored at a temperature of 20 °C.After drying at 105 °C, the mixture was compacted according to the required value. The process was performed to simulate liner contamination during disposal and backfilling processes.

a) **Direct shear tests**

As stated above, another important property for these insulation barriers is their mechanical behavior. The shear strength for the different mixtures (10% bentonite/crushed sand/tuff) was investigated. The direct shear test in the box was used to determine the parameters of the shear strength, i.e. cohesion and the angle of internal friction, according to NF P 94-071-1, (1994). Thus, the unconsolidated undrained (UU) direct shear test was used. This test allows studying the short-term behavior of the soil in place. The dimensions of the samples are 60x60x20 cm. The values of the apparent friction angle and cohesion are obtained analytically from the Coulomb law (Eq. 2):

$$\tau = C_{uu} + \sigma tg\phi_{uu} \tag{2}$$

where, τ: total shear strength (kPa); σ: normal stress (kPa); $\phi_{uu}$: apparent friction angle (°); $C_{uu}$: apparent cohesion (kPa).

The samples have been compacted by static compaction at a speed of 1.27 mm/min according to optimum Normal Proctor conditions (OWC and $\gamma_{dmax}$) of each mixture. For each direct shear test, three normal constraints have been used (100, 200, and 300 kPa with a speed of slow shear of 0.5 mm/min).

b) **Unconfined compression (UCS) test**

Crushing tests were carried out on partially saturated samples of mixtures subjected to air drying.

The unconfined compressive strength ($\sigma_c$) was measured on cylindrical specimens with a width of 5 cm and a height of 10 cm according to NF P94-420 (2000) standard. The test is fast, simple, compact and inexpensive. Because this test should determine the hardening phenomenon, called self-stabilizing, specimens of different mixtures were compacted and the change of the compressive strength ($\sigma_c$) versus time was measured. The specimens of the mixtures were statically compacted, extracted from the moulds and stored on a free surface. Then, the specimens were tested after 7 days, 14 days, 28 days, 60 days, and 90 days of curing. The unconfined compression test was determined at a loading rate of 1.27 mm/min. The average of the test results of three specimens was used to determine the unconfined compressive strength ($\sigma_c$) value.

Generally, the strength (or cohesion) of the soil depends on suction and $CaCO_3$ cementing (cemented bonds) (Schrefler and Delage 2001). It is therefore likely that matric suction interferes with the results presented. In addition, this suction tends to stiffen the soil and hinders rearrangements between grains, which increases soil cohesion (Demdoum 2019). The filter paper method (ASTM D 52980-094 1995). was used on the optimal mixture compacted with different water content from 3% to 22% to observe the suction change effect.

## 3 Results and Discussion

### 3.1 Swelling Characteristics (Free Swelling and Swelling Pressure)

The results of the free swelling G(%) showed that 10% of the total free swelling of bentonite (11825%) is an approach to swelling of all mixtures (see Table 5). This indicates

the stability of the swelling mixture with the interaction of tap water. Concerning bentonite, the ratio ($\Delta G$) between the two free swellings is about 35%. The free swelling of the leachate-bentonite interaction is due to the chemical composition of the landfill leachate. The theory of diffuse double-layer (DDL) montmorillonite predicts that the thickness of the diffuse double layer decreases (by reducing the repulsive force) with increasing chemical concentration of the pore-solution and, thus reduces bentonite swelling (Stewart et al. 2003). For G(%) with leachate, a decrease in free swelling was observed at a rate between 10% and 45% (Table 5).

**Table 5.** Maximum free swelling of $B_{10}CS_xT_y$ mixtures.

| Materials and mixtures | $G_{Water}$ (%) | $G_{Leachat}$ (%) | $\Delta G = \frac{(G_{Water} - G_{Leachat})}{G_{Water}}$ (%) |
|---|---|---|---|
| 100% CS | 0.1 | 0.1 | 0 |
| 100% T | 2,165 | 2.7625 | −27.60 |
| 100% B | 118.25 | 76.45 | 35.35 |
| $B_{10}CS_{10}T_{80}$ | 9.25 | 5.15 | 44.32 |
| $B_{10}CS_{20}T_{70}$ | 12.20 | 10.425 | 14.19 |
| $B_{10}CS_{30}T_{60}$ | 11.75 | 7.05 | 40.00 |
| $B_{10}CS_{45}T_{45}$ | 12.1 | 6.775 | 44.00 |
| $B_{10}CS_{60}T_{30}$ | 11.95 | 6.55 | 45.00 |

Table 5 also indicates that the $B_{10}CS_{20}T_{70}$ mixture has the highest value of the swelling pressure in cases of both cases, water and leachate. The swelling pressure of bentonite is about 850 kPa and 637 kPa with water and leachate, respectively. In both cases, water and leachate, the swelling pressure varies between 20 and 43 kPa (Fig. 2). The swelling pressure of the $B_{10}CS_{20}T_{70}$ mixture is relatively stable in the leachate interaction. It was noted that a low inflation pressure was found for all mixtures. Mishar et al. (2011) indicated that the hydraulic conductivity is inversely proportional to the exchangeable sodium percentage (ESP) and the free swelling of bentonite. Therefore, there is a possibility that the mixture with 20% CS, which has the highest free swelling in the leachate (Fig. 1), may show a very low permeability value.

### 3.2 XRD Result

The X-ray diffraction patterns of bentonite immersed in landfill leachate and tap water are shown in Fig. 3, noting that the peak of cristobalite and montmorillonite disappeared with immersion. The position of the montmorillonite peaks did not move to a larger value, but the peaks were considerably reduced, which means that the montmorillonite content became smaller. Some secondary minerals did not exist in the specimens after they were immersed in landfill leachate. However, amorphous products are not determined by X-ray diffraction.

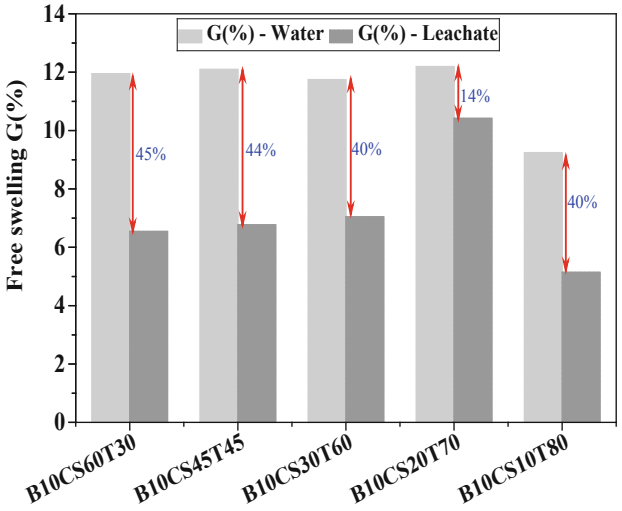


**Fig. 1.** Variation of free swelling versus mixtures in two case of saturation: water and leachate.

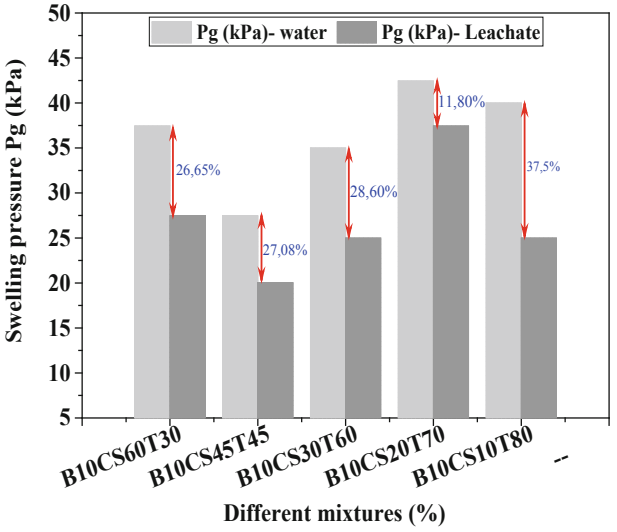


**Fig. 2.** Effect of leachate on the swelling pressure of $B_{10}CS_xT_y$ mixtures.

The montmorillonite content of the bentonite immersed in the landfill leachate is significantly reduced. For montmorillonite hydrolysis, $Mg^{2+}$, which is abundant in this landfill leachate (Table 3), can replace $Al^{3+}$ in the octahedral layer (e.g. Montmorillonite, Illite). These substitutions generate the exhaustion of positive charges and therefore an excess of negative charges, which will be compensated by interlayer or external cations (Kaufhold et al. 2008). Also, note that there is an increase in the silicate peaks.

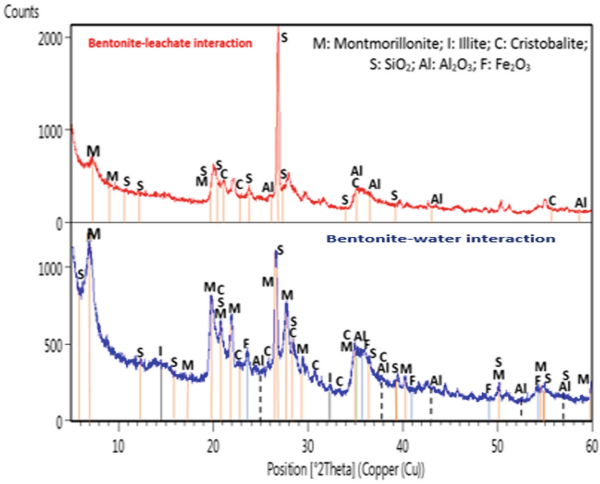


**Fig. 3.** X-ray diffraction patterns of bentonite immersed in landfill leachate (top) and tap water (bottom).

In the tuff, the $CaCO_3$ peak decreased in landfill leachate, unlike crushed sand, whose peaks remained almost constant (Fig. 4). Active calcium carbonate is abundant, particularly in the form of very fine particles ($< 20$ μm), its reactive surface is large and induces particularly high reactivity (Parker et al. 1993). The calcium carbonate-leachate reaction is very complex because the composition of the leachate is complex (microorganisms, ions, cations, and heavy metals). For example, the presence of metal ions (e.g. $Ni^{2+}$, $Zn^{2+}$ and $Cu^{+2}$) prevents the crystallization of calcite (Usmany et al. 2016). This is the opposite of the presence of high concentrations of $[Ca^{+2}]$ $[CO_3^{-2}]$ which increase the rate of crystallization (at laboratory room temperature). In addition, the interaction of the leachate with these fine particles induces a series of complex physico-chemical phenomena with highly variable kinetics that modify the properties of the swelling. In addition, the leachate could lead to the formation of new swelling compounds in the tuff (due to increased tuff swelling).

### 3.3 Hydraulic Conductivity (Falling-Head Method)

Figure 5 shows the results of the saturated hydraulic conductivity with the tuff addition. Two cases of measuring saturated hydraulic conductivity were considered: by tap water and by landfill leachate.

The tuff addition led to a decrease in hydraulic conductivity up to 70% tuff/20%crushed sand (the $B_{10}CS_{20}T_{70}$ mixture). In both cases, the hydraulic conductivity increased beyond this percentage. The decrease of hydraulic conductivity up to 70% tuff addition was significantly for all 4 specimens (for 30, 45, 60, 70% tuff) and could be explained by the following reasons: (1) The arrangement of granules between the tuff and sand after hydration can form a network of complex pores that impede fluid percolation; (2) Some substances, which were generated by the chemical reaction

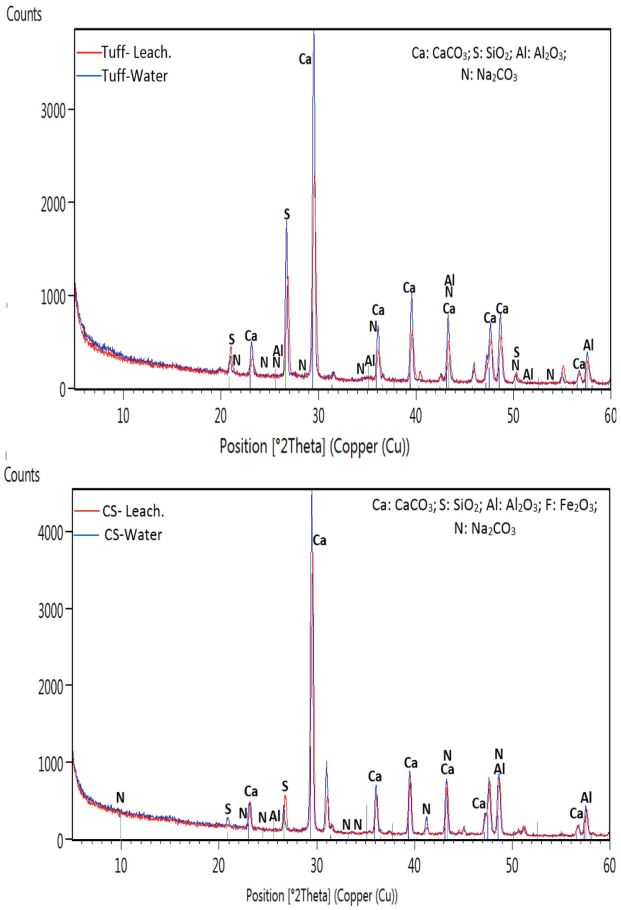


**Fig. 4.** X-ray diffraction patterns of crashed sand (CS, top) and tuff (T, bottom) immersed in landfill leachate and tap water.

between the compositions of leachate and $B_{10}CS_{20}T_{70}$ mixture; (3) Stability of swelling in this mixture is a significant factor in the stability of conductivity hydraulic.

Hydraulic conductivity varied between $10^{-9}$ and $10^{-8}$ m/s, for one period (24 h) in the test with leachate and tap water. For the same mixture, the values of hydraulic conductivity obtained in the case of water are slightly lower than that obtained by leachate. The $B_{10}CS_{20}T_{70}$ mixture presents the minimum value of the hydraulic conductivity: $k_{v20°}$=$1.97 \times 10^{-9}$ m/s with water permeated, and $k_{v20°} = 2.91 \times 10^{-9}$ m/s with leachate permeated. The increase in the hydraulic conductivity by leachate may be explained mainly by the decrease of free swelling. This is due to an irreversible reduction of the fixing of the spaces inter-layers, which leads to a stable aggregation and a significant increase in the hydraulic conductivity (Pansu and Gautheyrou 2006; Ören and Akar 2016).

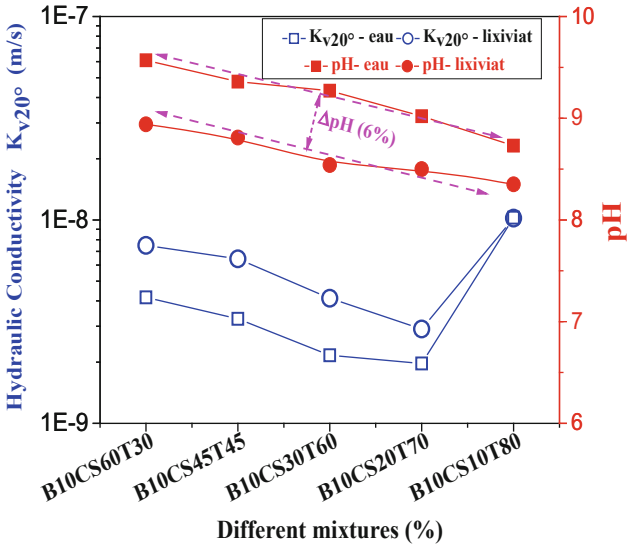


**Fig. 5.** Variations of hydraulic conductivity ($k_{v20°}$) and pH versus different mixtures (contaminated and uncontaminated).

The results of the hydraulic conductivity in relation to the pH in the solution (water and leachate) is also shown in Fig. 5. In the case of water, the hydraulic conductivity of the mixtures decreases with the decrease of the pH down to pH 9 corresponding to the $B_{10}CS_{20}T_{70}$ mixture; below (pH < 9), the hydraulic conductivity increases. The same is true for the case of leachate. The hydraulic conductivity of the mixtures decreases with the decrease of the pH down to 8.5 corresponding to the $B_{10}CS_{20}T_{70}$ mixture; below pH 8.5, the permeability increases. This pH remained constant for 24 h. The pH of the contaminated samples is by 6% lower than the pH of the uncontaminated samples. This is explained by an increase of $Ca^{2+}$ in the samples due to the interaction of three materials with landfill leachate. As explained before (free swelling), carbonates show acidity in mixtures after interaction with leachate. The pH of bentonite suspensions is known to be affected by carbonates (Parker et al. 1993). Furthermore, it is mentioned in the literature that the pH of a clay suspension is a determining parameter of the structural state of the suspension (Pusch 2015), so a change in pH will alter the structure of the suspension and, consequently, of its rheological behavior (hydraulic properties and compressibility). Nakayama et al. (2004) have confirmed an increase of porosity and hydraulic conductivity of a compacted bentonite in contact with a highly alkaline (NaOH, pH = 14) solution tank, due to montmorillonite dissolution. This observation is consistent with the results of a Gaomiaozi (Gao-Miao-Zi GMZ01) bentonite reported by Ye et al. (2014).

Table 6 shows that pH values increase with increasing proportion of crushed sand, which is contrary to the electrical conductivity results ($EC_{1:2}$).

Pansu and Gautheyrou (2006) and Kaufhold et al. (2008) show that the pH value can be used to predict the dominant cations on soil cation exchangers, such as pH > 5.5:

**Table 6.** pH and electrical conductivity (EC) Of contaminated and uncontaminated mixtures * (with leachate)

| Mixtures | pH | *pH | $EC_{1:2}$ (ms/cm) | *$EC_{1:2}$ (ms/cm) |
|---|---|---|---|---|
| $B_{10}CS_{10}T_{80}$ | 8.73 | 8.35 | 1.538 | 1.74 |
| $B_{10}CS_{20}T_{70}$ | 9.02 | 8.50 | 1.477 | 1.63 |
| $B_{10}CS_{30}T_{60}$ | 9.27 | 8.54 | 1.434 | 1.66 |
| $B_{10}CS_{45}T_{45}$ | 9.36 | 8.81 | 1.347 | 1.44 |
| $B_{10}CS_{60}T_{30}$ | 9.57 | 8.94 | 1.096 | 1.24 |

Hydroxide/polymer ions, pH 7.6-9: $CaCO_3$, pH > 9: $Na_2CO_3$. In addition, $Ca^{2+}$ is known to be more acidic than $Na^+$, due to hydrolysis (Callot and Dupuis 1980). The pH results confirmed the reaction of calcium carbonate. The degradation of minerals in reaction with leachate can lead to the formation of organic and inorganic acids (e.g. $H_2CO_3$) making mixtures less basic. The electrical conductivity ($EC_{1:2}$) fluctuated around 1.5-1.8 mS/cm at the end of the experiment for all mixtures. In the case of contaminated mixtures, the ($EC_{1:2}$) increased by more than 10% compared to mixtures saturated with tap water.

### 3.4 Shear Strength

The determination of the mechanical parameters of $B_{10}CS_xT_y$ mixtures is obtained by tracing the lines of Coulomb (intrinsic curves) on an orthonormal reference which presents on the horizontal axis the vertical stress ($\sigma_v$) and ordered the constraints of maximum shears ($\tau_{max}$), as shown in Fig. 6. Figure 6a shows that the friction angle φuu decreases with increasing crushed sand present. These results are in accordance with the available literature (Demdoum 2019) which indicates that the internal friction angle increases with grain size. The tuff shows a friction angle of about 34.45°. Variations in friction angles and cohesion show that the $B_{10}CS_{60}T_{30}$ mixture has maximum (denser) $C_{uu}$ and $\varphi_{uu}$ values. The results are presented in Table 7.

The friction angle of the $B_{10}CS_{20}T_{70}$ mixture is close to the results found by Kouloughli (2007) ($\varphi_{uu}$ values between 25° and 30°) for the 90% sand + 10% bentonite mixture. The short-term shear strength results for all the mixtures provide satisfactory stability of the literature's recommendations (friction angle of the mixture relatively high at 25°) for the compacted soil liners.

In the $B_{10}CS_{20}T_{70}$ mixture, shear parameters were modified by leachate pollution on a macroscopic scale. Figure 6b shows that the $C_{uu}$ value of the $B_{10}CS_{20}T_{70}$ mixture increased when saturated at 1.5LL by leachate prior to sample preparation while $\varphi_{uu}$ decreased. Li et al. (2013) made a similar observation on contaminated clay. Sunil et al. (2009) found that the C' value increased slightly with increasing leachate concentration in silty soil, while the φ' value decreased. The authors evaluated this result by increasing the clay content and specific surface area in the silt after interaction with the leachate. Therefore, it is presumed that the dissolution of minerals such as montmorillonite causes the increase in dry density of the sample and modifies the quality of the clay.

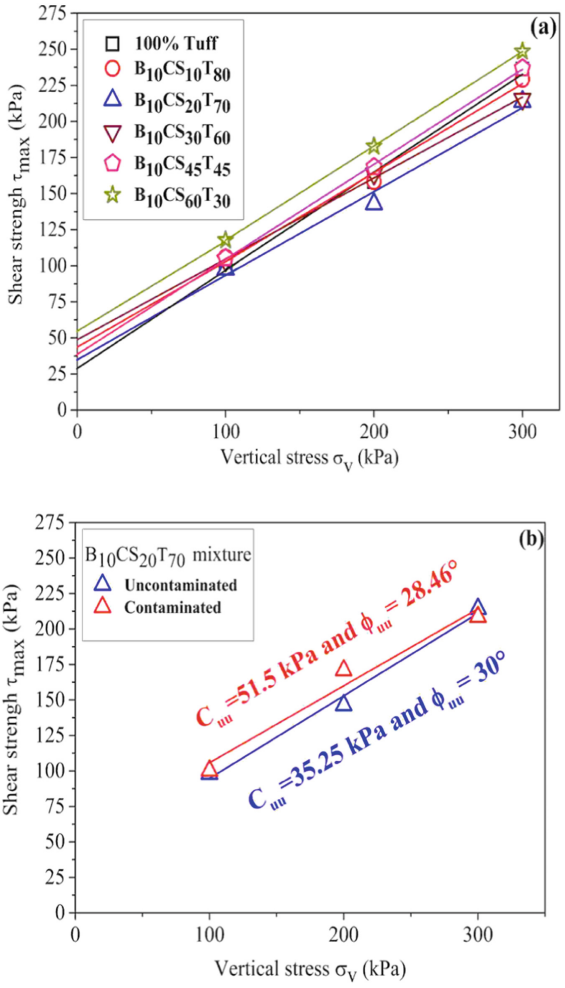


**Fig. 6.** Mohr-coulomb failure envelopes obtained from direct shear tests for: (a) all the mixtures ($B_{10}CS_xT_y$) and (b) contaminated $B_{10}CS_{20}T_{70}$ mixture.

Also, it causes the slight increase of shear strength or residual stress. In addition, leachate ions such as $Mg^{+2}$, $Ca^{+2}$ and $Na^{+}$ (Table 3) and its living microorganisms can also react rapidly with the materials' minerals (Ye et al. 2014), resulting in the emergence of new mineral compositions during saturation at 1.5LL. Therefore, this interaction can result in an increase in the cementitious components of the mixture leading to an increase its cohesion. Similarly, Ayininuola et al. (2009) studied the shear strength of a clay saturated with different concentrations of $CaSO_4$. The authors found that due to the presence of $CaSO_4$ salt and $Ca^{2+}$ provided by the formation of a strong bond between clay minerals, there was an initial increase in soil cohesion. In addition, after drying the contaminated samples, the organic matter becomes more soluble in compaction water, resulting in increased viscosity in the pore spaces and a slight decrease in the angle of friction.

**Table 7.** Shear properties (UU) of $B_{10}CS_xT_y$ mixtures and tuff.

| Mixtures | OWC (%) | $C_{uu}$(kPa) | $\phi_{uu}$ (degre) |
|---|---|---|---|
| 100% Tuff | 13.85 | 29.00 | 34.45 |
| $B_{10}CS_{10}T_{80}$ | 14.20 | 41.25 | 29.22 |
| $B_{10}CS_{20}T_{70}$ | 14.35 | 35.25 | 29.7 |
| $B_{10}CS_{30}T_{60}$ | 13.75 | 48.83 | 29.23 |
| $B_{10}CS_{45}T_{45}$ | 12.00 | 38.76 | 33.11 |
| $B_{10}CS_{60}T_{30}$ | 9.25 | 52.28 | 33.44 |

### 3.5 Unconfined Compression (UCS)

Figure 7(a) presents the evolution of unconfined compressive strength ($\sigma_c$) as a function of the curing time of all the mixtures. These results show that compressive strength ($\sigma_c$) increases rapidly at a young age (<7 days), which is explained by the rapid decrease in water content (Fig. 8(a)) due to the rapid drying of the surface areas and the increase suctions of specimens during curing (example illustrated in Fig. 8(b)).

The $B_{10}CS_{30}T_{60}$ mixture gave a maximum strength until day 14; after that, its strength is reduced for $B_{10}CS_{30}T_{60}$, $B_{10}CS_{45}T_{45}$ and $B_{10}CS_{60}T_{30}$ mixtures. For tuff, $B_{10}CS_{10}T_{80}$ mixture and $B_{10}CS_{20}T_{70}$ mixture, the compressive strength develops up to 90 days. As an indication, it can be seen at 90 days that the $B_{10}CS_{10}T_{80}$ and $B_{10}CS_{20}T_{70}$ mixtures acquire a maximum compressive strength ($\sigma_c$) of about 1.4 MPa corresponding to a 20% gain compared to the raw tuff and $B_{10}CS_{30}T_{60}$, $B_{10}CS_{45}T_{45}$ mixtures.

The results found can be compared to the maximum waste load over $1m^2$ of a landfill site in Laghouat region (Ben Nacer Ben Chohra Centre) (Demdoum et al. 2016). The tonnage of waste for 8 years of operation on this site is 177 870 tonnes and the maximum volume is 153 600 $m^3$ with a depth of 7 m. This results in a maximum waste pressure of around 79.5 kPa/$m^2$. If the cover is added, the load range is approximately 100 kPa/$m^2$. Obviously, the pressure value is lower compared to the compressive strength ($\sigma_c$) of all the mixtures and raw tuff.

Figure 8(b) shows an increase in compressive strength ($\sigma_c$) due to leachate effects on the composition of the $B_{10}CS_{20}T_{70}$ mixture. This increase can be explained by the increase in the apparent cohesion of the specimens as a function of curing time. This is a justification that was explained in the shear test.

On the other hand, the strength limits are influenced by the $CaCO_3$ level of the material (Alloul 1981; Ben Dhia 1983). This $CaCO_3$ content explains the deposition and recrystallization of calcite. It is a function of the evaporation of the quantity of water (change in water content) that was used for compaction (Ben Dhia 1983). Principally, calcium carbonate has three crystalline phases, namely calcite, vaterite and aragonite. The stability and formation of these phases are very temperature and concentration-dependent (Usmany et al. 2016). Here calcite is particularly stable at laboratory temperature, while aragonite can be formed at high T°. Moreover, vaterite occurs at the higher levels of supersaturated solution (Flaten et al. 2009). There is also an amorphous calcium carbonate (ACC) found as a scale deposit, which is thermodynamically unstable

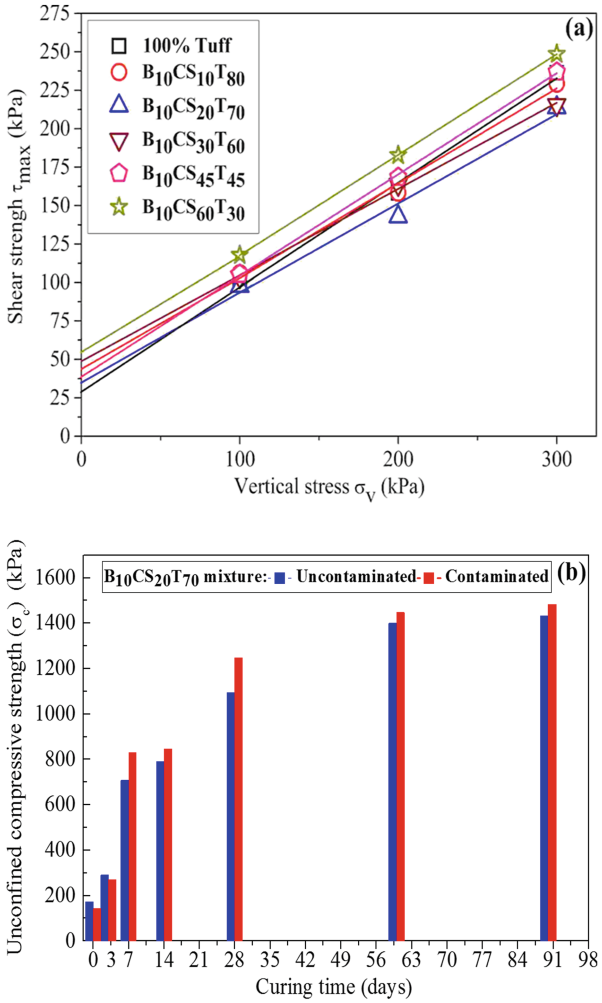


**Fig. 7.** Unconfined compressive strength ($\sigma_c$) of contaminated $B_{10}CS_{20}T_{70}$ mixture versus curing time.

and could spontaneously crystallize when suspended in an aqueous solution at laboratory temperature (Rodriguez et al. 2011). Further, the pure amorphous calcium carbonate will transform into to calcite via vaterite immediately at low temperatures (<30 °C) and to aragonite via vaterite at the higher temperatures (T ≥ 40 °C) (Rodriguez et al. 2011). The thermodynamically most stable phase is calcite and can be easily formed under normal conditions. The formation of the different polymorphs of $CaCO_3$ is strongly influenced by precipitation conditions. It is assumed that the change in the binding strength of Ca-$CO_3$ as a function of pH plays an important role in the determination of the different forms of ACC, which then develop into specific polymorphs of calcium carbonate. However, changes in the pH of the solution (i.e., the compaction water) will affect the

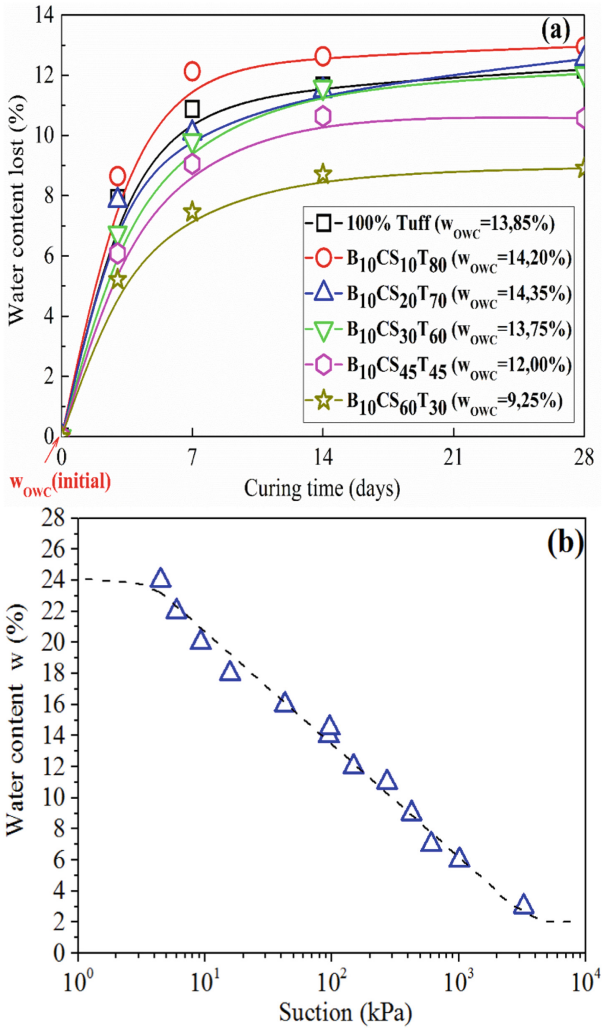


**Fig. 8.** (a) water content lost versus curing time of all the $B_{10}CS_xT_y$ mixtures (b) suction versus water contents of the $B_{10}CS_{20}T_{70}$ mixture

equilibrium concentration of the different carbon species (e.g., $HCO_3^-$ and $CO_3^{2-}$). This will affect the $Ca/CO_3$ ratio in solution, making it difficult to separate the effects of pH and stoichiometry of the solution.

The mixtures studied generally have a high carbonate content, indicating high cementing. To do this, the calcium carbonate ($CaCO_3$) level was measured by chemical analysis after crushing the specimens of each mixture stored for one year. The results obtained are given in Table 8 (by NF P 94-048, 1996 standard). It is notable that the $CaCO_3$ level changes according to the shelf life. In the presence of the leachate, cations and ions may act to make the vaterite more stable (Usmany et al., 2016) and not

turn into calcite. For this reason, we did not notice any increase in calcium carbonate crystallization.

**Table 8.** $CaCO_3$ content versus storage period for $B_{10}CS_XT_Y$ mixtures and tuff.

| % $CaCO_3$ of mixtures | | Storage period (days) | | | | | |
|---|---|---|---|---|---|---|---|
| | | 7 | 14 | 28 | 60 | 90 | 1an |
| $B_{10}CS_{10}T_{80}$ | | 59 | 58 | 60 | 61 | 61 | 62 |
| $B_{10}CS_{20}T_{70}$ | Contaminated | 59 | 60 | 60 | 60 | 60 | 60 |
| | Uncontaminated | 61 | 63 | 63 | 64 | 64 | 64 |
| $B_{10}CS_{30}T_{60}$ | | 60 | 60 | 61 | 61 | 61 | 61 |
| $B_{10}CS_{45}T_{45}$ | | 61 | 62 | 62 | 63 | 63 | 66 |
| $B_{10}CS_{60}T_{30}$ | | 62 | 63 | 64 | 66 | 68 | 69 |
| Tuff | | 67 | 67 | 68 | 70 | 70 | 71 |

## 4 Conclusions

This study was conducted to determine the effect of leachate contamination on the hydromechanical (compressibility, hydraulic conductivity, shear strength, unconfined compressive strength, unconfined tensile strength) and chemical characteristics of compacted $B_{10}CS_XT_Y$ mixtures. Several conclusions can be made as a result of this study:

i. For some formulations, leachate caused a reduction in the free swelling of more than 40% compared to water;
ii. The $B_{10}CS_{20}T_{70}$ mixture is relatively stable against chemical attack from leachate ($G_{water} = 12.20\%$ and $G_{Leach.} = 10.425\%$ after 12 days of saturation);
iii. Quartz mineral in with leachate contaminated bentonite increased while the montmorillonite content decreased;
iv. Tuff reacts better with leachate (decrease in carbonate peaks) than crushed sand, which showed high stability in mineralogy;
v. The leachate caused a slight increase in hydraulic conductivity obtained by the Falling-Head tests;
vi. The optimal mixture that satisfies hydraulic conductivity criteria is the $B_{10}CS_{20}T_{70}$ mixture in both cases of saturation with water ($k_v = 1.93x10^{-9}$ m/s) and with leachate ($k_v = 2.84x10^{-9}$ m/s);
vii. Measurements of the pH and electrical conductivity of leachate-contaminated mixtures revealed a decrease in pH values and an increase in electrical conductivity values;

viii. The shear strength parameters of the $B_{10}CS_{20}T_{70}$ mixture are affected by leachate contamination. For this mixture, the samples tested at Proctor density showed an increase in cohesion ($C_{uu}$) (from 35 to 51 kPa) and a decrease in friction angle ($\varphi_{uu}°$) (from 30° to 28.5°) due to leachate contamination;
ix. For unconfined compression tests on statically compacted $B_{10}CS_XT_Y$ mixtures, the strength was found to be in accordance with the recommended value in the literature (> 200 kPa);
x. The effect of leachate on mechanical behavior is a positive effect of an increase in mechanical strength (from 1.40 to 1.48 MPa, for compressive strength).

Finally, the adopted formulation of $B_{10}CS_{20}T_{70}$ perfectly meets the requirements of the regulations in force and is an economic product of local materials available in abundance for the design of bottom barriers especially in arid and semi-arid areas.

## References

Abdellah, D., Gueddouda, M.K., Goual, I., Souli, H., Ghembaza, M.S.: Effect of landfill leachate on the hydromechanical behavior of bentonite-geomaterials mixture. Constr. Build. Mater. **234**, 117356 (2020)

Abeele, W.V.: The influence of Bentonite on the permeability of sandy silt. Nuclear and chemical waste management **6**, 81–88 (1986). https://doi.org/10.1016/0191-815x(86)90091-4

AFNOR NF P 94-048. Sols : reconnaissance et essais-Détermination de la teneur en carbonate—Méthode du calcimètre. AFNOR, 11 p. (1996)

AFNOR NF P94-071-1: Sols : reconnaissance et essais - Essai de cisaillement rectiligne à la boîte - Partie 1 : cisaillement direct (1994)

AFNOR NF P94-420: Roches - Détermination de la résistance à la compression uniaxiale (2000)

AFNOR NF X 30-441: Déchets—Détermination en laboratoire du coefficient de la conductivité hydraulique à saturation d'un matériau—Essais de la conductivité hydraulique au permeamètre a' paroi rigide a' gradient hydraulique constant/variable (2008)

AFNOR XP P94-091: Sols: Reconnaissance et Essais–Essais de gonflement à l'œdomètre–Détermination des déformations par chargement de plusieurs éprouvettes (1995)

Alloul, B.: Étude géologique et géotechnique des tufs calcaires et gypseux d'Algérie en vue de leur valorisation routière. Thèse de docteur de 3ème cycle de l'Université de Paris VI (1981)

ASTM D 52980-094: Standard test method for measurement of soil potential (suction) using filter paper, vol. 4.09, pp. 154–159 (1995)

ASTM D1125: Standard test method for Resistivity and Consuctivity of Water and Soils (2009)

ASTM D4972–01: Standard test method for pH of soils." ASTM International, West Conshohocken (2007)

Ayininuola, G.M., Agbede, O.A., Franklin, S.O.: Influence of calcium sulphate on subsoil cohesion and angle of friction. J. Appl. Sci. Res. **5**, 297–304 (2009)

Ben Dhia, M.H.: Les encroûtements calcaires en Tunisie et dans le monde. Bulletin de liaison des laboratoires des ponts et chaussées **126**, 5–14 (1983)

Boulanger, M.V.: Performance D'une Couverture Avec Effets de Barrière Capillaire Fait de Mélanges Gravier-Bentonite Pour Contrôler La Migration D'oxygène En Conditions Nordiques Université de MONTRÉAL Département Des Génies Civil, Géologique Et, and D E S Mines, 196 p. (2015)

Callot, G., Dupuis, M.: Le calcaire actif des sols et sa signification, SCI Sol, n° 117-27 (1980)

Daniel, D.E., Benson, C.H.: Water content-density criteria for compacted soil liners. J. Geotech. Eng. **119**(2), 223–237 (1990). https://doi.org/10.1061/(asce)0733-9410(1990)116:12(1811)

Demdoum, A.: Comportement hydrique et mécanique d'un mélange de Bentonite-Sable Calcaire-Tuf: Application à la conception des Installations de Stockage des Déchets (ISD) (Doctoral dissertation). Français. ⟨tel-02099687⟩ (2019)

Demdoum, A., Gueddouda, M.K., Goual, I.: Experimental study on hydro-mechanical characteristics of compacted bentonite-moderately calcareous soil mixtures for landfill liners purposes. In: International Symposium on Construction Management And Civil Engineering (ISCMCE 2017), Skikda, Algeria (2017a)

Demdoum, A., Gueddouda, M.K., Goual, I.: Effect of water and leachate on hydraulic behavior of compacted bentonite, crushed sand and tuff mixtures for engineering barriers. Geotech. Geological Eng. **35**(6), 2677–2696 (2017b). https://doi.org/10.1007/s10706-017-0270-4

Demdoum, A., Gueddouda, M. K., Goual, I., Berkak, H.: Effect of liquid type on the hydraulic characteristic of compacted local geomaterials for use as hydraulic barriers. In: International Symposium on Materials and Sustainable Development, pp. 451–464. Springer, Cham (2018). https://doi.org/10.1007/978-3-319-89707-3_51

Demdoum, A., Gueddouda, M.K., Goual, I., Souli, H.: Unsaturated Hydraulic Characteristics of Compacted Local Geo-Materials for use as Landfill Liners. Algerian J. Res. Technol. **4**(1), 34–41 (2020)

Demdoum, A., Gueddouda, M.K., Goual, I., Souli, H., Anlauf, R., Ghembaza, M.S.: Effect of water content on hydraulic properties of bentonite–geomaterials mixture. Eur. J. Environ. Civ. Eng. 1-26 (2019). https://doi.org/10.1080/19648189.2019.1628108

Demdoum, A., Gueddouda, M.K., Goual, I., Benabed, B.: Geotechnical characterization of geomaterial blends with bentonite of Maghnia for use as landfill liners. J. Materials Process. Environ. **4**, 48–54 (2016)

Flaten, E.M., Seiersten, M., Andreassen, J.P.: Polymorphism and morphology of calcium carbonate precipitated in mixed solvents of ethylene glycol and water. J. Cryst. Growth **311**(13), 3533–3538 (2009)

Glatsteina, D.A., Francisca, F.M.: Hydraulic conductivity of compacted soils controlled by microbial activity. Environ. Technol. **35**(15), 1886–1892 (2014). https://doi.org/10.1080/09593330.2014.885583

Guney, Y., Aydilek, A.H., Demirkan, M.M.: Geoenvironmental behavior of foundry sand amended mixtures for highway subbases. Waste Manage. **26**(9), 932–945 (2005). https://doi.org/10.1016/j.wasman.2005.06.007

Guney, Y., Cetin, B., Aydilek, A.H., Tanyu, B.F., Koparal, S.: Utilization of sepiolite materials as a bottom liner material in solid waste landfills. Waste Manage. **34**, 112–124 (2014). https://doi.org/10.1016/j.wasman.2013.10.008

Harun, N.S., Rahman, A.Z., Rahim, A.S., Lihan, T., Idris, R.M.W.: Effects of leachate on geotechnical characteristics of sandy clay soil. AIP Conf. Proc. **1571**, 530–536 (2013)

Kaufhold, S., Dohrmann, R., Koch, D., Houben, G.: The pH of aqueous bentonite suspensions. Clays Clay Miner. **56**, 338–343 (2008). https://doi.org/10.1346/ccmn.2008.0560304

Kaza, S., Yao, L., Perinaz, B.T., Van Woerden, F.: What A waste 2.0: a global snapshot of solid waste management to 2050. World Bank Bonds & Investment Products (2018)

Koch, D.: Bentonites as a basic material for technical base liners and site encapsulation cut-off walls. Appl. Clay Sci. **21**, 1–11 (2002). https://doi.org/10.1016/s0169-1317(01)00087-4

Kouloughli, S.: Étude expérimentale des mélanges sable bentonite - leurs performances comme barrières de confinement dans les CET, Ph.D. thesis, of Mentouri University-Constantine (2007) http://bu.umc.edu.dz/md/index.php?lvl=notice_display&id=618

Li, B., Li, L., Grace, J.R.: Adsorption and hydraulic conductivity of landfill-leachate perfluorinated compounds in bentonite barrier mixtures". J. Environ. Manage. **156**, 236–243 (2015). https://doi.org/10.1016/j.jenvman.2015.04.003

Li, J.S., Xue, Q., Wang, P.: Influence of leachate pollution on mechanical properties of compacted clay: a case study on behaviors and mechanisms. Eng. Geol. **167**, 128–133 (2013)

Mishra, A.K., Ohtsubo, M., Li, L., Higashi, T.: Controlling factors of the swelling of various bentonites and their correlations with the hydraulic conductivity of soil-bentonite mixtures. Appl. Clay Sci. **52**(1–2), 78–84 (2011)

Morsli, M.: Contribution à la valorisation des tufs d'encroûtement en technique routière saharien. PhD Thesis. National Polytechnic School, ENP- Alger – Algeria (2007)

Nakayama, S., Sakamoto, Y., Yamaguchi, T., et al.: Dissolution of montmorillonite in compacted bentonite by highly alkaline aqueous solutions and diffusivity of hydroxide ions. Appl. Clay. Sci. **27**, 53–65 (2004)

Ören, A.H., Akar, R.Ç.: Swelling and hydraulic conductivity of bentonites permeated with landfill leachates. Appl. Clay Sci. **016**, 1317 (2016)

Ozcoban, M.S., Nejat, C., Suna, C., Guler, T.D., Cansiz, V., Tufekci, N.: Hydraulic conductivity and removal rate of compacted clays permeated with landfill leachate. Desalin. Water Treat **51**(31–33), 6148–6157 (2013). https://doi.org/10.1080/19443994.2013.769662

Pansu, M., Gautheyrou, J.: Handbook of Soil Analysis. Springer, New York (2006)

Parker, R.J., Bateman, S., Williams, D.: Design and management of landfills Geotechnical management of waste and contamination. In: Fell, P., Gerard (eds.) pp. 209–252, Balkema, Rotterdam (1993)

Pusch, R.: Bentonite clay: Environmental Properties and Applications CRC Press is an imprint of the Taylor & Francis Group an informa business 368 p. (2015)

Rodriguez-Blanco, J.D., Shaw, S., Benning, L.G.: The kinetics and mechanisms of amorphous calcium carbonate (ACC) crystallization to calcite, via vaterite. Nanoscale **3**(1), 265–271 (2011)

Schreler, B., Delage, P.: Géomécanique environnementale risques naturels et patrimoine. HERMES, Science Europe Ltd. (2001)

Stewart, D.I., Cousens, P.G., Studds, T.W.: The factors controlling the engineering properties of bentonite-enhanced sand source. Appl. Clay Sci. **23**(1–4), 97–110 (2003)

Sunil, B.M., Shrihari, S., Nayak, S.: Shear strength characteristics and chemical characteristics of leachate-contaminated lateritic soil. Eng. Geol. **106**(1–2), 20–25 (2009). https://doi.org/10.1016/j.enggeo.2008.12.011

Usmany, Y., Putranto, W.A., Bayuseno, A.P., Muryanto, S.: Crystallization of calcium carbonate (CaCO3) in a flowing system: Influence of Cu2 + additives on induction time and crystalline phase transformation. In: AIP Conference Proceedings, vol. 1725, No. 1, p. 020093. AIP Publishing LLC, April 2016

Xue, Q., Zhang, Q.: Effects of leachate concentration on the integrity of solidified clay liners. Waste Manage. Res. **32**, 198–206 (2014)

Ye, W.M., Zheng, Z.J., Chen, B, et al.: Effects of pH and temperature on the swelling pressure and hydraulic conductivity of compacted GMZ01 bentonite Appl. Clay. Sci. **101**, 192–198 (2014)

# Biosurfactants Production from Newly Isolated *Aspergillus sp.* FS11 Using Agro-Industrial Wastes

L. Derguine-Mecheri(✉) and S. Kebbouche-Gana

Laboratoire de conservation et valorisation des ressources biologiques, Université M'Hamed Bougara Boumerdès, Boumerdes, Algeria
louiza.derguine@gmail.com

**Abstract.** The aim of this work is the isolation, identification, production, characterization and properties of biosurfactant producing fungal strain. The fungal strain FS11 was isolated from water oil field collected in southern Algeria and identified as *Aspergillus sp.* FS11. In an attempt to provide cost-effective carbon source for biosurfactants production, crude olive mill wastewater (OMW) was used as fermentative medium for 9 days under conditions of pH 5, temperature of 28 °C and agitation of 150 rpm. After cultivation period, the emulsification index value $E_{24}$ reached 76% and ST reduction from 72 to 42 ± 0.20 mN/m. TLC and FTIR analysis of the crude extract, showed that crude biosurfactant was partially characterized as glycolipoprotein complex. The crude biosurfactant presented interesting properties such us; significant reduction in surface tension, important emulsifying activity and stability over a wide range of pH (2 to 12), temperature (4–100 °C) and salinity (1–10%). More interestingly, the produced biosurfactant, have proved great potential application in MEOR microbial enhanced oil recovery (removal rate greater than 50%).

**Keywords:** Biosurfactants · *Aspergillus sp.* FS11 · Crude OMW · ST · $E_{24}$

## 1 Introduction

Biosurfactants include a class of structurally diverse molecules synthesized by microorganisms such as bacteria, yeasts and filamentous fungi, they can be excreted in culture media (extracellular) or incorporated in the cell wall (intracellular), their molecular weight is generally between 500 and 1500 Da (Santos et al. 2016). Biosurfactants are amphiphilic molecules consisting of a polar hydrophilic part and a nonpolar hydrophobic part. The hydrophilic group is composed of mono- or polysaccharides, carboxylic acids, amino acids or peptides, while the hydrophobic group is composed of saturated or unsaturated fatty acids, hydroxylated fatty acids or alcohols (Bahia et al. 2018), which gives biosurfactants the ability to reduce interfacial tensions between two phases of different polarities such as oil and water, air and water, or water and a solid, allowing these two phases to mix and interact more easily (Pacwa-Plokiniczak et al. 2011). Biosurfactants


B. Safi et al. (Eds.): ISMSD 2019, *Proceedings of the 4th International Symposium on Materials and Sustainable Development*, pp. 115–127, 2020.
https://doi.org/10.1007/978-3-030-43211-9_10

have a wide range of biotechnological applications in various industries; petroleum, food, cosmetic, pharmaceutics, detergents, textiles, paints, mines and nanotechnology. Currently, the main market is the oil industry (Santos et al. 2016).

In addition, they show unique properties such us environmental compatibility, biodegradability, low toxicity, resistance to extreme conditions of temperature, pH and salinity. Therefore, the industry is increasingly interested in biosurfactants as potential substitutes for synthetic surfactants (Banat et al. 2014). However, although biosurfactants offer advantages over their synthetic counterparts, and have a promising use in various industries, they are not yet widely used on an industrial scale because of their low yields and high production costs (Banat et al. 2014). So, the success of the use of biosurfactants requires a reduction in production costs. This reduction can be achieved through the recovery of renewable and cheap wastes as substrates for biosurfactants production. The utilization of raw materials led to the development of an effective cost reduction strategy, associated with wastes management, by reducing the amount of wastes generated by different companies (Banat et al. 2014). As a result, a growing number of studies have investigated the production of biosurfactants using different low-cost substrates such as whey, molasses, corn steep liquor CSL, olive mill wastewater and frying oil as alternative substrates and media for biosurfactants production. Mediterranean countries covers 95% of the world olive wealth, Algeria is among them. The olive industry produces olive oil and two residues: one solid and the other liquid known as olive mill wastewater (OMW) (Dermeche et al. 2013). OMW is a concentrated black color liquor, it contains sugars (20–80 g/L), nitrogen compounds (12–24 g/L), organic acids (5–15 g/L), and residual oil (0.3–5 g/L). However, OMW contain polyphenols, which usually represents an environmental problem (Banat et al. 2014). Although the production of olive oil is a seasonal activity, the quantity of OMW produced is considerably reduced compared to other types of industrial wastes; the contribution of OMW to environmental pollution is not negligible. OMW is considered as one of the most harmful effluents from agro-food industries, because of their toxicity, in fact, 1 $m^3$ of OMW is equivalent to 200 $m^3$ of domestic wastewater (Cardinali et al. 2010). Thus, the OMW disposal is an environmental concern and a major challenge for Mediterranean countries. With that in mind, this study focused on providing a low cost effective media for biosurfactants production by fungal strain FS11 isolated from oil field water in Algeria. The kinetics of production, characterization and properties of produced biosurfactant (emulsifying, surface activity and stability studies) were evaluated. Assays on application of produced biosurfactants in microbial-enhanced oil recovery (MEOR) were also investigated.

## 2 Materials and Methods

### 2.1 Isolation of the Fungal Strain

Fungal strain was isolated from oil field water from the Algerian Sahara, province of Ouargla. 10 ml of water sample were aseptically introduced into Erlenmeyer flasks containing 90 ml of PDC potato dextrose broth supplemented by 0.1 g/L of chloramphenicol to inhibit bacterial growth, then incubated in a shaker with agitation of 120 rpm at 25 °C for 18 h. Isolation was made by the classical method of decimal dilutions. Distinguished colonies were isolated on PDA (potato infusion 200 g, dextrose 2%, 2% agar, 0.1 g/L

of chloramphenicol). Pure cultures of isolate were maintained at 4 °C in PDA chloramphenicol. Transfers were made to fresh agar plates each month to maintain viability (Botton et al. 1990).

### 2.2 Screening for Biosurfactants Producing Strains

Screening for biosurfactants production was done using different techniques such as the emulsification index test $E_{24}$, the drop collapse technique, the test of spred oil and the measurement of surface tension ST. Isolate was transferred to a 100 ml Erlenmeyer flask containing 50 ml of PDB supplemented by crude oil (2%, w/v) for a week at 25 °C with constant shaking of 150 rpm. The obtained cell free culture was subjected for emulsification index $E_{24}$, drop collapse, oil displacement and surface tension measurement using a digital tensiometer (Gibertini, Italy) as described by (Bodour and Miller-Maier 1998; Youssef et al. 2004; Pallas and Pethica 1983), respectively. All the screening experiments were performed in triplicates and the mean values were used as results.

### 2.3 Identification of Fungal Strain

The macroscopic observation of colonies like the texture of the thallus (velvety, woolly, powdery, granular ….), the color of the thallus (pigmentation of the mycelium, color of the conidia), the color of the reverse side of the culture and the presence of a diffusible pigment in the medium makes it possible to carry out a first characterization on special media (MEA and PDA). As well as microscopic observations of conidiophores, conidia, mode of implantation of conidiogenic cells, spores and their aspects (Botton et al. 1990).

### 2.4 Biosurfactants Production from OMW

OMW is an aqueous, reddish to black residual liquid with a strong olive odor and cloudiness. OMW used in this study was kindly supplied from an olive oil mill located in the north of Algeria, which uses a continuous three-phase centrifugation process for olive oil extraction. It was stored at 4 °C until use. The crude OMW was used without any treatment just diluted in order to adjust carbohydrates initial concentrations to 2% (v/v). Then, the medium based on crude OMW was filtered and then sterilized at 120 °C for 20 min.

### 2.5 Culture in Batch

Batch cultures were carried out in Minifors Bioreactor (INFORS HT) 2,5 L using crude OMW as substrate for low cost biosurfactants production. An initial spore concentration of $10^6$ spores/ml was prepared in sterile physiological water, and then transferred to 500 ml Erlenmeyer flasks, containing 100 ml of crude OMW medium, and incubated for 72 h at 28 °C in shaker incubator (150 rpm).

Kinetics of growth and biosurfactant production were conducted for 9 days. The inoculation was done from preculture. The temperature was set at 28 °C, orbital shaking at 150 rpm and pH 5. At regular intervals, different parameters were monitored such as biomass (g/L), pH, emulsification index $E_{24}$ (%) and surface tension TS (mN/m). All the experiments were performed in triplicate.

### 2.6 Isolation of Crude Biosurfactant

The crude OMW culture broth was centrifuged at 10.000 rpm for 20 min at 4 °C. The obtained supernatant was subjected to acid precipitation at 4 °C overnight (pH of the filtered supernatant was adjusted to 2 using 6N HCl). The obtained supernatant was extracted thrice with an equal volume of ethyl acetate and methanol (2/1, v/v). The biosurfactant was concentrated using a rotary evaporator at 40 °C. Biosurfactant yield was expressed in g/L (Derguine-Mecheri et al. 2018).

### 2.7 TLC Characterization

Biosurfactant was separated by TLC using different solvent systems; chloroform: methanol: water (60/30/10) for sugars, Acetone: acetic acid: water (70/20/10) for amino acids and chloroform: methanol: water (65/25/10) for lipids. Chemical revelation was done with ninhydrin for peptides detection, Molisch reagent for detection of sugar compounds. For lipids detection, plate was developed in a chamber saturated with iodine fumes. Isolated fractions were subjected to macromolecules quantification. Carbohydrate, protein and lipids estimations were carried out by the methods described by (Dubois et al. 1956; Bradford 1976; Goldsworthy et al. 1972), respectively.

### 2.8 Fourier Transform Infrared Spectroscopy (FTIR)

Samples were prepared by dispersing the solid uniformly in a matrix of potassium bromide. IR absorption spectra were obtained using a built-in plotter. Infrared absorption spectra of the sample were measured over the wave number range of 400–4000 $cm^{-1}$ with a resolution of 4 $cm^{-1}$.

### 2.9 Stability Studies

Stability studies regarding surface tension and emulsification activity were performed using cell free broth from crude OMW medium. Effect of temperature was studied by heating the cell free broth at high temperatures from (4 to 100 °C) for 1 h. Effect of pH was studied over a range of pH (2 to 12). The effect of salinity concentrations (1–10% NaCl) was also investigated.

### 2.10 Crude Biosurfactant in Microbial Enhanced Oil Recovery

20 g of sand impregnated with 2 g of crude oil were transferred to 250 ml Erlenmeyer flasks, followed by the addition of 40 ml of the cell-free broth, 40 ml of distilled water and 40 ml of SDS as negative and positive controls. The samples were incubated for 24 h at 27 °C with constant shaking of 150 rpm, and then centrifuged at 10000 g for 15 min to eliminate sand. The amount of oil in the sand after contact with the biosurfactant was gravimetrically measured after extraction by hexane and solvent evaporation (Derguine-Mecheri et al. 2018).

### 2.11 Statistical Analysis

All the experiments were run in triplicates. The standard errors for mean (SEM) values, at 95% confidence level, were calculated and represented as error bars in all the graphical representations.

## 3 Results and Discussion

### 3.1 Screening for Biosurfactants Producing Fungal Strains

Fungal isolate coded FS11 was a potent biosurfactants producer, as it presented the followings results: emulsification activity evaluated by calculation of $E_{24}$ ($E_{24} = 65.33 \pm 0.47\%$), drop collapse (**+++**), spread oil (+++, diameter of displacement zone = 2.1 cm) and reduction of surface tension of water from 72 to 42 mN/m. The drop collapse method is a sensitive and easy method for detecting the presence of biosurfactants; it can give positive results with a very small amount of biosurfactant, by the appearance of a flat drop in the 92 micro titter plate. In addition, oil displacement test is a quick and easy test to perform, and requires no specialized equipment. In light of these results, the isolate FS11 was selected for the rest of this study.

### 3.2 Isolate Identification

Isolate FS11 is green-brown, powdery, flat, and fluffy (Fig. 1a). The reverse of the colony is brown (Fig. 1b). It belong to the genus of *Aspergillus* because it showed the following criteria: A thallus with numerous upright conidiophores, unbranched, terminally vesiculated, phialides formed directly on the vesicle (Fig. 1c). The whole vesicle, metules, phialides and conidia constitute the *Aspergillus* head characteristic of the genus of *Aspergillus* (Botton et al. 1990). As results isolate FS 11 was identified as *Aspergillus sp.* FS11.

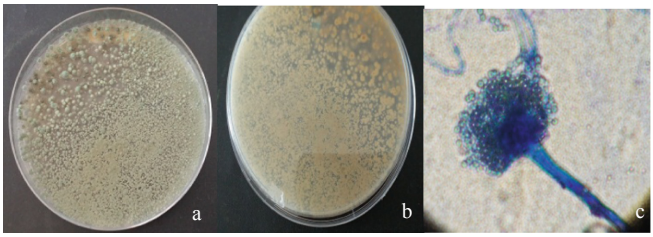


**Fig. 1.** Micrographs of *Aspergillus sp.* FS11. Cultures were grown for 3 days at 25 °C on PDA (a: fungal colony, b: reverse side of colony), (c) Micrographs of cells of *Aspergillus sp.* FS11. taken with photonic microscope x40.

### 3.3 Kinetics of Biosurfactants Production by *Aspergillus sp.* FS11 Using Crude OMW

Figure 2 displays the kinetic of batch fermentation of *Aspergillus sp.* FS11 isolate on crude OMW medium. The biomass reaches its maximum value after the 7$^{th}$ day of fermentation (biomass equal to 8.77 ± 0.05 g/L) corresponding to the highest emulsification index value $E_{24}$ (76 ± 0.28%) and also to the value of the lowest ST which is equal to 42 ± 0,20 mN/m. The production of biosurfactants took place from the 1$^{st}$ day of fermentation, to reach a maximum of production during the stationary phase with a biosurfactant concentration of 11.15 ± 0.7 g/L. This production is directly related to cell growth, when the biomass increases the ST decreases. The pH increased slightly after the 8$^{th}$ day of fermentation, in parallel with this increase, a slight increase in ST value and a slight decrease in the $E_{24}$ index followed by the decrease in biomass, which indicates the beginning of the decline phase.

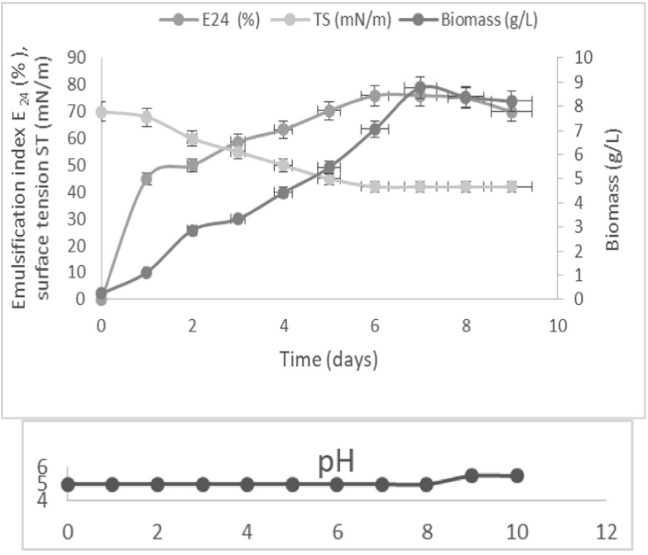


**Fig. 2.** Biosurfactant production profile; biomass, pH, surface tension, and emulsification index of *Aspergillus sp.* FS11 grown at 28 °C, pH 5 and agitation of 150 rpm on crude OMW medium in 2L bioreactor.

Colak and Kahraman (2013), reported that *Pseudomonas aeruginosa* produced a maximum of 400 mg/L of rhamnolipids using a 50% OMW as culture medium. In addition, Gudiña et al. (2016) studied the production of rhamnolipids by *Pseudomonas aeruginosa* # 112 using a medium containing 25% of OMW as culture medium, and found that *Pseudomonas aeruginosa* # 112 produced 5.124 ± 0.125 g/L of rhamnolipids after 168 h culture, with a reduction of the ST from 72 to 29.2 mN/m and $E_{24}$ of 58.4%. Mendes Souza et al. (2016), evaluated biosurfactant production by a fungal strain *Mucor polymorphosphorus* using CSL as a substrate for cultivation, fermentation was monitored for 96 h at 28 °C and 150 rpm. A reduction of the ST from 72 to 33.2 mN/m was

obtained. Qazi et al. (2014), studied the production of biosurfactants by *Fusarium sp.* BS-8 on PDB supplemented with vegetable oil, they noted that *Fusarium sp.* BS-8 produced biosurfactants with a concentration of 5.25 g/L, which was able to reduce surface tension from 72 mN/m to 32 mN/m, with an $E_{24}$ of 71%. Quantification of the crude biosurfactant extracts revealed that *Aspergillus sp.* FS11 produced biosurfactants with a concentration of 11.15 ± 0.7 g/L when grown on crude OMW medium at 28 °C, pH 5 and 150 rpm. *Ustilago maydis* FBD12 produced biosurfactants with a yield of 0.183 g/L and 0.096 g/L using fish oil and soybean oil as substrates, respectively, for 9 days of culture (Cortes-Sánchez et al. 2011).

### 3.4 Characterization of Biosurfactant

Figure 3 displays the CCM results of crude extract produced by *Aspergillus sp.* FS11, it showed several spots in chromatograms after the TLC analysis: 1 spot in carbohydrate chromatogram, 4 spots in proteins chromatogram and 1 spot after lipid revelation corresponding to the following Rf values: 0.25, 0.18, 0.59, 0.73, 0.80 and 0.74, respectively.

The estimation of macromolecules revealed the following concentrations: 1.07 ± 0.04 g/L of lipids, 2.76 ± 0.11 g/L of carbohydrates and 0.80 ± 0.02 g/L of proteins. According to the estimation and TLC analysis, the compound produced by *Aspergillus sp.* FS11 was partially characterized as a glycolipoprotein complex.

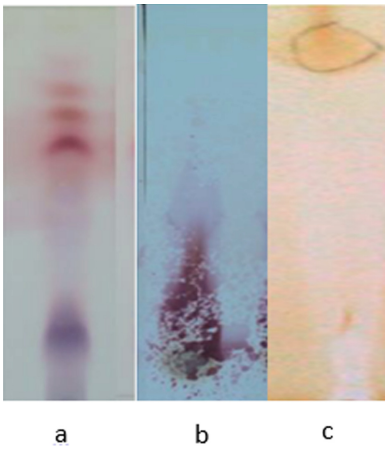


**Fig. 3.** TLC Analysis of crude biosurfactants produced by *Aspergillus sp.* FS11. grown on OMW medium after chemical revelation, A: Proteins, B Carbohydrates and C: Lipids.

The same results were reported by Kiran et al. (2009) for the strain *Aspergillus ustus* MSF3 grown on Sabouraud broth medium. The same authors reported that the biosurfactant from *Aspergillus ustus* MSF3 was partially characterized by TLC and macromolecules estimation as a glycolipoprotein mixture, with the following Rf values: 0.84 for lipids, 0.73 for carbohydrates and 0.80 for proteins, respectively with the following

concentrations: 0.38 g/L of lipids, 1.87 g/L of carbohydrates and 0.92 g/L of proteins. Recently, Pele et al. (2019) carried out a preliminary macromolecule estimation for crude biosurfactant extract produced by *Rhizopus arrhizus* UCP 1607. The authors reported that the produced biosurfactant from CSL and glycerol-based medium is composed of proteins (38%), carbohydrates (35.4%) and lipids (5.5%), suggesting that it is a glycolipoprotein. In addition, Akintunde et al. (Akintunde et al. 2015), used CCM analysis for preliminary characterization of crude biosurfactants produced by *Aspergillus niger* and *Aspergillus flavus*. Thus, they noted that two spots were appeared after spraying with the Molisch reagent with Rf values of 0.38 et 0.46, respectively for *Aspergillus niger* and *Aspergillus flavus*, this allowed the authors to suggest a glycolipidic nature of crude extracts.

### 3.5 FTIR Characterization of Produced Biosurfactant

The FTIR absorption spectrum of the extract produced by *Aspergillus sp.* FS11 given in Fig. 4 showed the following bands: 3443 $cm^{-1}$ (indicates the presence of a bound OH bond), 2850 to 2960 $cm^{-1}$ characterizing the presence of CH bonds, 1633 $cm^{-1}$ which indicates the presence of C=O (ketone), 1403 $cm^{-1}$ (C-N bond), 1451 $cm^{-1}$ (O-H bond of carboxylic acids), from 1266 to 1071 $cm^{-1}$, indicates the presence of C−O and C−O−C of alcohols of the sugars. Thus, IR spectroscopy revealed the presence of both aliphatic (C-H bond), peptide (C-N bond) and sugar moieties.

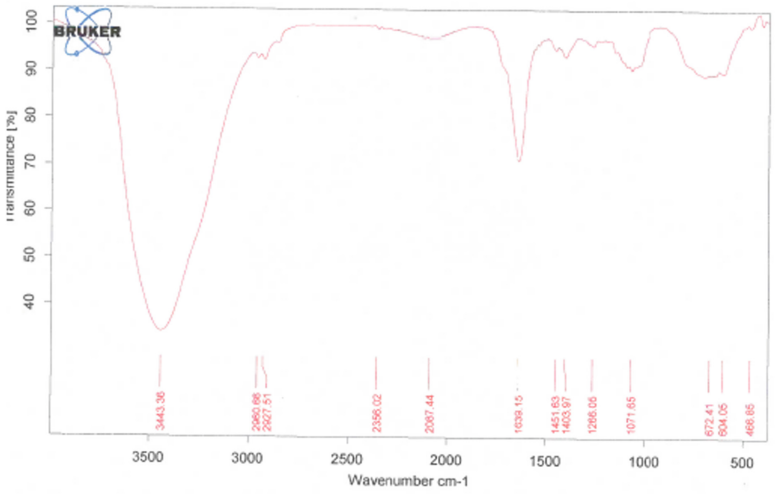


**Fig. 4.** FTIR spectra of the biosurfactant produced by *Aspergillus sp.* FS11 grown on OMW medium.

### 3.6 Stability Studies

The application of biosurfactants in several industries depend on their stability and their resistance to extreme environmental factors, such as: pH, salinity and temperature.

With this in mind, the effect of NaCl, temperature, and pH was studied and illustrated in Fig. 5a, b and c. For the influence of pH, crude biosurfactant produced by *Aspergillus sp.* FS11 was stable in a pH range from 2 to 12, with optimum stability at acidic pH 4, 6 and also at alkaline pH 8. At pH 10 and 12. Similar results have been reported by Abouseoud et al. (2008) for biosurfactants produced by *Pseudomonas fluorescens*. In addition, the stability of the emulsions was studied at different temperatures from 4 to 100 °C. The $E_{24}$ values and ST reduction showed very high stability over a temperature range 4 to 80 °C. Khopade et al. (2012) showed that the biosurfactant produced by *Nocardiopsis sp.* B4 was thermostable. Indeed, the heating of the biosurfactant at 100 °C did not have a significant effect on its performance. The emulsifying activity was stable at the temperatures tested. As for the effect of salinity, optimal stability of the biosurfactant was observed at concentrations of 1 to 8% NaCl. Few changes were observed at 10% (w/v). At the highest concentration of NaCl, produced biosurfactant retain 50% of their emulsifying activity. Kebbouche-Gana et al. (2009) reported that biosurfactant produced by a halophilic Achaea was stable at NaCl concentrations (up to 30%). In addition to the emulsifying activity, the reduction of ST is a relevant parameter for evaluation of an efficient production of biosurfactants. Results showed that ST remained stable under extreme pH, temperature and salinity conditions (Fig. 5a, b and c). These results are consistent with those reported by Kebbouche-Gana et al. (2009) and Kumar Gaur et al. (2019) for halophilic Achaea and *Candida spp*, respectively.

Significant stability at extreme conditions of pH, temperature and salinity provide to biosurfactants major importance in industrial food and environmental applications. Some of their potential applications in pollution and environmental control are control of oil spills, hydrocarbon degradation in contaminated soils, heavy metal removal from contaminated soil and hydrocarbon in aquatic environment and in microbial enhanced oil recovery MEOR as a tertiary method for recover remained oil using microorganisms or their metabolites including biosurfactants where pressure and salinity are at their extreme values (Pacwa-Płociniczak et al. 2011).

### 3.7 Microbial Enhanced Oil Recovery

The results showed that *Aspergillus sp.* FS11 have a potential in removal of crude oil from contaminated sand simple with recovery rate of 55%, relative to negative and positive controls, distilled water and synthetic surfactants SDS, Tween 80 with removal rate of 10% and 35% respectively. Different biosurfactants have been successfully used for the removal of petroleum products in contaminated soils. Batista et al. (2010) and Gusmão et al. (2010), studied the application of biosurfactants produced by *Candida tropicalis* and *Candida glabrata* UCP1002 in the remobilization of motor oil adsorbed to sand samples, and they recorded recovery rates of 80% and 92.6%, respectively. In addition, Luna et al. (2013), isolated a new biosurfactant, called Lunasan, produced by *Candida sphaerica* UCP 0995. This biosurfactant removed 95% of motor oil adsorbed to sand. Other surfactants produced by *Pseudomonas* species, rhamnolipids have been used successfully in this area (Silva et al. 2014).

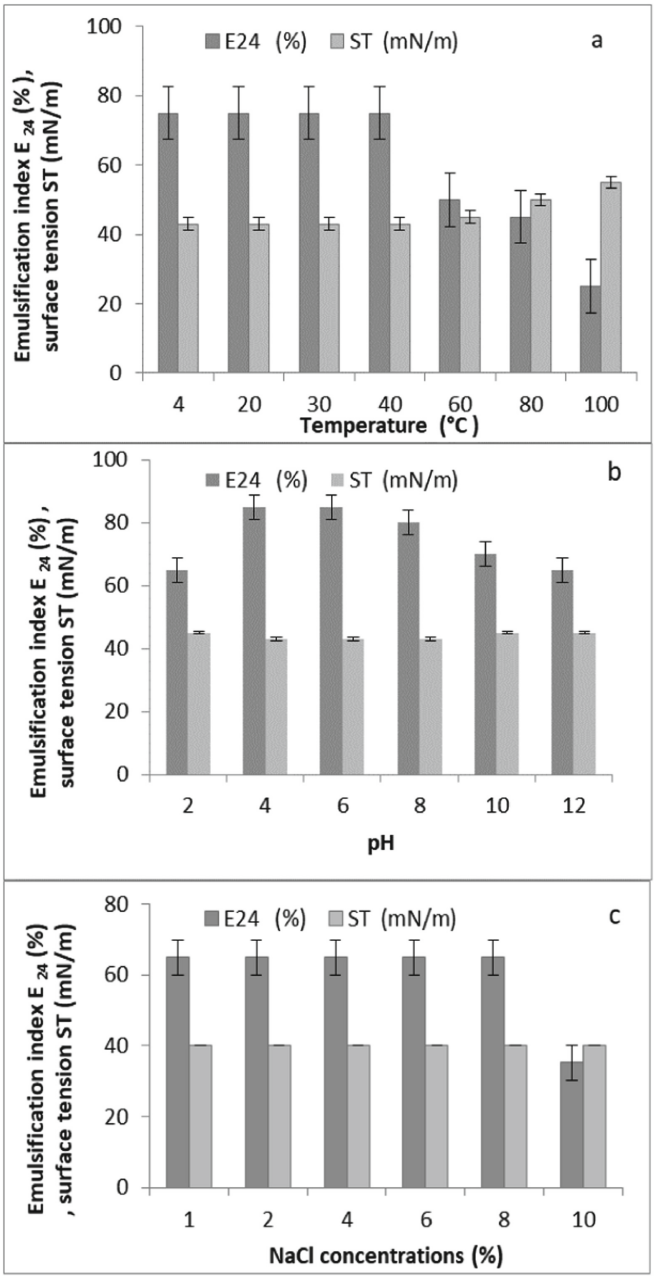


**Fig. 5.** Effect of temperature (a), pH (b) and salt concentrations (c) on stability of crude biosurfactant produced by *Aspergillus sp.* FS11. Grown on crude OMW regarding surface tension and emulsifying activity. Error bars illustrate experimental errors (standard deviations), calculated from three independent experiments.

## 4 Conclusions

The successful marketing of any biotechnology product depends largely on its economic bioprocesses. Currently, the high production costs and low yields of biosurfactants make them uncompetitive compared to their chemical counterparts. In order to obtain an economic fermentation process, we focused on the utilization of inexpensive substrates based on agro-industrial waste for the fermentation under known conditions. Therefore, the study provide a low cost-effective medium for biosurfactants production by conversion of hazardous OMW to a value-added biosurfactants by fungal strain FS11 newly isolated from oil field water in Algeria. The produced biosurfactant by *Aspergillus sp.* FS11 grown on crude OMW based medium at 28 °C, pH 5 and agitation of 150 rpm in 2L bioreactor exhibited excellent stability over temperature range (4 to 100 °C), pH range (2 to 12) and also NaCl concentrations (1–10%), providing possibility of its applications in sectors like bioremediation and microbial enhanced oil recovery. The effect of the biosurfactants on the removal of crude oil from contaminated sand, showed a potential for application in MEOR.

## References

Abouseoud, M., Maachi, R., Amrane, A., Boudergua, S., Nabi, A.: Evaluation of different carbon and nitrogen sources in production of biosurfactant by Pseudomonas fluorescens. Desalination **223**, 143–151 (2008)

Akintunde, T.A., Boboye Bolatito, E., Abioye Olabisi, P., Oyeleke, S.B., Ijjah Udeme, J.J., Suleiman, A.: Characterization of new glycosophorolipid-surfactant produced by *Aspergillus Niger* and *Aspergillus flavus*. Eur. J. Biotechnol. Biosci. **3**, 34–39 (2015)

Bahia, F.M., Carneiro de Almeida, G., Pereira de Andrade, L., Gonçalves Campos, C., Queiroz, L.R., Vieira da Silva, R.L., Verardi Abdelnur, P., Corrêa, J.R., Bettiga, M., Parachin, N.S.: Rhamnolipids production from sucrose by engineered Saccharomyces cerevisiae. Sci. Rep. **8**, 2905 (2018)

Batista, R.M., Rufino, R.D., Luna, J.M., De Souza, J.E.G., Sarubbo, L.A.: Effect of medium components on the production of a biosurfactant from *Candida tropicalis* applied to the removal of hydrophobic contaminants in soil. Water Environ. Res. **82**, 418–425 (2010)

Banat, I.M., Satpute, S.K., Cameotra, S.S., Patil, R., Nyayanit, N.V.: Cost effective technologies and renewable substrates for biosurfactants' production. Front Microbiol. **5**, 697 (2014)

Bodour, A.A., Miller-Maier, R.M.: Application of a modified drop-collapse technique for surfactant quantitation and screening of biosurfactant-producing microorganisms. J. Microbiol. Methods **32**, 273–280 (1998)

Botton, B., Breton, M., Fevre, M., Gautier, S., Guy, Ph., Larpent, J.P., Reymond, P., Sanglier, J.J., Vayssier, Y., Veau, P.: Moisissures utiles et nuisibles Importance industrielle, 2ème édn. Collection Biotechnologies, Masson (1990)

Bradford, M.M.: A rapid and sensitive method for the quantitation of microgram quantities of protein utilizing the principle of protein-dye binding. Anal. Biochem. **72**, 248–254 (1976)

Cardinali, A., Cicco, N., Linsalata, V., Minervini, F., Pati, S., Pieralice, M.: Compounds in the phenolic fraction of olive oil. Clin. Chem. **46**, 976–988 (2010)

Colak, A.K., Kahraman, H.: The use of raw cheese whey and olive oil mill wastewater for rhamnolipid production by recombinant *Pseudomonas aeruginosa*. Environ. Exp. Biol. **11**, 125–130 (2013)

Cortes-Sánchez, A., Hernández-Sánchez, H., Jaramillo-Flores, M.: Production of glycolipids with antimicrobial activity by *Ustilago maydis* FBD12 in submerged culture. Afr. J. Microbiol. Res. **5**, 2512–2523 (2011)

Derguine-Mecheri, L., Kebbouche-Gana, S., Khemili-Talbi, S., Djenane, D.: Screening and biosurfactant/bioemulsifier production from a high-salt-tolerant halophilic Cryptococcus strain YLF isolated from crude oil. J. Petrol. Sci. Eng. **162**, 712–724 (2018)

Dermeche, S., Nadour, M., Larroche, C., Moulti-Mati, F., Michaud, P.: Olive mill wastes: biochemical characterizations and valorization strategies. Process Biochem. **48**, 1532–1552 (2013)

Dubois, M., Gilles, K., Hamilton, J., Rebers, P., Smith, F.: Colorimetric method for determination of sugars and related substances. Anal. Chem. **28**, 350–356 (1956)

Goldsworthy, G.J., Mordue, W., Guthkelch, J.: Studies on insect adipokinetic hormones. Gen. Comp. Endocrinol. **18**, 545–551 (1972)

Gudiña, E.J., Rodrigues, A.I., de Freitas, V., Azevedo, Z., Teixeira, J.A., Rodrigues, L.R.: Valorization of agro-industrial wastes towards the production of rhamnolipids. Biores. Technol. **212**, 144–150 (2016)

Gusmão, C.A.B., Rufino, R.D., Sarubbo, L.A.: Laboratory production and characterization of a new biosurfactant from *Candida glabrata* UCP1002 cultivated in vegetable fatwaste applied to the removal of hydrophobic contaminant. World J. Microbiol. Biotechnol. **26**, 1683–1692 (2010)

Kebbouche-Gana, S., Gana, M.L., Khemili, S., Fazouane-Naimi, F., Bouanane, N.A., Penninckx, M., Hacene, H.: Isolation and characterization of halophilic Archaea able to produce biosurfactants. J. Ind. Microbiol. Biotechnol. **36**, 727–738 (2009)

Khopade, A., Biao, R., Liu, X.: Production and stability studies of the biosurfactant isolated from marine *Nocardiopsis sp.* B4. Desalination **285**, 198–204 (2012)

Kiran, G.S., Hema, T.A., Gandhimathi, R., Selvin, J., Thomas, T.A.: Optimization and production of a biosurfactant from the sponge-associated marine fungus *Aspergillus ustus* MSF3. Coll. Surf. B Biointerfaces **73**, 250–256 (2009)

Kumar Gaur, V., Regara, R.K., Dhiman, N., Gautam, K., Srivastava, J.K., Patnaik, S., Kamthane, M., Manickam, N.: Biosynthesis and characterization of sophorolipid biosurfactant by *Candida spp.*: application as food emulsifier and antibacterial agent. Biores. Technol. **285**, 121–131 (2019)

Luna, J.M., Rufino, R., Sarubboa, L.A., Campos-Takaki, G.B.: Characterisation, surface properties and biological activity of a biosurfactant produced from industrial waste by *Candida sphaerica* UCP0995 for application in the petroleum industry. Colloids Surf. B **102**, 202–209 (2013)

Mendes Souza, P., Freitas-Silva, M., Alves de Lima, E., Silva, T., Silva, G.K.B., Lima, M.A.B., Nascimento, A.E., Marques, N., Santos, V.P., Oliveira, L.T., Campos-Takaki, G.M.: Factorial design based medium optimization for the improved production of biosurfactant by *Mucor polymorphosphorus*. Int. J. Curr. Microbiol. App. Sci. **5**, 898–905 (2016)

Pallas, N.R., Pethica, B.A.: The surface tension of water. Colloids Surf. **6**, 221–227 (1983)

Pacwa-Płociniczak, M., Płaza, G.A., Piotrowska-Seget, Z., Cameotra, S.S.: Environmental applications of biosurfactants: recent advances. Int. J. Mol. Sci. **12**, 633–654 (2011)

Pele, M.A., Rubio Ribeaux, D., Rodrigues Vieira, E., Souza, A.F., Luna, M.A.C., Montero Rodríguez, D., Andrade, R.F.S., Sales Alviano, D., Sales Alviano, C., Barreto-Bergter, E., Santiago, A.L.C.M.A., Campos-Takaki, G.M.: Conversion of renewable substrates for biosurfactant production by *Rhizopus arrhizus* UCP 1607 and enhancing the removal of diesel oil from marine soil. Electron. J. Biotechnol. **38**, 40–48 (2019)

Qazi, M.A., Kanwal, T., Jadoon, M., Ahmed, S., Fatima, N.: Isolation and characterization of a biosurfactant-producing *Fusarium sp.* BS-8 from oil contaminated soil. Biotechnol. Progress **30**, 1065–1075 (2014)

Santos, D.K.F., Rufino, R.D., Luna, J.M., Santos, V.A., Sarubbo, L.A.: Biosurfactants: multifunctional biomolecules of the 21st Century. Int. J. Mol. Sci. **17**, 401 (2016)

Silva, R.C.F.S., Almeida, D.G., Luna, J.M., Rufino, R.D., Santos, V.A., Sarubbo, L.A.: Applications of biosurfactants in the petroleum industry and the remediation of oil spills. Int. J. Mol. Sci. **15**, 12523–12542 (2014)

Youssef, N.H., Duncan, K.E., Nagle, D.P., Savage, K.N., Knapp, R.M.: Comparison of methods to detect biosurfactant production by diverse microorganisms. J. Microbiol. Methods **56**, 339–347 (2004)

# Analyses of the Micromechanics of Stress Transfer in Single Fiber Pull-Out Tests

Fatiha Teklal(✉), Bachir Kacimi, and Arezki Djebbar

Laboratory of Mechanics, Structures and Energetics (L.M.S.E), University of Mouloud MAMMERI, BP 17 RP, 15000 Tizi-Ouzou, Algeria
fatiha.teklal@ummto.dz

**Abstract.** Fiber composite technology is based on taking advantage of the high strength and high stiffness of fibers, which are combined with matrix materials of similar/ dissimilar natures in various ways, creating inevitable interfaces. In fiber composites, both the fiber and the matrix retain their original physical and chemical identities, yet together they produce a combination of mechanical properties that cannot be achieved with either of the constituents acting alone, due to the presence of an interface between these two constituents. Fibre-matrix interface is known to have contribution to the mechanical performance of fibre-reinforced composite by its potential for load transfer between the fibre and the matrix. The understanding of the interface (or interphase) in composites is the central point of this interdisciplinary effort. In this work, we are interested in the qualitative study of the interface by the means of' a micromechanical test, which defined by a behavior of a fiber embedded in a matrix block (test pull-out) to characterize the fiber/matrix interfacial adhesion solicited in traction. Initially, a theoretical study of the test is highlighted. Equations which give the evolution of the normal constraints to the level of the enchased filament and the sheath of matrix surrounding it, as well as the shear stress on the level of the interface are presented. In second place, we have to carry out a simulation of the mathematical equations under Matlab by varying the various parameters which present an influencing on the value of the interfacial shear stress, such as, the geometry of the model, embedded length of the fiber, fiber diameter and loading conditions, including components (fiber, matrix, interface). Curves are plotted and of interpretations are presented.

**Keywords:** Interface · Pull-out · Interfacial shear strength · Micromechanics · Damage

## 1 Introduction

The study of the mechanical behavior of composite materials often boils down to two basic constituents, i.e. matrix, and reinforcement. If the literature is rich on the theme of composites, it much more discreet about the influence of the interface or the interphase. Since the 1970 and the last few years alone, less than 30% of published articles dealing with interfaces while only 2% of the interphase. The notion of interface or interphase


B. Safi et al. (Eds.): ISMSD 2019, *Proceedings of the 4th International Symposium on Materials and Sustainable Development*, pp. 128–135, 2020.
https://doi.org/10.1007/978-3-030-43211-9_11

remains relatively vague, the interfacial zone does not exist in itself, it is created during the implementation of the composite. Therefore, it appears very difficult to assign to him the mechanical properties. However, this zone (interface/interphase) plays a leading role as shows it Drzal (1986) and Piggott (2004) in its works. Indeed, the interface and/or interphase ensure the transmission of the efforts between the relatively soft matrix and the stiffer reinforcement. From then, the contribution of the reinforcement on the mechanical properties of the composite is directly related to the quality of the interfacial zone Kim and Mai (1991). Kim et al. (1993), Kim and Mai (1995) show that the mastery of the interfacial zone is considered one of the criteria for composite design.

The interface is the key region which determines, on a macroscopic scale, the properties of any systems heterogeneous, Baley et al. (2004). The latter plays a vital role in the performance (In particular the holding in service) of composites by controlling the propagation of the cracks (in particular their kinetics), its role is all the more fundamental as a composite is a containing material of the defects, Muller and Sehlnauder (1993), Wu and Davies (2005), Wang et al. (2013), Sun et al. (2015), and Tran et al. (2019). The optimization of the interface appears as a condition necessary in order to be able to fully draw party from the coupling fiber/matrix in the composites Orifici et al. (2008). From an industrial point of view, this optimization should be realized regarding both the respective performances of the fiber and matrix, but still with respect to the elaboration process of the material (wettability, held in temperature …), to limit the potential defects of implementation of the material. A solution to improve the mechanical performance of the interface/interphase is coming treating the fiber for improving the chemical compatibility between the inorganic fiber and the organic matrix Keusch and Haessler (1999), Piggott (1997), and Bellini et al. (2019).

As mentioned earlier, the notion of the interface is not easy to understand and can cover, even if it is limited to the case of unidirectional composites, different realities: interphase fiber matrix but also the interfaces are many and varied in natures. We can distinguish two important classes: the interfaces related to the structure itself of the composite or interfaces generated by the process of implementation of the composite. The first result from the association of constituents' matrix and reinforcement (fiber/matrix interface). The seconds are one of the signatures of the implementation process, as the inter-layer interface, defined by the superposition of layers and/or intra-layers or inter-wick to the level of a layer Sun and Pan (2006), Mohammadi et al. (2015), and Dhiman et al. (2015). As for their influence on the behavior of composites, it is also difficult to model as to characterize. To study the behavior pull-out (push back) of a fiber embedded in a matrix block to characterize the interfacial adhesion fiber/matrix an analytical models has been proposed to measure the shear strength at the interface. The parameters influencing these properties, geometry models, the embedding length of the fiber, the fiber diameter and loading conditions, including the components (fiber, matrix, interface), the manufacture and defects itinerary will be widely discussed.

## 2 Principle and Interest of the Drop Test

The drop test is different from that of heaving the particular configuration of the samples: here, the fiber is embedded in a resin micro drop deposited on the monofilament before

cooking. During the tensile test, it is maintained by using two plates (Fig. 1. a). Can, by this technique, reach lengths of very low entrenchment, up to 30 μm, which is rarely possible pull-out. The only limiting factor is the test, in the case of a thermosetting resin, the initial viscosity of the resin, if it is too high, prevents the deposition of small drops. Finally, the drop test allows, from the pull-out, achieving relatively fast for a large number of samples (the implementation of these do not require specific mounting) Drzal (1986). Figure 1.b shows the curves obtained from tensile testing of gout. As in pull-out, these curves to determine the strength of groundwood $F_d$. The whole problem is then to relate this experimental scale to a specific parameter of the interface Piggott (2004), Kim and Mai (1991), Kim et al. (1993), Kim and Mai (1995), and Baley et al. (2004).

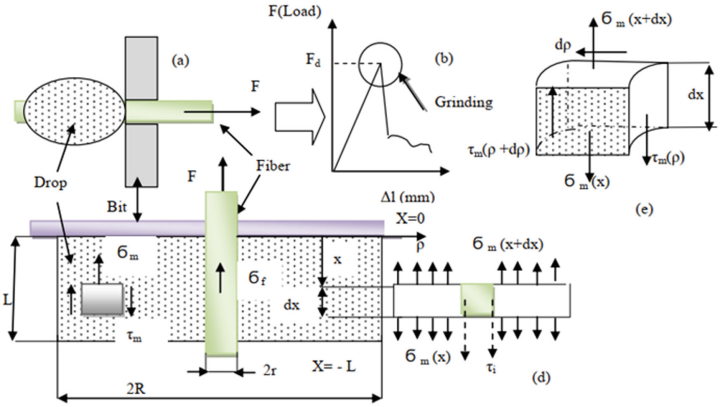


**Fig. 1.** Model of the drop/Fiber (a); load- displacement curve (b); balance of forces on a section (c), (d) and (e).

## 3 Geometry of the Drop and Put into Equation

### 3.1 Geometry of the Drop

The debonding test (pull-out) is a micromechanical characterization test of the interfacial adhesion fiber/ matrix is considered to be the most advanced technology. It consists of making a tensile test on a monofilament partially embedded in resin and measuring the force required to extract this fiber of its sheath of the matrix. The test of debonding was originally developed by Shiriajeva and Andreevskaya (1962), improved by Favre and Perrin (1972), Piggott et al. (1985), Hampe 1988 and Hampe et al. 1989. Different configurations of pull-out exist, the fiber may be embedded either in a microdroplet of resin or in a resin button or still, more typically, in a block of resin. In all cases, the resin is bonded to the lower part of the traction device.

Thus, it appears that the actual geometry of the test can be modeled as shown in Fig. 1.a, a cylinder of length L represents gout, or L is the length of entrenchment, but the length of the drop. Index, “m”, “f”, refers to the matrix and the fiber, τ means the

shear stress at the interface that is to say ρ = r. We put in elastic, linear, with axial symmetry (no twist). We assume that the axial stresses in the matrix $\sigma_m$, and in the fiber $\sigma_f$, radial effects are negligible. These effects include swelling of the matrix and fiber contraction due to the effects of Poisson's ratio.

### 3.2 Setting Equation

Let us now apply the balance of forces on various parts of the system, Fiber + drop (Fig. 1-a). The balance of forces operating on the fiber we get the whole Eq. (1).

$$F = \int_{x=-L}^{x=0} (2\pi r)\tau_i(x)dx \tag{1}$$

$$\frac{d\sigma_f}{dx} = \frac{2\tau_i(x)}{r} \tag{2}$$

$$\tau_i'' - \alpha^2\tau_i = 0 \tag{3}$$

The resolution of Eq. (3) gives the evolution of shear stresses at the fiber/matrix interface $\tau_i$ (x), the normal stress at the fiber level $\sigma_f$ and at the matrix level $\sigma_m$, are given by the Eqs. (4), (5) and (6) respectively:

$$\tau_i(x) = \frac{-\alpha F}{2\pi(ch(\alpha L) - 1)} sh[\alpha(x + L)] \tag{4}$$

$$\sigma_f = \frac{F[ch(\alpha(x + L)) - 1]}{\pi^2[ch(\alpha L) - 1]} \tag{5}$$

$$\sigma_m = \frac{-F[ch(\alpha(x + 1)) - 1]}{\pi(R^2 - r^2)[ch(\alpha L) - 1]} \tag{6}$$

For our simulation, we used a calculation software Matlab. The graphical representation of Eqs. (4), (5) and (6) depending on the length embedded in Fig. 2 and 3. We chose for our simulation; thermosetting epoxy matrix (drop) in diameter, 2R = 30 μm whose mechanical properties ($E_m$ = 4.5 GPa, $G_m$ = 1.6 GPa) and two types of E-glass filament (r = 4 μm, $E_f$ = 73 GPa) and carbon-HT (r = 3.5 μm, $E_f$ = 230 GPa).

### 3.3 Results of Drop Test

#### 3.3.1 Interpretation of Test Results Drop

The evolution of profile of the stresses $[\sigma_f, |\sigma_m|, |\tau_i|]$ according to the length enchased for the various values of the load applied are represented by Figs. 2 and 3.

From the plotted curves we find that evolutionary constraints $[\sigma_f, |\sigma_m|, |\tau_i|]$ is the same for both types of fiber (carbon, glass).

The value of the stress $\sigma_m$ of the matrix and shearing of the interface $\tau_i$ varies in a decreasing way with the length of the enshrining until they become null; same for

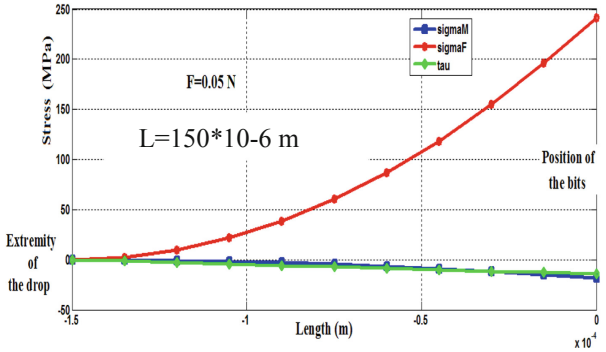


**Fig. 2.** Evolution constraints $[\sigma_f, |\sigma_m|, |\tau_i|]$ based on the embedded length for an applied force of 0.05 N (drop test, epoxy/glass).

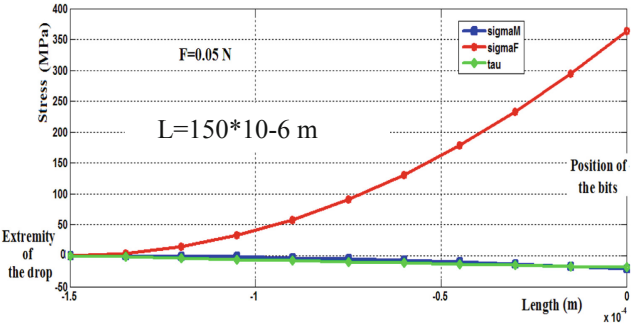


**Fig. 3.** Evolution constraints $[\sigma_f, |\sigma_m|, |\tau_i|]$ based on the embedded length for an applied force of 0.05 N (drop test, couples epoxy/carbon).

the longitudinal stress fiber $\sigma_f$ which decreases with the length embedded. Through the results obtained for the test of drop, we could highlight:

The high values of $\tau_i$ obtained for the various couples (carbon/epoxy, glass/epoxy) are not due to a bad evaluation of $\tau_i$ nor even to a numerical overvaluation of the force applied.

It is for this reason that the rupture occurs at the interface rather than in the matrix (for lengths of 45 μm to 125 μm entrenchment). Several explanations can be raised: It appears that the shear stress decreases rapidly away from that of the fiber; this then means that only the interfacial zone is subject to strong constraints, and this could pose a greater resistance than the matrix. According to the results, we see three cases that appear:

For the first case when $\tau_i > \sigma_m$ two cases may appear, strong adhesion of the material tested, or due to modeling error. The characteristics of the interface are higher than those of the matrix and what are the properties of the latter that restrict the behavior of the composite. In this case, we cannot characterize the interface and this case is not real.

For the 2nd case $\tau_i \approx \sigma_m$ values of the embedding length ranges from 135 μm to 150 μm the two curves show the stress at the interface and the normal stress at the

matrix are close to the two lines of evolution and superimposed. In this case, the interface behavior follows that of the matrix.

For the 3rd case $\tau_i < \sigma_m$ lengths embedding 400 μm to 175 μm variants of $\sigma_m$ values obtained for the matrix are larger than the interface; the characteristics of the interface are lower than those of the matrix and thus constitute the weak point at the origin of the rupture; This is the case we will consider in the tests because he represents the reality.

The profile of the stresses $\tau_i$, $\sigma_f$ and $\sigma_m$ is represented by curves, for the drop test simulated according to the length of 45 μm to 150 μm entrenched and 30 μm diameter we find that it can have a grinding (detaching from its sheath fiber matrix). By cons for values of embedding lengths ranging from 150 μm to 400 μm causing failure of the fiber before you, get the heaving.

### 3.3.2 Presentation of the Maximum Interfacial Stresses According to the Length Enchased for the Test of Drop

The true test of mastery of the drop thus inevitably means a thorough mechanical analysis, associated with a good knowledge of the behavior of the tested material (plasticity?…). This is not specific to this test but is very characteristic of all the techniques that micromechanical, all, fish generally by the simplicity of the assumptions. However, the problem of an absolute determination of interfacial characteristics remains unsolved.

It now appears that any interpretation of the drop test and any test micromechanical, in terms interfacial characteristics absolute, must take into account the effect of the radial stresses. This undoubtedly limits the possibilities of analytical resolution in favor of numerical methods.

We have seen that the complete modeling (taking into account radial effects, residual stresses), from a mechanical point of view, this test is a complex problem, unresolved. Nevertheless, it appears that a simple approach, who evaluates only one mean stress of shearing to the interface, appears acceptable and representative of quality of adhesion fiber/matrix; we thus obtain a good relative evaluation of the interfacial properties.

The maximum stresses at the interface for a constant force of 0.075 N and 0.09 N evolve linearly with the length embedded, such as the shear stress $\tau_{i,max}$ is high for carbon/epoxy (Figs. 4.c and 4.d). We cannot claim with the determination of the absolute values of interfacial resistance, having high values of obtained: up to 173 MPa in test of the drop, and up to 86 MPa in test of indentation. These values are indeed greater than the shear strength of epoxy ($\tau = 80$ MPa); if they represented really interfacial resistance, an interfacial failure could occur, matrix having sold well before. However, we can wonder whether the value of τ, determined by a macroscopic mechanical test on pure resin, really corresponds to resistance to local intrinsic rupture of material. In a massive test-tube, the final rupture generally intervenes by the propagation of a fissure started on a defect, however, in the vicinity of this defect, leading to the rupture of material, is much higher than the measured nominal stress. The apparent discrepancy between our estimate of the interfacial strength and matrix strength is probably less important than it seems.

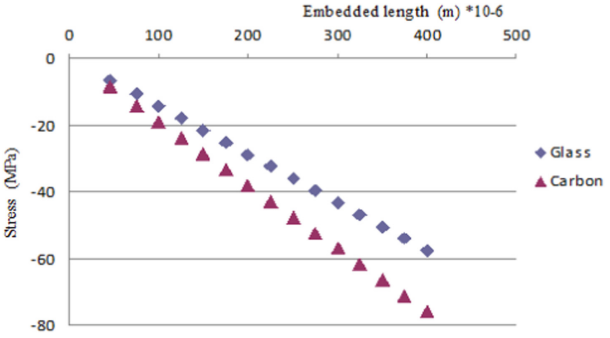


c) Constant force F = 0.075 N

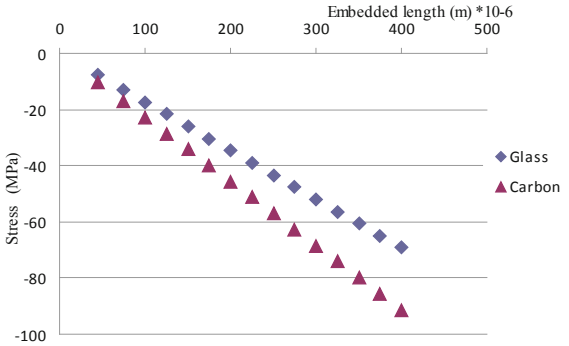


d) Constant force F=0,09N

**Fig. 4.** Evolution of maximum interfacial stresses as a function of embedded length for a constant force F = 0.09 N for the drop test.

## 4 Conclusion

Micromechanical tests developed so far, have kept a share of simplicity and specific characteristics; such as type of stress, the dimension and nature of specimens and the boundary conditions. These tests allow a qualitative study of the interface. Based on these tests, interface stand for values below the calculated interfacial resistance but the reality is that the interfaces become damaged at values far below those ound numerically for parameters not considered in the assumptions may intervene in the case of finished products. While this study particularly interesting to validate the experimental results of tests. In addition, it will optimize couples reinforcements/matrix and determine the effect of surface treatment of the reinforcement.

## References

Drzal, L.T.: The Interphase in Epoxy Composites, Advances in Polymer Science, edited by K. Dušek, vol. 75, pp 1–32 (1986)

Piggott, M.R.: The Effect of the interface/interphase on fiber composite properties. Polym. Compos. **8**(5), 291–297 (2004)
Kim, J.K., Mai, Y.W.: High strength, high fracture toughness fibre composites with interface control a review. Compos. Sci. Technol. **41**, 333–378 (1991)
Kim, J.K., Zhou, L., Mai, Y.W.: Stress transfer in the fiber fragmentation test-Part I. An improved analysis based on a shear strength criterion. J. Mater. Sci. 28, 6233 6245 (1993)
Kim, J.K., Mai, Y.W.: Stress transfer in the fiber fragmentation test-Part II. Multiple fiber composites. J. Mater. Sci. **30**, 3024–3032 (1995)
Baley, C., Grohens, Y., Busnel, F., Davies, P.: Application of interlaminar tests to marine composites. Relation between glass fibre/polymer interfaces and interlaminar properties of marine composites. Appl. Compos. Mater. **11**, 77–98 (2004)
Muller, W.H., Sehlnauder, S.: Interface stresses in fiber-reinforced materials with regular fiber arrangements. Compos. Struct. **24**, 1–21 (1993)
Wu, Z.J., Davies, J.M.: Effect of interphase on fibre-bridging toughness of a unidirectional FRP composite thin plate. Compos. Struct. **69**, 510–515 (2005)
Wang, H., Wang, H., Li, W., Ren, D., Yan, Yu.: An improved microbond test method for determination of the interfacial shear strength between carbon fibers and epoxy resin. Polym. Testing **32**, 1460–1465 (2013)
Sun, Q., Luo, X., Yang, Y.Q., Li, J.H., Hung, B., Li, C.: Analysis on the interfacial shear strength of fiber reinforced titanium matrix composites by shear lag method. Mater. Sci. Eng. A **642**, 262–267 (2015)
Tran, M.T., Vu, X.H., Ferrier, E.: Effect of carbon textile treatment and embedded textile length on textile/matrix interface behaviour from pull-out test. In: SMAR 2019, Fifth Conference on Smart Monitoring, Assessment and Rehabilitation of Civil Structures, September 2019
Orifici, A., Herszberg, I., Thomson, R.: Review of methodologies for composite material modelling incorporating failure. Compos. Struct. **86**, 194–210 (2008)
Keusch, S., Haessler, R.: Influence of surface treatment of glass fibres on the dynamic mechanical properties of epoxy resin composites. Compos.: Part A **30**, 997–1002 (1999)
Piggott, M.R.: Why interface testing by single-fibre methods can be misleading. Compos. Sci. Technol. **51**, 965–974 (1997)
Bellini, A., Bovo, M., Mazzotti, C.: Experimental and numerical evaluation of fiber-matrix interface behaviour of different FRCM systems. Compos. Part B: Eng. **161**, 411–426 (2019)
Sun, H., Pan, N.: Mechanical characterization of the interfaces in laminated composites. Compos. Struct. **74**(2006), 25–29 (2006)
Mohammadi, B., Olia, H., Toudeshky, H.H.: Intra and damage analysis of laminated composites using coupled continuum damage mechanics with cohesive interface layer. Compos. Struct. **120**, 519–530 (2015)
Dhiman, S., Potluri, P., Silva, C.: Influence of binder configuration on 3D woven composites. Compos. Struct. **134**, 862–868 (2015)
Shiriajeva, G.V., Andreevskaya, G.D.: Sov. Plastics **4**, 40 (1962)
Favre, J.P., Perrin, J.: Carbon fibre adhesion to organic matrices. J. Mater. Sci. **7**, 1113–1118 (1972)
Hampe, A.: Amts und Mitteilungsblatt der BAM **18**, 3 (1988)
Hampe, A., Boro, I., Schumacher, K.: Composites, France **29**, 3 (1989)

# Effect of Reinforcement Shear and Buckles Defects on the Low Velocity Impact Behavior of a Composite

B. Kacimi(✉), F. Teklal, and A. Djebbar

Laboratory of Mechanics, Structures and Energetics (L.M.S.E), Mouloud MAMMERI University, BP 17 RP 15000, Tizi-Ouzou, Algeria
bachir.kacimi@ummto.dz

**Abstract.** This paper presents an experimental study of the effect of mesoscopic buckles defect and shear deformation of the reinforcement, which result from shaping, on the low velocity impact behavior of a composite laminate. The material studied is a glass/polyester composite with three layers of mat and one layer of taffeta fabric. To assess the properties induced on the final composite, plates with calibrated defects and deformations were manufactured. Results of the impact tests and observations performed on the materials with calibrated defects identified a negative effect of buckling on elastic parameters and revealed greater damage relative to the healthy material. The reinforcement shear had a beneficial effect on the impact properties of the laminate, which was attributed to the increase in local fiber density.

**Keywords:** Defects · Impact · Induced properties · Laminates · Textiles

## 1 Introduction

Composite materials with organic matrix are increasingly used for structures in many industrial fields such as shipbuilding, aeronautics and automotive. This attraction is mainly motivated by their high performance (strength/specific mass) and their anisotropy, which can be adapted to the mechanical loadings undergone. In addition, the rapid growth of composite materials shaping techniques has contributed significantly to their global growth. However, the characterization and mastering of the behaviors and damage processes of these materials, taking into account the effect of the manufacturing processes, remains a challenge when they are subjected to complex mechanical loadings.

The sensitivity of composite structures to low velocity impacts, which is a part of these loadings, raises many concerns and relatively restricts their scope of application. Indeed, a structure can be exposed to shocks from various strange bodies (of varying size, shape and rigidity) during the production, maintenance or service phases. These shocks generally cause internal damage, that ca is not visible on structures surfaces, often with dramatic consequences on the mechanical performance of structures in service (Cantwell and Morton 1991; Abrate 2005; Zhang and Richardson 2007)


B. Safi et al. (Eds.): ISMSD 2019, *Proceedings of the 4th International Symposium on Materials and Sustainable Development*, pp. 136–144, 2020.
https://doi.org/10.1007/978-3-030-43211-9_12

However, to our knowledge, studies in this area do not take into account the effect of shaping processes. In general, the composite materials tested are made under ideal conditions (stratification of undeformed fabrics and resin injection) without taking into account deformations and/or defects of the fibrous network. Indeed, the fabric is mechanically loaded (tension, shear, bending, compaction …) during shaping which can lead to residual deformations as well as the appearance of local defects on the reinforcement (Lightfoot et al. 2013; Allaoui et al. 2014, 2015a), especially when the part is of complex geometry.

Shaping defects can be divided in two types (Fig. 1): macroscopic defects (at the fabric scale) and mesoscopic defects (at the yarn scale). Macroscopic defects (wrinkles) are widely studied in terms of phenomenology and effect on the final composite behavior. On the phenomenological level, studies have shown that wrinkle defect, which is an out-of-plane phenomenon, is highly dependent on the coupling of shear/tension/bending/friction behaviors of the reinforcement (Allaoui et al. 2011, 2014; Wilems et al. 2008). This defect, appearing at the reinforcement scale, generates a significant over-thickness that affects the geometrical tolerances and aesthetics of the final part. Furthermore, studies have shown that the mechanical performance induced on the final composite drops drastically, reaching up to 40% loss of maximum breaking stress (Potter et al. 2008; Bloom et al. 2013; Hallander et al. 2013).

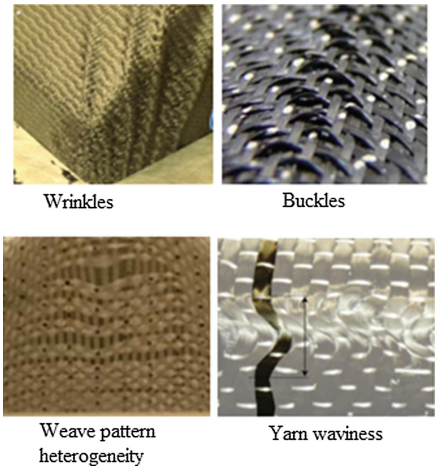


**Fig. 1.** Shaping defects: Macroscopic (wrinkles) and Mesoscopic.

Mesoscopic defects, meanwhile, appear locally at the yarn scale. We can distinguish yarn breakage, weave pattern heterogeneity, buckles, yarn waviness, etc. (Lightfoot et al. 2013; Allaoui et al. 2014; Potter et al. 2008; Tephany et al. 2016). The composite's behaviors induced by these mesoscopic defects, is significant on the service life of the composite (Piggott 1995; Allaoui et al. 2015b; Cruanes et al. 2018). However, only few studies deal with this aspect while these mesoscopic defects are among the most recurrent when shaping complex preforms (Allaoui et al. 2014, 2015a; Wilems et al. 2008; Capelle et al. 2014). In addition, the inter-ply friction substantially increases their quantity and

extent of appearance, when dealing with multilayer forming (Allaoui et al. 2015a; Cruanes et al. 2018), hence, the importance to understand the mechanisms involved and characterizes criticality of these defects on the behavior of the final composite.

It is within this framework that this work is situated, which is interested in the effect of the mesoscopic buckles defect and reinforcement shear on the composite impact behavior. For this, calibrated defects and shear were generated on glass fabric, taking care to reproduce the amplitudes observed during forming of complex composite part. Glass/polyester composite plates w were manufactured by the contact molding process and then tested. The results and observations were analyzed and compared with those obtained on a healthy composite material in order to evaluate the effect of the mesoscopic buckles defect and reinforcement shear on the behavior and generated damage.

## 2 Material and Preparation of Calibrated Specimens

### 2.1 Material

The composite material used in this study is a GFRP from the company Iselman (Bejaïa, Algeria, www.iselman.com). It is mainly intended for the manufacture of marine navigation and fishing equipment. The same manufacturing process used by the company, namely contact molding, was used to produce composite plates with and without defects. The reinforcements used are of type E glass, in the form of mats and taffetas. An unsaturated polyester thermosetting resin (with an appropriate hardener) was used to impregnate the various stacks.

The final average thickness of the composite plates obtained is approximately 3.7 mm. The fold order of this laminate is shown in Fig. 2. The impact tests will be carried out on the outside face of the laminate (Fig. 2), which is subject to this type of loading during navigation.

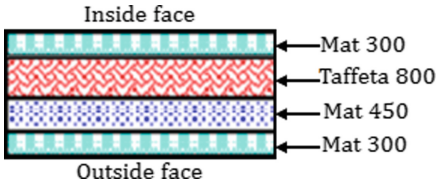


**Fig. 2.** Order of the reference laminate layers.

### 2.2 Preparation of Calibrated Specimens

Plates with calibrated defects have been produced in accordance with the stacking arrangement of the reference laminate. Defects are generated only on the taffeta fabric. The defects were generated in such a way as to reproduce the amplitudes observed in a feasibility study of a complex and undevelopable part for nautical application. Plies were made with shear angles of $30^{\pm 1\circ}$ on each of the zones delimiting the buckle band seen the amplitude of the defect is proportional to this shear (Fig. 3).

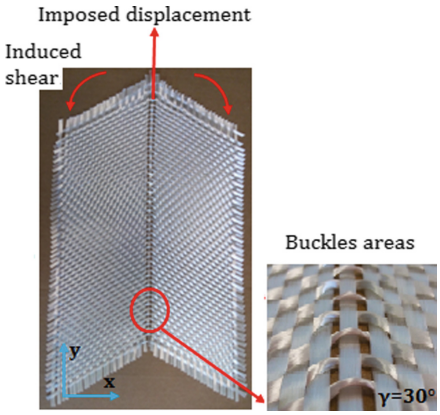


**Fig. 3.** Protocol for making calibrated specimens.

## 3 Comparison Between Healthy Materials and Materials with Calibrated Defect and Shear

### 3.1 Reference Material

The reference laminate was tested for low impact energies. Figure 4 highlights the variation of the impact properties according to the three energies used 10J, 20J and 30J. Good reproducibility of the results for the drop weight impact test was observed for the same material.

It is interesting to see that loading and unloading regions are almost symmetrical (Fig. 4a), suggesting that the contact duration is almost unchanged. The rising part of the curves (Fig. 4b) corresponds to the loading phase of the material up to a maximum value equivalent to the impact energy. It can also be seen that after about 14 ms the energy stabilizes indicating that the impactor has lost contact with the sample. Some of the energy has been restored in an elastic way. The residual energy then corresponds to the energy dissipated by the damage of the laminate. We also observe that the absorbed energy and damaged areas generated after impact evolve linearly with the impact energy for this type of material.

### 3.2 Material with Calibrated Defects

Impact tests were conducted to characterize the properties induced by the calibrated buckles defects (AB samples) as well as the shear deformation (AS samples) of the reinforcement. This comparison will be made at impact conditions at 20J corresponding to a speed of 1.68 m/s.

Despite almost symmetrical behavior, there is a variation in the maximum load (Fig. 5a). Thus, the maximum load of the specimens with sheared reinforcement (AS) is slightly higher than that measured for the reference laminate (A), which is attributed to the increase in the stiffness of the laminate. This increase in stiffness is attributed to the effect of reinforcement shear which induces an increase in fiber content (by 6.68% in this

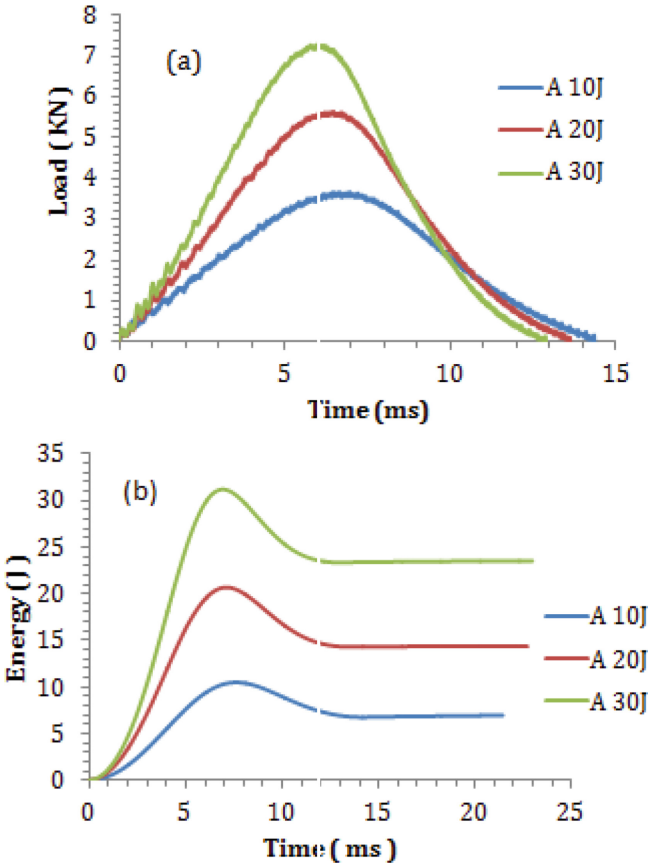


**Fig. 4.** Evolution of load vs. time (a), energy vs. time (b) for the three levels of impact energy.

case) associated with the contribution of transverse yarns to mechanical behavior in the longitudinal direction of the material. The trend is reversed for specimens with buckles defect (AB) where a maximum load reduction is measured (Fig. 4a). This indicates that the effect of the buckles mesoscopic defect is not negligible on the mechanical impact behavior of the composite as is also the case for fatigue behavior (Allaoui et al. 2015b; Cruanes et al. 2018).

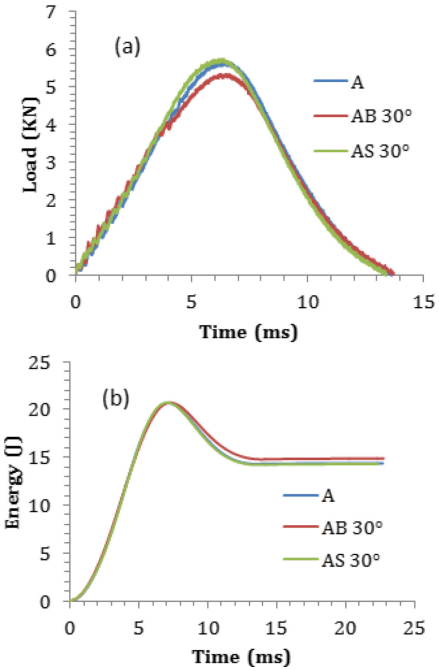


**Fig. 5.** Comparison of healthy material behavior/with defect/with shear: load vs. time (a), energy vs. time (b)

In addition, this drop in performance is associated, by the nature of the defect, with a greater predisposition to damage leading to higher absorbed energy for the laminate with defects than for the healthy material (Fig. 5b).

This fact has been verified with the help of the SEM observations, which have been made in the thickness of the samples passing through the center of the buckles defect. These observations showed the presence of significant damage, located on the opposite side, with numerous fiber breakage, multiple cracks and fragmentations of the matrix, combined with a fiber/matrix debonding (Fig. 6). These fractographies also highlighted the presence of areas rich in resin or fibers. The SEM observations highlighted significant damage in out-of-plane mode for the specimens with calibrated defects relatively to the reference material (Fig. 6).

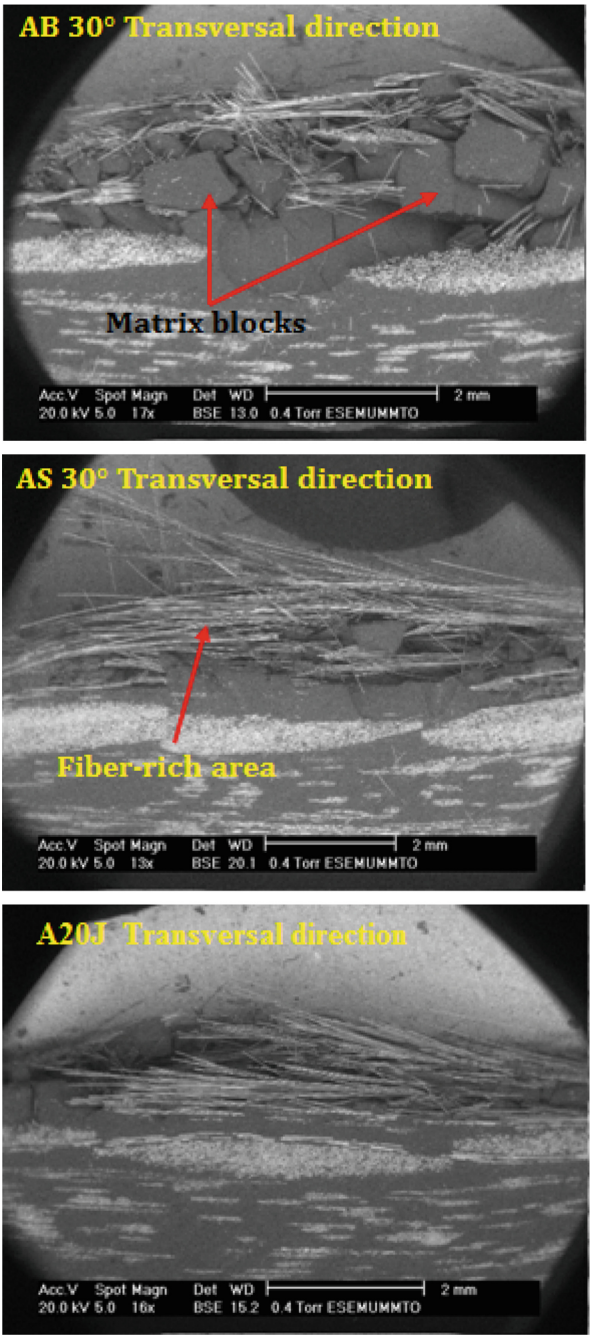


**Fig. 6.** SEM observation of specimens with buckles defect (AB), sheared (AS) and healthy specimen (Reference A).

## 4 Conclusion

The results of the impact tests showed that the buckles defect has a negative effect on the elastic parameters of the material. This effect is the consequence of a local fiber impoverishment caused and a disorganization of the fibrous network, with a reorientation of the fibers following the out-of-plane buckling of the yarns, in the area where were located the defects.

For the material with calibrated shear of the reinforcement, the significant contribution to stiffness of the transverse yarns and the increased local fiber rate due to the shear deformations led to an increase in mechanical properties.

The SEM observations made on the impacted specimens highlighted significant damage in out-of-plane mode, both in the case of specimens with buckles defect and those with shear , relative to the healthy material where the in plane damages are predominant.

## References

Cantwell, W.J., Morton, J.: The impact resistance of composite materials – a review. Composites **22**, 347–362 (1991)

Abrate, S.: Impact on Composite Structures. Cambridge University Press, Cambridge (2005)

Zhang, Z.Y., Richardson, M.O.W.: Low velocity impact induced damage evaluation and its effect on the residual flexural properties of pultruded GRP composite. Compos. Struct. **81**, 195–201 (2007)

Lightfoot, J.S., Wisnom, M.R., Potter, K.: Defects in woven preforms: formation mechanisms and the effects of laminate design and layup protocol. Compos. Part A- Appl. Sci. Manuf. **51**, 99–107 (2013)

Allaoui, S., Hivet, G., Soulat, D., Wendling, A., Ouagne, P., Chatel, S.: Experimental performing of highly double curved shapes with a case corner using an interlock reinforcement. Int. J. Mater Form **7**, 155–165 (2014)

Allaoui, S., Cellard, C., Hivet, G.: Effect of inter-ply sliding on the quality of multilayer interlock dry fabric. Compos. Part A- Appl. Sci. Manuf. **68**, 336–345 (2015a)

Allaoui, S., Boisse, P., Chatel, S., Hamila, S., Hivet, G., Soulat, D., Vidal-Salle, E.: Experimental and numerical analyses of textile reinforcement forming of a tetrahedral shape. Compos. Part A- Appl. Sci. Manuf. **42**, 612–622 (2011)

Wilems, A., Lomov, S., Verpoest, I., Vandepitte, D., Harrison, P., Yu, W.R.: Forming simulation of a thermoplastic commingled woven textile on a double dome. Int. J. Mater Form **1**, 965–968 (2008)

Potter, K., Khan, B., Wisnom, M., Bell, T., Stevens, J.: Variability fibre waviness and misalignment in the determination of the properties of composite materials and structures. Compos. Part A- Appl. Sci. Manuf. **39**, 1343–1354 (2008)

Bloom, L.D., Wang, J., Potter, K.D.: Damage progression and defect sensitivity: an experimental study of representative wrinkles in tension. Compos. Part -B Eng. **45**, 449–458 (2013)

Hallander, P., Akermo, M., Mattei, C., Petersson, M., Nyman, T.: An experimental study of mechanisms behind wrinkle development during forming of composite laminates. Compos. Part A- Appl. Sci. Manuf. **50**, 54–64 (2013)

Tephany, C., Gillibert, J., Ouagne, P., Hivet, G., Allaoui, S., Soulat, D.: Development of an experimental bench to reproduce the tow buckling defect appearing during the complex shape forming of structural flax based woven composite reinforcements. Compos. Part A- Appl. Sci. Manuf. **81**, 22–33 (2016)

Piggott, M.R.: The effect of fiber waviness on the mechanical properties of unidirectional fiber composite: a review. Compos. Sci. Tech. **53**, 201–205 (1995)

Allaoui S., Hivet G., Haddad, M., Agogué, R., Khellil, K., Beauchene, P., Aboura, Z.: Effect of the buckles mesoscopic defects on the composite properties. In: ICCM-20 Copenhagen (2015b)

Cruanes, C., Shanwan, A., Méo, S., Allaoui, S., Deffarges, M.P., Lacroix, F., Hivet, G.: Effect of mesoscopic out-of-plane defect on the fatigue behavior of a GFRP. Mech. Mater. **117**, 214–224 (2018)

Capelle, E., Ouagne, P., Soulat, D., Duriattic, D.: Complex shape forming of flax woven fabrics: design of specific blank-holder shapes to prevent defects. Compos. Part - B Eng. **62**, 29–36 (2014)

# Reinforcement of Building Plaster with Plastic Waste and Glass Powder

S. Kennouche[1(✉)], H. Abdelli[2], B. Amrane[1], and B. Hami[1]

[1] Civil Engineering Department, Bouira University, Bouira, Algeria
kennouchesalim@gmail.com
[2] ME Laboratry, Civil Engineering Department, Ferhat Abbas University, Setif, Algeria

**Abstract.** Plaster is a building material widely used in finishing buildings work, known for its qualities, which allow it a growing demand in the construction market; it is a favorable material to protection of the environment, very malleable, low density, also its thermal and sound insulation, regulator of the hygrometry of the enclosures and decorative, but the fragility of plaster poses a problem in design of decorative pieces with a langue size dimension, which causes problems for the users; in this study the plaster will be reinforced by fiber from waste plastic and powder glass, by introducing ratio (1 and 2% for plastic fiber and 5 and 10% of glass powder) of the introducing volume of reference specimens plaster studied. The results shows the positive effect of the introducing the waste plastic fiber and glass, that the results shows increasing the values of stress in flexion testing of reinforcing plaster beams, and also improving of the fragile behavior, in the other hand including waste glass has improving too the density various comparing in to reference plaster beam.

**Keywords:** Construction plaster · Plastic fiber · Glasses powder · Stresses of rupture

## 1 Introduction

Plaster has been used as finishing material in construction for walls and ceilings for its excellent performance favorable to the protection of the environment, easy application, and low density, with notable functional properties as firebreak, thermal insulation, hygrometry regulator speakers, decorative Iucolano et al. (2015).

In addition, the large availability, relative low cost, easy handling and mechanical characteristics suitable for different uses, makes the gypsum a widely used construction material Arikan et al. (2002). However, the fragility of plaster material is the subject of much research works. In order to overcome these limitations, the mechanical properties of all the binders can be enhanced with the addition of fibers to produce fiber-reinforced composites Hamzaoui et al. (2014).

Recently, eco-friendly materials are playing an important role in the building materials market, most of all-natural fibers used to reinforce several typologies of composites materials like plastics Sullins et al. (2017), but the use of natural fibers as reinforcement in


B. Safi et al. (Eds.): ISMSD 2019, *Proceedings of the 4th International Symposium on Materials and Sustainable Development*, pp. 145–151, 2020.
https://doi.org/10.1007/978-3-030-43211-9_13

building materials is the weak interaction between fiber and binder matrix. Accordingly, a large number of studies focused on chemical (such as silane alkalization or mercerization and acetylation treatments) or physical treatments of the fibers to enhance their surface roughness improve the fiber-matrix adhesion and reduce the moisture absorption Van de Weyenberg et al. (2006).

Concerning the reuse of recycled plastic in mortars and concrete, extensive studies have been conducted on used tyre modified concrete and mortars Turatsinze (2007).

The use of PET waste in cement-based composites will provide benefit in the disposal of wastes and, in addition, will reduce the environmental damages due to the use of natural mineral aggregates resources. The use of waste plastic as lightweight aggregate in the production of concrete provides both the recycling of the plastic waste and the production of a lightweight concrete in an economical way Frigione (2010).

Glass waste is representing urgent environmental problems all over the world. Du et al. (2013), and the usability of fine glass powder as a value-added product as it could replace a proportion of an expensive concrete constituent such as Portland cement was possible. Du and Tan (2014), these materials occupy huge parts of the land fills spaces. due to the non-biodegradable nature of glass, and causing serious environmental pollutions (air, water and soil pollutions). Also, the lack of spaces for new landfills is a problem facing the dense population cities in different countries. The reuse of glass wastes can be an interesting to reduce the environmental impact. Recycling of these wastes will help to conserve the earth's natural resources, minimizes the landfills spaces and saves energy and money Hogland (2002). Different studies have been done to investigate the optimum percentage of waste glass that can be used as a partial replacement to cement to produce concrete, investigated the use of (5–10 and 20%) of waste glass as a partial replacement to cement. The glass waste powder used was slightly higher in particle size distribution than that of Portland cement. Schwarz et al. (2008), but the introducing of waste glass in plaster is not cited in studied, in the work we proposed the effect of similar introducing of plastic fiber and powder glass in plaster beam, in physical and mechanical properties of the composite plaster materiel.

## 2 Materials and Methods

The materials used in this work are: Plaster: KNAUF [FLEURIS], glass powder from glass waste, having undergone a fine grinding, and plastic waste type PET polyester high resistant with depth is 2 mm, recover as waste, that is used as packaging cord in industry, as shown in Fig. 1.

### 2.1 Composite Formulation

The absence of a universal method for the formulation of plaster-based compositions the compositions are formulated as according to the following steps:

At the beginning the normal consistency is determined and the ratio E/P = 0.60 is fixed.

We will cut the plastic with a thickness of 2 mm and length of 14 to 15 cm, with depth is 2 mm, the plastic fibers are placed horizontally to provide reinforcement of

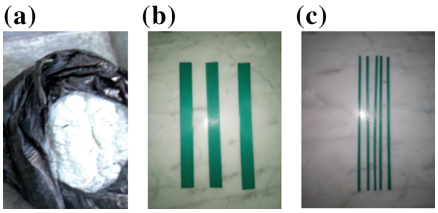


**Fig. 1.** a: Glass powder b: Plastic fiber (20 mm) c: Plastic fiber (2 mm).

the composite. The percentages (water. glass powder. plastic waste) are related to the amount of plaster of the composition concerned.

The studied compositions are given in the Table 1:

**Table 1.** Summary of the compositions studied.

| Compositions | % Powder glass | % Plastic fiber |
|---|---|---|
| Composition 1 | 0% | 0% |
| Composition 2 | 0% | 1% |
| | 0% | 2% |
| Composition 3 | 5% | 1% |
| | 10% | 1% |
| Composition 4 | 5% | 1% |
| Composition 5 | 5% | 2% |
| Composition 6 | 10% | 1% |
| Composition 7 | 10% | 2% |

## 2.2 Tensile Strength of Fibers

The tensile tests of the plastic strapping (PET), are doing in tensile machine, the dimension of plastic specimen are (200 × 20 × 2) $mm^3$, as shown in Fig. 2.

**Fig. 2.** Tensile test of plastic fiber

The Fig. 3 shows the strain-strain curves of tensile tests on plastic fibers.

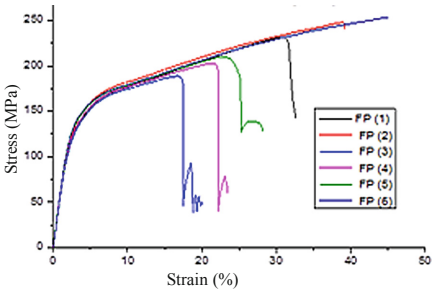


**Fig. 3.** Tensile curve test result of plastic fiber

## 2.3 Mechanical Characterization

### 2.3.1 Mechanical Resistances

The mechanic tests are realized in a hydraulic press. The beams dimension is (4 × 4 × 16) $cm^3$ with constant (W/P) ratio W/P = 0.6, the bending tests are carried out, with a loading speed of 50 N/s ± 10 N/s. The failing of each specimen in flexion is carried out according to the device shown in Figure 4 below, the results are showed in the Table 2.

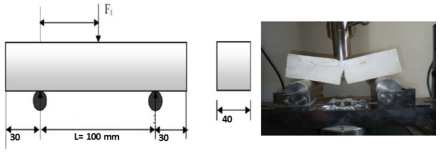


**Fig. 4.** Flexural strength test of plaster specimen.

Flexural breaking strength is given by the following formula:

$$R_f = \frac{x1.5 \times Ff \times L}{b^3}$$

L: Distance between the test rolls of the beam is
(40 × 40 × 160) $mm^{3;}$ (L = 100 mm);
Rf: Flexural strength in MPa;
Ff: Breaking force.

The following Figs. 5, 6, 7 and 8, represent the variation of the force as a function of the displacement of all the specimens studied in this work.

### 2.3.2 Discussion and Interpretation of the Results

According to the results that the Figs. 6, 7 and 8 represent the curves of the flexural tests, we observe the amelioration of mechanical resistance to flexural test for all the compositions with addition of plastic fiber as shows the Figs. 5, 6, 7 and 8 with 1% and 2% of plastic fiber), and (5% and 10% of glass powder) which represented in Figs. 7

**Table 2.** Summarize the composition of the variant specimens studied.

| Compositions | % Powder glass | % Plastic fiber | ρ (g/cm$^3$) | Fmax (N) | σ bending stress (MPa) |
|---|---|---|---|---|---|
| Composition 1 | 0% | 0% | 1.24 | 936.94 | 2.20 |
| Composition 2 | 0% | 1% | 1.33 | 1965.73 | 4.61 |
| | 0% | 2% | 1.37 | 1854.10 | 4.35 |
| Composition 3 | 5% | 1% | 1.35 | 1792.38 | 3.86 |
| | 10% | 1% | 1.37 | 1843.16 | 4.61 |
| Composition 4 | 5% | 1% | 1.33 | 1282.09 | 3.00 |
| Composition 5 | 5% | 2% | 1.31 | 1852.05 | 4.34 |
| Composition 6 | 10% | 1% | 1.28 | 1921.53 | 4.39 |
| Composition 7 | 10% | 2% | 1.36 | 1958.79 | 4.43 |

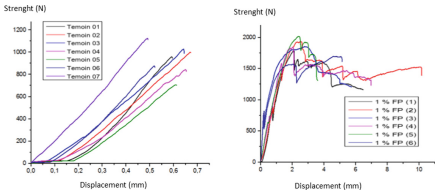


**Fig. 5.** Three point flexural curve test results (Compositions 1 and 2)

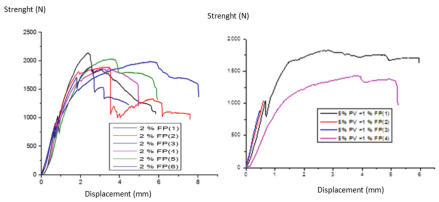


**Fig. 6.** Three point flexural curve test results (Compositions 3 and 4)

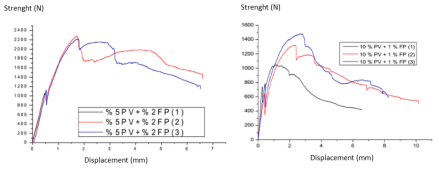


**Fig. 7.** Three point flexural curve test results (Compositions 5 and 6)

and 8, compared to the reference specimen, the results shows the increasing of flexural straight, which exceeds 100% in the specimen of the compositions: composition 2:

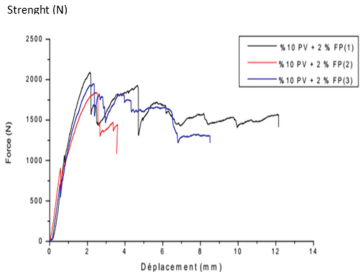


**Fig. 8.** Three point flexural curve test results (Composition 7)

(+2.41 MPa), composition 3: (+2.86 MPa), composition 4: (+0.8 MPa, composition 5: (+2.14 MPa, composition 6: (+2.19 MPa, and the composition 7: (+2.23 MPa) comparing to the reference composition without plastic fiber addition (composition 1 (2.2 MPa), as showed in the Table 2, this increasing is explained by the effect of plastic waste which plays the role of reinforcement in the composite and there horizontal disposition in the composite studied.

The flexural curves, shows a variation of the mechanical comportment under flexural tests, the specimens without fiber (composition 1) indicate the fragile comportment, but the others composition shows the amelioration of mechanical behavior, the corves shows this modifications, explained by the presence of plastic fiber which contribute to the strength of the composite, that the values of flexural strength has increasing with a percentage that exceeds 100% in some varieties as showed in the Table 2.

The introduction of waste glass as a powder is benefic to the densification of composite do to this finesse, that showed by the increasing of density of composite, which increasing the mechanical properties of the specimens studied, with is explained by the double impact of the plastic fiber and the powder glass.

## 3 Conclusion

The effect of plastic waste fibers and glass powder on the mechanical properties of plaster composite was investigated in this paper. Furthermore, the effect of different rate additions of fibers and the consequent in flexural resistance was too improving by increasing the flexural strength, in addition the powder glass participate to the densification of composite.

Too, we investigated the possible uses of glass and plastic waste in the plaster material, as reinforcement, the results of flexural testing of all beams with plastic fiber, confirms the amelioration of mechanical behavior after reinforcement by the waste fiber that we have improving the tensile resistance, the fiber with high tensile strength, which contributed to the improvement of the mechanical flexural strength of the plaster.

In the light of the results, this work can offer a new construction material with an improvement of the mechanical properties in bending of the plaster material.

## References

Turatsinze, A., et al.: Potential of rubber aggregates to modify properties of cement, based-mortars. Constr. Build. Mater. **21**(1), 176–181 (2007)

Du, H., et al.: Use of waste glass as sand in mortar: part II-Alkali-silica reaction and mitigation methods. Cem. Concr. Compos. **35**, 118–126 (2013)

Iucolano, F., et al.: Evaluation of bio-degummed hemp fibers as reinforcement in gypsum plaster. Constr. Build. Mater. **99**(2015), 184–191 (2015)

Hamzaoui, R., et al.: Microstructure and mechanical performance of modified mortar using hemp fibers and carbon nanotubes. Mat. Des. **56**, 60–68 (2014)

Du, H., Tan, K.H.: Concrete with recycled glass as fine aggregates. ACI Mater. J. **111**, 47–58 (2014)

Hogland, W.: Remediation of an old landfill site. ESPR-Environ. Sci. Pollut. 572 Res. **1**, 49–54 (2002)

Arikan, M., et al.: The optimization of a gypsum-based composite material. Cem. Concr. Res. **32**(11), 1725–1728 (2002)

Frigione, M.: Recycling of PET bottles as fine aggregate in concrete. Waste Manage. **30**, 1101–1106 (2010)

Schwarz, N., et al.: Influence of a fine glass powder on the durability characteristics of concrete and its comparison to fly ash. Cem. Concr. Compos. **30**, 486–496 (2008)

Sullins, T., et al.: Fiber reinforced polypropylene composites: the effects of material treatments. Compos. Part B Eng. **114**, 15–22 (2017)

Van de Weyenberg, I., et al.: Improving the properties of UD flax fiber reinforced composites by applying an alkaline fiber treatment. Compos. Part A **37**, 1368–1376 (2006)

# Compliance with RPA of an Old Building

R. Madi[1(✉)], A. Bordjiba[2], and M. Guenfoud[1]

[1] Université 8 Mai 1945, Guelma, Algerie
madi.rafik@univ-guelma.dz
[2] Université Badji Mokhtar, Annaba, Algérie

**Abstract.** Most of the old buildings in Algeria were built before the appearance of the Algerian seismic regulation. They were designed to resist the vertical loads without considering the impact of the earthquake. In this case, compliance with the RPA against the earthquake is necessary to ensure the safety of these structures. The solution adopted in the present research is the reinforcement by the insertion of reinforced concrete bracing shear walls in both directions of the structure. The objective of this article is the study of the influence of reinforcement on the strength of the resistance of the structure and the methodology of compliance with RPA 99 version 2003 of a building built before the appearance of the first Algerian seismic code RPA 81. The results obtained after reinforcement, from a Pushover analysis in terms of ductility demand $\mu_D$, the elastic stiffness of the structure $K_e$, The stiffness performance point $K_p$ and the global degradation indicator $I_d$ show an increase in capacity in terms of displacement and shear force.

**Keywords:** Rehabilitation · Reinforced concrete building · Pushover analysis · Compliance · Algerian seismic regulation

## 1 Introduction

The reinforcement of existing buildings is a recent concern of earthquake engineering. Most of the old buildings in Algeria are built before the appearance of the Algerian seismic code RPA. The first version RPA81, was developed after the El-Asnam earthquake of 10 October 1980 (Ministère de l'Habitat et de la Construction 1981). It is followed by the RPA 83 (Ministère de l'Habitat et de la Construction 1983). These two calculation codes are based on the equivalent static method for the evaluation of seismic forces applied to the structures. The spectral modal analysis method was introduced in RPA 88 (Ministère de l'Habitat et de la Construction 1988). Both methods are integrated in the RPA 99 (Ministère de l'Habitat et de la Construction 2000) and the RPA 99 version 2003 (Ministère de l'Habitat et de la Construction 2003). Most of the old buildings are designed to resist only to vertical loads without considering the action of horizontal forces calculated from the seismic codes. In this case the conformity of the constructions is necessary. In the case of an old building in good condition, Compliance requires the reinforcement of the structure, in order to meet the requirements of the calculation code such as displacements, the participation of the modal masses, ductility, etc. There are


B. Safi et al. (Eds.): ISMSD 2019, *Proceedings of the 4th International Symposium on Materials and Sustainable Development*, pp. 152–162, 2020.
https://doi.org/10.1007/978-3-030-43211-9_14

several methods of strengthening: addition of bracing shear walls, concrete jacketing of columns and beams (Kim 2008), use of composite materials (Leng and Teng 2008), etc. Therefore the use of shear walls is strongly recommended by the RPA.

## 2 Building Reinforcement

An old building designed and built without seismic consideration, but located in a seismic zone is subject to a seismic reinforcement regulatory obligation (Madi et al. 2011a, b). Reinforcement is an operation that involves increasing the level of service of a construction such as resistance, ductility or both simultaneously, to allow normal use in conditions not originally intended or to provide him with sufficient protection against demands that have not been taken into account in calculations such as the earthquake (Madi et al. 2014). The reinforcement strategy is to find the optimal solution that takes into account the cost, the construction period and inconvenience to the occupants. There are two methods:

- reinforcement inside the existing structure;
- design a new structure, often outside the building, and which alone resists the total action of the earthquake. This solution is often optimal. It consists in putting in each horizontal direction two bracing walls based on a new foundation sole. The diagnosis of the existing structure and its environment is necessary before beginning the study of reinforcement (Madi et al. 2011a, b; Madi 2012). It gives a detailed statement on the status of construction. This is an analysis of resistance to seismic action by searching and examining: site data, the quality of materials, architectural and civil engineering plans (formwork and reinforcement), the most suitable dynamic calculation and the feasibility of different reinforcement solutions. It is a complete and expensive approach that can be adapted and possibly simplified case by case, depending on the complexity of the building. The general approach to follow is: study of the state of the building to be reinforced, definition of objectives to be achieved: enhance the bearing capacity or bearing capacity and ductility capacity or only ductility capacity, choice of means and methods to use and detailed study of the operation. The different methods of strengthening structures are mentioned in Fig. 1. Inserting new elements into an existing structure significantly changes its dynamic behavior during an earthquake. There will be a new redistribution of horizontal forces between the various bracing elements. In this case, the concentration of forces in low resistance elements must be avoided and/or low ductility and reduce the effects of twisting and irregularities.
  The increase of the capacity of the structures against the earthquake can be done either by a global reinforcement based on:
- The insertion of the shear walls bracing (Fig. 2): reinforcement by reinforced concrete walls is undoubtedly the best method to increase the resistance capacity to the seismic forces of a structure. These walls can be placed outside the building, on the periphery or inside.
- reinforcing the structural elements (CGS 1992):

***a. Beams:*** the jacketing can be made on one, three or four sides (Fig. 3).

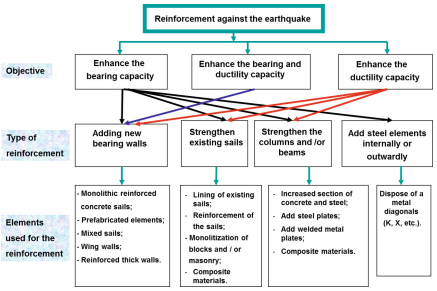


**Fig. 1.** Organizational methods of reinforcements

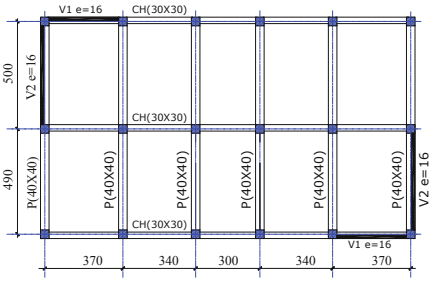


**Fig. 2.** Reinforcement by adding bracing shear walls

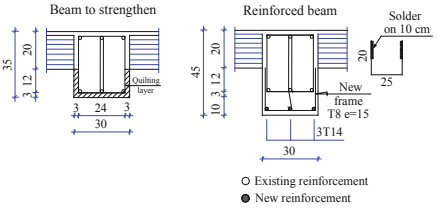


**Fig. 3.** Reinforcement of a beam by jacketing

***b. Columns:*** in this case reinforced concrete or metal jacketing can be used. Metal jacketing consists of enclosing the column in a metal cage. The reinforced concrete jacketing depends on the free space around the column and it can be made on one, two, three or four faces (Fig. 4).

***c. Concrete Walls:*** the increase of the thickness of a wall by jacketing it with concrete can be realized if its resistance is insufficient (Fig. 5).

***d. Soles:*** the reinforcement of existing soles requires the increase of their dimensions to increase the surface of contact with the ground (Fig. 6). It is easy to achieve a simple reinforcement of the sole in the case where the column is itself reinforced by sheathing. Belt surrounding the existing sole and directed at its base is of great importance for the transmission of efforts inclined. For this it is necessary to achieve a fairly rigid belt.

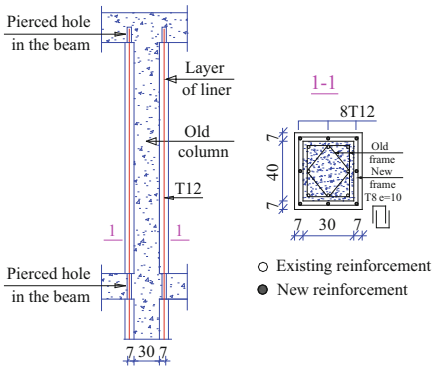


**Fig. 4.** Reinforcement of a column by lining

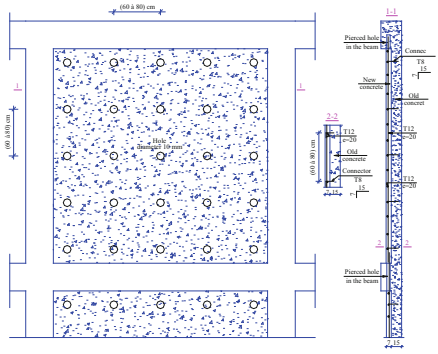

**Fig. 5.** Reinforcement of the concrete wall by jacketing

## 3 Pushover Analysis

Pushover analysis is a method of computation by nonlinear static analysis to study the vulnerability of the existing structures against the earthquake. It allows tracing the flow sequence, the ruin of the elements, the level of structural damage and the progress of the overall structure curve. The safety levels according to ATC 40 (Fig. 7) are: Immediate occupation (IO), Life Safety (LS) and Collapse Prevention (CP). The other points: collapse (C) and Ruin (D).

In this analysis, the beams and columns are modeled by elements having linear elastic properties. The nonlinear behavior is reflected by the introduction of the plastic hinges defined by the ATC 40 (Applied technology council 1996) and FEMA 273 (FEMA 1997) integrated in SAP 2000 (SAP 2000 2014). For the calculation of plastic rotations, $M_3$ is used for the beams and P-$M_2$-$M_3$ for the columns. The shear wall is modeled by an equivalent column-beam element located on the axis of the wall. Two plastic hinges type P-M-M are introduced at the base and at the top of the wall and a shear hinges type V2 or V3 in the middle (John 2008). The beams framing the wall are considered as rigid zone. The ductility demand $\boldsymbol{\mu_D}$ depending on the elastic displacement of the structure

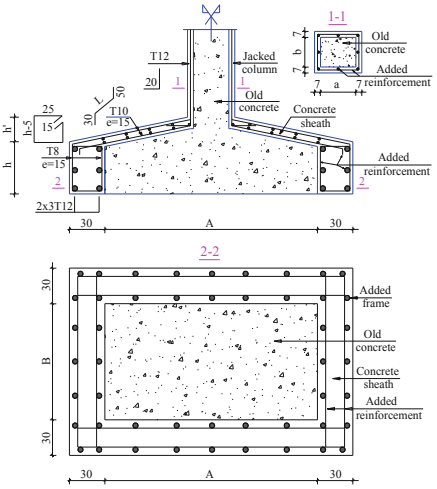


**Fig. 6.** Reinforcement of soles and columns by lining

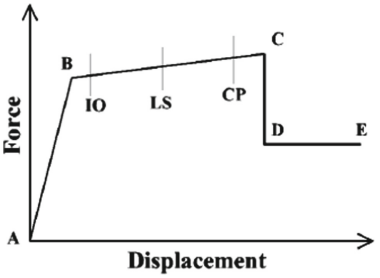


**Fig. 7.** Force-displacement relationship used in SAP2000

$D_y$ and displacement to the point of performance $D_p$ is given by:

$$\mu_D = \frac{D_p}{D_y} \tag{1}$$

As the factor $\mu_D$ is large, the degree of penetration of the structure in the plastic field is important. The initial stiffness (elastic) of the structure $K_e$ according to the elastic shear force $V_y$ and the elastic displacement $D_y$ is given by:

$$K_e = \frac{V_y}{D_y} \tag{2}$$

As the structure elements plasticize, the structure suffers damage which results in a decrease of $K_e$. Stiffness at the point of performance $K_p$ according to the shear force $V_p$ and the displacement $D_p$ is given by:

$$K_p = \frac{V_p}{D_p} \tag{3}$$

The global degradation indicator $\boldsymbol{I_d}$ is given by:

$$I_d = 1 - \frac{K_p}{K_e} \tag{4}$$

We study the structure in the y direction, which is the most vulnerable.

## 4 Study of an Existing Building Autostable Frames

According to the expertise of the construction (Fig. 8): This is a reinforced concrete structure (ground floor + 5 floors), symmetrical in both directions, built in 1980 and located in the city of Guelma in eastern Algeria. The floor of the various stages is hollow body of 20 cm thick. The dimensions are (30 × 35) cm for the beams, (30 × 30) for chaining and (30 × 40) for columns. The floor height is 3,15 m. The structure is located in a class IIa seismic zone. The foundation soil is of the loose type. The characteristics of the materials are as follows:

Concrete: $f_{c28} = 25$ MPa, $E_c = 32164$ MPa. Steels: *FeE400* for longitudinal reinforcement, $E_s = 2.10^5$ MPa, $f_y = 400$ MPa and *FeE235* for transverse reinforcement, $E_s = 2.10^5$ MPa, $f_y = 235$ MPa. Permanent loads G and overloads Q are as follows: $G_{terrace} = 0{,}57$ tf/m$^2$, $Q_{terrace} = 0{,}10$ tf/m$^2$, $G_{floor} = 0{,}50$ tf/m$^2$, $Q_{floor} = 0{,}10$ tf/m$^2$.

## 5 Compliance of the Existing Structure with RPA 99 Version 2003

The RPA 99 version 2003, requires the presence of bracing shear walls in both directions of the structure. The best disposition of the sails is that which are placed at the end of the structure with perfect symmetry (Madi et al. 2017). Which requires the symmetrical insertion of the walls with respect to the x and y directions. The thickness of the shear walls is 15 cm (Fig. 9).

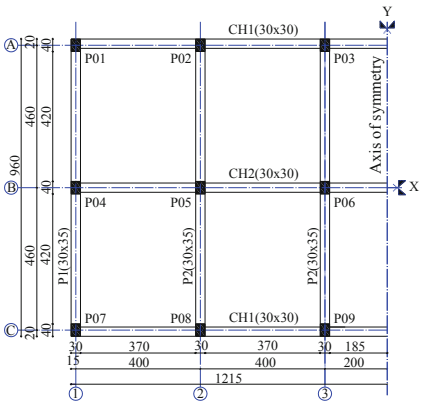


**Fig. 8.** Coffrage of the existing structure

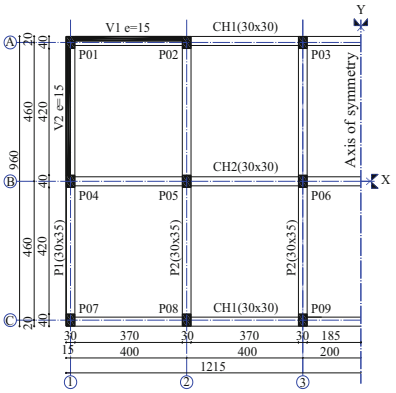


**Fig. 9.** Coffrage of the reinforced structure

## 6 Comparison of Results

### 6.1 Dynamic Study

The results of the dynamic analysis are shown in Table 1.

**Table 1.** Dynamic analysis results

| N° | Variant | Fundamental period (s) | Participation of the masses | Displacement at the top (cm) | | |
|---|---|---|---|---|---|---|
| | | | X (%) | Y (%) | X (cm) | Y (cm) |
| 01 | Frames | 1,39 | 99 | 99 | 3,04 | 3,04 |
| 02 | Frames + Shear walls | 0,57 | 91 | 91 | 0,94 | 0,98 |

### 6.2 Pushover Analysis

The results of the Pushover analysis are shown in Tables 2 and 3.

The analysis of the results shows an increase in the resistance, a decrease in displacements and good penetration in the plastic field of the reinforced structure with respect to the initial structure.

## 7 Reinforcement Detail

The joining details of the existing columns with the new reinforcing shear walls are mentioned in the Figs. 10, 11, 12 and 13. The steps to follow for realization reinforcement are as follows:

**Table 2.** Pushover Analysis Results

| Variant | Sens y-y | | | | | |
|---|---|---|---|---|---|---|
| | Capacity curve | | | | Pushover analysis | |
| | | | | | Performance point | |
| | $V_{max}$ (tf) | $D_{max}$ (m) | Vy (tf) | Dy (m) | Vp (tf) | Dp (m) |
| Frames | 214,78 | 0,15 | 73,08 | 0,029 | 91,59 | 0,046 |
| Frames + Shear walls | 374,64 | 0,09 | 78,46 | 0,007 | 129, 390 | 0,020 |

**Table 3.** Parameters of Pushover Analysis Results

| Variant | Sens y-y | | | |
|---|---|---|---|---|
| | Parameters | | | |
| | $\mu_D$ | Ke (tf/m) | Kp (tf/m) | Id (%) |
| Frames | 1,59 | 2520 | 1991,10 | 0,22 |
| Frames + Shear walls | 2,85 | 11208,60 | 6469,50 | 0,42 |

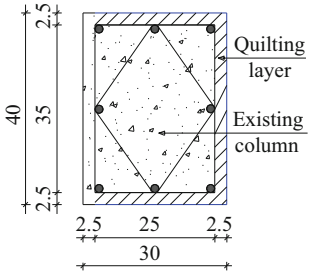


**Fig. 10.** Column stitching

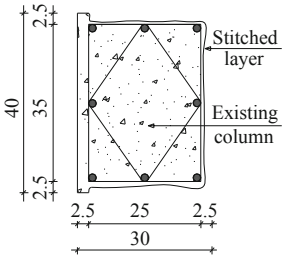


**Fig. 11.** Stitched column

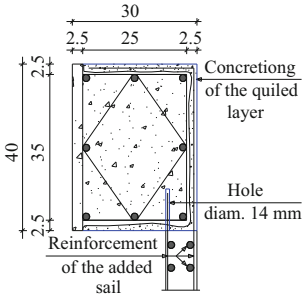


**Fig. 12.** Column-new wall junction detail

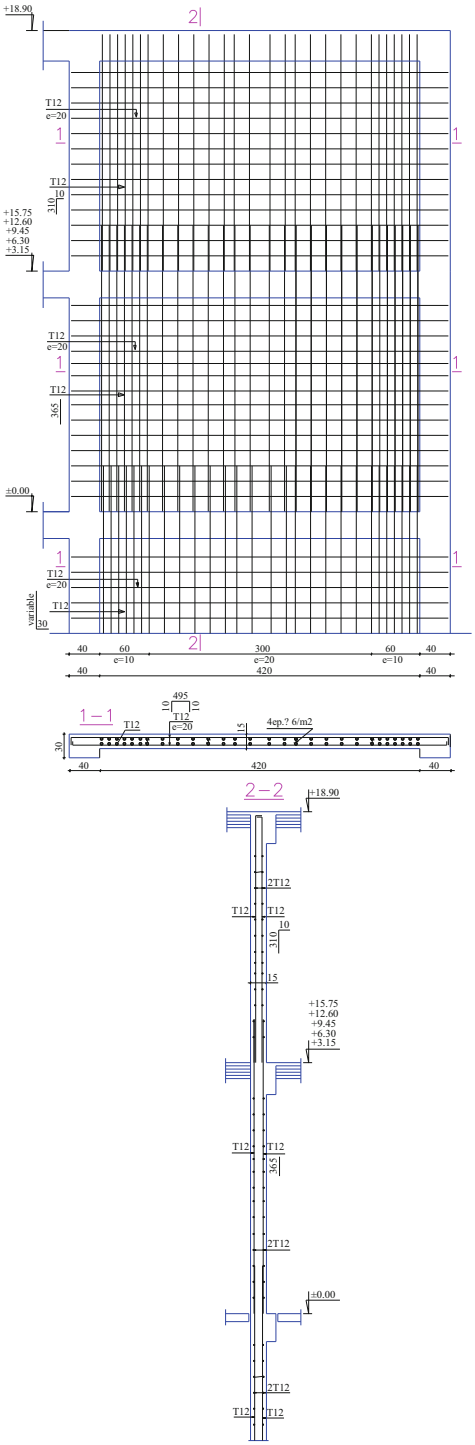


**Fig. 13.** Reinforcement detail of the added walls

– proceed to the jacketing of the columns by removal of the coating layer;
– Drill 14 mm diameter holes in the columns and beams at the crossing point of the horizontal and vertical reinforcement;
– seriously clean stitched surfaces with an air jet;
– apply a layer of Sika impregnation on quilted surfaces;
– the stuffing of the drilled holes is done by the sealing sika;
– set up of coffrage and reinforcement;
– setting up concrete with vibration.

## 8 Conclusions

The compliance of old buildings with the Algerian RPA seismic regulation is an essential requirement to preserve people and the environment. There are several methods of reinforcing structures or repairing structural elements: metal or concrete sheathing, containment and bandage by FRP, steel plating, etc. The addition of shear walls is an effective measure for strengthening existing structures. It increases the resistance and ductility capacity. We must place the shear walls in a way that allow us to avoid the twisting effect. The junction detail is necessary to ensure a good connection between the old and the new elements.

The results presented show the improvement of the ductility and strength of the structure in case of reinforcement by shear walls: reduction of the period and displacements and a good penetration in the plastic field. They are an example of compliance of buildings built before the appearance of seismic codes and decision support government in the rehabilitation of structures in medium and high seismicity areas.

## References

Ministère de l'Habitat et de la Construction: Règles Parasismiques Algériennes RPA81 (1981)
Ministère de l'Habitat et de la Construction: Règles Parasismiques Algériennes RPA81 version (1983)
Ministère de l'Habitat et de la Construction: Règles Parasismiques Algériennes RPA 88, Edition CGS (1988)
Ministère de l'Habitat et de l'Urbanisme: Règles Parasismiques Algériennes RPA 99, Edition CGS (2000)
Ministère de l'Habitat et de l'Urbanisme: Règles Parasismiques Algériennes RPA 99/Version 2003, Edition CGS (2003)
Kim, E.S.: A new steel jacketing method for concrete cylinders and comparison of the results with a constitute model. Int. J. Railway **8**(1), 72–81 (2008)
Leng, C.H., Teng, J.G.: Strengthening and Rehabilitation of Civil infrastructures Using Fibers. Woodhead Publishing Limited, CRC Press, Boca Raton, Boston, New York, Washington, DC (2008)
Madi, R., Guenfoud, M.: Etude de la vulnérabilité des constructions vis-à-vis du séisme. Revue Technologie et développement ANDRU **8**, 207–220 (2011a)
Madi, R., Guenfoud, M.: Réhabilitation des bâtiments en béton armé vis-à-vis du séisme. In: 1ère conférence Internationale sur la mécanique des matériaux et des structures MSM (2014)

Madi, R., Guenfoud, M.: Techniques de réparation des bâtiments en béton armé vis-à-vis au séisme. In: 1er séminaire national sur les matériaux et protection de l'environnement SNMPE 2011, Université Abdelhamid Ibn Badis, Mostaganem, Algérie, 14–15 March 2011 (2011b)
Madi, R., Guenfoud, M.: Evaluation de la capacité des sructures après réhabilitation vis-à-vis du séisme. In: 1er congrés sur le génie civil ICCE 2012, Université Ammar Thelidji de Laghouat, Algérie, 6–7 November 2012 (2012)
CGS: Catalogue des méthodes de réparation et de renforcement. CGS Alger, Algérie (1992)
Applied Technology Council: The seismic Evaluation and Retrofit of concrete buildings. ATC 40, Redwood city, California (1996)
FEMA: NEHRP comentary of the guidelines of seismic rehabilitation of buildings. FEMA (1997)
CSI: SAP2000 V-14 Integrated finite element analysis and design of structures basic analysis reference manual. Computers and Structures Inc., Berkeley (2014)
John, W.: Slender Wall Behavior Modeling. University of California, Los Angeles (2008)
Madi, R., Guenfoud, M.: Recherche de la position optimale des voiles. In: Second International Congress on Materials & Structural Stability CMSS 2017, Rabat, Morocco, 21–24 November 2017 (2017). MATEC Web of Conferences, vol. 149, p. 02010 (2018)

# Study of Physico-Mechanical Characteristics of Concrete Made with Recycled Gravel and Prepared Sand

B. Mehsas[1,2(✉)], A. Noui[2], L. Belagraa[3,4], and S. Slimani[2]

[1] Laboratory of Materials and Mechanics of Structures LMMS, University of M'sila, 28000 M'sila, Algeria
boumediene.mehsas@univ-msila.dz
[2] Department of Civil Engineering, University of Bordj Bou Arreridj, 34000 El Anseur, Algeria
[3] Laboratory of Materials and Electronic Systems, University of Bordj Bou Arreridj, 34000 El Anseur, Algeria
[4] Department of Civil Engineering, Faculty of Technology, University of M'sila, 28000 M'sila, Algeria

**Abstract.** The depletion of natural deposits of aggregates and the difficulties to open new quarries make it necessary to look for new sources of supply. Recycling and waste recovery are now considered as an alternative solution in the future. Aggregates are considered essential components in the composition of ordinary concrete or concrete for specific use. Such utilization of recycled aggregates is of great importance from a technical and environmental point of view. The present study concerns the use of aggregates from the crushing of concrete waste as a replacement for natural aggregates with a sand of standardized particle size of determined fractions. An experimental program for the characterization of a local recycled concrete based on prepared sand was planned. Four types of concrete were formulated including a control concrete mixture with crushed aggregates, 8/16 recycled concrete gravel fraction and prepared sand. The substitution amount of the fine fraction of prepared sand was 15% for slag and 10% pozzolan as mineral additions. The principal objective of this research work is to study the effect of partial substitution of recycled aggregates on the physical and mechanical characteristics and on the resistance to aggressive environments of a local recycled concrete based on prepared sand. The results obtained show the positive effect of using a recycled local sand-based concrete on the mechanical properties of concrete while keeping an acceptable workability for the studied concrete mixtures.

**Keywords:** Recycled concrete · Prepared sand · Aggressive environment · Slag · Pozzolan

## 1 Introduction

The concrete is one of the most used materials in the world, this composite material resulting from carefully balanced mixture of a granular skeleton (aggregates) and a


B. Safi et al. (Eds.): ISMSD 2019, *Proceedings of the 4th International Symposium on Materials and Sustainable Development*, pp. 163–174, 2020.
https://doi.org/10.1007/978-3-030-43211-9_15

blending pasty matrix composed of cement, water and usually admixtures (Dreux and Festa 2000; Aitcin 2001). The use of aggregates by huge amounts in the concrete manufacturing industry drives us to find an alternative solution such as the case of a concrete based on recycled aggregates, which could be a solution to reduce the impact on the environment and save natural aggregate resources. Previous studies on plain concrete utilizing prepared sand found the advantageous effect of replacing the prepared sand with additions slag on physical, mechanical properties and holding in aggressive environments (durability) mortars and concretes. These concretes based on this sand showed improved performances especially at an optimal percentage range of 10 to 15% replacements. Bouglada et al. (2017), Noui et al. (2018). The partial or total substitution of aggregates for the formulation of a recycled aggregate concrete (RAC) satisfying the requirements of quality and durability; currently present a topic of great interest for construction researchers and specialists in domain of concrete industry (Rao et al. 2007; Belagraa 2015; Belagraa et al. 2017). This study uses recycled aggregate (RA) from prepared from old concrete site to standardized particle sizes of fine (sand) as well as coarse fractions in the presence of active mineral additives blast furnace slag(S), and natural pozzolan (PZ) beside introducing additions replacement to substitute the fine fractions of the novel prepared sand. The fine (0.08–0.16 mm) sieve fraction replacement by the mineral additions, slag (S) and pozzolan (PZ) in this experimental program. The objective of the present research is to study the physico-mechanical properties of concrete with recycled aggregates, prepared sand and compared to an ordinary concrete (control) with natural aggregates. Thus a possible future use of RAC in the engineering civil field and public works. The total substitution of 100% recycled aggregates can generate a strength of fall, however, a partial replacement of natural aggregates by recycled only with a defined percentage could be a solution for making commonly used concrete within acceptable performances (Topcu and Sengel 2004; Marta and Gutierrez 2004; Falek 2017). The study will address the following investigation parts; firstly to see the effect of the prepared sand on the physico-mechanical properties of recycled concrete gravel base. In the second stage a comparison between the results obtained by direct compressive strength testing for conventional concrete and RAC regarding the aggressive environment sustainability. Thus, the durability could be assessed for studied mixtures.

## 2 Experimental Program, Materials and Methods

This section presents the different materials used in this study, their characteristics, the experimental methods and formulations of concrete mixtures.

### 2.1 Materials

See Figs. 1 and 2.

#### 2.1.1 Crushed Gravel CG

The crushed gravel used in the testing program for concrete control mix is based on a local quarry site from the region of Bordj BouArréeridj, (3/8), (8/16) fractions.

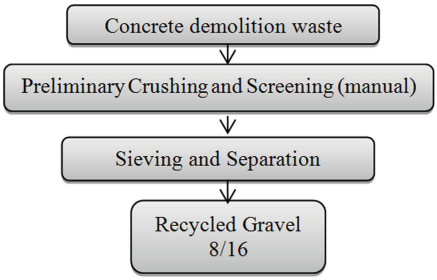


**Fig. 1.** Preparation process of recycled aggregates

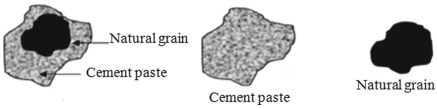


**Fig. 2.** Shape and constituents of recycled aggregates.

The characteristics are listed in Table 1. These, were studied in civil the engineering laboratory at the University of Bordj BouArreridj.

### 2.1.2 Recycled Gravel RG

Crushing operations and preliminary screening of concrete waste are made on site, then at the laboratory of civil engineering of the university we conduct a screening and separation to obtain the desired fractions 3/8 and 8/16. The composition of the recycled aggregate concrete is different from natural aggregates by their composition, indeed the recycled aggregate concrete is a composite material, and the two components are: natural aggregates crushed partially or paste of crushed hydrated cement, coating the natural aggregates. De Juan and Gutiérrez (2009), Douara et al. (2009) indicate these features are on the Table 1.

### 2.1.3 Prepared Sand SP

The sand used in our work is a dune sand from the desert region, Oued Souf locality, prepared at a determined granularity fractions sizes: (0,08 to 0,16) = 11%, (0,16 to 0,315) = 16%, (0,315 to 0,63) = 29%, (0.63 to 1.25) = 19%, (1.25–2.5) = 15% and (2.5 to 3.15) = 10%, their characteristics are cited in Table 1 (Fig. 3).

### 2.1.4 Cement (MATINE) C

The used cement CEM II/B 42.5 N is chosen to formulate the mixtures; it is delivered from a local plant LafargeHolcimin the region of Hammam Dhalaa, M'sila; its chemical compositions and physical characteristics are reported in Table 2.

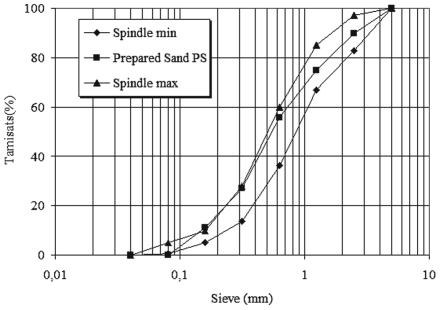


**Fig. 3.** Sieve analysis curve of prepared sand (PS).

**Table 1.** Characteristics of aggregates

| Properties | CG 3/8 | CG 8/16 | RG8/16 | PS |
|---|---|---|---|---|
| Bulk density (g/cm$^3$) | 1,55 | 1,40 | 1,38 | 1,70 |
| Specific density (g/cm$^3$) | 2,69 | 2,57 | 2,37 | 2,39 |
| Porosity P (%) | 42,21 | 45,49 | 41,91 | – |
| Compacity C (%) | 57,79 | 54,51 | 58,09 | – |
| Voidtatio e | 0,73 | 0,83 | 0,72 | – |
| Sand equivalent | – | – | – | 100 |
| Finesse modulus Mf | – | – | – | 2,41 |

**Table 2.** Chemical composition and physical properties of Cement, Slag and Pozzolan.

| | CEM II/B 42.5 N | Slag | Pozzolan |
|---|---|---|---|
| SiO2 | 17.35 | 35,40 | 74.48 |
| Al2O3 | 4.51 | 10.58 | 12.83 |
| Fe2O3 | 2.92 | 0.85 | 3.92 |
| CaO | 59.87 | 35.64 | 1.51 |
| MgO | 1.62 | 6.62 | 0.32 |
| SO3 | 3.08 | 0.52 | – |
| K2O | 0.62 | 0.61 | – |
| Cl | 0.014 | 0.016 | – |
| LOI | 10,02 | 9.53 | 7.21 |
| SSB (cm$^2$/g) | 4150 | 3627 | 3575 |
| ρ (g/cm$^3$) | 3.02 | 2.87 | 2.73 |

### 2.1.5 The Blast Furnace Slag(S)

Slag is a byproduct of the manufacture of cast iron in the blast furnaces of steel plants, granulated slag was taken from a fresh production of the factory of El Hadjar (Annaba east Algeria). The physico-chemical properties are provided in Table 2.

### 2.1.6 Natural Pozzolan (PZ)

Pozzolan of a volcanic origin extracted from Bou Hamidi deposit located 2.5 km from Beni Saf (Algeria northwest) represented by a cone-shaped mountain called El Kalcoul is used in the experimental program and their characteristics are listed in Table 2.

## 2.2 Experimental Methods

In our study the absolute volume method known as method SCRAMTAIEV has been used in the formulation of our concrete, the principle of this method is: the sum of all components of the concrete should be equal to 1000 L or 1 $m^3$ and the porosity P = 0 for a compressed concrete (Naceri 2004; Belagraa 2011), the concrete composition, that is to say the cost (amount) of: cement, water, sand and gravel is determined approximately by calculation. Finally it is specified by experimental test, the mix concrete in Table 4 later. Remember that the goal of our work is to see the effect of partially recycled aggregates on the mechanical behavior a concrete and given to aggressive media prepared with different types of sand. To reach the objectives, it has been adopted a testing methodology based on the preparation of wasted four types of concrete according to Table 3 later.

**Table 3.** The different types of concrete mixtures used

| Type concrete | CG (%) | RG (%) | SP (%) | Slag (%) | PZ (%) |
|---|---|---|---|---|---|
| Control 1 concrete CC1 | 100 | 0 | 100 | 0 | 0 |
| Control 2 concrete CC2 | 40 | 60 | 100 | 0 | 0 |
| Concrete CS | 40 | 60 | 85 | 15 | 0 |
| Concrete CPZ | 40 | 60 | 90 | 0 | 10 |

The molds used for making test specimens are steel cubes (10 × 10 × 10) $cm^3$.

**At fresh state,** the slump test was utilized to assess the workability of concrete mix according to the standard (NF EN 12350-2 2012).

**In the hardened state,** the density and the compressive strength were performed at 14 and 28 days according to the standard (EN 12390-3 2012).

**The durability tests,** were performed according to the standard (EN 197-1 2012) on specimens of 10 × 10 × 10 $cm^3$. Four types of concrete were made up, after 24 h they were removed from the molds and stored in water up to 28 days. After 28 days of curing in water, the specimens were weighted and cleaned after which they were immersed in two separate aggressive media for 15 days: A solution of 5% HCl acid see Fig. 4, and a solution of 3.5% H2SO4 Fig. 5.

**Table 4.** Concrete formulation for 1 $m^3$

| Components | CC1 | CC2 | CS | CPZ |
|---|---|---|---|---|
| Water E (l) | 200.00 | 200.00 | 217.00 | 214.00 |
| CG 3/8 (kg) | 482.30 | 482.30 | 482.30 | 482.30 |
| CG 8/16 (kg) | 723.45 | / | / | / |
| RG 8/16 (kg) | / | 723.45 | 723.45 | 723.45 |
| Cement C (kg) | 336.00 | 336.00 | 336.00 | 336.00 |
| PS 2.5/3.15 (kg) | 51.63 | 51.63 | 51.63 | 51.63 |
| PS 1.25/2.5 (kg) | 77.44 | 77.44 | 77.44 | 77.44 |
| PS 0.63/1.25 (kg) | 98.09 | 98.09 | 98.09 | 98.09 |
| PS 0.315/0.63 (kg) | 149.72 | 149.72 | 149.72 | 149.72 |
| PS0.16/0.315 (kg) | 82,60 | 82,60 | 61.95 | 82,60 |
| PS 0.08/0.16 (kg) | 56.79 | 56.79 | / | 5.16 |
| Slag (kg) | / | / | 77.44 | / |
| Pozzolan (kg) | / | / | / | 51.63 |
| Spoil concrete (kg) | 2258.02 | 2258.02 | 2275.05 | 2272.05 |

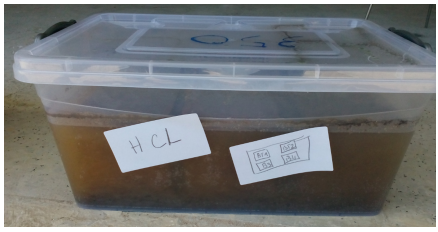


**Fig. 4.** Concrete test cubes submerged in solution: HCl

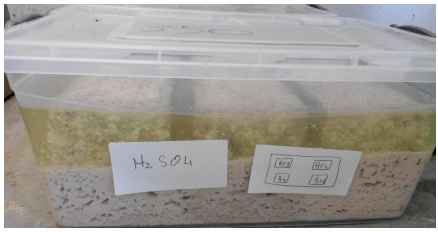


**Fig. 5.** Concrete test cubes submerged in solution: H2SO4

**Weight Loss:** The degree of attack is evaluated by the following weight loss formula:

$$\textbf{Weight loss } (\%) = [(M1 - M2)/M1] \times 100 \quad (1)$$

With: M1: the weight of the specimens before immersion, M2: mass of the test pieces after immersion for 15 days.

**Strength Loss:** a second parameter of the degree of chemical attack effect on the resistance is evaluated by the following formula strength loss:

$$\textbf{Strength loss } (\%) = [(R28 - RCD)/R28] \times 100 \quad (2)$$

With; R28: The compressive strength at 28 days,
RCD: The compressive strength after immersion for 15 days.

## 3 Results and Discussion

### 3.1 Properties at Fresh State

From Fig. 6, the effect of substitution of recycled aggregates shows a decrease in the density in the fresh state what correlates with previous work (Topcu and Guncan 1995; Katz 2003), a rate of order of 04% is justified for the difference of the volume mass of the aggregate, the introduction of the mineral additives in the prepared sands has not given an increase in density of the concrete as compared to the control concrete aggregates partially recycled (Table 5).

**Table 5.** Physical properties of concrete mixtures (fresh state).

| Concrete type | Density D (kg/m$^3$) | Slump Af (cm) | W/C |
|---|---|---|---|
| CC1 | 2466 | 4.20 | 0.596 |
| CC2 | 2368 | 4.20 | 0.596 |
| CS | 2325 | 4.00 | 0.647 |
| CPZ | 2357 | 4.00 | 0.657 |

The introduction of mineral additions prepared sand in concrete with partially recycled aggregates leads to an amount of water increases to reach a constant workability for all types of concrete or Af = 04 cm, the one speaker is the presence additions that have an additional water absorption capacity which affects the ratio W/C Fig. 7. The results found in this work show an increase of water cement ratio of around 9% Table 4, whereas previous studies show that an amount of water added to the case of a concrete based on recycled aggregate totally recycled is approximately 18% (Zemmit and Maafi 2013).

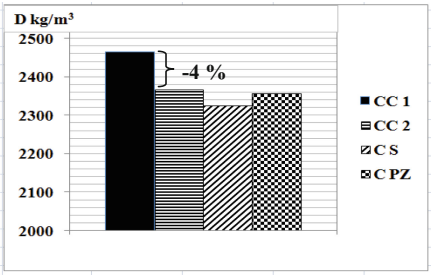


**Fig. 6.** The Density for the different concrete types.

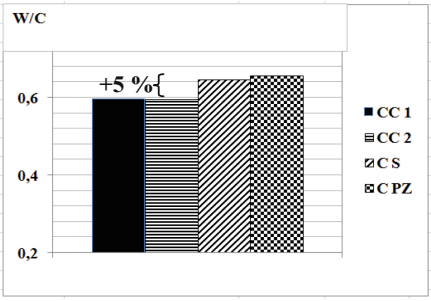


**Fig. 7.** The W/C Ratio for the different concrete types.

## 3.2 Properties at Hardened State

### 3.2.1 The Density

Figure 8 shows the density at hardened state of concrete as a function of the age at 7, 14 and 28 days. The concrete based on crushed gravel CC1 without replacement has a higher density compared to control concrete CC2 with recycled gravel at 0% mineral additions. However, the slag addition mixture CS and that with Pozolan, register a light decrease in density compared to the former concrete types. This is due to the difference in density of the nature of gravel which lighter as recycled one at 60% replacement is with lower density. The substitution effect based on recycled aggregates and prepared sand mixtures has a lower density at the hardened state about 2% (Zemmit and Maafi 2013).

### 3.2.2 The Compressive Strength

From the Fig. 9, a normal development of the resistance to compression (Rc) at [7, 14 and 28 days] for different types of concrete is observed. At 28 days the mechanical response of the different type of concrete is greater than the desired value Rb = 30 MPa by about 20% improvement, it is due to the use of a prepared sand of particle size with active addition (slag and Pozzolan) that contributes for the enhancement of strength. The formation of new hydrates in the cement matrix might be advantageous using the prepared sand with mineral substitution.

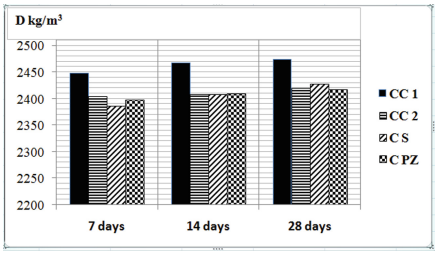


**Fig. 8.** The density for the different concrete types at hardened state.

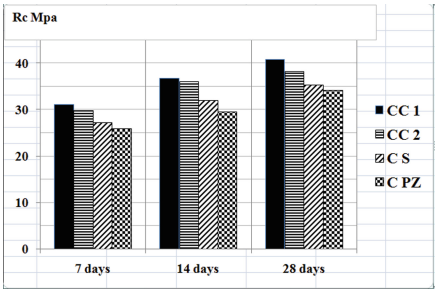


**Fig. 9.** Compression strength of different concrete types at 7, 14 and 28 days.

It is noted, that the compressive strength at different ages of concretes based on partially recycled aggregates with sand prepared without mineral additives CC2 at a reduction of 8% compared to the strength of concrete based on aggregates crushed with prepared sand CC1 those are similar to the finding of previous studies (Falek 2017; Zemmit and Maafi 2013). So the partial substitution effect of recycled aggregates based on standard sand of particle size does not influence on the compressive strength of concrete. The addition of slag or pozzolanic in prepared sand tend to increase the W/C ratio which has a negative influence on the compressive strength at different ages with a reduction of about 10% relative to the two control concretes CC1 and CC2, respectively.

### 3.2.3 Durability Test

*3.2.3.1 Mass Loss in Aggressive Media H2SO4 and HCl*

According to the Figs. 10 and 11 later, it is noted that the loss of almost identical mass loss for all the concrete mixtures after fifteen days exposure in aggressive environment, this or aggregates or prepared sand, a loss rate of 6.5% H2SO4 in the middle and 2.5% in HCl solution for the two types of concrete with recycled aggregate and that with partial substitution by slag and pozzolan for prepared sand mixtures.

*3.2.3.2 Compression Strength Loss in Aggressive Media H2SO4 and HCl*

According to Figs. 12 and 13 the loss of compressive strength is around 57% in the aggressive environment H2SO4 Also, it is observed o resistance loss in HCl medium of about 33%. So, the influence of H2SO4counts almost twice compared to HCl aggressive medium for all types of concrete studied.

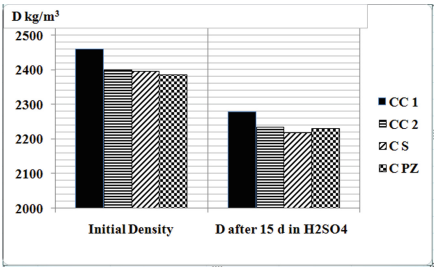


**Fig. 10.** The weight loss after 15 days exposure in H2SO4.

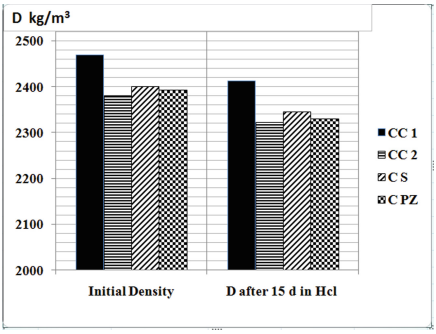


**Fig. 11.** The weight loss after 15 days exposure in HCl.

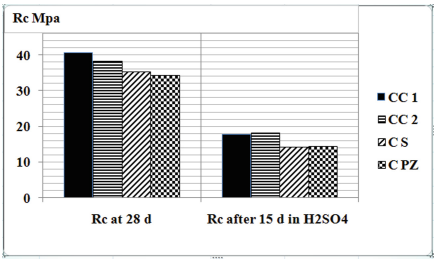


**Fig. 12.** Compressive strength loss in H2SO4.

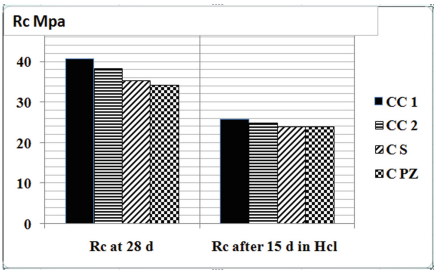


**Fig. 13.** Compressive strength loss in HCl.

## 4 Conclusions

Based on the results obtained in this study, the following conclusions could be drawn;

The partial substitution of aggregates by a recycled gravel of prepared sand mixtures has no influence on the compressive strength of the concrete types so far, which is comparable with a normal concrete their density shows a slight decrease of about 2% (Falek 2017).

The introduction of mineral additions prepared sand in concrete with a partial replacement of recycled gravel leads to an increase in the demand for water for recycled concrete mixtures.

At 28 days of age the mechanical response of the different types of concrete is greater than the desired value Rb = 30 MPa, it is due to the use of a prepared sand and the mineral additive effect (slag and pozzolan), this improvement is about 20%.

The weight loss is considerable for all types of concrete regardless gravel or sand prepared.

It is noted that the recycled concrete gravel and sand at a better resistance to H2SO4 and HCl medium compared to other concrete containing the mineral slag or pozzolanic addition. And H2SO4 environment influences much more than HCl the concrete types in terms of durability. Strength losses of around 57% in the middle H2SO4 and 33% for HCL are noticed, respectively.

In general, it can be concluded that the formulation of concrete with prepared sand for recycled concrete types up to 60% replacement is advantageous and improved performance in regards to the mechanical compressive strength.

## References

Aitcin, P.C.: High performance concrete. Ed. Eyrolles, Paris (2001)

Belagraa, L.: Building material, Course. University of M'sila/Algeria (2011)

Belagraa, L., Beddar, M., Bouzid, A.: Marble fillers effect on the mechanical properties of recycled aggregate concrete Environ. Eng. Manag. J. EEMJ **16**(1), 197–204 (2017)

Belagraa, L.: Characterization of local aggregate concrete. Ph.D. thesis, submitted in the department of civil engineering, University of M'sila, Algeria (2015)

Bouglada, M.S., Noui, A., Belagraa, L., Achour, Y., Bouzid, A., Benyaiche, T.: Study of physico-mechanical characteristics of a concrete high performance based with prepared sand. In: International Symposium on Construction Management and Civil Engineering ISCMCE, Skikda, Algeria, 15–16 November 2017 (2017)

De juan, M.S., Gutiérrez, P.A.: Study on the influence of attached mortar content on the properties of recycled concrete aggregate. Constr. Build. Mater. **23**(2), 872–877 (2009)

Dreux, G., Fest, J.: New Guide of Concrete and These Constituents. Ed. Eyrolles, Paris (2000)

Douara, T.H., Benhouna, M., Nezerui, B.: Physical and chemical characterization of recycled aggregates and natural aggregates. In: 1st International Conference on Sustainable Built Environment Infrastructures in Developing Countries ENSET Oran/Algeria, 12–14 October 2009, pp. 289–294 (2009)

EN 12350–3: Test standard for fresh concrete slump test (2012)

EN 12390–3: Standard for hardened concrete, compressive strength (2012)

EN197–1: Standard specifications compositions and conformity criteria for common cements (2012)

Falek, K., Aoudjane, K., Kadri, E.H.: Effect of recycled aggregates on the mechanical and rheological properties of concrete. J. Wulfenia **24**(3) (2017)

Katz, A.: Properties of concrete made with recycled aggregate from partially hydrated old concrete. Cem. Concr. Res. **33**(5), 703–711 (2003)

Marta, S., Gutierrez, P.A.: Influence of recycled aggregate quality on concrete properties. In: International RILEM Conference on the Use of Recycled Materials in Buildings and Structures/Spain, pp. 545–553 (2004)

Naceri, A.: Comparative Study of the concrete formulation methods. Algeria equipment, pp. 13–17 (2004)

Noui, A., Bouglada, M.S., Belagraa, L., Achour, Y., Bouzid, A., Lamrani, M.: The influence of prepared sand on the physico-mechanical characteristics of self-compacting concretes. In: International Congress on Materials, Strasbourg France, November 2018 (2018)

Rao, A., Jha, K.N., Misra, S.: Use of aggregate from recycled construction and demolition waste in concrete. Resour. Conserv. Recycl. **50**, 71–81 (2007)

Topcu, B.I., Sengel, S.: Properties of concretes produced with waste concrete aggregate. Cem. Concr. Res. **34**, 1307–1312 (2004)

Zemmit, A., Maafi, N.: Study of the effect of the type of aggregate on the mechanical behavior of concrete. Master thesis, University of M'sila/Algeria (2013)

# Behavior of Concrete Using Coal Waste (Heap) in Hot Weather

M. Miloudi(✉) and M. Merbouh

Faculty of Technology, Department of Civil Engineering, FIMAS Laboratory (Fiability of Materials and Structures Laboratory), TAHRI Mohammed University, BP. 417, 08000 Bechar, Algeria
miloudi_maamar@yahoo.fr

**Abstract.** Concreting in hot regions (eg. southern regions of Algeria) suffers from enormous difficulties in the conservation of materials, mixing, setting up, setting and hardening concrete. The consequences pose major short- and long-term problems, in terms of both fresh and hardened behavior, affecting the good performance and long-term performance of concrete, as well as its durability especially in aggressive environments. Coal waste in the Bechar region are abundant and a worrying waste. The incorporation of aggregates of waste is a recovery method and a contribution to environmental protection. This study was carried out to investigate the effects of temperature and coal waste (heap) addition on concrete strength under simulated hot weather conditions. The study consists of comparing the properties of a reference concrete with concretes incorporating aggregate of coal waste (heap) at six levels of heap as content (1, 2, 3, 4, 5 and 6% fine aggregate replacement) and two levels of temperature (25 and 50 °C). The simulation of the hot climate in the laboratory is subjected to temperature 50 °C with relative humidity of about 10%, wind speed at 10 km/h and E/C ratio constant between all mixtures. The results revealed that coal waste (heap) inclusion was more effective can be used for enhancement of properties of concrete. The optimum heap as content varied between 1 to 4%. However, the strength at higher temperatures was positively affected by inclusion of coal waste.

**Keywords:** Hot weather concreting · Coal waste (heap) · Environment · Compressive and flexural strength · X ray diffraction

## 1 Introduction

Hot weather concreting is defined in ACI 305 as mixing concrete, placing it and curing it with any factors that tend to impair concrete (ACI 1994). The requires prevention curing of water loss from freshly placed concrete and the creation of high humidity in the immediate vicinity of the concrete surface. The creation and maintenance of high humidity depends not only on the type of curing used, but also on the surrounding environment around the concrete. As for the latter, factors such as high air temperature, wind speed and relative humidity and the intensity of solar radiation also have a significant


B. Safi et al. (Eds.): ISMSD 2019, *Proceedings of the 4th International Symposium on Materials and Sustainable Development*, pp. 175–186, 2020.
https://doi.org/10.1007/978-3-030-43211-9_16

influence contribute to the heating effect (Ibrahim et al. 2013; Al-Gahtani 2010; Ortiz et al. 2009; Janos and Ahmad 1991; Alsayed and Amjad 1994; Austin et al. 1992). The undesirable effects of hot weather on the properties of fresh concrete according to many literatures include increasing, Water demand for required consistency; Rate of slump loss; Velocity of setting and hardening; Plastic shrinkage….

Because of the detrimental effects of high concrete temperature, direct all operations on hot weather should toward keeping the concrete as cool as possible. The most economical way to decrease the temperature of the concrete is to decrease the temperature of the mixing water (Neville 2000).

Curing in hot and dry weather compounds can reduce evaporation loss of from concrete (Janos and Ahmad 1991; Faattuhi 1986), however, it is also recognised that there are significant difficulties arising in evaluating the correct time to apply curing membrane on freshly placed concrete surfaces for maximum efficiency. In addition, the efficiency of curing compounds can be highly variable, can be significantly reduced with increased temperature, and reduced relative humidity. There is a paucity of information about the effectiveness of traditional curing systems in reducing evaporation loss from the surface of fresh concrete placed in a hot, dry environment. Ambient temperature conditions ($\approx$ 50 °C and low relative humidity ($\approx$15% are typical of inland areas of southern regions of Algeria.

Recent developments in concrete technology take into account the inclusions of bottom ash, coal waste, fuel ash, fly ash, etc.… in the preparation of concrete. The use of this waste as a partial or total fine aggregate replacement is reported in the literature (Andrade et al. 2007; Kula et al. 2002; Amir and Pooyan 2014; Ciarán et al. 2016; Andrade et al. 2016; Saeid et al. 2016; Maamar 2017). So this totally wastes produced by thermoelectric power plants have the ability to be used in concrete and mortar. At present in America, coal waste is mainly used for the following applications: (Aggregate for concrete, Road base and sub-base, Structural fill, Backfill, asphalt and masonry, manufactured soil products…).

Environmental problems caused by the presence of coal waste near urban areas are still making life difficult for thousands of people, which is a major source of greenhouse gas emissions, this coal waste is destroying farms, threatening Biodiversity, refines its lungs, pollutes the atmosphere of cities, and distorts the extracted landscape.

Coal waste (heap) can be beneficially utilized in a variety of manufacturing and construction applications. At present, Coal waste (heap) is predominantly used for the following applications: • Road base and sub-base • Structural fill • Backfill• Aggregate for concrete, asphalt and masonry…

Hot weather conditions in many parts of the world are causing problems for cleanliness of concrete in the fresh state and in the cured state. Reduced durability is considered a major problem for cast concrete in hot weather. Faced with these problems encountered by the industrialists on the site, it becomes essential to undertake much more in-depth studies on the reduced durability in the face of chemical aggressions caused by sulphate in soils and acids in sewerage networks on the other hand.

The objective of this study is to contribute to the use of coal waste in hydraulic concrete. This makes it possible to eliminate these wastes by recycling, hence the protection of the environment. This helps to solve some problems related to the lack of

**Table 1.** Chemical and physical properties of the materials used and Coal waste (heap).

| Content (%) | Cement | Sand | Coarse aggregates | Coal waste (heap) |
|---|---|---|---|---|
| Chemical analysis | | | | |
| Silicon dioxide $SiO_2$ | 17.50 | 41.15 | 03.46 | 35.42 |
| Aluminum oxide $Al_2O_3$ | 4.87 | 02.11 | 00.71 | 19.57 |
| Iron (III) oxide $Fe_2O_3$ | 2.88 | 25.76 | 42.87 | 29.88 |
| Potassium $K_2O$ | 0.61 | 00.45 | 00.06 | 02.52 |
| Calcium oxide CaO | 59.98 | 28.64 | 52.29 | 4.68 |
| Titanium $TiO_2$ | - | 00.17 | 00.03 | 00.52 |
| Sulfur $SO_3$ | 2.59 | 00.02 | 00.01 | 05.40 |
| Sodium $Na_2O$ | 0.12 | 00.08 | 00.07 | 00.84 |
| Magnesium oxide MgO | 1.76 | 01.58 | 00.46 | 01.07 |
| CaO free | 1.398 | - | - | - |
| $P_2O_5$ | - | 00.04 | 00.04 | - |
| Tricalcium Aluminate $C_3A$ | 05 | - | - | - |
| Tricalcium Silicate $C_3S$ | 56 | - | - | - |
| Physical tests | | | | |
| Blaine ($cm^2/g$) | 4130 | - | - | - |
| Initial setting time (min) | 145 | - | - | - |
| Final setting time (min) | 250 | - | - | - |
| Specific gravity ($g/cm^3$) | 3.10 | 2.50 | 2.75 | 2.00 |

aggregates, and allows the study of the durability to evaluate the addition of coal waste on the strength of concrete under hot weather conditions with low relative humidity and as well wind. The results obtained in this investigation would be useful in determining the performance of waste heap concrete structures in hot weather.

## 2 Experimental Work

### 2.1 Material and Mix Proportions

The cement used in this study was CEM II/B 42.5 (conforming to the Algerian standard NA 442 (similar to type EN197-1/NF P15-301)). Crushed sand (0–3 mm) with specific gravity of 2.50 and fineness modulus of 2.20 and two class aggregate (3–8 and 8–15 mm) with specific gravity of 2.50 and 2.73 respectively. Table 1 shows the chemical and physical characteristics of the materials used.

Coal waste (heap) used in current study has been collected from the settling of the Kenadsa olden Coal mine, in Bechar, southern-west Algeria. The chemical and physical characteristics are given in Table 1.

The W/C ratio for all mixtures considered in this study was 0.51. The details of mixing with and without coal (heap) are shown in Table 2.

### 2.2 Climatic Data of the Studied Areas

The region of Béchar is located in the south west of Algeria in the Saharan desert, the climate is of continental desert type which is characterized by a very hot summer which can reach (+43 °C in the shade), which can exceed 45 or 50 °C on the ground, and a very cold winter (1 °C to 2 °C). Knowing that the hot period during the days of the year is too long (8/12 months approximately).

### 2.3 Casting and Curing

To simulate a setting and curing in hot weather in the laboratory, a climatic room of $1800 \times 1000 \times 800$ mm$^3$ was used. This room is equipped with electric heaters, an electric fan and a thermo-hygrometer to regulate and monitor the conditions inside. The temperature was maintained at 50 °C for 24 h with relative humidity (RH) of about 10% and wind speed at 10 km/h (Maamar 2017).

An extensive program of tests has been prepared to study the effect of these concreting conditions in hot weather on the behavior of the various concretes, the testimony of ordinary concrete and concretes with coal waste. Specimens of $100 \times 100 \times 100$ mm$^3$ were made for the compression test and $70 \times 70 \times 280$ mm$^3$ for flexural.

All batches of concrete were cast inside the laboratory. Batch 0 was prepared using the mix proportions shown in Table 2 and contained ordinary concrete without additions of coal waste (heap); Batch 1 to 6 was prepared using the same mix proportions except that used to substitute the volume of fine aggregates (sand) by the coal waste. Each sample was cast in 3 layers in a steel mold, each layer being compacted by external vibration.

All Batch was use to cast 03 concrete cubes that were tested for compressive strength and 03 concrete prismatic specimens were tested for flexural strength, with the aim of comparing the severe hot climate 50 °C use curing plastic sheet cover and without using plastic cover, with the normal climate 25 °C. After demolding, the specimens were subjected at $20 \pm 2$ °C under water to enable us to test the compressive strength at 2, 7 and 28 days, as well as test the flexural strength at 2, 7 and 28 days.

## 3 Results and Discussion

### 3.1 Compressive Strength

After 2 days, the compressive strength of the concrete poured in hot weather increases slightly compared to that of the same poured concrete in the laboratory. On the other hand, at 28 days, it becomes weaker. The increase and decrease in the compressive strength of cast concrete in hot weather is explained by the decrease in the amount of water evaporation due to both the high temperature (50 °C) and the wind speed. This is justified by the acceleration of hydration reactions by raising the temperature of the average

**Table 2.** Chemical and physical properties of the materials used and Coal waste (heap).

| | Mix proportion (Kg/m$^3$) | | | | | |
|---|---|---|---|---|---|---|
| Concrete | Cement | 8–15 mm Coarse aggregate | 3–8 mm Coarse aggregate | Sand | Coal waste (heap) | Water |
| $C_{0\%}$ | 350 | 940 | 164 | 743 | 0 | 180 |
| $C_{1\%}$ | 350 | 940 | 164 | 735.57 | 7.43 | 180 |
| $C_{2\%}$ | 350 | 940 | 164 | 728.14 | 14.86 | 180 |
| $C_{3\%}$ | 350 | 940 | 164 | 720.71 | 22.29 | 180 |
| $C_{4\%}$ | 350 | 940 | 164 | 713.28 | 29.72 | 180 |
| $C_{5\%}$ | 350 | 940 | 164 | 705.85 | 37.15 | 180 |
| $C_{6\%}$ | 350 | 940 | 164 | 698.42 | 44.58 | 180 |

environment, the concrete hydrates further, which contributes to the improvement of its compactness and its strength to compression.

As a result, the physical, chemical, and mineralogical properties of fine sand or aggregates can have a significant impact on water demand, affecting most of the properties of hardened concrete. The setting time and hydration faster. This leads to accelerated hydration and lower strength in the long term (Muhammad et al. 2017; Abdullah 2001).

Concrete sand substitution rate by coal waste cast in hot climate gains between 44 and 46% of its strength in two days. It is also clear in hot weather, that concrete acquire strength in 7 days compared to concrete poured in normal condition (in the laboratory), this gain being between 3 and 8%. Therefore, the results obtained indicate that, in the influence more of hardening in hot weather, the compressive strength of concrete cubes of coal waste with 1%, 2%, 3% and 4% is higher than that concrete 0% coal waste.

Thus, there is not much difference in strength between 0 and 4% of sand substitution rate by coal waste. In addition, the strength observed at 4% was higher than that of other coal waste mixtures, but higher than that of the 0% concrete mix of coal waste (reference concrete). Maximum concrete strength was achieved when replacing 4% sand with coal waste, which can be considered an optimal mix. The compressive strength of all coal waste mixtures increased with age. In 2 days, all the coal waste mixtures were more resistant than the 0% coal waste mix, but at age increased to 365 days, they achieved slightly higher strengths than the 0% concrete coal waste in the middle of normal condition casting and hot weather condition as shown in Fig. 1.

In general, the results obtained in these studies show the important effect of the heat of hydration of the cement and the high ambient temperature on the reduction of the workability and the strength to the compression, still the formation of the microstructure of the cement paste and concrete.

It has been observed that the difference in strength in the various mixtures from the coal waste concrete mixture may be equal for various concrete mixtures without coal waste (reference concrete), with an increase in age from 2 to 28 days. The reference concrete mix increased from 2 to 7 days of 80.45% and from 7 to 28 days of 43.73% which is a characteristic of normal concrete. Coal waste mixtures have reached a relatively

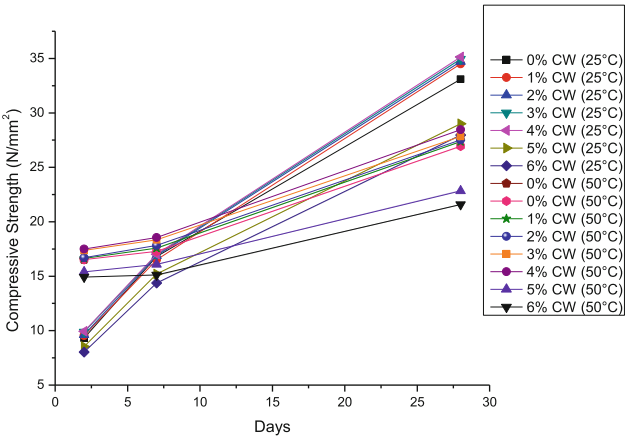


**Fig. 1.** Effect of % age replacement of CW on compressive strength at curing temperatures of 25 °C and 50 °C

constant strength of 71 to 73% from 2 to 7 days and of 46 to 49% from 7 to 28 days, in the normal condition (in the laboratory).

Nevertheless, in the condition of hot weather the reference concrete mixture increased from 2 to 7 days of 4.66% and from 7 to 28 days of 43.30%. Coal waste mixtures have reached a relatively constant strength of 1 to 7% from 2 to 7 days and from 25 to 43% from 7 to 28 days.

In order to improve the mechanical strength of cast concrete under hot weather conditions, the plastic film was used as a solution. The results of this mechanical test study are presented in Fig. 2.

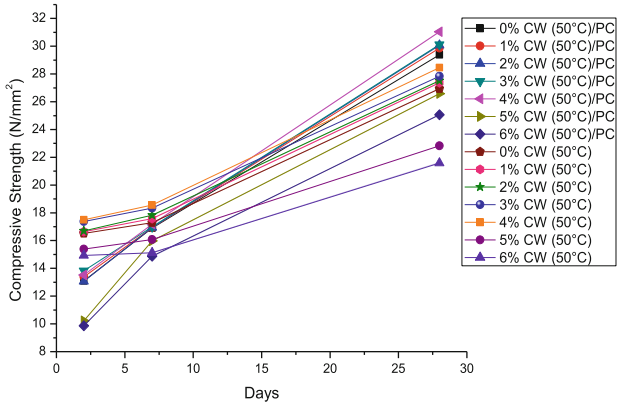


**Fig. 2.** Effect of % age replacement of CW on compressive strength at curing temperatures of 50 °C and 50 °C/Plastic Cover

From Fig. 2 that the use of plastic film, applied to the surface of fresh concrete poured in hot weather, significantly improves the compressive strength of all concretes irrespective of the rate of substitution of sand by the coal waste.

Thus, early-age water releases, related to temperature, concrete's humidity, wind speed, and air temperature, do not allow to maintain in the concrete the moisture necessary for the proper cooling process hydration (Balayssac et al. 1997; El-Dieb 2007). Indeed the purpose of different protection (plastic film, burlap, curing product, ….) Is to prevent the rapid departure of water inside the fresh concrete, to allow a good hydration of the cement paste (Alsayed and Amjad 1994; Sharon and Ling 2006). As a consequence of the best mechanical performances, and a good durability of the works against the external attacks.

The compressive strength of cast concrete in hot weather increases slightly to 2 days compared to that of the same cast concrete even condition (hot weather), but a plastic film was used for protection. On the other hand, at 28 days it becomes weaker, same remark from the previous explanation. The increase and decrease in the compressive strength of cast concrete in hot weather is explained by the decrease in the amount of water evaporation due to both the high temperature (50 °C) and the wind speed important (12 Km/h). This is justified by the acceleration of hydration reactions by raising the temperature of the average environment, the concrete hydrates further which contributes to the improvement of its compactness and its compressive strength.

As soon as 2 days have elapsed, the compressive strength of the sand substitution rate concrete by the hot-rolled coal waste gains between 21 and 34% of its strength in two days. It is also clear in hot weather, that the concrete acquire strength in 7 days compared to concrete poured in normal condition (laboratory), this gain being between 2 and 6%. Therefore, the results obtained indicate that, in the influence more of hardening in hot weather, the compressive strength of concrete cubes of coal waste with 1%, 2%, 3% and 4% is higher than that concrete 0% coal waste.

It was observed that the concrete of coal waste had risen differently from concrete 0% of coal waste at age increases to 365 days; except coal waste mixture of 5% and 6% which showed a larger decrease at all ages. Incomplete adhesion of coal waste to cement paste is also responsible for this decrease in strength. On the other hand, the values close to the strengths of control concretes and concretes of 1 to 4% coal waste could be explained by a better adhesion of these aggregates to the matrix.

Thus, there is not much difference in strength between 0 and 4% of sand substitution rate by coal waste. In addition, the strength observed at 4% was higher than that of other coal waste mixtures, but higher than that of the 0% concrete mix of coal waste (reference concrete). Maximum concrete strength was achieved when replacing 4% sand with coal waste, which can be considered an optimal mix. The compressive strength of all coal waste mixtures increased with age. In 2 days, all the coal waste mixtures were more resistant than the 0% coal waste mix, but at age increased to 28 days, they achieved slightly higher strengths than the concrete 0% coal waste in the middle of the casting condition hot weather without/with plastic film as shown in Fig. 2.

It has been observed that the difference in strength in the various mixtures from the coal waste concrete mixture may be equal for various concrete mixtures without coal waste (reference concrete), with an increase in age from 2 to 28 days. The reference

concrete mix increased from 2 to 7 days of 29.01% and from 7 to 28 days of 37.48% which is a characteristic of normal concrete. Coal waste mixtures have reached a relatively constant strength of 23 to 30% from 2 to 7 days and of 32 to 41% from 7 to 28 days, in the condition of hot weather with protection by plastic film. Nevertheless in the condition of hot weather without plastic film same previous explanation.

### 3.2 Flexural Strength

Figure 3 shows the flexural strength results of concrete beams tested at 2, 7 and 28 days.

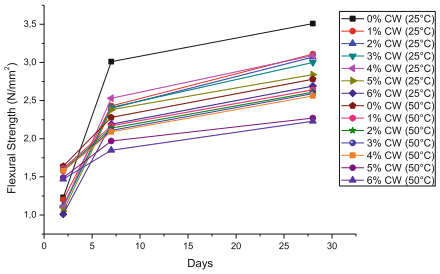


**Fig. 3.** Effect of % age replacement of CW on flexural strength at curing temperatures of 25 °C and 50 °C

The flexural strength of the concrete beams of the coal waste and the reference concrete tested in 2 days increased uniformly, for cast concrete in the hot weather condition, the reference concrete was higher than that of the coal waste concretes correspondents.

On the other hand, the flexural strength of concrete beams of reference coal and concrete wastes tested at 7 days showed a substantial increase in cast concrete under normal conditions (in the laboratory) to compare those cast concrete in hot weather condition. The beams hardened to cast in hot weather conditions are regressed by about 16 to 24%.

The flexural strength of the 28-day cast concrete beams in normal condition increases compared to cast concrete under hot weather conditions, since the reference concrete is always higher than that of the corresponding coal waste concretes. In fact, at high curing temperatures, the flexural strength of these two concretes at 28 days was always lower than the normal temperature.

The flexural strength of the tested coal waste concrete beams remained substantially the same as the cure temperature and the test age. This finding indicates that the curing temperature has little effect on the bending strength of a concrete of coal waste.

For all concretes cast at cure temperatures and test ages, the flexural strength of the reference concrete beams tested was still higher than that of the corresponding coal waste concretes. This finding indicates that cast coal concrete cured and cured at elevated temperatures generally does not have a greater flexural strength than cured reference concrete under similar conditions.

In addition, the results show that the method of hardening with the use of plastic film makes it possible to reduce the transfer of concrete humidity to its environment

and thus to retain the water inside the microstructure of the concrete, to guarantee the hydration of the concrete and it gives an adequate mechanical strength. These results are consistent with the work of Al-Amoudi, Al-Gahtani, Bouziadi and Ibrahim (Al-Amoudi et al. 1995; Ibrahim et al. 2013).

In fact, the substitution of sand for coal waste. At the age of 2 days increased uniformly, for cast concrete in the hot weather condition without protection by the plastic film, the reference concrete was higher than that of the coal waste concretes test presented in Fig. 4.

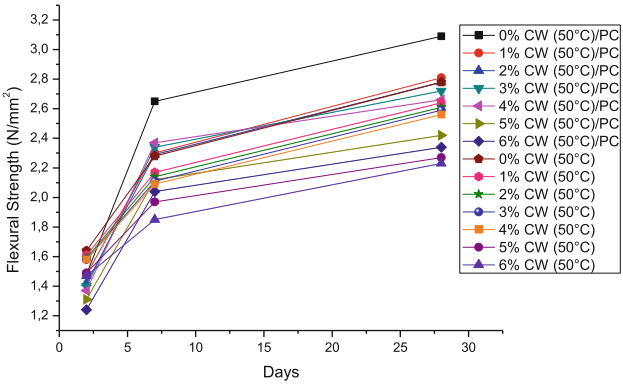


**Fig. 4.** Effect of % age replacement of CW on flexural strength at curing temperatures of 50 °C and 50 °C/Plastic Cover

On the other hand, the flexural strength of the 7-day reference and coal waste concrete beams showed a substantial increase in cast concrete in hot weather condition with the plastic film protection to compare those of cast concretes in hot weather conditions without plastic film. Beams cast in hot weather conditions experienced a regression of about 7 to 12%.

The flexural strength of cast concrete beams in hot weather condition with the plastic film protection tested at 28 days increases compared to cast concrete under hot weather conditions without plastic film, the reference concrete being always superior to that of corresponding coal waste.

### 3.3 X-ray Diffraction

The X-ray diffraction technique was performed to analyze the components of the 0% CW and 4% CW concrete mixes cast under hot climatic conditions, the results are shown in Figs. 5, 6. One of the main problems encountered in the qualitative and quantitative analysis of cement is that there is a significant overlap of the major diffraction peaks of all the principal phases of cement components in the angular range of 2θ 30 to 35 allowing the identification of individual components extremely difficult. In all mixtures, peaks $C_2S$, $C_3S$ and $C_3A$ are not visible indicating that they can be totally consumed or that the unheated cement peaks overlap with those of $SiO_2$ because all the mixtures analyzed

are concrete samples with large number of aggregates containing quartz that resulted in intensive $SiO_2$ peaks. Thus, as indicated, the free silica indicating the $SiO_2$ peak in the reference mixture was observed at 10,000. The X-ray diffraction pattern observed in the 4% CW mixture was similar to the 0% CW mixture as the sand contained than 4% of coal waste.

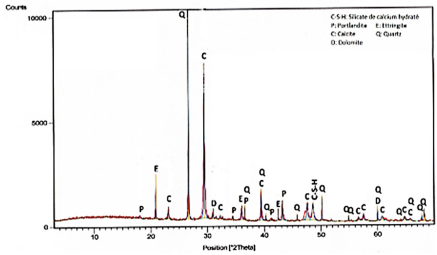


**Fig. 5.** X-ray Diffraction analysis for 0% CW concrete at curing temperatures of 50 °C

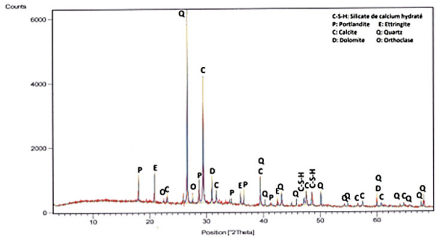


**Fig. 6.** X-ray Diffraction analysis for 4% CW concrete at curing temperatures of 50 °C

The X-ray diffraction analysis indicated a peak of dolomite is a calcium and magnesium carbonate having a chemical composition of CaMg $(CO_3)_2$ and peaks of the hydrated phase crystals of portlandite, hydrated calcium silicate and ettringite.

Concrete 4% coal waste cast in hot conditions, analysis indicated crystals of the hydrated phase, portlandite, ettringite and a broad quartz that represented the sand and coal waste used in the formulation of the mixture. Orthoclase is an aluminum silicate potassium having a chemical composition of $KAlSi_3O_8$. The formation of this compound was expected due to the presence of $K_2O$, $Al_2O_3$ and $SiO_2$ contents in the coal waste. This mineral is responsible for improving the bond between cement slurries and aggregates in concrete resulting in higher compressive strength of concrete containing coal waste aggregates (Fig. 6).

## 4 Conclusions

The properties of fresh as well as hardened concrete are closely associated with the characteristics and relevant proportioning of its constituent materials. The research reports show that inclusion of coal waste (heap) as sand replacement in concrete influences

the workability, setting times, loss of water through bleeding, bleeding rate and plastic shrinkage of fresh concrete and density, strength, porosity, durability of hardened mass.

The addition of coal waste (heap) beyond 4% is ineffective, which can be deduced from a sharp drop in performance of 5% and 6%. The optimal percentage of charcoal waste was 4% based on the test results. This research has shown that the use of fine aggregates from crushed coal waste can produce relatively strong structural concrete, with a weight saving of up to 10%, compared to normal concrete.

The decrease in strength of concrete is mainly due to higher porosity and higher water demand on use of coal waste (heap) in concrete. The compressive strength can be improved by reducing the water demand by using super plasticizers, it is concluded that:-

- coal waste (heap) is the potential viable material to be used as fine aggregate to produce durable concrete.
- Its use as fine aggregate in concrete will help in alleviating the potential problem of dwindling natural resources.
- Its use will also help in protecting the environment.
- Furthermore, the concretes made in this study, based on coal waste aggregates, have given satisfactory results, despite the mechanical failure of these (secondary) aggregates; consequently, a grain strength defect may not prevent the use of these aggregates in structural concrete.

## References

ACI Committee 305: Hot weather concreting. American Concrete Institute, USA Committee Report ACI 305 R-91 (1994)

Ibrahim, M., Shameem, M., Al-Mehthel, M., Maslehuddin, M.: Effect of curing methods on strength and durability of concrete under hot weather conditions. Cement Concr. Compos. **41**, 60–69 (2013)

Al-Gahtani, A.S.: Effect of curing methods on the properties of plain and blended cement concretes. Constr. Build. Mater. **24**, 308–314 (2010)

Ortiz, J., Aguado, A., Agulló, L., García, T., Zermeño, M.: Influence of environmental temperature and moisture content of aggregates on the workability of cement mortar. Constr. Build. Mater. **23**, 1808–1814 (2009)

Janos, E.U., Ahmad, J.: Hot weather concreting with hydraulic additives. Cem. Concr. Res. **21**, 345–354 (1991)

Alsayed, S.H., Amjad, M.A.: Effect of curing conditions on strength, porosity, absorptivity, and shrinkage of concrete in hot and dry climate. Cem. Concr. Res. **24**, 1390–1398 (1994)

Austin, S.A., Robins, P.J., Issaad, A.: Influence of curing methods on the strength and permeability of GGBFS concrete in a simulated arid climate. Cement Concr. Compos. **14**, 157–167 (1992)

Neville, A.M.: Properties des bétons, Paris (2000)

Faattuhi, N.I.: Curing compounds for fresh and hardened concrete. Build. Environ. **21**, 119–125 (1986)

Andrade, L.B., Rocha, J.C., Cheriaf, M.: Evaluation of concrete incorporating bottom ash as a natural aggregates replacement. Waste Manage. **27**, 1190–1199 (2007)

Kula, I., Olgun, A., Sevinc, V., Erdogan, Y.: An investigation on the use of tincal ore waste, fly ash, and coal bottom ash as Portland cement replacement materials. Cem. Concr. Res. **32**, 227–232 (2002)

Amir, M., Pooyan, A.: Coal waste application in recycled asphalt mixtures with bitumen emulsion. J. Clean. Prod. **83**, 263–272 (2014)

Ciarán, J.L., Ravindra, K.D., Gurmel, S., Ghataora, B.: Municipal incinerated bottom ash characteristics and potential for use as aggregate in concrete. Constr. Build. Mater. **23**, 609–614 (2016)

Andrade, L.B., Rocha, J.C., Cheriaf, M.: Influence of coal bottom ash as fine aggregate on fresh properties of concrete. Constr. Build. Mater. **23**, 504–517 (2016)

Saeid, H., Amir, M., Mostafa, S., Hesam, M.: Mechanical properties of roller compacted concrete pavement containing coal waste and limestone powder as partial replacements of cement. Constr. Build. Mater. **111**, 625–636 (2016)

Maamar, M., M'hammed, M., Bachir, G.: Mechanical Properties of Concrete Using Coal Waste (Heap) as Partial Replacements of Fine Aggregate in Hot Weather. Int. Rev. Civ. Eng. (IRECE) **8**, 120–124 (2017)

Muhammad, N., Al-Amoudi, O.S.B., Maslehuddin, M.: Effect of placement temperature and curing method on plastic shrinkage of plain and pozzolanic cement concretes under hot weather. Constr. Build. Mater. **152**, 943–953 (2017)

Abdullah, A.A.: Effect of environmental conditions on the properties of fresh and hardened concrete. Cement Concr. Compos. **23**, 353–361 (2001)

Balayssac, J.P., Détriché, Ch.H., Diafat, N.: Effect of wet curing duration upon mechanical properties of commonly used concretes. Mater. Struct. **30**, 284–292 (1997)

El-Dieb, A.S.: Self-curing concrete: water retention, hydration, and moisture transport. Constr. Build. Mater. **21**, 1282–1287 (2007)

Sharon Huo, X., Ling, U.W.: Experimental study of early-age behavior of high performance concrete deck slabs under different curing methods. Constr. Build. Mater. **20**, 1049–1056 (2006)

Al-Amoudi, O.S.B., Almusallam, A.A., Khan, M.M., Maslehuddin, M.: Effect of hot weather on compressive strength of plain and blended cement mortars. In: Proceedings of the 4th Saudi Engineering Conference, vol. 2, pp. 193–199. King Abdulaziz University, Jeddah (1995)

# Influence of Nitrogen Partial Pressure on the Structural, and Mechanical Properties of Ti-N Thin Films

F. Salhi[1(✉)], L. Aissani[1,2], C. Nouveu[3], and A. Alhussein[4]

[1] Mater Science Department, ABBES Laghrour University, P. O 1252, 40004 Khenchela, Algeria
faiza.salhi40@gmail.com
[2] Laboratory of Active Components and Materials, Larbi Ben M'Hidi. University, 04000 Oum El Bouaghi, Algeria
[3] La.Bo.Ma.P. ENSAM, Rue Porte de Paris, 71250 Cluny, France
[4] ICD – LASMIS, Université de Technologie de Troyes. Antenne de Nogent, Pôle Technologique de Sud Champagne 26, Rue Lavoisier, 52800 Nogent, France

**Abstract.** Modern technologies based on the exploitation of the typical thin film properties (adhesion, thermal stability, low porosity, desirable stoichiometry), have strongly developed to become one of the most essential industrial interests during recent years. TiN coatings, for example, usually used to edge retention and corrosion resistance on machine tools besides, it discovered applications in the nuclear industry as hard facing material mainly due to its high thermal stability. This work aims to develop and characterize, titanium nitride thin films deposited by the magnetron sputtering method on silicon and XC100 steel substrates, containing 1% wt. of carbon, under ($N_2$ and Ar) mixed atmosphere. The influence of nitrogen concentration on the structural, mechanical and tribological properties of the coatings was determined by EDS, DRX, AFM, MEB, Nano-indentation and alternative tribometer test. By varying the nitrogen flow rate from 0 to 20 sccm, it's thus formed a titanium nitrides mixture ($Ti_2N$ and TiN). The study's interest in the mechanical behavior of titanium nitride films on this steel type, and in this range of nitrogen percentage, is particularly because the obtained hardness, and adhesion in this area are extremely important. Also, the deposited titanium thin films on the XC100 steel show that the hardness achievement in the inter-critical area is as important as that obtained in the uncoated XC100 due to the change in the phase's proportion.

**Keywords:** Ti-N · Magnetron sputtering · Structure · Hardness · Tribological behavior

## 1 Introduction

Wear, corrosion, and oxidation, considered the principle cause for large losses in industries worldwide [1]. In machining operations, cutting tools are used to reshape materials


B. Safi et al. (Eds.): ISMSD 2019, *Proceedings of the 4th International Symposium on Materials and Sustainable Development*, pp. 187–195, 2020.
https://doi.org/10.1007/978-3-030-43211-9_17

workpieces in desired final forms, the process in which cutting tools are exposed to high contact pressures, and temperatures, excessive cutting forces, and intensive chemical attack in the cutting zone, so as a result, tools surface rapidly worn out [2, 3]. Transition metal nitrides (TMN) are ceramic materials with remarkable properties. TMN coatings are generally deposited on engine components and cutting tools to protect them toward heat, erosion, scratch, abrasion, corrosion, wear and oxidation [2, 4]. Among them, Titanium nitride (TiN) which is a rock-salt structure (NaCl structure) compound consisting of titanium atoms contained in a face-centered cubic (fcc) based lattice, with all octahedral sites filled with nitrogen atoms [5]. High hardness and chemical stability, good wear and corrosion resistance, raised melting temperature, farther excellent chemical inertness, unique and diverse characteristics, enabled the use of TiN coatings in a wide range not only as hard coatings in industrial applications, but also decorative, and wear-resistant coatings, diffusion barrier in microelectronics [6–9] and, biomedical instruments [10].

In the literature, many experimental studies demonstrated that the microstructural, mechanical, and tribological proprieties of titanium nitride films have a substantial correlation with the deposition parameters such as substrate type, temperature, or bias voltage, and nitrogen flow rates. In a previous research Sh. Valedbagi et al. [6] investigated the physical properties of titanium nitride thin film under different substrate temperatures (300°–500 °C) utilizing the reactive DC magnetron sputtering technique. At high substrate temperature AFM images show the creation of nanostructured thin films with an increase in the surface roughness. Moreover, D. Zhou et al., prepared TiN thin films on Si (100) wafers, utilizing DC reactive magnetron sputtering using a pure Ti target in ($N_2$ and Ar) mixed atmosphere at 350 °C, to clarify the influence of thickness on the proprieties of Ti-N thin films. It was found that the increase in the film thickness accompanied by an improvement in grain sizes and enhancement in density, and an increase in the surface roughness [11].

Besides, V. I. Shapovalov et al. [12] found that the titanium nitride films with the highest hardness (up to 30 GPa) and Young's modulus (up to 300 GPa) have the largest grains, that obtained at a low nitrogen flow rate and high discharge current density. Recently, E. Ajenifujaa et al. [13] sputtered $TiN_x$ films on LCS substrate using the magnetron sputtering method to evaluate the chemical, and microstructural properties dependent on film thickness. Scanning electron microscopy observation gave an indication of fine-grained microstructure that confirms the good hardness, and adhesion. The purpose of this work is to study, develop and characterize the structural as well as, the mechanical, and tribological properties of titanium-nitride thin films deposited by the RF magnetron sputtering method on Si (100) and XC100 steel substrates, containing 1% wt. of carbon.

## 2 Experimental

Series of TiN films were deposited on Si (100) wafer and XC100 steel, containing 1% wt. of carbon, using a RF magnetron sputtering technique. The typical composition of XC100 steel as follows: 0.95 to 1.05 wt-% C, 0.5 to 0.8 wt-% Mn, 0.05 wt-% S, 0.25 wt-% Si, 0.035 wt-% P and S, with Fe as the balance [3].

A Ti target (99.98% of purity) has set in vacuum chamber wall. The sputtering chamber was evacuated to a pressure of $2 \times 10^{-5}$ Pa. The Si (100) (for structure detected)

and polished steel (for mechanical detected) substrates were cleaned ultrasonically in acetone and de-ionized water, then in the sputtering chamber for 15 min at 1 Pa (Ar) pressure with the substrate bias voltage of − 700 V. The 120 min deposition time of coating process carried out at a total 0.4 Pa pressure with various nitrogen and argon ($N_2$ + Ar) gas mixture at − 900 V.

In this study, the film thickness determined using scanning electron microscopy (JeolJSM-6400FS), equipped with an energy dispersive X-ray spectrometer (EDS) to determine the chemical composition.

The crystalline structure of the films was explored by X-ray diffraction (XRD) using a Bruker D8 Advance diffractometer with Co cathode (Co–Kα radiation λ = 1.78 Å) wavelength. An AFM 100, APE research was performed to observe the topographic surface and the roughness of the TiN films.

The grain size (D) of the TiN films was calculated using the Scherrer's formula [3].

$$D = \frac{0.9\,\lambda}{\beta \cos\theta} \tag{1}$$

where 0.9 is a dimensionless shape factor, λ wavelength of the incidence, $\beta$ is the width at half-maximum of the diffraction peak and $\theta$ the Bragg's angle of TiN phase.

The mechanical properties (hardness and Young's modulus) of TiN films measured using a Nanoindenter XP (MTS-XP) system in continuous stiffness mode having a Berkovich diamond indenter tip, with a tip radius of 200 nm.

The friction coefficient performed using the pin-on-disk micro-tribometer with a 100Cr6 steel ball. The tests were performed in the ambient atmosphere under a temperature of 27 °C.

## 3 Results and Discussion

### 3.1 Microstructure Analysis

The evolution of deposition rate as a function of the nitrogen content is presented in Fig. 1. The deposition rate of the films decreases gradually from (16.33 ± 0.15 nm/min) to (10.16 ± 0.15 nm/min), with increasing nitrogen content from 0 to 53.7 at.%. This decrease in the deposition rate corresponding to the poor sputtering capability of nitrogen compared with pure argon [14].

The analysis shows that the oxygen level doesn't exceed 3 at%, which is relatively acceptable for a secondary vacuum produced. We note that the increase in the nitrogen percentage accompanied by an increase in the nitrogen content of the TiN coating and a decrease in the Ti content. Also we obtain a ratio of (0.49 ≈ 0.5) for 10 sccm of nitrogen in the plasma corresponds the hexagonal phase of $Ti_2N$ and a stoichiometry equal to 1 (N/Ti = 0.98≈1) for 20 sccm of the TiN cubic phase. Lu et al. [15] found that the N/Ti stoichiometry ratio increased from 0.69 to 0.98 with the $N_2$ flow rate rise from 1 to 20 sccm that is in good argument with that we obtained at 20 sccm.

The information of phases and crystallinity of the Ti-N coatings obtained with XRD indicate that the structure of Ti-N films depends on the nitrogen content in the sputtering process. The films deposited at 10 sccm of $N_2$ shows a strong $Ti_2N$ (1 1 0) orientation

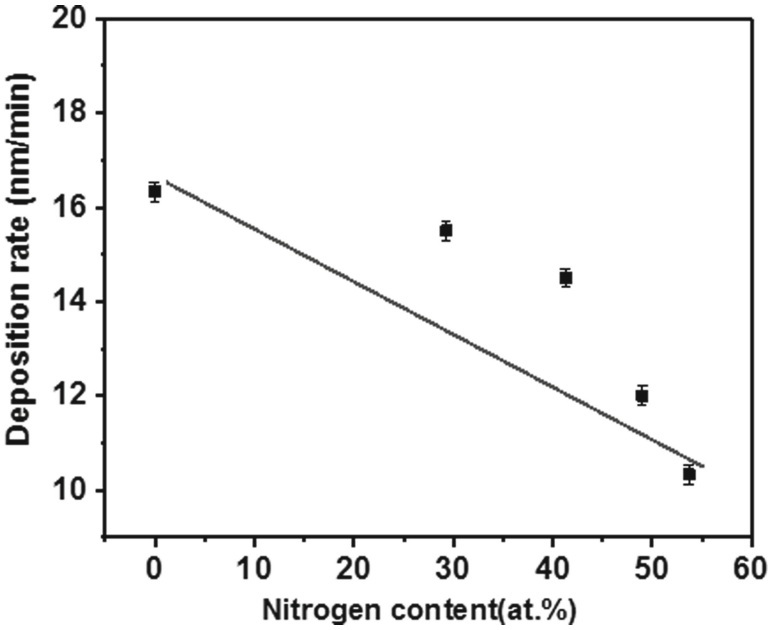


**Fig. 1.** Evolution of the deposition rate as a function as a nitrogen content of TiN films

**Table 1.** Compositions and coating thicknesses of Ti-N deposits as a function of the nitrogen percentage in the plasma.

| $N_2$, Sccm | Film thickness (μm) | N %.at | Ti at. % | O at. % | G.Size (nm) |
|---|---|---|---|---|---|
| 0 | 1950 ± 15 | 0 | 97 | 3 | – |
| 10 | 1860 ± 15 | 29.3 | 69 | 1.7 | 36 |
| 15 | 1750 ± 15 | 41.3 | 57 | 1.7 | 30 |
| 20 | 1480 ± 15 | 49 | 49.8 | 1.2 | 24 |
| 25 | 1220 ± 15 | 53.7 | 45 | 1.3 | 28 |

(JCPDS card number 71-0299). At 20 sccm, the film contains mainly $Ti_2N$ phase with (1 1 0) preferred orientations and TiN (1 1 1), (2 0 0) and (121) orientations (JCPDS card number 71-0299). It was confirmed that a mixture of $Ti_2N$ and TiN compounds could be formed via varying the $N_2$ content in deposition process (Fig. 2). N. Arshi et al. [16] found that FCC TiN phase with (111) preferred orientation appeared when the nitrogen flow rate varied from 3 to 9 sccm.

The investigation of the SEM morphology shows a dense structure and appearance columnar morphology with a rough surface (Ra = 15.6 nm) at10 sccm. The film surface roughness decreases with increasing the nitrogen flow rate (Fig. 3 "a") with an increasing the N content. At 20 sccm (Fig. 3 "b"), a globular and columnar type structure observed for the TiN film with a surface roughness of 7 nm. Compared to the film deposited at

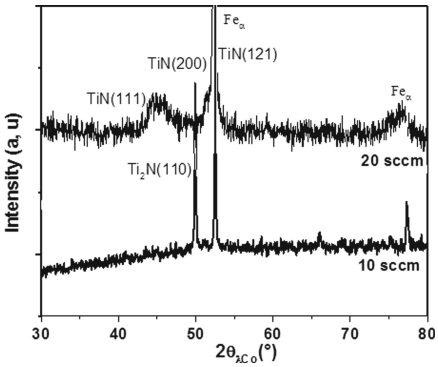


**Fig. 2.** XRD patterns of TiN films as a function as $N_2$ flow rate

10 sccm, the topography shows small columns with regular tops average column size around 100 nm. The TiN film grain size at 10 sccm was of the order of 36 nm. However, at 20 sccm, the grain size was found to be 24 nm as shown in Table 1. The decrease in both surface roughness and grain size are related to the dense structure and the smooth surface. According to Zhou et al. [17] the nitrogen plays a significant role on the film densification due to the presence of further nuclei.

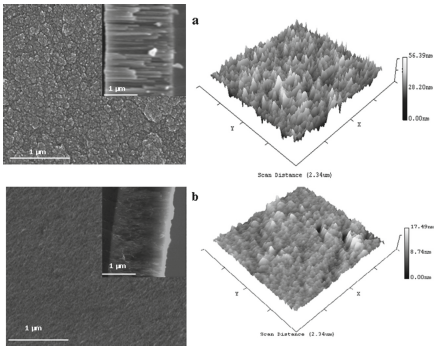


**Fig. 3.** AFM and SEM images of the TiN films deposited at: "a" 10 sccm, "b" 20 sccm

Y. L. Jeyachandran et al. [18] found that the TiN films deposited at low $N_2$ concentration of 0.5% showed smooth and uniform morphology with densely packed crystallites. However, at higher nitrogen concentration conditions, uniformity developed in the films with increase in thickness. Moreover, N. White et al. [19] showed that the RMS roughness decreases from 7.5 nm at 0 sccm to approximately 1 nm with the oriented columnar grain structure for higher flow rates (20 sccm and above) with the disappearance of the columnar structure and a decrease in the calculated grain size.

### 3.2 Mechanical Properties

The hardness for the pure Ti (6 GPa) increases gradually by increasing $N_2$ content up to a maximum of 27 GPa at 10 sccm of $N_2$ (Fig. 4). Further, increasing the nitrogen content reduces the hardness to a value of 16 GPa at 25 sccm of $N_2$ due to the decrease in the residual stress and the structure densification. As the columnar microstructure became dense, the residual stress induced by sputtering could be released and consequently decreased. Meanwhile, the decrease in the residual stress could be associated with an absence in the significant number of defects produced during the film growth, and a decrease in the energy of ions bombarding the substrate surface. The Young's modulus of all films reflects the same trend as the coatings' hardness. According to S. Kataria et al. [20] the increase of the nitrogen flow rate leads to an increase in the hardness value, which is the result of the coatings microstructure refinement. The smaller crystallite size can also lead to an increase in the film hardness.

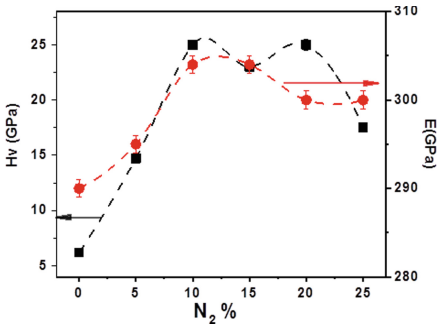


**Fig. 4.** Hardness and Young's modulus of TiN coatings obtained for different $N_2$ flow rate

### 3.3 Tribological Properties

The friction coefficients of the TiN film obtained for different $N_2$ flow rate plotted in Fig. 5. The pure Ti films (0 sccm of $N_2$) show a high friction coefficient against the 100Cr6 steel ball ($0.59 \pm 0.01$). This cause the steel ball was harder than the Ti film. Between 10 ($0.5 \pm 0.01$) and 20 sccm of $N_2$ ($0.51 \pm 0.01$), a lower friction coefficient was obtained. However, for the higher nitrogen content (25 sccm), the friction coefficient increased slightly to ($0.52 \pm 0.01$). The existence of the dense and smooth surface of the film deposited at 20 sccm $N_2$ may act as a relatively lower frictions coefficient in the wear process.

The main reason for that is the crystals orientations of TiN thin coatings that have a direct effect on the tribological properties [21], according to S. Zhang et al. [22] TiN thin films deposited at ratio of 1:1 ($Ar/N_2$) gave a suitable COF (0.12) and a best wear resistance, which are the best coating TiN thin film condition; due to the dense columnar structure and low surface roughness. In contrast, the presence of oxygen cause changes in the friction and wear characteristics [23]. L. Aissani et al. [24] explained the

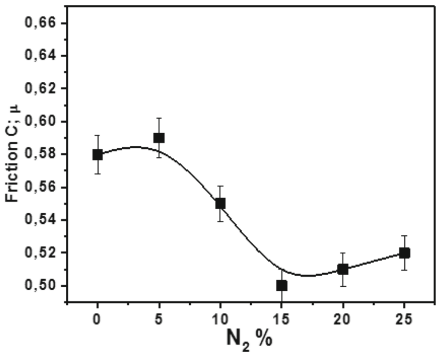


**Fig. 5.** Friction coefficients of TiN coatings obtained for different $N_2$ flow rate

relationship between the friction coefficient and the presence of oxidation in the films, where she reported that the removal of the superficial oxidative layer (via annealing at 700 °C) formed during the Cr–N film deposition, allow a significant increase in the friction coefficient (from 0.53 to 0.62).

The wear test marks effected on the film's surface was observed by SEM and analyzed by EDS to check the state of degradation. In Fig. 6. "a", we notice that the layer deposited at 10 sccm (corresponding to the $Ti_2N$ hexagonal phase) exhibits total delamination of the film inside, and in the edges of the friction traces, and we only detect the presence of the relative iron of XC100 substrate and oxygen at these areas of damage, which evidence their oxidation. This is in direct connection with the surface condition of these layers despite its good mechanical properties. The damage of the films deposited at 20 sccm, corresponding to the nitrogen stoichiometry of the TiN cubic phase, that was less because we detect only very local flaking in the corresponding traces of friction. According to a previous study [22], the TiN films have a lower friction coefficient and a better wear behavior than that of $Ti_2N$. The increase in the wear volume is the consequence of the difference between both Young's modulus of coating and substrate leads to a higher concentration of shear stresses in the interfacial zone (coating-substrate) [24].

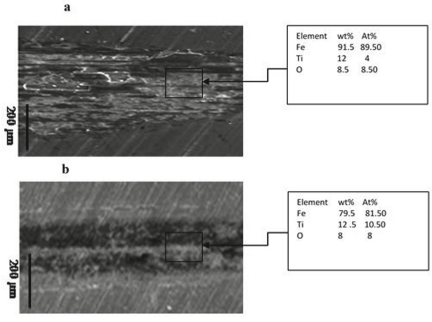


**Fig. 6.** Analysis by EDS and WDS of the wear track obtained at the bottom of the made on the TiN films deposited at: "a" 10 sccm, "b" 20 sccm on the XC100 steel substrate

## 4 Conclusions

TiN films with different nitrogen contents were deposited using RF magnetron sputtering to analyze the structural, mechanical and tribological properties.

- XRD diffraction patterns reveal the formation of mixed $Ti_2N$ and TiN phases, and the SEM image showed a dense and a columnar-type structure.
- The TiN films showed a higher hardness value of around 27 GPa at 10 sccm of $N_2$.
- The pure Ti film shows a high friction coefficient against the 100Cr6 steel ball. However, the friction coefficient decreases to lower values between 10 and 20 sccm of $N_2$ flow rates, with good adhesion, then it increased to about 0.73 with a further increase in nitrogen content.

## References

1. Valdez, B., Schorr, M., Zlatev, R., Carrillo, M., Stoytcheva, M., Alvarez, L., Eliezer, A., Rosas, N.: Corrosion control in industry. In: Environmental and Industrial Corrosion - Practical and Theoretical Aspects (2012). https://doi.org/10.5772/51987
2. Sangiovanni, D.G.: Transition metal nitrides: alloy design and surface transport properties using Ab-initio and classical computational methods. Linkoping Studies in Science and Technology, dissertation no. 1513 (2013)
3. Aissani, L., Alhussein, A., Nouveau, C., Radjehi, L., Lakdhar, I., Zgheib, E.: Evolution of microstructure, mechanical and tribological properties of vanadium carbonitride coatings sputtered at different nitrogen partial pressures. Surf. Coat. Technol. (2019). https://doi.org/10.1016/j.surfcoat.2019.06.034
4. Oyama, S.T.: The Chemistry of Transition Metal Carbides and Nitrides. Blackie Academic & Professional, Glasgow (1996)
5. Ţălu, Ş., Stach, S., Valedbagi, S., Elahi, S.M., Bavadi, R.: Surface morphology of titanium nitride thin films synthesized by DC reactive magnetron sputtering. Mater. Sci.-Pol. **33**(1), 137–143 (2015). https://doi.org/10.1515/msp-2015-0010
6. Bavadi, R., Valedbagi, S.: Physical properties of titanium nitride thin film prepared by DC magnetron sputtering. Mater. Phys. Mech. **15**, 167–172s (2012)
7. Ponon, N.K., Appleby, D.J.R., Arac, E., King, P.J., Ganti, S., Kwa, K.S.K., O'Neill, A.: Effect of deposition conditions and post deposition anneal on reactively sputtered titanium nitride thin films. Thin Solid Films **578**, 31–37 (2015). https://doi.org/10.1016/j.tsf.2015.02.009
8. Bailey, E., Ray, N.M.T., Hector, A.L., Crozier, P., Petuskey, W.T., McMillan, P.F.: Mechanical properties of titanium nitride nanocomposites produced by chemical precursor synthesis followed by High-P T, treatment. Materials **4**(10), 1747–1762 (2011). https://doi.org/10.3390/ma4101747
9. Grosso, S., Latu-Romain, L., Berthomé, G., Renou, G., Le Coz, T., Mantel, M.: Titanium and titanium nitride thin films grown by dc reactive magnetron sputtering Physical Vapor Deposition in a continuous mode on stainless steel wires: Chemical, morphological and structural investigations. Surf. Coat. Technol. **324**, 318–327 (2017). https://doi.org/10.1016/j.surfcoat.2017.05.089
10. Wu, W.-Y., Chan, M.-Y., Hsu, Y.-H., Chen, G.-Z., Liao, S.-C., Lee, C.-H., Lui, P.-W.: Bioapplication of TiN thin films deposited using high power impulse magnetron sputtering. Surf. Coat. Technol. (2019). https://doi.org/10.1016/j.surfcoat.2019.01.106

11. Liang, H., Xu, J., Zhou, D., Sun, X., Chu, S., Bai, Y.: Thickness dependent microstructural and electrical properties of TiN thin films prepared by DC reactive magnetron sputtering. Ceram. Int. **42**(2), 2642–2647 (2016). https://doi.org/10.1016/j.ceramint.2015.10.070
12. Babinova, R.V., Smirnov, V.V., Useenov, A.S., Kravchuk, K.S., Gladkikh, E.V., Shapovalov, V.I., Mylnikov, I.L.: Mechanical properties of titanium nitride films obtained by reactively sputtering with hot target. J. Phys: Conf. Ser. **872**, 012035 (2017). https://doi.org/10.1088/1742-6596/872/1/012035
13. Ajenifuja, E., Popoola, A.P.I., Popoola, O.M.: Thickness dependent chemical and microstructural properties of DC reactive magnetron sputtered titanium nitride thin films on low carbon steel cross-section. J. Mater. Res. Technol. **8**(1), 377–384 (2019). https://doi.org/10.1016/j.jmrt.2018.02.010384
14. Vaz, F., Ferreira, J., Ribeiro, E., Rebouta, L., Lanceros-Méndez, S., Mendes, J.A., Alvesb, E., Goudeauc, Ph., Rivièrec, J.P., Ribeirod, F., Moutinhod, I., Pischowe, K., de Rijke, J.: Influence of nitrogen content on the structural, mechanical and electrical properties of TiN thin films. Surf. Coat. Technol. **191**(2–3), 317–323 (2005). https://doi.org/10.1016/j.surfcoat.2004.01.033
15. Lu, L., Luo, F., Huang, Z., Zhou, W., Zhu, D.: Influence of the nitrogen flow rate on the infrared emissivity of TiN x films. Infrared Phys. Technol. **88**, 144–148 (2018). https://doi.org/10.1016/j.infrared.2017.11.015
16. Arshi, N., Lu, J., Koo, B.H., Lee, C.G., Ahmed, F.: Effect of nitrogen flow rate on the properties of TiN film deposited by e beam evaporation technique. Appl. Surf. Sci. **258**(22), 8498–8505 (2012). https://doi.org/10.1016/j.apsusc.2012.04.179
17. Zhou, W., Liang, J., Zhang, F., Mu, J., Zhao, H.: A comparative research on TiAlN coatings reactively sputtered from powder and from smelting TiAl targets at various nitrogen flow rates. Appl. Surf. Sci. **313**, 10–18 (2014). https://doi.org/10.1016/j.apsusc.2014.05.053
18. Jeyachandran, Y.L., Narayandass, S.K., Mangalaraj, D., Areva, S., Mielczarski, J.A.: Properties of titanium nitride films prepared by direct current magnetron sputtering. Mater. Sci. Eng.: A **445–446**, 223–236 (2007). https://doi.org/10.1016/j.msea.2006.09.021
19. White, N., Campbell, A.L., Grant, J.T., Pachter, R., Eyink, K., Jakubiak, R., Martinez, G., Ramana, C.V.: Surface/interface analysis and optical properties of RF sputter-deposited nanocrystalline titanium nitride thin films. Appl. Surf. Sci. **292**, 74–85 (2014). https://doi.org/10.1016/j.apsusc.2013.11.078
20. Kataria, S., Srivastava, S.K., Kumar, P., Srinivas, G., Siju, Khan, J., Rao, D.V.S., Barshilia, H.C.: Nanocrystalline TiN coatings with improved toughness deposited by pulsing the nitrogen flow rate. Surf. Coat. Technol. **206**(19–20), 4279–4286 (2012). https://doi.org/10.1016/j.surfcoat.2012.04.040
21. Bahri, A., Guermazi, N., Elleuch, K., Ürgen, M.: Tribological performance of TiN coatings deposited on 304L stainless steel used for olive-oil extraction. Wear **342–343**, 77–84 (2015). https://doi.org/10.1016/j.wear.2015.08.012
22. Zhang, S., Yan, F., Yang, Y., Yan, M., Zhang, Y., Guo, J., Li, H.: Effects of sputtering gas on microstructure and tribological properties of titanium nitride films. Appl. Surf. Sci. **488**, 61–69 (2019). https://doi.org/10.1016/j.apsusc.2019.05.148
23. Hamzah, E., Ourdjini, A., Ali, M., Akhter, P., Mohd Toff, M.R.H.J., Abdul Hamid, M.: Influence of nitrogen flow rate on friction coefficient and surface roughness of tin coatings deposited on tool steel using arc method. Surf. Rev. Lett. **14**(05), 1007–1013 (2007). https://doi.org/10.1142/s0218625x07010408
24. Aissani, L., Fellah, M., Radjehi, L., Nouveau, C., Montagne, A., Alhussein, A.: Effect of annealing treatment on the microstructure, mechanical and tribological properties of chromium carbonitride coatings. Surf. Coat. Technol. **359**, 403–413 (2019). https://doi.org/10.1016/j.surfcoat.2018.12.099

# Author Index




B. Safi et al. (Eds.): ISMSD 2019, *Proceedings of the 4th International Symposium on Materials and Sustainable Development*, pp. 197–198, 2020.
https://doi.org/10.1007/978-3-030-43211-9